Investigation of the mechanisms underlying the vascular relaxation mediated by n-3 PUFAs (fish oils), docosahexaenoic acid (DHA) and eicosapentaenoic acid (EPA), in resistance and conduit arteries

PhD

School of Pharmacy

Roshan Limbu

2019

Declaration

I confirm that this is my own work and the use of any material from other sources has been properly and fully acknowledged.

Roshan Limbu

Acknowledgements

I would like to start off by thanking my supervisors, associate professor Alister McNeish and Dr Graeme S. Cottrell, for the exceptional guidance and support that was given throughout my PhD journey both in and outside the lab. I will be forever grateful for the level of expertise and scientific knowledge that was imparted to me by both of them.

I would also like to express my sincere gratitude to professor Andrew Tinker from Queen Mary University of London and his team, especially Dr Qadeer Aziz Hussain and Mark Specterman, for the tremendous supervision and support that was given during my visits. The amount of experience and understanding that I gained was immense.

I want to thank my colleagues and friends from the Hopkins building, you guys have been amazing to work with. I want to personally thank Dr Claudia Bauer for being a wonderful mentor and for all the help that she provided. I also want to thank Dr Francesco Tamagnini for helping me with my patch-clamp experiments.

I want to thank British Heart Foundation for funding my PhD and providing the generous travel grant which allowed me to present my work throughout the globe.

Lastly, I want to acknowledge my parents, close friends and Paruhangma Rai for always believing in me and being there for me through thick and thin.

धन्यवाद

Abstract

There is extensive evidence demonstrating the protective effects of fish oils or omega-3 polyunsaturated fatty acids (n-3 PUFAs) against cardiovascular diseases. It is widely accepted that the main n-3 PUFAs involved with these therapeutic effects are DHA and EPA. These PUFAs have been reported to reduce blood pressure by improving various vasodilation pathways. However, most of these studies focus on either DHA or EPA in a single artery. Therefore, this PhD project involved the comprehensive characterisation of the underlying vasodilation mechanisms of both n-3 PUFAs using conduit and resistance rat arteries.

Wire myograph was used to examine acute vasodilation effects of n-3 PUFAs in pre-constricted rat arteries, mostly via the use of pharmacological inhibitors. Stable cells that allowed inducible expression of TRPV4 was generated to assess changes in channel activity with n-3 PUFAs, using Fluo-4 AM based calcium imaging. n-3 PUFA mediated activation of K_{ATP} channels was also examined by using stable cells and whole cell patch clamp.

The novel role of IK_{Ca} was observed in DHA-induced relaxation. Consistent with previous studies, BK_{Ca} was also involved in the relaxation effects of n-3 PUFAs. The presence of K_{ATP} and K_v7 component in n-3 PUFA-mediated vasodilation was also demonstrated for the first time. One of the most important highlights of my findings is the heterogeneity in the vasodilation mechanisms that was dependent upon both the type of n-3 PUFA and artery. These findings will be invaluable for future vascular studies that focus on investigating the prospect of using n-3 PUFA and novel fatty acid analogues as treatments that target specific vasodilation pathways, that are involved in providing therapeutic benefits against certain cardiovascular disorders.

Table of contents

List of figures

Chapter 5 Page

Fig 5.14	**Expression of K_{ATP} channels in HEK_{KATP}**	221
Fig 5.15	**DHA is not involved in the direct modulation of K_{ATP} channels**	224
Fig 5.16	**Original representative traces demonstrating the effect of XE991 (1 µM) in DHA-induced relaxation of rat mesenteric artery**	227
Fig 5.17	**Original representative traces demonstrating the effect of XE991 (1 µM) in DHA-induced relaxation of rat aorta**	228
Fig 5.18	**Concentration response curves demonstrating relaxation mediated by (A) DHA (*n*=5) and (B) EPA (*n*=5) in rat mesenteric artery following inhibition of K_v7 channels (mainly Kv7.1 homomer and Kv7.2+Kv7.3) with XE991 (1 µM)**	229
Fig 5.19	**Concentration response curves demonstrating relaxation mediated by (A) DHA (*n*=6) and (B) EPA (*n*=5) in rat aorta following inhibition of K_v7 channels (mainly Kv7.1 homomer and Kv7.2+Kv7.3) with XE991 (1 µM)**	230

Chapter 6 Page

List of tables

Abbreviations

A	Adrenic acid
AA	Arachidonic acid
ABC	Adenosine triphosphate-binding cassette
AC	Adenylate cyclase
ACh	Acetylcholine
ADMA	Asymmetric dimethylarginine
ADP	Adenosine diphosphate
ALA	Alpha-linoleic acid
ANOVA	Analysis of variance
AP1	Activator protein 1
ATP	Adenosine triphosphate
AT_1	Angiotensin II receptor type 1
ATPase	Adenosinetriphosphatase
AWERB	Animal Welfare and Ethical Review Board
BK_{Ca}	Large conductance calcium activated potassium channel
BSA	Bovine serum albumin
$[Ca^{2+}]_i$	Intracellular calcium
CaM	Calmodulin
cAMP	Cyclic adenosine monophosphate
CaV	Voltage-gated calcium channels
cGMP	Cyclic guanosine monophosphate
CHD	Coronary heart disease
COX	Cycloxygenase

CPI-17	C-kinase potentiated protein phosphatase-1 inhibitor
Cx	Connexin
CVDs	Cardiovascular diseases
CYP	Cytochrome P450
DAG	1,2-diacylglycerol
DDW	Double distilled water
DGLA	Dihomo-gammalinolenic acid
DHA	Docosahexaenoic acid
DHETs	Dihydroxyeicosatrienoic acid
DMEM	Dulbecco's modified eagle's medium
DMSO	Dimethyl sulfoxide
DPA	Docosapentaenoic acid
dNTPs	Deoxyribonucleotide triphosphate
ECs	Endothelial cells
EDH	Endothelium-dependent hyperpolarization
EDHF	Endothelium-derived hyperpolarization factor
EDPs	Epoxydocosapentaenoic acids
EDRF	Endothelium-derived relaxing factor
EDTA	Ethylenediaminetetraacetic acid
EETs	Epoxyeicosatrienoic acids
EGF	Epidermal growth factor
eNOS	Endothelial NO synthase
EPA	Eicosapentaenoic acid
EPAC	Exchange protein activated by cAMP

EPETEs	Epoxyeicosatetraenoic acids
FADS	Fatty acid desaturase
FBS	Foetal bovine serum
Fluo-4 AM	Fluo-4 acetoxymethyl ester
GLA	Gamma linolenic acid
GOI	Gene of interest
GPCR	G protein-coupled receptors
GPR40	Free fatty acid receptor 1
GSK	GSK1016790A
GTP	Guanosine triphosphate
HA	Human influenza hemagglutinin
HC	HC-067047
HDHA	Hydroxy-docosahexaenoic acid
HEK	Human embryonic kidney cells
HETEs	Hydroxyeicosatetraenoic acids
HRP	Horseradish peroxidase
IC_{100}	Internal circumference corresponding to the transmural pressure of 100 mm Hg
ICC	Immunocytochemistry
IgG	Immunoglobulin
IK_{Ca}	Intermediate conductance calcium activated potassium channel
IL-17	Interleukin-17
IP	Prostaglandin I2 receptor
IP_3	Inositol 1,4,5-triphosphate

K_{ATP}	ATP-sensitive potassium channel
K_{Ca}	Calcium activated potassium channel
Kir2.1	Voltage-gated channel subfamily J member 2
Kir6.1	Inward-rectifier potassium channel 6.1
KO	Knockout
K_v	Voltage-gated potassium channel
K_v7	Potassium voltage-gated channel subfamily Q member
LA	Linoleic acid
LT	Leukotriene
LTR	Long terminal repeats
M_3	Muscarinic acetylcholine receptor M3
MAPK	Mitogen-activated protein kinase
MEGJ	myo-endothelial gap junctions
MLCK	Myosin light chain kinase
MLCP	Myosin light chain phosphatase
mRNA	Messenger ribonucleic acid
Na+/K+-ATPase	Sodium-potassium adenosine triphosphatase
NADPH	Nicotinamide adenine dinucleotide phosphate
NBD	Nucleotide binding fold
NEB	New England biolabs
NF-κB	Nuclear factor kappa-light-chain-enhancer of activated B cells
NICE	National institute for health and care excellence
NO	Nitric oxide
PCR	Polymerase chain reaction

PE	Phenylephrine
PFA	Paraformaldehyde
PG	Prostaglandin
PIP2	Phosphatidylinositol 4,5-bisphosphate
PKA	Protein kinase A
PKC	Protein kinase C
PKG	Protein kinase G
PLA_2	Phospholipase A_2
PLC	Phospholipase C
PUFA	Polyunsaturated fatty acid
qPCR	Quantitative PCR
RAG-1	Recombination activating gene 1
RCK	Regulator of conductance for K+
RE	Restriction enzyme
RhoA	Ras homolog gene family, member A
ROCK	Rho-associated protein kinase
ROI	Regions of interest
ROS	Reactive oxygen species
RRE	Rev response element
RT-PCR	Reverse transcription PCR
RV	Resolvin
SDS	Sodium dodecyl sulfate
sEH	Soluble epoxide hydrolase
SERCA	Sarco/endoplasmic reticulum Ca2+-ATPase

SHR	Spontaneously hypertensive rats
sGC	Soluble guanylate cyclase
SK_{Ca}	Small conductance calcium activated potassium channel
SMCs	Smooth muscle cells
SOB	Super optimal broth
SOC	Super optimal broth with catabolite repression
SR	Sarcoplasmic reticulum
STOCs	Spontaneous transient outward currents
SUR	Sulfonylurea receptor
TAE	Tris-acetate-ethylenediaminetetraacetic acid
TEMED	Tetramethylenediamine
TMD	Transmembrane domain
TNF-α	Tumour necrosis factor-alpha
TP	Thromboxane A2 receptor
TRPC1	Transient Receptor Potential Cation Channel Subfamily C Member 1
TRPV1	Transient receptor potential cation channel subfamily V member 1
TRPV4	Transient receptor potential cation channel subfamily vanilloid member 4
TX	Thromboxane
TXA2	Thromboxane A2
VIP	Vasoactive intestinal polypeptide
VSV-G	Vesicular stomatitis virus
VSMCs	Vascular smooth muscle cells

WB	Western blot
WKY	Wistar Kyoto

Chapter 1

Introduction

1.1 Introduction

The cardiovascular system is a complex network of organs that function together to deliver oxygen and nutrients to different parts of the body. The main components that are involved are the heart, blood and blood vessels. As the heart pumps blood into the arteries, pressure is exerted against the vessel wall. Blood pressure is affected by various factors such as the cardiac output (volume of blood ejected from the left ventricle per minute), blood viscosity and systemic vascular resistance (Betts et al. 2013). The vascular resistance can be calculated by using the Poiseuille's equation of blood flow where (Pfitzner 1976);

Resistance = $\frac{8\eta\lambda}{\pi r^4}$

η = Blood viscosity

λ = Length of the blood vessel

r = Radius of the blood vessel

According to the equation, viscosity and length of the blood vessels are directly proportional to the resistance, however, these variables are fairly consistent throughout the body and do not undergo drastic changes. The radius of blood vessels on the other hand can be readily altered and as demonstrated by the above equation is raised to the power of 4, indicating that minute changes in the radius can significantly affect the arterial resistance. Based on the size, the arteries can be further subdivided into conduit and resistance arteries. Conduit arteries are the larger blood vessels such as aorta and are mainly involved in the distribution of blood throughout the body (London 1997). Resistance arteries are the smaller arteries (lumen diameter <300 μm) that are involved in blood pressure regulation (Davis et al. 1986; Schiffrin 1992). The greatest vascular

resistance and reduction in pressure occurs in resistance arteries and as demonstrated by Poiseuille's equation, minute changes in their radius can significantly influence blood pressure (Pocock et al. 2013). Although the diameter of capillaries are the smallest in the circulatory system, the vascular resistance that they offer is relatively small due to their large total cross-sectional area which is 25 times greater than resistance arteries (Pocock et al. 2013). Majority of the blood is found in the larger veins which are also known as capacitance vessels. However, these vessels also offer little vascular resistance due to relatively thinner walls and higher compliance compared to arteries. Therefore, the venous pressure ranges from 2-20 mmHg whereas the average arterial pressure is about 100 mmHg in humans (Pocock et al. 2013).

Anatomical differences depending upon the size and the type of blood vessels are present throughout the body, however arteries and veins are mainly composed of three layers; tunica intima, tunica media and tunica externa (Fig 1.1) (Betts et al. 2013). Tunica intima forms the inner layer and is composed of endothelial cells (ECs) and internal elastic lamina. ECs can regulate the vascular tone via the production of various vasoconstrictors and vasodilators. Tunica media is mostly composed of smooth muscle cells (SMCs) which can directly alter the diameter of blood vessels, whereas the outer layer also known as tunica externa is composed of connective tissue. Most blood vessels involved in the systemic circulation, excluding cerebral arteries, are surrounded by an outer layer of perivascular adipose tissue (Brown et al. 2014). This adipose layer is involved in various physiological processes including regulation of the vascular tone (Lynch et al. 2013; Withers et al. 2014).

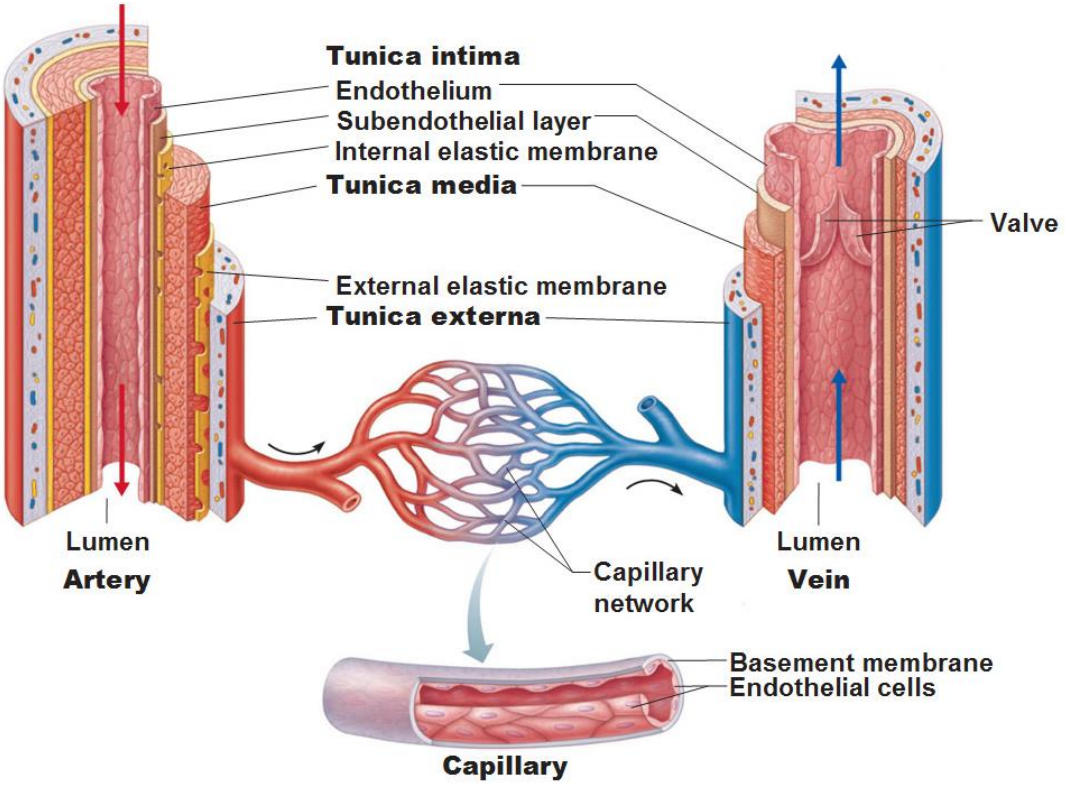

Fig 1.1 Anatomy of blood vessels. The three main layers of blood vessels are; tunica intima, tunica media and tunica externa. Capillaries are made up of single layer of endothelial cells. The endothelium is involved in the production of various vasodilators and vasoconstrictors that can regulate the vascular tone. Image taken from (Marieb 2014).

The vascular tone is regulated by vasoconstriction and vasodilation which involves the narrowing and widening of the blood vessels, respectively. SMCs are non-striated spindle-shaped cells composed of actin and myosin filaments that are involved in constriction of the blood vessels. Unlike striated muscle cells, SMCs lack troponin and therefore require calmodulin to reversibly bind to Ca^{2+}. Elevated levels of intracellular Ca^{2+} $[Ca^{2+}]_i$ promotes formation of the calcium-calmodulin (CaM) complex, which subsequently activates myosin II light chain kinase (MLCK). Myosin regulatory light chain (20 kDa) is then phosphorylated at Ser^{19} by MLCK, facilitating binding with the actin filaments (Dabrowska et al. 1982; Allen and Walsh 1994). This results in subsequent activation of myosin adenosine triphosphatase (ATPase) initiating the cross

bridge cycle and contraction of the SMCs (Dabrowska et al. 1982; Allen and Walsh 1994). Myosin light chain phosphatase (MLCP) present in SMCs can inhibit the effects of MLCK by dephosphorylating the myosin regulatory light chain (Jianhua Feng et al. 1999). Therefore, the relative proportions of MLCK and MLCP can be crucial in determining the phosphorylation state of myosin light chain and the vascular tone.

Certain agonist-mediated smooth muscle contractions can be biphasic, involving an initial rapid increase (Phasic) and subsequent steady sustenance (Tonic) of contractile tone. As shown in Fig 1.2, agonists such as phenylephrine can bind to alpha-1 adrenergic receptor, which is a G protein-coupled receptor (GPCR) present in SMCs, resulting in activation of phospholipase C (PLC) via $G\alpha_q$ protein. This subsequently results in the production of inositol 1,4,5-triphosphate (IP_3) (Daykin et al. 1993) and 1,2-diacylglycerol (DAG) (Berridge 1987; Exton 1985). IP_3 can bind to receptors present in the sarcoplasmic reticulum (SR) facilitating the transient release of $[Ca^{2+}]_i$ that results in the phasic contraction of SMCs (Patel et al. 1999). DAG can further activate protein kinase C (PKC) which phosphorylates C-kinase potentiated protein phosphatase-1 inhibitor (CPI-17) (Eto et al. 1995; Li et al. 1998; Kitazawa et al. 1999). The phosphorylated CPI-17 then inhibits MLCP resulting in enhancement of smooth muscle contraction at a given $[Ca^{2+}]_i$, this phenomenon is also referred as calcium sensitisation and is involved in the tonic contraction of SMCs (Eto et al. 1995; Li et al. 1998; Kitazawa et al. 1999). Other GPCR agonists such as U46619, a thromboxane A_2 (TXA_2) mimetic, can bind to thromboxane A2 receptor (TP) resulting in activation of multiple G proteins such as $G\alpha_{12/13}$ and $G\alpha_q$ (Moers et al. 2004) [for more information regarding other GPCRs that bind to $G\alpha_{12/13}$, see review (Riobo and Manning 2005)]. $G\alpha_{12/13}$ can elicit ras homolog gene family member A (RhoA) mediated activation of rho-associated protein kinase (ROCK) (Swärd et al. 2003; Somlyo and Somlyo 2000). ROCK then inhibits MLCP by phosphorylating the

myosin targeting subunit present in MLCP (J Feng et al. 1999). This also results in calcium sensitisation and tonic contraction of SMCs.

In 1902, a study demonstrated that resistance arteries were able to autoregulate blood flow by either contracting (myogenic tone) during elevation in intravascular pressure or relaxing when the pressure declined (Bayliss 1902). It has been reported that this mechanism of maintaining a constant blood flow with changes in arterial pressure is primarily elicited by vascular SMCs and is known as the myogenic response, as it does not necessarily require the presence of endothelium (Falcone et al. 1991) and nerve innervation (Bayliss 1902). The degree of myogenic response can vary depending upon the vascular bed, however most studies indicate that this response is the strongest in smaller resistance blood vessels such as coronary (Liao and Kuo 1997), mesenteric (Sun et al. 1992) and renal (Edwards 1983) arteries. Mechanistic studies have revealed that an increase in arterial pressure can elevate $[Ca^{2+}]_i$ following opening of voltage-dependent calcium channels through membrane depolarization, subsequently generating the myogenic tone (Davis 2012). Furthermore, angiotensin II receptor type 1, a Gαq GPCR (Hong et al. 2016), has been reported to act as a membrane pressure sensor that depolarizes vascular SMCs resulting in myogenic constriction. There is also evidence of ROCK signalling in myogenic tone via activation of the purinergic GPCRs (Kauffenstein et al. 2016).

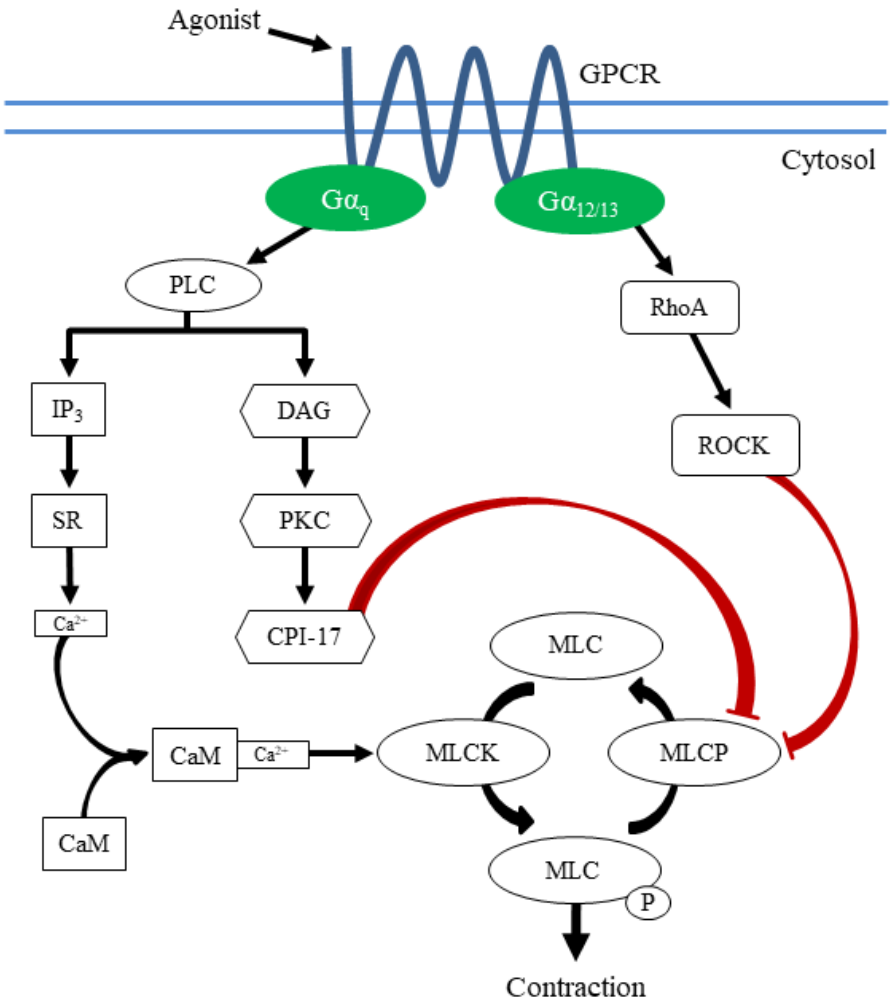

Fig 1.2 Pathways involved in GPCR-induced contraction of smooth muscle cells. Activation of GPCR by an agonist can result in dissociation of G proteins that affect the phosphorylation state of MLC. $G\alpha_q$ can enhance the production of $[Ca^{2+}]_i$ that binds to CaM resulting in subsequent activation of MLCK. The dephosphorylation of MLC by MLCP is inhibited by CPI-17 and ROCK following activation of $G\alpha_q$ and $G\alpha_{12/13}$ respectively. CaM = calmodulin, CPI-17 = C-kinase potentiated protein phosphatase-1 inhibitor, DAG = 1,2-diacyglycerol, GPCR = G protein coupled receptors IP_3 = inositol 1,4,5-triphosphate, MLC = myosin light chain, MLCK = MLC kinase, MLCP = MLC phosphatase, PKC = protein kinase C, PLC = phospholipase C, RhoA = ras homolog gene family, member A, ROCK = rho-associated protein kinase and SR = sarcoplasmic reticulum.

1.2 Pathways involved in vasodilation

1.2.1 NO

The inner endothelium layer (Fig 1.1) of blood vessels has an integral role in the regulation of vasomotor parameters. Various vasodilator pathways have been associated with the endothelium including nitric oxide (NO) signalling. In 1980, Furchgott first discovered that acetylcholine (ACh) mediated relaxation was inhibited in endothelium-denuded rabbit aorta (Furchgott and Zawadzki 1980). Subsequent studies revealed that the mechanism involved activation of soluble guanylate cyclase (sGC) in SMCs (Furchgott et al. 1984) via an endothelium-derived relaxing factor (EDRF) which was later identified as NO (Ignarro et al. 1987). There is also extensive evidence demonstrating that endothelial NO is the predominant vasodilation mechanism in conduit arteries whereas resistance arterial tone is mostly under the influence of NO-independent pathways (Triggle and Ding 2011). The heterogeneity in the vasodilation mechanisms due to anatomical differences between blood vessels will be further discussed throughout section 1.2.

1.2.1.i Mechanisms involved with NO-induced vasodilation

In the endothelium, NO pathway can be activated by various GPCRs such as muscarinic 3 receptors (M_3) (Eglen and Whiting 1990), bradykinin 2 receptors (B_2) (Agostoni and Cugno 2001), neurokinin 1 receptor (Andoh and Kuraishi 2003) and mechanical stimulus such as shear stress [for review see (Busse and Fleming 2003)]. Stimulation of this pathway increases $[Ca^{2+}]_i$ levels, resulting in activation of endothelial NO synthase (eNOS) (Fig 1.3). eNOS is a homodimer and each monomer is composed of N-terminal oxygenase and a C-terminal reductase subunits with a CaM-binding domain in the middle (Wu et al. 2012). Elevation in $[Ca^{2+}]_i$ levels facilitates formation of Ca^{2+}-CaM complex

which binds to eNOS resulting in the conversion of L-arginine into L-citrulline and NO (Marlettaz 1993). NO diffuses into SMCs where it activates sGC converting guanosine triphosphate (GTP) to cyclic guanosine monophosphate (cGMP) which enhances protein kinase G (PKG) activity (Moncada et al. 1991). PKG is a homodimer connected by a leucine zipper and is further subdivided into PKGI and PKGII encoded by two distinct genes, pkrg1 and pkrg2 respectively (Orstavik et al. 1997). PKGI is the isoform expressed in vascular SMCs (Tamura et al. 1996) and is involved in the activation of MLCP resulting in dephosphorylation of MLCK and inhibition of vasoconstriction (Wu et al. 1996; Lee et al. 1997). PKGI has also been reported to induce vasodilation through mechanisms that can reduce the levels of $[Ca^{2+}]_i$. Direct stimulation of Ca^{2+} activated potassium channels (K_{Ca}) by PKGI has been reported in porcine tracheal SMCs (Yamakage et al. 1996) and myometrial cells (Zhou et al. 1998), resulting in hyperpolarization and subsequent inhibition of voltage-gated Ca^{2+} channels. In addition, using patch clamp electrophysiology NO has also been reported to directly activate K_{Ca} channels in SMCs derived from rat mesenteric artery (Mistry and Garland 1998). PKGI has also been reported to inhibit PLC mediated IP_3 production (Hirata et al. 1990; Pfeifer et al. 1995) and IP_3 receptor activity via phosphorylation (Komalavilas and Lincoln 1996; Komalavilas and Lincoln 1994), leading to the reduction of the intracellular Ca^{2+} release. Sarco/endoplasmic reticulum Ca^{2+}-ATPase (SERCA) is a pump involved in transporting cytoplasmic Ca^{2+} into SR (Cornwell et al. 1991). PKGI is involved in the upregulation of calcium sequestration by phosphorylating and therefore suppressing phospholamban, a protein involved in the inhibition of SERCA (Cornwell et al. 1991). As mentioned earlier, studies have indicated that endothelial NO is the predominant vasodilation mechanism in conduit arteries (Shimokawa et al. 1996; Waldron et al. 1999). This could be explained by the higher expression of eNOS that was reported in rat aorta compared to mesenteric

arteries (Shimokawa et al. 1996). Furthermore, it was also demonstrated that ACh-mediated relaxation was completely abolished in aorta derived from eNOS knockout (KO) mice, whereas relaxation of mesenteric arteries from the same animal remained unaffected (Waldron et al. 1999).

1.2.1.ii Role of NO-induced vasodilation in cardiovascular diseases

Although there are other endothelium-dependent vasodilation pathways, vascular studies mostly refer endothelial dysfunction as an impairment of NO mechanism in the endothelium (Zhao et al. 2015). It is well documented that various risk factors for cardiovascular diseases (CVDs) such as aging and hypertension can promote endothelial dysfunction (Hadi et al. 2005; Sitia et al. 2010). Studies also indicate that diet can affect endothelial function by modifying the NO signalling pathway. For example; in a porcine study, high-fat diet was reported to impair cGMP production due to enhanced eNOS uncoupling resulting in the formation of inactive eNOS monomers, although protein expression of eNOS was unaffected by the diet (Musicki et al. 2008). In contrast, hyperglycaemia has been indicated to promote NO production in rats and humans (Adela et al. 2015). Dose-dependent elevation of both eNOS expression and NO levels were reported in human umbilical vein endothelial cells following treatment with glucose (Adela et al. 2015). Furthermore, plasma level of NO was also enhanced in both hyperglycaemic rats and patients with type 2 diabetes compared to the normal control groups (Adela et al. 2015). There is also evidence indicating that high-salt diet can elevate eNOS expression in thick ascending limb derived from rats, however, it did not result in the subsequent increase of NO production (Ortiz et al. 2003).

Endothelial dysfunction can develop in both conduit and resistance arteries (Blackwell et al. 2004; Csiszar et al. 2007; Lesniewski et al. 2009). Although smaller resistance arteries

are predominantly involved in the regulation of peripheral resistance and mean blood pressure; the larger conduit arteries, especially aorta, also have an important role in providing the dampening effect against the pulsatile ventricular pressure (Marchais et al. 1993). Furthermore, aortic stiffening can significantly attenuate vascular compliance resulting in the subsequent increase of systolic central blood pressure and cardiac afterload (Chen et al. 2017); ultimately promoting ventricular hypertrophy (Yucel et al. 2015) and impairment of smaller peripheral arteries (Van Sloten et al. 2015). In comparison to elevated peripheral resistance, studies indicate that aortic stiffening has a greater role in the development of isolated systolic hypertension (Wallace et al. 2007; McEniery et al. 2009). The impairment of NO pathway has been associated with the elevation of central pressure, resulting in the subsequent enhancement of arterial stiffness in conduit arteries including aorta (Wilkinson et al. 2002; Wilkinson et al. 2004). This is consistent with studies indicating that the improvement of NO production can reduce arterial stiffness in aorta, resulting in the subsequent attenuation of central blood pressure (McEniery et al. 2004; Dhakam et al. 2006; Kampus et al. 2011). Arotinolol, a nonselective α/β-blocker, was also reported to induce eNOS phosphorylation and NO-dependent vasodilation in aorta, resulting in the subsequent reduction of central blood pressure and aortic stiffness (Zhou et al. 2014). Although the peripheral resistance is predominantly regulated by resistance arteries, findings from these studies clearly demonstrate that vasodilation of conduit arteries via NO pathway can also elicit therapeutic effects. Therefore, to enable a complete understanding of the beneficial effects of vasodilators, it is crucial to investigate their mechanisms using both conduit and resistance arteries (Pocock et al. 2013).

The absence of NO signalling in mice has been reported to facilitate the development of CVDs such as hypertension and atherosclerosis (Huang et al. 1995; Kuhlencordt et al.

2001). Similarly, human studies have also reported an impairment of NO pathway in hypertension. A study demonstrated that L-N^G-monomethyl arginine citrate (L-NMMA), an eNOS inhibitor, mediated attenuation of forearm blood flow was not as profound in hypertensive patients compared to the control (Panza et al. 1990). There is also evidence indicating reduction in NO bioavailability due to increased oxidative stress in arterial hypertension (Hermann et al. 2006). Oxidative stress is characterized by an increased production of reactive oxygen species (ROS) and an impairment in the antioxidant defence systems (Rodrigo et al. 2011). Nicotinamide adenine dinucleotide phosphate (NADPH) oxidase is the main enzyme involved in the production of superoxide in blood vessels (Rodrigo et al. 2011). An increase in NADPH oxidase expression and subsequent enhancement in superoxide production has been associated with hypertension by numerous studies, using various hypertensive animal models such as angiotensin II-induced hypertensive rats (Fukui et al. 1997; Mollnau et al. 2002), deoxycorticosterone acetate-salt hypertensive rat (Beswick et al. 2001) and SHR (Zalba et al. 2000; Wassmann et al. 2001; Hamilton et al. 2002; Wassmann et al. 2002). NADPH oxidase-derived superoxide can react with NO to form peroxynitirte, which oxidizes and uncouples eNOS, resulting in an additional increase in ROS and attenuation in NO production (Laursen et al. 2001; Kuzkaya et al. 2003). As a result, these mechanisms can further elevate oxidative stress in the vasculature and impair NO-induced vasodilation, subsequently contributing to the development of hypertension [for an in-depth review regarding the role of oxidative stress in hypertension see (Rodrigo et al. 2011)]. Oxidative stress has also been reported to promote vascular inflammation through activation of pro-inflammatory transcription factors such as nuclear factor kappa-light-chain-enhancer of activated B cells (NF-κB) and activator protein 1 (AP1) (Sen and Packer 1996; Imhoff and Hansen 2009). This in turn results in the subsequent production of inflammatory

cytokines such as interleukin-17 (IL-17) and tumour necrosis factor-alpha (TNF-α), facilitating further activation of adhesion molecules that promote leukocyte adhesion in the vasculature (Libby et al. 2002; Park et al. 2014). These mechanisms can contribute to the formation of atherosclerotic lesions and ultimately, lead to thrombotic events associated with atherosclerosis.

There is also evidence indicating that T cells are involved in hypertension; for example, a study demonstrated that loss of mature T cells in recombination activating gene 1 (RAG-1) KO mice led to attenuation in angiotensin II-induced; elevation of blood pressure, superoxide production and inhibition of endothelium-dependent vascular relaxation (Guzik et al. 2007). Furthermore, this inhibition of angiotensin II mediated effects was completely reversed following adoptive transfer of T cells into RAG-1 KO mice (Guzik et al. 2007). It was also indicated that angiotensin II facilitated the activation of effector T cells and chemokines, therefore suggesting the role of T cell-dependent inflammation in hypertension (Guzik et al. 2007). Furthermore, pro-inflammatory cytokines such as IL-17 and TNF-α produced by T cells are involved in hypertension. An elevated production of IL-17 was observed in mice following administration of angiotensin II (Madhur et al. 2010). Although an initial increase in blood pressure was observed with angiotensin II, IL-17 KO mice failed to maintain this hypertensive state in contrast to wild type mice (Madhur et al. 2010). Additionally, marked reduction in angiotensin II-induced T cell infiltration and superoxide production was also observed in IL-17 KO mice (Madhur et al. 2010). Higher plasma levels of IL-17 were reported in diabetic patients with hypertension compared to the normotensive diabetic control group (Madhur et al. 2010). There is also evidence indicating that TNF-α can activate NADPH and enhance ROS production (De Keulenaer et al. 1998). Etanercept, a TNF-α antagonist, was found to inhibit angiotensin II-induced hypertension and superoxide production in

mice (Guzik et al. 2007). Furthermore, etanercept prevented hypertension in fructose-fed rats (Tran et al. 2009) and lowered blood pressure in a mouse model of systemic lupus erythematosus (Venegas-Pont et al. 2010). Thus, hypertension is a complex disorder that not only involves endothelial dysfunction characterized by the impairment of vasodilation pathways such as NO signalling, but also involves mechanisms that promote oxidative stress and inflammation.

An increase in the plasma levels of asymmetric dimethylarginine (ADMA), an endogenous eNOS inhibitor, is also associated with endothelial dysfunction, hypercholesterolemia and atherosclerosis (Böger et al. 1998; Ignarro and Napoli 2005). It is not surprising that the impairment of NO signalling would have such detrimental effects since in addition to having a role in blood pressure regulation; NO is also involved in inhibiting adhesion of leukocytes, platelet aggregation and proliferation of SMCs in the vasculature, all of which attenuate the development of atherosclerotic plaques (Kuhlencordt et al. 2001). Therefore, treatment drugs that are involved in the modulation of NO pathway are still being used against CVDs. According to the national institute for health and care excellence (NICE) guidelines, glyceryl trinitrate (NO donor) is used generally for the treatment of angina whereas sodium nitroprusside (another NO donor) is used for hypertension related emergencies, heart failure and during surgery with anaesthesia for controlled hypotension (NICE 2019f). Phosphodiesterase-5 are enzymes involved in the breakdown of cGMP (Corbin and Francis 1999). Currently, inhibitors of these enzymes such as tadalafil and sildenafil are used for the treatment of pulmonary arterial hypertension (NICE 2019a).

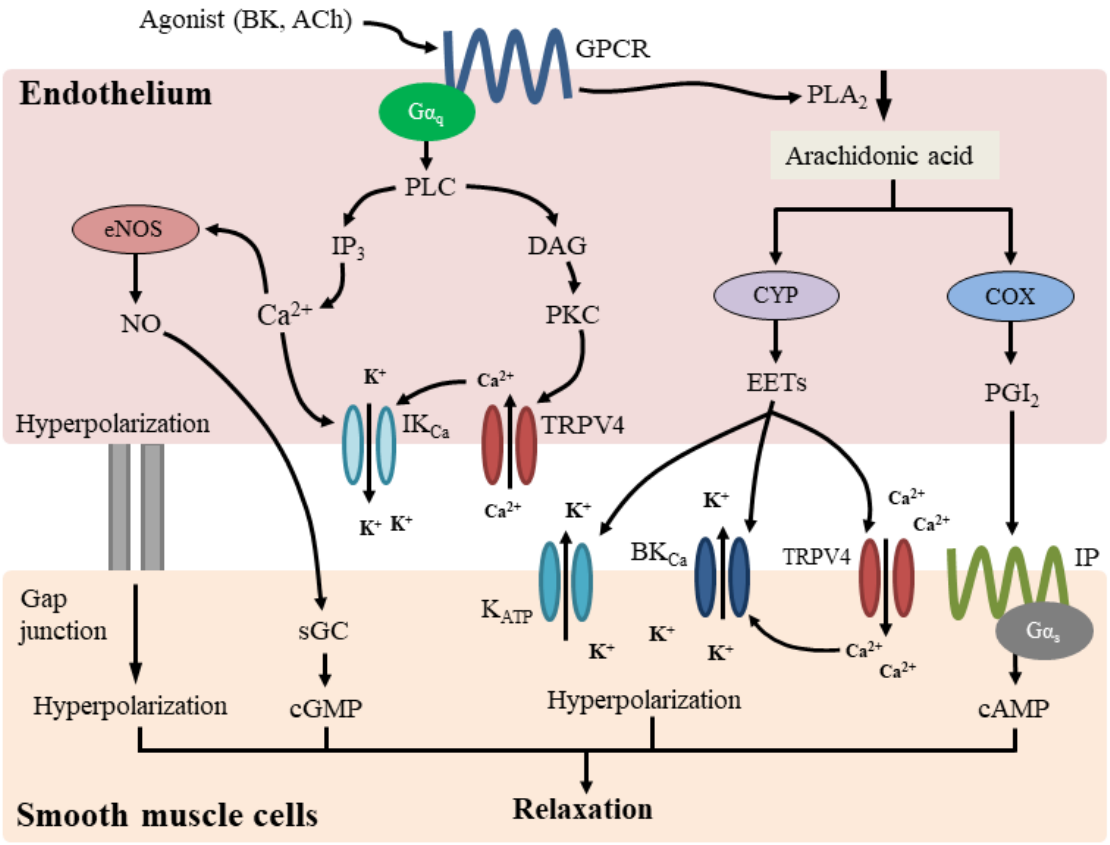

Fig 1.3 Pathways involved in vasodilation. Various agonists such as ACh can activate M_3 receptors present in the endothelium, that subsequently triggers the complex signalling cascade resulting in the relaxation of vascular smooth muscle cells. ACh = acetylcholine, BK = bradykinin, BK_{Ca} = large conductance calcium activated potassium channels, cAMP = cyclic adenosine monophosphate, cGMP = cyclic guanosine monophosphate, COX = cycloxygenase, CYP = cytochrome P450 epoxygenase, DAG = 1,2-diacyglycerol, EETs = epoxyeicosatrienoic acids, eNOS = endothelial nitric oxide synthase, GPCR = G protein coupled receptors, IK_{Ca} = intermediate conductance calcium activated potassium channels, IP = prostaglandin I2 receptor, IP_3 = inositol 1,4,5-triphosphate, K_{ATP} = adenosine triphosphate-sensitive potassium channel, NO = nitric oxide, PGI_2 = prostaglandin I_2, PKC = protein kinase C, PLA_2 = phospholipase A_2, PLC = phospholipase C, sGC = soluble guanylate cyclase and TRPV4 = transient receptor potential cation channel subfamily vanilloid member 4.

1.2.2 Metabolites of AA in relaxation

1.2.2.i COX-derived metabolites of AA

a) Structure and function of COX

Arachidonic acid is an omega-6 (n-6) polyunsaturated fatty acid (PUFA) involved in the regulation of various physiological processes including vasodilation. There is evidence indicating that activation of GPCRs such as M_3 receptors, can enhance the release of AA following activation of phospholipase A_2 (PLA_2) (Fig 1.3) (Wang et al. 2004). Depending upon the enzymes, metabolites of AA also known as eicosanoids which are derived from the oxidation of AA are further subdivided into series-2 prostaglandins (PGs), leukotrienes (LTs), hydroxyeicosatetraenoic acids (HETEs) and epoxyeicosatrienoic acids (EETs). Cycloxygenase (COX) is a homodimeric enzyme and each monomer is composed of a membrane binding domain, an epidermal growth factor (EGF) domain and a catalytic domain containing the COX and peroxidase active sites (Smith et al. 2000) (Fig 1.4). There are two isoforms of COX; COX-1 (71 kDa) and COX-2 (73 kDa), which are both involved in the initial metabolism of AA into PGG_2, which occurs in the COX active site. Subsequently, PGG_2 is converted into PGH_2 in the peroxidase active site (Smith et al. 2000). COX-1 is constitutively expressed in various tissues and is coupled with synthases that are involved in the production of TXA_2, PGF_2 and PGD_2 (Naraba et al. 1998). COX-2 lacks constitutive expression and as a result require inflammatory stimuli such as bacterial endotoxin and cytokines to induce its expression. Synthases that couple with COX-2 catalyse the production of PGI_2 and PGE_2 (Hata and Breyer 2004). These COX-derived eicosanoids have an important role in the

body as they are involved in the regulation of various physiological processes such as inflammation, nociception, renal function and cardiovascular homeostasis (Smyth et al. 2009).

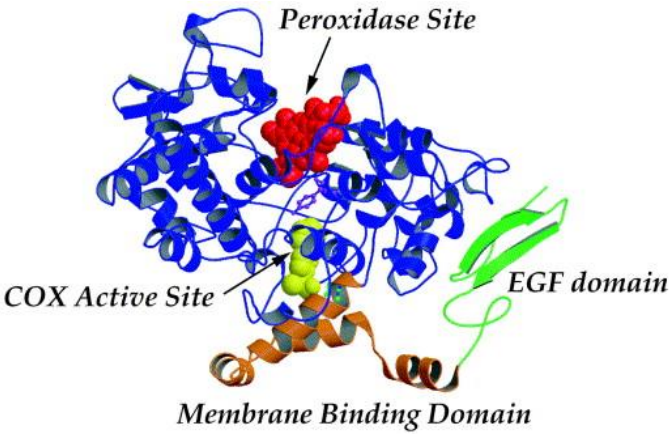

Fig 1.4 3D schematic representation of the COX monomer. Each monomer is composed of three domains; EGF, membrane binding and catalytic domain which involves the COX and peroxidase active site. The EGF-domain forms the N-terminus. The COX active site is involved in conversion of AA to PGG_2 and the peroxidase site subsequently converts PGG_2 to PGH_2. COX = cycloxygenase and EGF = epidermal growth factor. Image obtained from (Garavito and DeWitt 1999).

b) Mechanisms involved with COX-induced vasodilation

PGI_2 initially known as "prostaglandin X", was first discovered by John Vane along with Salvador Moncada during 1970s and this discovery was crucial in understanding the pharmacology of aspirin (Bunting et al. 1976; Dusting et al. 1977). PGI_2 is converted from AA mainly via the action of COX-2 (Ricciotti et al. 2013) (Fig 1.3). It can elicit vasodilation by binding to prostaglandin I2 receptor (IP) which is a GPCR ($G\alpha_s$) and promotes adenylate cyclase (AC)-mediated production of cyclic adenosine

monophosphate (cAMP), subsequently enhancing intracellular protein kinase A (PKA) activity (Majed and Khalil 2012). Depending upon the type of vascular cells, PKA can induce vasodilation through different mechanisms. For example, in ECs derived from human and bovine aorta, PKA has been shown to elevate expression of eNOS resulting in enhanced NO production following administration of PGI_2 analog, beraprost (Niwano et al. 2003). Depending upon the type of tissue, PGI_2-activated PKA has been reported to elicit vasodilation through different mechanisms which include; (i). Enhanced calcium sequestration via SERCA, (ii). Inhibition of TP receptor activity in human aortic SMCs (Wikström et al. 2008), (iii). Activation of potassium channels such as K_{Ca} in rat cerebral artery (Dong et al. 1998) along with rat pulmonary artery (Dumas et al. 1997), adenosine triphosphate-sensitive potassium channels (K_{ATP}) in rat pulmonary artery (Dumas et al. 1997) and voltage-gated potassium channels (K_v) in rat cerebral artery (Dong et al. 1998) and (iv). Phosphorylation and subsequent inhibition of MLCK (Horman et al. 2008).

c) *Role of PGI_2-induced vasodilation in cardiovascular diseases*

PGI_2 is primarily involved in vasodilation and inhibits platelet activation whereas TXA_2 (COX-1 derived) is a vasoconstrictor and has prothrombotic effects. Due to the opposite effects of these prostanoids in the vasculature, the balance between these metabolites is important in the maintenance of cardiovascular health. In IP receptor/ApoE (Apolipoprotein E) KO mice (animal model for studying atherogenesis), elevated atheroma formation and platelet activation were reported (Kobayashi et al. 2004). However, these effects were reversed in TP receptor/ApoE KO mice (Kobayashi et al. 2004).

Using ovariectomized female mice, another study demonstrated that estrogen-derived PGI_2 was involved in the inhibition of atherogenesis (Egan et al. 2004). R212C polymorphism of the IP receptor that results in impairment of receptor signalling was also reported to enhance atherothrombosis and disease severity in cardiovascular patients (Arehart et al. 2008). The pathophysiological mechanisms involved in pulmonary hypertension (PH) are associated with an increase in TXA_2 production, thrombosis, vasoconstriction and vascular remodelling (Mitchell et al. 2014). As a result, various studies have indicated a protective role of PGI_2 in PH (Mitchell et al. 2014) and PGI_2 analogues such as iloprost and epoprostenol are currently used in the clinical setting. Iloprost is used for the treatment of idiopathic PH (NICE 2019c) and epoprostenol is used for primary PH resistant to other treatments (NICE 2019b).

1.2.2.ii CYP-derived metabolites of AA

a) Structure and function of CYP

Cytochrome P450 (CYP) are haemoproteins made up of 400-500 amino acid residues with an iron-containing cofactor present in the active site (Manikandan and Nagini 2018). CYP is encoded by more than 17,000 genes throughout the biological kingdoms and currently about 57 CYP genes have been identified in humans (Pikuleva and Waterman 2013). Although there are 18 families of human CYP, predominant expression occurs within three families; CYP2, CYP3 and CYP4 (Nebert et al. 2013). AA can be converted into epoxyeicosatrienoic acids (EETs) and hydroxyeicosatetraenoic acids (HETEs) by CYP epoxygenase and omega-hydroxylase respectively (Panigrahy et al. 2010). In SMCs, CYP omega-hydroxylase from the 4A and 4F families are generally involved in inserting a hydroxyl group into the AA molecule, resulting in the formation of 20-HETE (Fig 1.5) (Roman 2002). CYP epoxygenases are predominantly expressed in vascular ECs and belong to 2C along with 2J family (Fig 1.5) (Node et al. 1999; Zeldin 2001). These epoxygenases are found in the endoplasmic reticulum and they metabolize AA by adding an epoxide group to one of the double bonds, resulting in the production of four regioisomers, which include; 5,6-EET, 8,9-EET, 11,12-EET and 14,15-EET (Zeldin 2001). CYP2C is mainly involved in the production of EETs in ECs. 11,12-EET and 14,15-EET are the main metabolites produced, accounting for up to 70-80% of the total EETs. In the presence of soluble epoxide hydrolase (sEH), EETs can be converted into less active metabolites known as dihydroxyeicosatrienoic acids (DHETs) (Yu et al. 2000).

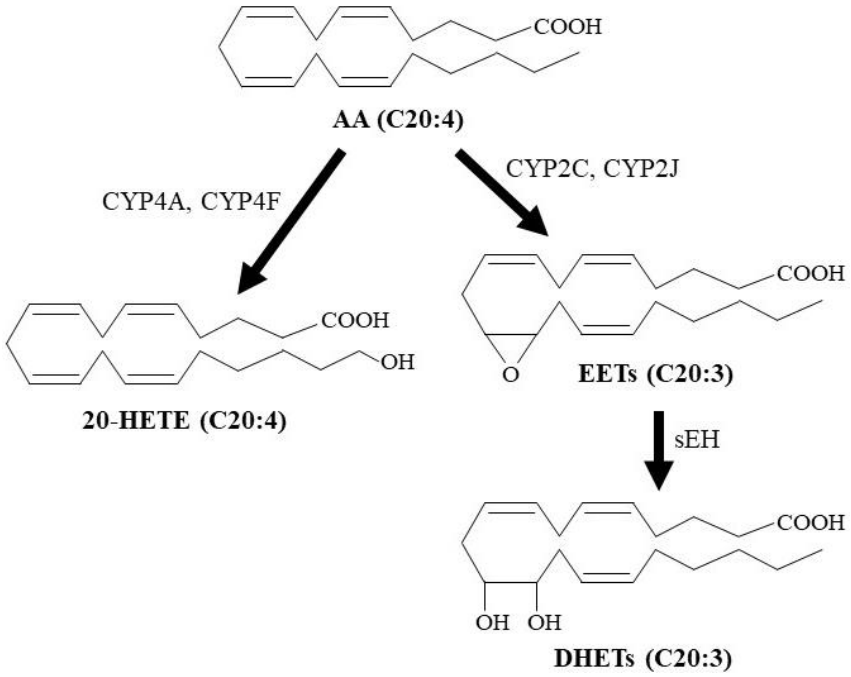

Fig 1.5 Metabolism of AA by CYP epoxygenase and omega-hydroxylase. AA is converted into 20-HETE by CYP4A and CYP4F omega-hydroxylase. CYP2C and CYP2J epoxygenase are involved in metabolism of AA into EETs which is further metabolised by sEH into DHETs. AA = arachidonic acid, CYP = cytochrome P450, DHETs = dihydroxyeicosatrienoic acids, EETs = epoxyeicosatrienoic acids HETE = hydroxyeicosatetraenoic acid and sEH = soluble epoxide hydrolase.

b) Mechanisms involved with CYP mediated vasodilation

20-HETE is a CYP omega-hydroxylase metabolite found in resistance arteries such as cerebral (Harder et al. 1994), mesenteric (Zhang et al. 2001) and renal arteries (Marji et al. 2002; Roman 2002). The biosynthesis of this metabolite is predominantly observed in SMCs whereas its endothelial production has only been reported in pulmonary arteries (Zhu et al. 2002). 20-HETE is involved in eliciting vasoconstriction through activation of kinases such as mitogen-activated protein kinase (MAPK) (Muthalif et al. 1998), PKC (Lange et al. 1997; Sun et al. 1999) and src-type tyrosine kinase

(Sun et al. 1999); subsequently leading to inhibition of K_{Ca} channels and augmentation of depolarization through opening of L-type calcium channels (Gebremedhin et al. 1998). 20-HETE can also induce vasoconstriction through activation of ROCK resulting in MLCP inhibition and calcium sensitisation (Randriamboavonjy et al. 2003). In contrast to 20-HETE, the four regioisomeric EETs are involved in relaxation of the blood vessels and were first identified as an endothelium-derived hyperpolarization factor (EDHF) in 1996 by Campbell *et al* (Campbell et al. 1996). Their findings indicated that EETs-mediated relaxation of bovine coronary arteries involved K_{Ca} opening. 11,12-EET and 14,15-EET are the most abundant regioisomers in ECs. The general mechanism of EETs-induced vasodilation involves an initial release of these eicosanoids from ECs, followed by subsequent binding to potassium channels present in the SMCs, resulting in hyperpolarization of the arteries. Majority of the literature reports that EETs are involved in activation of large conductance K_{Ca} (BK_{Ca}) in various vascular beds including bovine coronary arteries (Li et al. 2002; Campbell et al. 2006), human mammary arteries (Archer et al. 2003) and rat mesenteric artery (Dimitropoulou et al. 2007) (Fig 1.3). However, some studies also indicate that EETs can activate adenosine triphosphate-sensitive potassium channels (K_{ATP}) resulting in relaxation of rat mesenteric arteries (Ye et al. 2005; Ye et al. 2006). Furthermore, in depth mechanistic investigation revealed that EETs can stimulate $G\alpha_s$-dependent activation of PKA which can subsequently activate both K_{Ca} and K_{ATP} (Imig et al. 1999; Ye et al. 2005; Ye et al. 2006; Dimitropoulou et al. 2007). EETs have also been reported to indirectly facilitate BK_{Ca} opening via initial activation of transient receptor

potential cation channel subfamily vanilloid member 4 (TRPV4) (Ma et al. 2015; Vriens et al. 2005; Watanabe et al. 2003).

c) Role of EET-induced vasodilation in cardiovascular diseases

The protective effects of EETs in the cardiovascular system have been demonstrated by various studies. For example, attenuation in EET production due to decreased CYP2C expression (Imig and Hammock 2009) and increased activity of sEH enzyme (Zhao et al. 2003; Zhao et al. 2004) has been associated with hypertension. Although CYP2C44 KO mice initially remained normotensive with normal levels of dietary salt, these mice developed hypertension after 4-5 weeks of high salt diet whereas only a small increase in systolic blood pressure was observed with the wild type control mice (Capdevila et al. 2014). In spontaneously hypertensive (Yu et al. 2000) and angiotensin II-induced (Imig et al. 2002) hypertensive rats, increased expression of sEH was reported. Furthermore, sEH inhibitors have also been reported to inhibit inflammation and atherosclerosis of the vasculature [reviewed in (Imig and Hammock 2009; Imig 2012)]. Recently, two phase I clinical trials investigated the effects of a novel sEH inhibitor, GSK2256294, in overweight smokers (Yang et al. 2017; Lazaar et al. 2016). Results from these studies demonstrated that the inhibitor was well-tolerated and the suppression of sEH was effectively maintained for 24 h (Lazaar et al. 2016). Furthermore, administration of this inhibitor was also reported to potentiate bradykinin mediated vasodilation (Yang et al. 2017). Thus, the protective effects of EETs are currently under investigation for their therapeutic benefits against CVDs (Imig 2016).

1.2.3 EDH

It was during the late 1970s that Hirosi Kuriyama *et al* first reported ACh-induced hyperpolarization of SMCs in rabbit mesenteric artery (Kuriyama and Suzuki 1978) and guinea pig coronary artery (Kitamura and Kuriyama 1979); but surprisingly, vasoconstriction was also observed. A later study led by Bolton *et al*, also demonstrated a similar effect involving hyperpolarization and constriction of SMCs by carbachol (an ACh mimetic) in guinea pig mesenteric artery (Bolton et al. 1984). It was this study that first identified the role of endothelium in this hyperpolarization response and therefore, the authors concluded by indicating that a diffusible factor released from ECs was possibly involved (Bolton et al. 1984). Similar to the earlier study, Bolton *et al* also reported the dual constrictive and hyperpolarization effects of these agonists. It was indicated that this effect was observed due to the expression of M_3 receptors in both SMCs and ECs of these arteries, highlighting variability in vascular expression of these receptors between different species (Bolton et al. 1984). "EDRF" which involved the NO pathway was also discovered by Furchgott *et al* (Furchgott and Zawadzki 1980) during that time and as a result, it was speculated that EDRF was potentially involved in the hyperpolarization response. These speculations were later addressed by a Chen *et al* study demonstrating that the ACh-induced hyperpolarization of endothelium-intact rat aorta and pulmonary artery was independent of NO and COX pathway (Chen et al. 1988). The hyperpolarization was associated with an increase in the efflux of $^{86}Rb^{+}$ efflux (a marker for K^{+}), indicating the role of potassium channels (Chen et al. 1988). This endothelial factor was identified to be distinct from the EDRF and therefore was named as the "endothelium derived hyperpolarization factor" (EDHF) (Taylor and Weston 1988). It was only after another 6 years that Waldron and Garland demonstrated that this EDHF response was completely inhibited through the combined application of both apamin, a

small conductance K_{Ca} (SK_{Ca}) blocker and charybdotoxin which was considered to be a selective BK_{Ca} blocker at that time (Edwards et al. 2010). Zymunt and Högestätt then reported that combination of apamin and iberotoxin (a more selective inhibitor of BK_{Ca} compared to charybdotoxin) could not abolish the EDHF response in rat hepatic artery (Zygmunt and Högestätt 1996). It was later recognized that this discrepancy was due to the additional inhibition of intermediate conductance K_{Ca} channel (IK_{Ca}) by charybdotoxin (Vázquez et al. 1990; Garcia et al. 1995). As it was originally speculated that an EDHF released from the endothelium was involved in subsequent activation of SK_{Ca} and IK_{Ca}, these channels were considered to be possibly expressed in SMCs. However, SK_{Ca} and IK_{Ca} were only detected in the endothelium (Edwards et al. 1998). Therefore, this hyperpolarization response is generated from the endothelium itself and it does not always involve a diffusible factor. Due to these findings, this pathway is currently more accurately referred as the "endothelium-dependent hyperpolarization" (EDH) response [extensively reviewed by (Feletou and Vanhoutte 2006; Edwards et al. 2010)]. As described earlier the EDH response is mainly regulated by SK_{Ca} and IK_{Ca}, however other potassium channels present in the SMCs such as K_{ATP}, potassium voltage-gated channel subfamily Q member (K_v7) and especially BK_{Ca} can also be subsequently activated following the release of endothelial factors, resulting in hyperpolarization and vasodilation. These channels will be further discussed in the later sections.

1.2.3.i SK_{Ca} and IK_{Ca}

a) Structure and distribution of SK_{Ca} and IK_{Ca}

SK_{Ca} and IK_{Ca} are tetramers composed of four α-subunits and each subunit contains six transmembrane segments (S1-S6) with a pore forming loop between S5 and S6 (Fig 1.6) (Guéguinou et al. 2014). There are three

subtypes of SK_{Ca}; SK1 ($K_{Ca}2.1$), SK2 ($K_{Ca}2.2$) and SK3 ($K_{Ca}2.3$) (Guéguinou et al. 2014). Due to similarities in the structure and function, IK_{Ca} is also referred as SK4, however it has a higher conductance (20-90 pS) in comparison to SK_{Ca} (5-20 pS) (Clements et al. 2015). Both SK_{Ca} and IK_{Ca} have calmodulin constitutively bound to intracellular carboxyl terminus of each subunit allowing binding of $[Ca^{2+}]_i$ (Xia et al. 1998; Fanger et al. 1999). These channels do not have a voltage-sensing region and therefore their activities are insensitive to changes in membrane potentials.

SK_{Ca}, particularly SK3 (Marchenko and Sage 1996), and IK_{Ca} are expressed in vascular ECs (Félétou 2009) but not in SMCs, although IK_{Ca} expression has been reported in proliferating SMCs in culture and also following an injury (Neylon et al. 1999; Kohler et al. 2003; Tharp et al. 2006). There is evidence indicating that the differential expression of K_{Ca} channels can partly elicit heterogeneity in the functional phenotype of vascular SMCs; for example, BK_{Ca} channels are predominantly expressed in contractile SMCs whereas an increased expression of IK_{Ca} channels is associated with proliferative SMCs (Neylon et al. 1999; Kohler et al. 2003; Tharp et al. 2006). SK_{Ca} are generally found in homocellular endothelial gap junctions and in caveolar microdomains with other receptors such as IP_3 and cationic channels including TRPV4 (Fig 1.8) (Félétou 2009; Sonkusare et al. 2012). IK_{Ca} are mostly expressed in endothelial projections that are in direct contact with the membranes of SMCs via myo-endothelial gap junctions (MEGJ) (Félétou 2009). Similar to SK_{Ca}, studies also report TRPV4 and IP_3 receptor-dependent activation of IK_{Ca} (Fig 8) (Sonkusare et al. 2012). There is extensive evidence indicating the predominance of EDH vasodilation

mechanism in resistance arteries compared to conduit arteries. An increase in the expression of both K_{Ca} channels (Hilgers et al. 2006) and MEGJ with decreasing arterial size has been reported in rats (Sandow and Hill 2000). Furthermore, the thicker internal elastic lamina of conduit arteries, compared to resistance arteries, has been suggested to provide a greater barrier against electrotonic signalling, resulting in inhibition of EDH dispersal (Triggle and Ding 2011). It has also been indicated that microdomains found in endothelial projections that consists of IK_{Ca}, IP_3 receptors, calcium-sensing receptors and MEGJ are predominantly involved in the regulation of resistance arterial tone [for review see (Triggle and Ding 2011)].

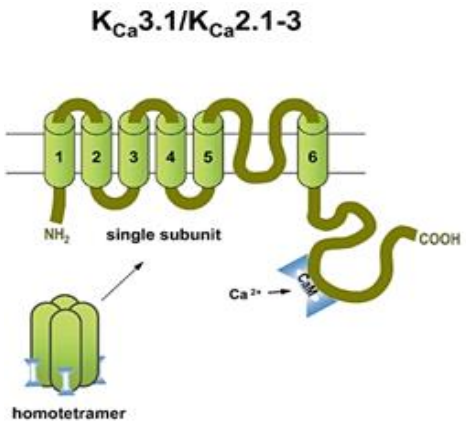

Fig 1.6 Structure of the endothelial K_{Ca} channels. (A) SK_{Ca} ($K_{Ca}2.3$) and IK_{Ca} ($K_{Ca}3.1$) are composed of six transmembrane segments (S1-6) with calmodulin attached to carboxyl terminus that confers calcium sensitivity. CaM = calmodulin, K_{Ca} = calcium activated potassium channel, $K_{Ca}2.1\text{-}3$ = small conductance K_{Ca} and $K_{Ca}3.1$ = intermediate conductance K_{Ca}. Image obtained from (Grgic et al. 2009).

b) Mechanisms involved with SK_{Ca}- and IK_{Ca}-induced vasodilation

ACh and shear stress (involving TRPV4 channels) can activate endothelial K_{Ca} channels by increasing $[Ca^{2+}]_i$ levels resulting in the efflux of K^+ and hyperpolarization of the ECs (Fig 1.3) (Félétou 2009). The hyperpolarization can further facilitate the influx of Ca^{2+} into ECs through non voltage-gated calcium channels such as TRP channels [for review see (Guéguinou et al. 2014)], resulting in the activation of calcium-sensitive enzymes such as eNOS and PLA_2 (Clark et al. 1991). This can subsequently enhance the production of vasodilators such as NO, PGI_2 and EETs. Furthermore, electric transmission of EDH from ECs to SMCs via myoendothelial gap junctions has also been reported, especially in resistance arteries, leading to the subsequent hyperpolarization of SMCs (Feletou and Vanhoutte 2006). The main gap junction connexin (Cx) proteins that are expressed in the vasculature are Cx37, Cx40 and Cx43 (Lang et al. 2007). Evidence of their involvement in the EDH response has mostly been found in *in vitro* experiments using human subcutaneous resistance arteries (Lang et al. 2007), rat cerebral and mesenteric arteries (Matchkov et al. 2006; Haddock et al. 2006). On the contrary, results from most *in vivo* experiments have failed to indicate the role of myoendothelial gap junctions in the EDH response [reviewed by (de Wit et al. 2008)]. This discrepancy may be partly explained by differences in the type of arteries that were studied, since *in vitro* experiments involved mesenteric artery whereas skeletal muscle arterioles were mostly used *in vivo* experiments (de Wit et al. 2008). Furthermore, multiple *in vivo* physiological factors such as mechanical stress, sympathetic innervation and signalling molecules present in the

blood, may also influence these gap junctions. The opening of endothelial K_{Ca} can also result in a modest increase of K^+ ions (1-15 mmol/L) in the intercellular space between ECs and SMCs (Haddy et al. 2006). This elevation of K^+ ions can activate potassium voltage-gated channel subfamily J member 2 ($K_{ir}2.1$) (Bradley et al. 1999) and sodium-potassium adenosine triphosphatase (Na^+/K^+-ATPase) (Prior et al. 1998), resulting in hyperpolarization of the neighbouring SMCs. However, these mechanisms are not ubiquitous to all arteries (Feletou and Vanhoutte 2006) and there is heterogeneity in the pathways involved depending upon the type of species and the vascular bed under investigation.

c) Role of SK_{Ca}- and IK_{Ca}-induced vasodilation in cardiovascular diseases

In transgenic mice using Tet-off inducible expression system, SK_{Ca} was reported to be involved with the hyperpolarization of SMCs and inhibition of SK_{Ca} expression through dietary doxycycline led to an increase in blood pressure (Taylor et al. 2003). In addition, it was also demonstrated that this effect on blood pressure was subsequently reversed following exclusion of doxycycline, further suggesting the role of SK_{Ca} in pressure regulation (Taylor et al. 2003). Loss of IK_{Ca} expression in mice also led to impairment in ACh-induced dilation of carotid artery and subsequent elevation of blood pressure (Si 2006). Numerous *in vitro* and *in vivo* studies involving the eNOS KO mice have demonstrated the compensatory role of EDH in different vascular beds such as femoral artery (Waldron et al. 1999), mesenteric artery (Waldron et al. 1999; Ding et al. 2000; Chen et al. 2012) and skeletal arterioles (Huang et al. 2000; Huang et al. 2001). In female eNOS/COX KO mice, the EDH-like response was found to act as a compensatory

vasodilation mechanism that prevented these animals from being hypertensive (Scotland et al. 2005). This was also reported in coronary arteries from rats with congestive heart failure (Ueda et al. 2005). Similarly, the compensatory role of EDH following hypercholesterolemia-induced inhibition of the NO pathway, has also been demonstrated in porcine brachial artery (Woodman et al. 2005), rabbit renal artery (Brandes et al. 1997; Taniguchi et al. 2005), renal arteries from SHR (Kagota et al. 1999), mesenteric artery from ApoE-deficient mice (Ding et al. 2009) and gracilis artery from dislipidaemic mice (Krummen et al. 2005). On the contrary, significant attenuation of EDH response was associated with severe hypercholesterolemia and aging in human gastroepiploic arteries (Urakami-Harasawa et al. 1997). This indicates that the severity of physiological disorders may influence the compensatory role of the EDH pathway. Currently, there are no treatments that primarily focus in opening the endothelial K_{Ca} channels. This may be due to their role in other physiological processes that could introduce unwanted adverse effects; for example, IK_{Ca} is involved in the proliferation of ECs (Grgic et al. 2005), SMCs (Neylon et al. 1999), pancreatic cancer cell (Jager et al. 2004) and endometrial cancer cells (Wang et al. 2007). In addition, SK_{Ca} are also involved in neuronal excitability (Blank et al. 2004) and therefore, sustained activation of these channels in the body can have multiple effects which is yet to be investigated. These findings suggest that these channels might not be an ideal therapeutic target against CVDs. However, there is some evidence of an improvement in the EDH response with current treatment drugs such as losartan (angiotensin receptor antagonist) (Feletou and Vanhoutte 2004), cizalaprilat

(angiotensin-converting enzyme blocker) (Feletou and Vanhoutte 2004) and cilostazol (phosphodiesterase inhibitor) (Matsumoto et al. 2005), although these drugs primarily act via other vasodilation pathways.

1.2.3.ii BK_{Ca}

a) Structure and distribution of BK_{Ca}

Endothelial factors such as EETs (Dimitropoulou et al. 2007) and NO (Félétou 2009) have been reported to activate BK_{Ca} resulting in hyperpolarization of the SMCs. BK_{Ca} ($K_{Ca}1.1$) is composed of four α- (Slo1 α) and four accessory β-subunits with a conductance of ~100-300 pS (Fig 1.7) (Lee and Cui 2010). The α subunit is encoded by a single gene (*KCNMA1*) and is made up of seven transmembrane segments (S0-S6) (Lee and Cui 2010). The S4 segment is composed of positively charged residues involved with voltage sensitivity and the S5-S6 segments form the channel pore with the selectivity filter for potassium ions (Lee and Cui 2010). The intracellular carboxyl-terminus of the α subunit contains a regulator of conductance for K^+ (RCK) domain and Ca^{2+} bowl regions which confer sensitivity to Ca^{2+} (Lee and Cui 2010). The β-subunit (β1-4) is encoded by four genes (KCNMB1-4) and is made up of two transmembrane segments with intracellular amino- and carboxyl-terminals (Lee and Cui 2010). The β1 subunit is predominantly expressed in the vascular SMCs and interacts with the amino-terminus along with S0 segment of the α subunit (Lee and Cui 2010).

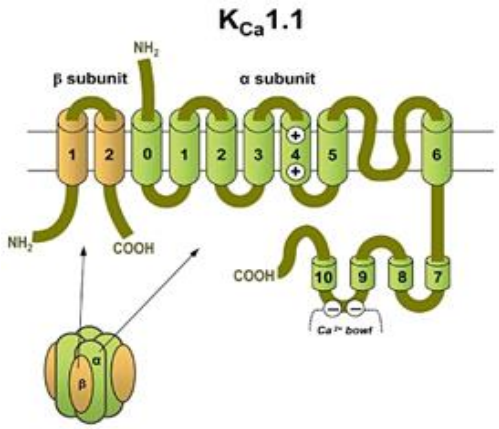

Fig 1.7 Structure of the BK_{Ca} channels. BK_{Ca} ($K_{Ca}1.1$) is made up of α subunits with seven transmembrane segments (S0-6) and β subunits with two transmembrane domains. α subunit contains a calcium binding region (Ca^{2+} bowl) in the C-terminus and voltage sensing S4 region. CaM = calmodulin, K_{Ca} = calcium activated potassium channel and $K_{Ca}1.1$ = large conductance K_{Ca}. Image obtained from (Grgic et al. 2009).

b) Mechanisms involved with BK_{Ca}-induced vasodilation

BK_{Ca} channels can be modulated by both changes in membrane potential and $[Ca^{2+}]_i$. Depolarizing potential can activate these channels during low $[Ca^{2+}]_i$ conditions (McManus 1991) and increase in $[Ca^{2+}]_i$ can shift the voltage dependence of these channels to a more negative and physiological membrane potentials facilitating channel opening (Fig 1.3) (McManus 1991). Furthermore, depolarization of the membrane has also been reported to increase sensitivity of these channels to $[Ca^{2+}]_i$ (McManus 1991). BK_{Ca} are predominantly expressed in vascular SMCs and are found in clusters of 20-100 units (Félétou 2009). The clustered arrangement amplifies channel activation as localized Ca^{2+}-release events (Ca^{2+} sparks) from the ryanodine receptors are able to generate large spontaneous transient outward currents (STOCs) (Bolton and Imaizumi 1996; Zhuge et al. 2002); subsequently

leading to hyperpolarization, reduction in $[Ca^{2+}]_i$ and vasodilation. Electrophysiological techniques have been used to demonstrate that NO can directly activate BK_{Ca} in SMCs derived from rat mesenteric artery (Mistry and Garland 1998). Indirect activation of BK_{Ca} by NO through PKG mediated phosphorylation has also been reported in pulmonary artery (Archer et al. 1994). Another group of endothelial factors reported to activate BK_{Ca} are the EETs and has been demonstrated in various vascular beds including bovine coronary (Rosolowsky et al. 1990; Rosolowsky and Campbell 1993; Campbell et al. 1996), human mammary (Archer et al. 2003) and rat cerebral arteries (Earley et al. 2005). Most studies indicate an indirect activation of BK_{Ca} by EETs through mechanisms such as stimulation of $G\alpha_s$ protein-dependent activation of PKA which can subsequently facilitate opening of BK_{Ca} channels (Imig et al. 1999; Fukao et al. 2001; Dimitropoulou et al. 2007). Furthermore, EETs have also been reported to activate BK_{Ca} by upregulating the production of carbon monoxide in rat mesenteric arteries (Sacerdoti et al. 2006). Lastly, a study led by Earley *et al* demonstrated that EETs can facilitate BK_{Ca} channel opening by initially activating TRPV4-mediated release of Ca^{2+} sparks from the SR (see section 2.6, ii) (Fig 1.3 and 1.9) (Earley et al. 2005).

c) *Role of BK_{Ca}-induced vasodilation in cardiovascular diseases*

An increase in oxidative stress has been associated with atherogenesis (Singh and Jialal 2006) and studies report that vasodilation pathways involving NO, K_{ATP} and K_v channels can be impaired by ROS (Liu and Gutterman 2002). However, BK_{Ca} channels were less sensitive to this ROS-mediated inhibition and were reported to act as a compensatory relaxation pathway in

atherosclerosis (Liu and Gutterman 2002). This was further confirmed by studies conducted using SHRs which demonstrated increased expression of α (Liu et al. 1998) and β1 (Chang et al. 2006) BK_{Ca} subunits in cerebral arteries and mesenteric arteries, respectively. In addition, elevated expression of β1 subunits in cerebral arteries were also found in aging rats which prevented the impairment of BK_{Ca} function (Nishimaru, Eghbali, Stefani, et al. 2004). In contrast, depending upon the type of arteries and animal models, reduced expression of the BK_{Ca} subunits has also been reported. The reduction in the expression of α subunit was demonstrated in pulmonary artery from rats with pulmonary hypertension (Bonnet et al. 2003), superior mesenteric artery from N-nitro-L-arginine hypertensive rats (Bratz et al. 2005) and coronary artery from aging rats (Nishimaru, Eghbali, Lu, et al. 2004). Similarly, decreased expression of β1 subunit was also reported in cerebral arteries from SHR (Amberg and Santana 2003) and angiotensin II-induced hypertensive rats (Amberg et al. 2003). Currently, BK_{Ca} openers are not used for the treatment of CVDs since these drugs have mostly failed in clinical trials due to insufficient selectivity and potency (Nardi and Olesen 2008; Bentzen et al. 2014). However, a BK_{Ca} opener, andolast, is undergoing clinical investigation at the moment for the treatment of mild to moderate asthma (Malerba et al. 2015). A lot of the current medicinal treatments that elicit NO and PGI_2 mediated vasodilation have also been reported to activate BK_{Ca} and these drugs include; sildenafil (phosphodiesterase inhibitor) (Werner et al. 2008), iloprost (PGI_2 analog) (Clapp et al. 1998) and nitroglycerin (NO donor) (Gruhn et al. 2002).

Therefore, there is still some potential for these channels to act as therapeutic targets with more selective and potent BK_{Ca} openers.

1.2.3.iii TRPV4

a) Structure and distribution of TRPV4

It was initially thought that EETs hyperpolarized SMCs through direct activation of BK_{Ca} channels. However, currently there is extensive evidence indicating an indirect modulation of BK_{Ca} channels by these PUFAs (Imig et al. 1999; Fukao et al. 2001; Dimitropoulou et al. 2007) via various mechanisms including initial activation of TRPV4 channels (Earley et al. 2005). TRPV4 is a non-selective cationic tetramer from the vanilloid sub group (Everaerts and Owsianik 2010). It contains six transmembrane segments (TM1-6) with intracellular amino- and carboxyl-terminus (Fig 1.8) (Everaerts and Owsianik 2010). The region between TM5-6 forms the pore of the channel (Everaerts and Owsianik 2010). The cytoplasmic N-terminus is composed of an ankyrin repeat domain which is involved in interaction between different ligands and proteins (Sullivan et al. 2015). The C-terminus also contains binding sites for calmodulin and cytoskeletal proteins (Takahashi et al. 2014). It has a conductance of 50-60 pS for inward current and 90-100 pS for outward currents (Everaerts and Owsianik 2010). TRPV4 channels can be activated by various stimuli such as heat, mechanical stress, AA and EETs (Everaerts and Owsianik 2010). Endothelial expression of TRPV4 has been reported in both conduit and resistance arteries, examples include mouse aorta along with mesenteric artery, rat carotid artery and rat pulmonary artery (Filosa et al. 2013). TRPV4 expression in vascular SMCs

has also been reported in rat aorta, rat cerebral artery, rat pulmonary and mesenteric artery (Filosa et al. 2013).

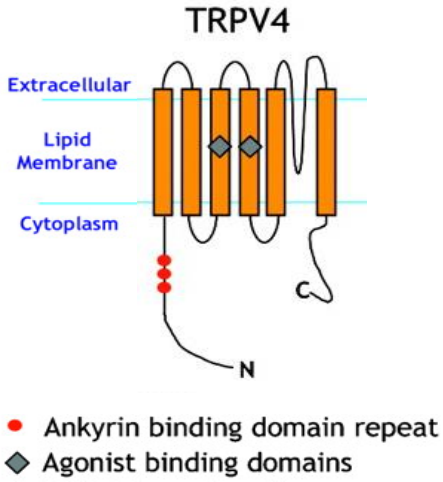

Fig 1.8 Structure of TRP channels. TRPV4 is a tetramer and each subunit is composed of six transmembrane segments with the N- and C-terminus located in the cytoplasm. TRPV4 is expressed in both endothelial and the smooth muscles cells of the vasculature. The region between TM5-6 forms the pore of the channel. TRPV4 = transient receptor potential cation channel subfamily vanilloid member 4. Image was obtained from (Blackshaw et al. 2010).

b) Mechanisms involved with TRPV4-induced vasodilation

The signalling pathway involving TRPV4 and BK_{Ca} channels in EET-induced vasodilation was first reported in rat cerebral arteries (Fig 1.3 and 1.9) (Earley et al. 2005). This study demonstrated that EETs initially activated TRPV4 channels resulting in the subsequent stimulation of the ryanodine receptors. The localized Ca^{2+} sparks released from these receptors then activated the neighbouring BK_{Ca} channels, generating STOCs which hyperpolarized and relaxed the pressurized arteries (Earley et al. 2005). Similarly, Sonkusare *et al.* also demonstrated regulation of endothelial SK_{Ca} and IK_{Ca} channels by TRPV4 in carbachol-induced relaxation of pressurized

mouse mesenteric arteries (Fig 1.3 and 1.9) (Sonkusare et al. 2012). However, this pathway did not involve the BK_{Ca} channels and the release of Ca^{2+} from intracellular stores (Sonkusare et al. 2012). TRPV4 was indicated to function cooperatively forming a cluster of four-channels resulting in an amplified influx of Ca^{2+} that directly activated the endothelial K_{Ca} channels (Sonkusare et al. 2012). In addition, IK_{Ca} was found to be primarily activated by the TRPV4 and SK_{Ca} activation required higher concentration of the TRPV4 agonist. A subsequent study led by the same group investigated the mechanisms involved with TRPV4 activation in carbachol-induced relaxation (Sonkusare et al. 2014). Carbachol activates the muscarinic M_3 GPCR present in the endothelium, resulting in subsequent production of PKC. This study revealed that PKC stimulates PKC-anchoring protein (AKAP150) which facilitates the opening of TRPV4 channels resulting in the subsequent activation of IK_{Ca} (Sonkusare et al. 2014). Furthermore, AKAP150 was also found to be localised in the myoendothelial projections, suggesting the presence of microdomains involving the TRPV4, IK_{Ca} and AKAP150 (Sonkusare et al. 2014). Consistent with the earlier findings another study also confirmed the interaction between SK_{Ca} and TRPV4 channels in rat mesenteric arteries (Ma et al. 2013). Using coimmunoprecipitation and double immunolabeling, these channels were shown to be physically associated with each other and shared a functional interaction in ECs (Ma et al. 2013).

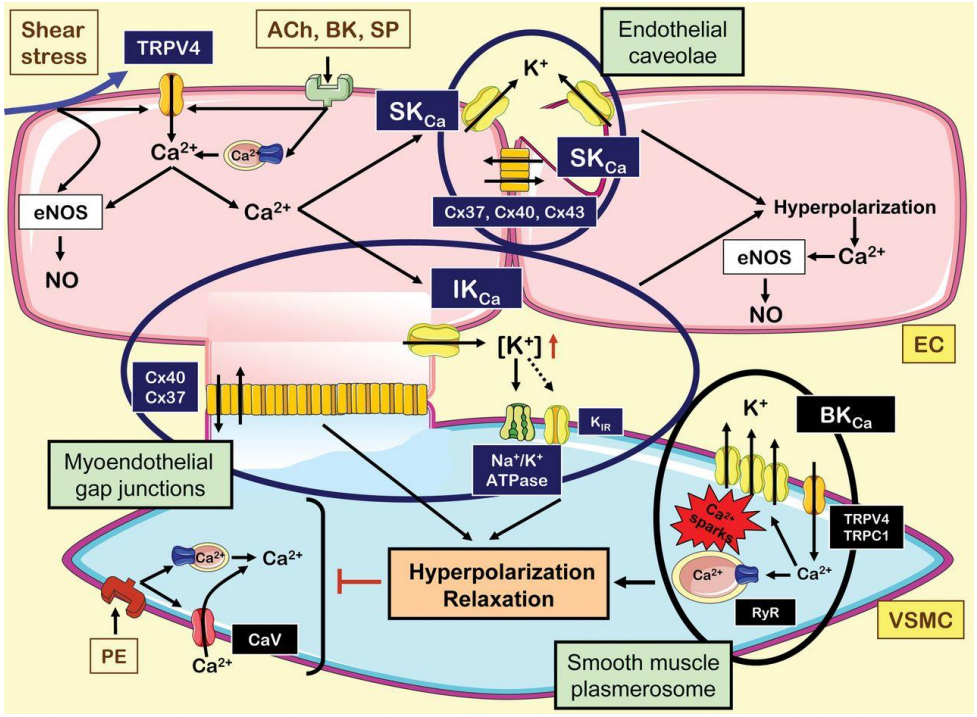

Fig 1.9 Mechanisms involved in the regulation of EDH response by TRP channels. TRP channels were found to directly activate endothelial SK_{Ca} and IK_{Ca} channels whereas BK_{Ca} channels were indirectly activated by TRP channels through the release of calcium sparks, resulting in the hyperpolarization of SMCs and relaxation of the arterial bed. ACh = acetylcholine, BK = bradykinin, BK_{Ca} = large calcium activated potassium channels, CaV = voltage-gated calcium channels, Cx = connexin, EC = endothelial cell, eNOS = endothelial nitric oxide synthase, IK_{Ca} = intermediate conductance calcium activated potassium channels, K_{IR} = inward-rectifier potassium ion channel, Na^+/K^+-ATPase = sodium-potassium adenosine triphosphatase, NO = nitric oxide, PE = phenylephrine, RyR = ryanodine receptor, SK_{Ca} = small conductance calcium activated potassium channels, SP = substance P, TRPC1 = transient receptor potential cation channel subfamily C member 1, TRPV4 = transient receptor potential cation channel subfamily vanilloid member 4 and VSMCs = vascular smooth muscle cells. Figure was obtained from (Félétou and Vanhoutte 2009).

c) Role of TRPV4-induced vasodilation in cardiovascular diseases

There is evidence indicating the role of TRPV4 in the regulation of vascular tone; for example, loss of TRPV4 expression in KO mice led to impairment of shear stress mediated vascular relaxation in carotid (Hartmannsgruber et al. 2007) and mesenteric arteries (Mendoza et al. 2010). Studies also indicate inhibition of ACh-mediated vasodilation both *in vivo* and *in vitro* using mesenteric arteries derived from TRPV4 KO mice (Zhang et al. 2009; Earley, Pauyo, et al. 2009). In human coronary arteries, TRPV4 was associated with flow mediated dilation and the mechanism involved the release of mitochondrial ROS (Bubolz et al. 2012). AA was also reported to activate endothelial TRPV4 that resulted in hyperpolarization and relaxation of human coronary arteries (Zheng et al. 2013). TRPV4 KO mice did not develop hypertension, however, administration of eNOS inhibitor led to significant increase in blood pressure in these KO mice compared to the wild type controls (Earley, Pauyo, et al. 2009). These findings indicate that there is therapeutic potential for TRPV4 modulation against CVDs, however it should be noted that these channels are also involved in other physiological processes such as nociception (Qu et al. 2016), pulmonary fibrogenesis (Rahaman et al. 2014) and epithelial permeability (Reiter et al. 2006). Therefore, in contrast to the beneficial effects of TRPV4 activation with CVDs, studies also report that antagonism of TRPV4 would be therapeutically advantageous for diseases that involve oedema, pain and bronchoconstriction (Grace et al. 2017). Perhaps targeting signalling mechanisms, that are more specific to a certain disorder or tissue of the body,

would be the safer approach for cardiovascular treatments that involve TRPV4 channels.

1.2.4 Other potassium channels involved in vascular relaxation

1.2.4.i K_{ATP}

a) Structure and distribution of K_{ATP}

In 1983, an ATP-sensitive potassium channel (K_{ATP}) was first reported in cardiac myocytes by Noma (Noma 1983). The study demonstrated that intracellular ATP inhibited these channels and therefore were distinct from the inward rectifier potassium channels (Kir) (Noma 1983). Six years after this discovery, a similar current was observed in rabbit mesenteric SMCs and was found to regulate vasodilation (Standen et al. 1989). K_{ATP} channel is a hetero-octameric complex composed of four sulfonylurea receptor (SUR) subunits and four pore-forming Kir6 subunits (Fig 1.10) (Shi et al. 2012). Kir6 subunits are further divided into Kir6.1, encoded by *KCNJ8* and Kir6.2, encoded by *KCNJ11* (Shi et al. 2012). SUR subunits are also subdivided into SUR1 encoded by *ABCC8* and SUR2A along with SUR2B are encoded by *ABCC9* (Shi et al. 2012). Kir6 is composed of two transmembrane regions (M1-M2), a pore-forming loop and both the N- and C-termini located in the cytoplasm (Shi et al. 2012). SUR subunits are part of the ATP-binding cassette family and are composed of seventeen transmembrane segments (Shi et al. 2012). These segments are divided into three transmembrane domains (TMD0, TMD1 and TMD2) (Shi et al. 2012). TMD1 and TMD2 are connected by intracellular nucleotide binding fold (NBF1) containing Walker A and Walker B domains which are involved in nucleotide hydrolysis [for review see (Foster and Coetzee 2016)]. Another nucleotide

binding fold (NBF2) is present in the intracellular carboxyl-terminus and also contains Walker A along with Walker B domains (Foster and Coetzee 2016). NBF1 and NBF2 are involved in the binding of MgATP and MgADP respectively (Foster and Coetzee 2016). Kir6.1 has been reported to be ubiquitously expressed whereas Kir6.2 are mostly expressed in pancreatic beta, cardiac and skeletal muscle cells (Foster and Coetzee 2016). SUR2A is highly expressed in cardiac and skeletal muscle cells (Foster and Coetzee 2016). The expression of SUR2B has been detected in tissues such as heart, lung epithelium, astrocytes, vascular ECs and SMCs (Foster and Coetzee 2016). Most studies report lower expression of SUR1 and SUR2A messenger ribonucleic acid (mRNA) compared to SUR2B in SMCs (Inagaki et al. 1995; Chutkow et al. 1996; Isomoto et al. 1996). Although the presence of Kir6.2 mRNA was reported in SMCs, the protein expression of this subunit was not detected (Yoshida et al. 2004). In ECs derived from guinea pig cardiac capillaries and human coronary artery, the K_{ATP} complex was made up of Kir6.1, Kir6.2 and SUR2B subunits (Mederos y Schnitzler et al. 2000; Yoshida et al. 2004). Therefore, majority of the studies indicate that the vascular K_{ATP} channels, present in both ECs and SMCs, are mainly composed of Kir6.1 and SUR2B (Foster and Coetzee 2016).

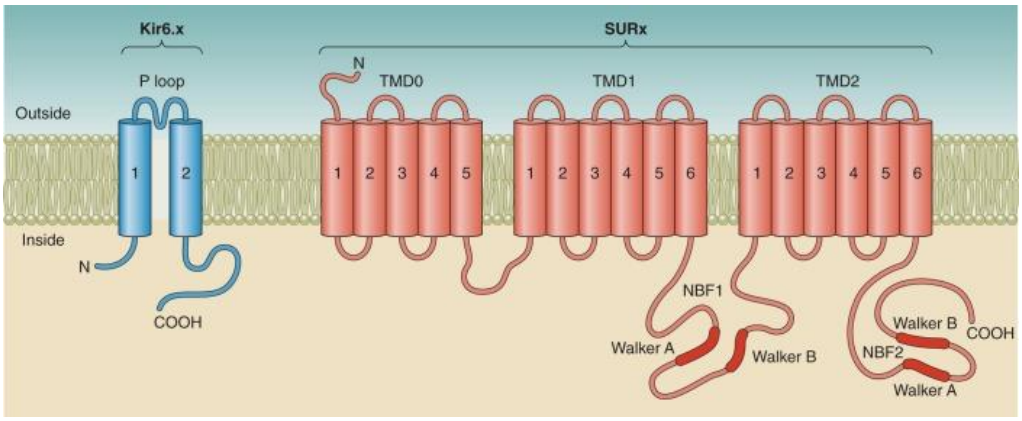

Fig 1.10 Schematic representation of the structure of the K_{ATP} channels. K_{ATP} is composed of Kir6 and SUR subunits. Kir6 subunit is composed of two transmembrane helices linked by an extracellular pore-forming loop (P loop). SUR is composed of three transmembrane domains (TMD0-2) and two nucleotide binding folds (NBF1-2) located intracellularly. NBF1 and NBF2 are involved in the binding of MgATP and MgADP respectively. Walker A and Walker B domains are involved in nucleotide hydrolysis. Kir6 = inwardly rectifier potassium channels and SUR = sulfonylurea receptor. Figure obtained from (Foster and Coetzee 2016).

b) Mechanisms involved with K_{ATP}-induced vasodilation

One of the main features of the K_{ATP} channels is the direct inhibition mediated by intracellular ATP (Foster and Coetzee 2016). Using the inside-out patch clamp technique, about 100 µM of ATP was able to reduce K_{ATP} channel activity by half in cardiac myocytes (Foster and Coetzee 2016). As a result, these channels have a reduced activity at basal conditions in the vasculature since the intracellular concentration of ATP is at the millimolar range (1-11.7 mM) (Foster and Coetzee 2016). Studies also indicate that these channels are inhibited to a lesser extent by other nucleotides such as adenosine diphosphate (ADP) and GTP (Foster and Coetzee 2016). However, ADP in the presence of Mg^{2+} can activate K_{ATP} channels and therefore the intracellular ATP/ADP ratio determines the channel opening.

Most studies indicate that PKA is involved in K_{ATP}-induced vasodilation (Fig 1.3). Vasoactive intestinal polypeptide (VIP) is a vasodilator that activates GPCRs ($G\alpha_s$), VIP receptor 1 and 2, resulting in the subsequent production of PKA. VIP was reported to induce hyperpolarization and relaxation of rat mesenteric artery through a PKA-dependent pathway (Yang et al. 2008). PKA phosphorylates serine residues (Ser1351 and Ser1387) present in NBF2 region of the SUR2B subunit resulting in channel activation (Shi et al. 2007). In contrast, exchange protein activated by cAMP (EPAC) which forms a complex with K_{ATP} channels is involved in the activation of Ca^{2+}-sensitive protein phosphatase 2B (PP-2B, calcineurin) and subsequent inhibition of K_{ATP} (Purves et al. 2009). A higher concentration of cAMP was required to activate EPAC compared to PKA. Therefore, it is currently suggested that the differential cAMP-mediated modulation of K_{ATP} is dependent upon the concentration of cAMP. CYP metabolites of AA, EETs, have also been reported to dilate rat mesenteric arteries through activation of $K_{ATP.}$ However, the pathways were indicated to differ depending upon the type of EET regioisomers. Activation of K_{ATP} channels by 11,12-EET (Ye et al. 2005) was dependent upon PKA activity whereas 14,15-EET (Ye et al. 2006) mediated activation required ADP-ribosylation of $G\alpha_s$. NO has also been reported to activate K_{ATP} channels by upregulating the production of cGMP in rabbit mesenteric arteries (Murphy and Brayden 1995). However, sodium nitroprusside was unable to stimulate these channels in SMCs derived from pig coronary (Wellman et al. 1998) and rabbit mesenteric artery (Quayle et al. 1994). Hydrogen sulphide was also reported to activate K_{ATP} channels in

porcine cerebral arterioles (Liang et al. 2011) and rat aorta (Zhao and Wang 2002) along with mesenteric arteries (Tang et al. 2005).

c) Role of K_{ATP}-induced vasodilation in cardiovascular diseases

Loss of Kir6.1 and SUR2 expression in the coronary artery was associated with coronary artery vasospasm, sudden cardiac death and hypertension [for review see (Nichols et al. 2013)]. The vasospasm was reported to decrease following treatment with nifedipine (Ca^{2+} channel blocker) in SUR2 KO mice (Nichols et al. 2013), indicating a protective role of K_{ATP} channels in vasospasms. Moreover, expression of a dominant negative Kir6.1 subunit in transgenic mice increased the coronary perfusion pressure which was attributed to the elevated levels of the vasoconstrictor, endothelin-1 (Nichols et al. 2013). In transgenic mice expressing gain of function mutants of Kir6.1 in SMCs, attenuation of blood pressure was reported (Nichols et al. 2013). In SUR2 null mice, re-establishing the expression of SUR2 was associated with reduction in infarct size and increased recovery in cardiac function compared to the control mice (Stoller et al. 2010). However, compared to the animal models, loss of function mutations of Kir6.1 and SUR2 in humans were not involved in hypertension and coronary vasospasm (Nichols et al. 2013). In contrast, genetic variation in the *KCNJ8* (Kir6.1) was associated with several disorders involving the heart such as J wave syndromes along with ventricular and atrial fibrillation (Foster and Coetzee 2016). It is possible that this inconsistency in human studies might have occurred partly due to the expression of K_{ATP} channels in multiple tissues other than the vascular bed. Therefore, it is crucial to develop openers that selectively target the vascular K_{ATP} isoform. Due to lack of selectivity, the current K_{ATP}

openers are only used for the treatment of severe hypertension (Minoxidil with diuretic and beta-blocker) (NICE 2019d) and stable angina (Nicorandil, second line) (NICE 2019e).

1.2.4.ii K_v7

a) Structure and distribution of K_v7

Potassium voltage-gated channel subfamily KQT (K_v7) are tetramers composed of four α subunits (Fig 1.11) (Fosmo and Skraastad 2017). Each subunit has six transmembrane segments (S1-S6) with the intracellular amino- and carboxyl-terminus. The voltage sensing domain is present between S1-S4 whereas S5-S6 regions form the pore of the channel (Fosmo and Skraastad 2017). The α subunits can be divided into five $K_v7.1$-7.5 subtypes encoded by *KCNQ*1-5 genes respectively (Fosmo and Skraastad 2017). K_v7 subunits can form both homomers and heteromers depending upon where they are expressed (Fosmo and Skraastad 2017). There are six positively charged arginine residues present in the S4 segment which is involved in closing and opening of the channel following changes in the membrane potential (Fosmo and Skraastad 2017). K_v7 subunits can also coassemble with auxiliary β subunits (*KCNE1-5*) that are involved in regulating the function and expression of K_v7 channels (Fosmo and Skraastad 2017). In cardiac muscle cells, $K_v7.1$ subunits can assemble with *KCNE1* to form the I_{KS} channel involved with the repolarization of ventricles (Fosmo and Skraastad 2017). In the neuronal system, M-currents are associated with the regulation of action potentials and release of neurotransmitters (Fosmo and Skraastad 2017). These currents are generated by homomeric and heteromeric complexes formed with $K_v7.2$, $K_v7.3$ and

K_v7.5 subunits (Fosmo and Skraastad 2017). Studies using rat renal arteries (P. S. Chadha et al. 2012) and human visceral arteries (Fosmo and Skraastad 2017) report that K_v7.1, K_v7.4 and K_v7.5 subunits were predominantly expressed in SMCs. K_v7.4 and K_v7.5 channels were reported to be mostly involved in the regulation of vascular tone (Fosmo and Skraastad 2017).

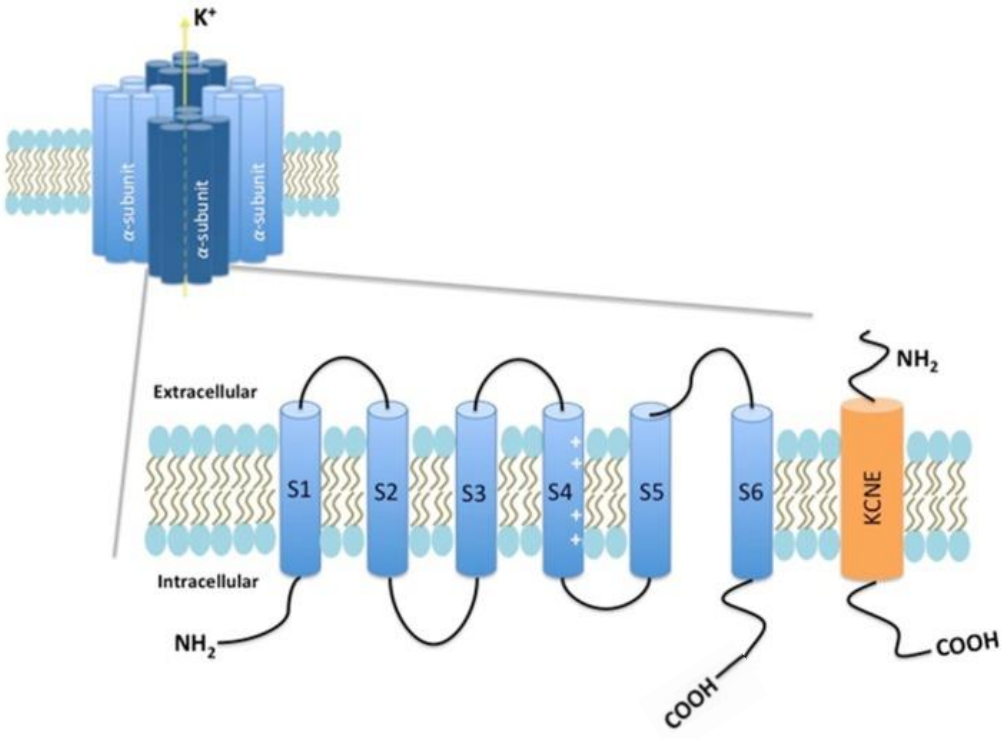

Fig 1.11 Structure of the K_v7 channels. K_v7 channel is a tetrameric complex composed of α subunits containing six transmembrane regions (S1-6). S4 segment contains positively charged arginine residues involved in channel opening and closing following changes in the membrane potential. S5-S6 regions form the pore of the channel. Auxiliary *KCNE1* subunits can also coassemble with K_v7 and regulate channel function. Figure obtained from (Foster and Coetzee 2016).

b) Mechanisms involved with K_v7-induced vasodilation

In rat renal arteries, isoproterenol (β2 adrenoceptor agonist)-induced relaxation was mediated via the cAMP-dependent activation of K_v7.4

channels (P. S. Chadha et al. 2012). A recent electrophysiological study also demonstrated that isoproterenol elicited activation of the β2 adrenoceptor (G_S) resulting in the cAMP-induced production of PKA that subsequently activated $K_v7.4/K_v7.5$ heteromers and $K_v7.5$ homomers (Mani et al. 2016). Furthermore, $K_v7.5$ was found to be more sensitive to PKA activation compared to the $K_v7.4/K_v7.5$ heteromers. In contrast to K_{ATP} channels, EPAC is involved in the activation of K_v7 (Stott et al. 2016). Using proximity ligation, $K_v7.4$ channels were reported to be localized with EPAC in rat renal and mesenteric artery (Stott et al. 2016). Moreover, there was heterogeneity in the pathway involved with isoproterenol-induced relaxation depending upon the type of vascular bed (Stott et al. 2016). In rat renal artery, relaxations were reduced via inhibition of EPAC and was not associated with PKA activity. On the contrary, relaxations were only sensitive to PKA activation in rat mesenteric artery. cGMP was also found to be involved in the relaxation of rat aorta and renal artery through activation of $K_v7.4$ channels (Stott et al. 2015). Although there are no studies indicating the role of AA in the activation of K_v7 channels in the vasculature, 12-lipoxygenase metabolites of AA were involved in activation of M-currents in the sympathetic neurons of bullfrogs (Yu 1995).

c) *Role of Kv7-induced vasodilation in cardiovascular diseases*

In SHR, a decrease in expression of $K_v7.4$ subtype and attenuation of agonist-induced relaxation has been reported in aorta, coronary and mesenteric artery (Jepps et al. 2011). PKA-induced relaxation of rat renal arteries following application of β adrenergic agonist (Isoproterenol) was also inhibited in SHR (P. S. Chadha et al. 2012). This study also indicated

that decreased $K_v7.4$ activity was associated with hypertension (P. S. Chadha et al. 2012). cGMP-dependent vasodilation pathway involving the activation of K_v7 was also attenuated in aorta and renal artery derived from SHR (Stott et al. 2015). Small GTPase Ras-related protein 1 (Rap1b) is a GTP-binding protein involved in different cellular functions including regulation of vascular tone and can be activated by EPAC (Lakshmikanthan et al. 2014). Inactivation of Rap1b in mice was associated with hypertension (Lakshmikanthan et al. 2014). Since $K_v7.4$ channels are reported to be localized with EPAC (Stott et al. 2016), it can be speculated that inhibition of these channels is possibly involved. A K_v7 opener, flupirtine, was reported to elicit vasodilation in pulmonary arteries and reduce right ventricular pressure and hypertrophy in mouse models of pulmonary hypertension (Morecroft et al. 2009). Furthermore, flupirtine was also indicated to reduce pulmonary pressure and prevent pulmonary hypertension in rats (Sedivy et al. 2015). Currently, there are only two studies that have reported the effects of flupirtine in human blood pressure. Chronic treatment with flupirtine for 52 weeks led to reduction in blood pressure (Herrmann et al. 1987), however an elevation in pressure was reported following a single dose administration after 2h (Hummel et al. 1991). These findings indicate that the therapeutic effects of K_v7 openers can depend upon the duration of the treatment and as a result, further studies need to be conducted to validate these findings using more selective K_v7 openers.

1.3 Role of n-3 PUFAs in vasodilation

1.3.1 Arachidonic acid

In the beginning of the 20th century, dietary fatty acids were only known as a great source of energy and were not considered as an essential nutrient (Spector and Kim 2015). It was only after three decades that a deficiency disease was initially reported in rats fed with fat-excluded diet resulting in the development of severe symptoms such as necrosis of the tail, hair loss, scaly skin, abrogation of growth, lesions in the urinary tract and kidney resulting in premature death (Burr and Burr 1929). Furthermore, it was later indicated that inclusion of linoleic acid (LA), an n-6 PUFA with 18 carbon chain and two double bonds, reversed these detrimental effects and therefore this established the role of fats as an essential nutrient (Burr and Burr 1930). Numerous studies were then conducted investigating the physiological effects of fatty acids and by 1940s, substantial amount of evidence demonstrated that LA could be endogenously converted into arachidonic acid (AA) (Nunn and Smedley-Maclean 1938; Holman and Burr 1948; Rieckenhoff et al. 1949; Widmer and Holman 1950). AA is an omega-6 PUFA composed of 20-carbon chain and four cis-double bonds. AA can be physiologically acquired either through a dietary source or by enzymatic elongation and desaturation of precursor PUFAs as shown in figure 1.12. This enzymatic metabolism of LA into AA has been demonstrated in various tissues including vascular ECs and SMCs (Rosenthal and Whitehurst 1983; Garcia et al. 1990; Harmon et al. 2003). In 1964, there was another breakthrough discovery demonstrating further conversion of AA into COX metabolites, prostaglandins (section 1.2.2.i) (Bergstroem et al. 1964; Van Dorp et al. 1964). Prostaglandins have a major role in maintaining homeostasis throughout the body as they are involved in various physiological processes including inflammation (Ricciotti and FitzGerald 2011).

Therefore, the insufficient production of prostaglandins due to a fat-deficient diet provided an explanation for the fatal symptoms that were previously reported in rats by Burr (Bergstroem et al. 1964; Van Dorp et al. 1964). PUFAs such as AA can be found in membrane phospholipids and are released as a free fatty acid into the cytosol following hydrolysis of the phospholipid ester bond by calcium-sensitive phospholipase A_2 (PLA_2) (Clark et al. 1991; Dennis 1994). As previously described (section 1.2.2.ii), AA can be metabolised by various enzymes including CYP, resulting in the production of different types of PUFA metabolites that have diverse functions throughout the body. Studies also indicate that AA itself can also elicit some of the responses mediated by its metabolites; for example, AA can directly activate BK_{Ca} channels involved in vasodilation, however, EETs (CYP metabolites of AA) were reported to be 1000 times more potent than AA (Lu, Katakam, et al. 2001; Martín et al. 2014). Due to the reported functional similarities between AA and its metabolites, it is important to consider that perhaps other types of fatty acids such as n-3 PUFAs could also elicit similar effects. In fact, both n-3 and n-6 PUFAs have been reported to activate identical pathways involved in vasodilation and these studies will be further discussed in the following sections.

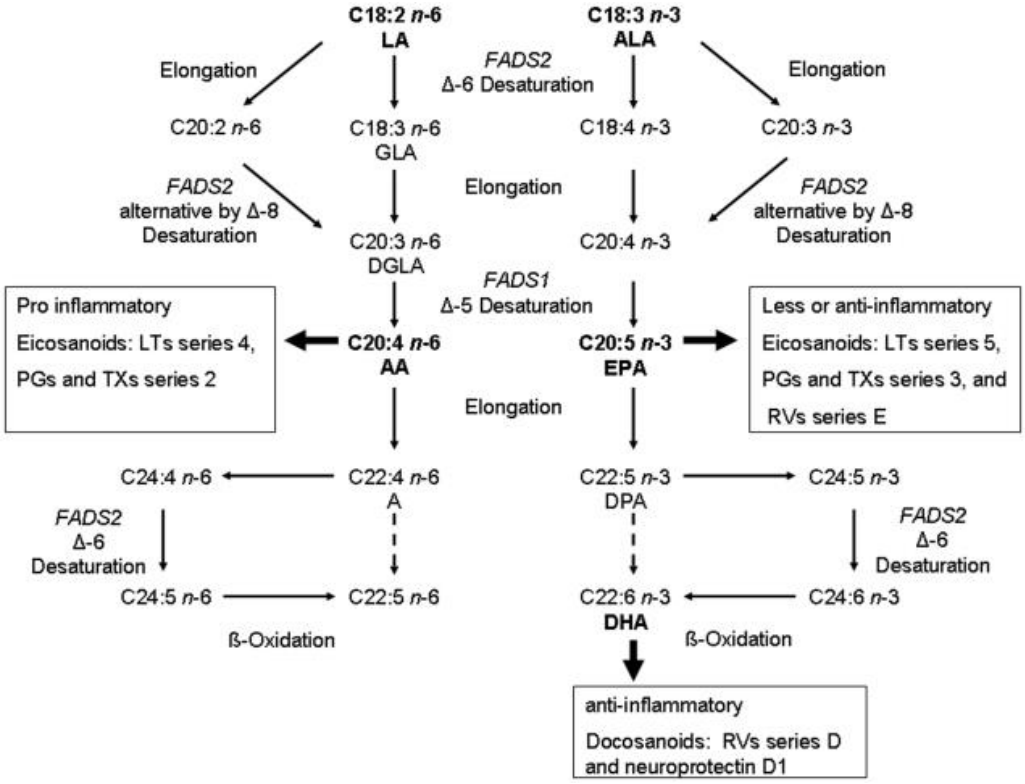

Fig 1.12 Enzymatic conversion of omega-3 and omega-6 PUFAs in the human body. LA and ALA act as precursors which undergo elongation and desaturation processes producing a range of PUFAs. A = adrenic acid, AA = arachidonic acid, ALA = alpha-linoleic acid, DGLA = dihomo-gammalinolenic acid, DHA = docosahexaenoic acid, DPA = docosapentaenoic acid, EPA = eicosapentaenoic acid, FADS = fatty acid desaturase, GLA = gamma linolenic acid, LA = linoleic acid, LTs = leukotrienes, PGs = prostaglandins, RVs = resolvins, TXs = thromboxanes. Figure obtained from (Rzehak et al. 2010).

1.3.2 n-3 PUFAs

According to World Health Organization, CVDs are number one cause of deaths worldwide (WHO 2017). Endothelial dysfunction, hypertension and dyslipidemia are some of the major risk factors for CVDs. Vascular endothelial dysfunction refers to the abnormality in the vasomotor pathways of the endothelium. This dysfunction results in impaired vasodilation and enhanced vasoconstriction (Sitia et al. 2010). Dyslipidemia is another disorder that involves an imbalance in the circulating lipids of the blood stream. It can result in lower levels of high density lipoprotein and higher levels of low density lipoprotein, promoting the formation of atherosclerosis. There is evidence indicating that atherogenesis mostly occurs in larger and medium-sized elastic and muscular arteries (Glagov et al. 1988). Furthermore, the interaction between endothelium and haemodynamic forces such as shear stress and circumferential tensile stress (stretch), was reported to influence the localization of atherorsclerotic lesions in various vascular beds (Glagov et al. 1988). Major arterial sites with bifurcations and branches were indicated to be more prone to plaque formations due to their increased susceptiblility of developing an impairment in unidirectional laminar flow, via reduction in shear stress and flow velocity [for a comprehensive review see (Glagov et al. 1988; Frangos et al. 1999)]. As a result, studies suggest that carotid bifurcation, coronary arteries, major branches of aortic arch and abdominal aorta have the highest risk of developing atherosclerosis (Glagov et al. 1988; Frangos et al. 1999).

Omega-3 (n-3) PUFAs or in more popular term “Fish oils” have been identified as healthy fats and so far numerous studies have investigated the protective effects of these PUFAs in the cardiovascular health of different subpopulations (Miller et al. 2014; Aung et al. 2018). Earliest records of the protective effects of n-3 PUFAs in the vasculature were found during the late 1970s, in studies involving Greenland Eskimo and Japanese people

(Bang et al. 1976; Hirai et al. 1980). The diets of these people were found to be low in carbohydrates whereas high in protein and omega-3 fatty acids, due to an increased intake of fish compared to the western population. These studies also reported lowering of plasma triglycerides and low-density lipoprotein levels. Following these novel findings, numerous human supplementary and dietary intervention studies were carried out to investigate the protective effects of n-3 PUFAs in CVDs. Reduction in plasma triglyceride levels present in very low-density lipoprotein were reported both in healthy volunteers and hypertriglyceridemic (elevated plasma triglyceride levels) patients (Harris et al. 1988). Triglycerides containing n-3 PUFAs had a reduced intestinal absorption rate resulting in lowered plasma levels. In addition, another study confirmed reduction in esterified eicosapentaenoic acid (EPA) absorption due to decreased rate of hydrolysis by the pancreatic lipase (Chen et al. 1987). An extensive review regarding n-3 PUFAs and lipoproteins can be found elsewhere (Harris 1997). However, depending upon the target subpopulations, there are also reports indicating an ineffectiveness of n-3 PUFAs in providing cardiovascular benefits. A recent study that involved meta-analysis of ten randomized clincial trials with a minimum of 500 participants with coronary heart disease (CHD), demonstrated that treatments with n-3 PUFAs (0.226-1.8 g/day) for an average duration of 4.4 years, did not cause any signifcant reduction in adverse events which include myocardial infraction, fatal coronary heart disease (CHD) and stroke (Aung et al. 2018). It is possible that depending upon the dosage and type of CVD, the efficacy of n-3 PUFAs in improving cardiovascular health may differ. For example, a meta-analysis study of randomized trials revealed that a higher dose (3.7 g/day) of n-3 PUFAs lowered both systolic and diastolic blood pressure especially in older and hypertensive patients (Geleijnse et al. 2002). Campbell *et al* also verified these findings, following meta-analysis of 17 studies, by indicating that that n-3 PUFA supplementation led to significant

reduction of blood pressure in hypertensive patients but not in healthy volunteers (Campbell et al. 2013). Furthermore, a more recent meta-analysis study that evaluated 70 randomized trials, reported that the decrease in blood pressure associated with n-3 PUFAs (≥1 g/day) was the most potent in unmedicated hypertensive participants (Miller et al. 2014). Therefore, the discrepancy that has been reported between n-3 PUFA studies could be explained by the heterogeneity involved with the protective effects of n-3 PUFAs, that seems to depend upon the type of; target subpopulation (eg: normotensive vs hypertensive), CVDs (eg: CHD vs hypertension) and possibly the dosage of these PUFAs. Furthermore, genetic variations in the vasodilation pathways between different subpopulations should also be considered when comparing these studies. As mentioned earlier (section 1.2.2.ii), CYP2C and CYP2J are the main epoxygenases that are expressed in the ECs and are involved in the production of EETs, which are known to elicit vasodilation (Zeldin 2001). Similar to the n-3 PUFAs, conflicting findings have been reported by studies investigating the role of CYP polymorphisms in various CVDs [reviewed by (Zordoky and El-Kadi 2010)]. Besides the expected differences in diet, ethnicity and family history between different subpopulations (Arun Kumar et al. 2011); the reported inconsistency could also be perhaps explained by the propensity of specific CYP polymorphisms to affect certain CVDs. For example; in African American population, CYP2J polymorphism was reported to lower the risk of coronary artery disease (Lee et al. 2007), however this polymorphism was not involved with hypertension (Dreisbach et al. 2005). CYP2C polymorphism on the other hand was not associated with both coronary artery disease (Lee et al. 2007) and hypertension (Dreisbach et al. 2005) in African Americans. There is extensive evidence indicating that both n-3 PUFAs and its CYP metabolites can elicit vasodilation by directly activating BK_{Ca} channels (discussed in section 1.3.3.iii) (Ye et al. 2002; Hercule et al. 2007; Wang et al. 2011;

Toshinori Hoshi, Wissuwa, et al. 2013; Nagaraj et al. 2016). As discussed earlier in section 1.2.3.ii.c, the expression profile of BK_{Ca} has been reported to alter depeding upon the type of CVD. An increase in β1 BK_{Ca} subunit expression was reported in SHR (Liu et al. 1998) whereas reduction in the expression of α subunit of BK_{Ca} was demonstrated in rats with pulmonary hypertension (Bonnet et al. 2003). Therefore, depending upon the disorder of the subpopulation, it seems that the therapeutic effectiveness of n-3 PUFA supplementation may differ due to changes in the expression and the functional activity of the vasodilation pathways.

n-3 PUFAs are essential fats which comprise of alpha-linoleic acid (ALA, C18:3), EPA (C20:5), docosapentaenoic acid (DPA, C22:5) and docosahexaenoic acid (DHA, C22:6). Figure 1.12 illustrates the endogenous enzymatic pathway involving fatty acid desaturase enzymes, which orchestrate elongation and desaturation reactions that convert ALA into eicosanoids, DPA, EPA and DHA. EPA and DHA are considered as essential fatty acids since the enzymatic conversion of ALA into EPA and DHA in the human body is very inefficient, and only about 0.2 to 8% of EPA and 0 to 4% of DHA are produced (Burdge et al. 2002; Mozaffarian and Wu 2011). As a result, optimum levels of EPA and DHA are only achieved through diet and supplementation.

Similar to AA, n-3 PUFAs are also released from the membrane phospholipids via the activity of PLA_2 and can compete with AA for similar enzymes (Bogatcheva et al. 2005). As a result, EPA also produces various eicosanoids including series-3 PG, series-5 LTs and epoxyeicosatetraenoic acids (EPETEs) (Thomson et al. 2012). DHA is also converted into metabolites such as epoxydocosapentaenoic acids (EDPs) and hydroxy-DHA (HDHA) (Arnold, Konkel, et al. 2010). Figure 1.13 summarises the metabolism of these fatty acids and the enzymes involved.

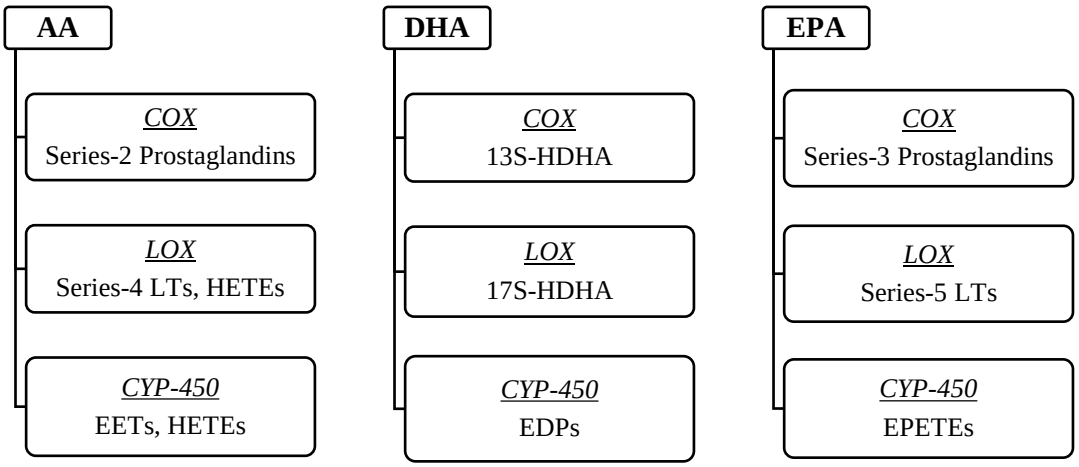

Fig 1.13 Enzymes involved in the metabolism of AA, DHA and EPA. Dietary intake of DHA and EPA results in incorporation of these fatty acids into the cell membrane. Following its release from membrane phospholipids, it can compete with enzymes that metabolise AA. AA, Arachidonic acid; COX, cyclooxygenase; CYP, cytochrome P450; DHA, docosahexaenoic acid; EETs, epoxyeicosatrienoic acids; EDPs, epoxydocosapentaenoic acids; EPETEs, epoxyeicosatetraenoic acid; EPA, eicosapentaenoic acid; HDHA, hydroxy-docosahexaenoic acid; HETEs, hydroxyeicosatetraenoic acids; LOX, lipoxygenase and LTs, leukotrienes.

1.3.3 n-3 PUFAs and vasodilation

As discussed earlier, although n-3 PUFAs were not involved in improving the cardiovascular health of participants with CHD (Aung et al. 2018), various meta-analysis studies have reported that these PUFAs are involved in the reduction of blood pressure in patients suffering from hypertension (Geleijnse et al. 2002; Campbell et al. 2013; Miller et al. 2014). Likewise, improvements in vasodilation response of arteries have also been reported as a common effect of n-3 PUFAs supplementation (Mori 2014). This section of the introduction will discuss both the endothelium-dependent and -independent mechanisms that have been associated with n-3 PUFAs in various vascular beds.

1.3.3.i Effects of n-3 PUFAs in NO production

n-3 PUFAs have been shown to improve endothelial dysfunction and reduce progression of CVDs. Many studies indicate that n-3 PUFAs enhance endothelial NO levels; for example, EPA was reported to induce calcium-independent increases in endothelial NO, resulting in relaxation of bovine coronary arteries (Omura et al. 2001). Similarly, DHA enhanced interleukin-1β-mediated NO production in SMCs derived from rat aorta (Hirafuji et al. 2002). An increase in eNOS mRNA and protein levels in isolated aortic tissues are possible mechanisms of n-3 PUFA-induced NO production (López et al. 2004). In SHR, dietary supplementation with DHA and EPA for two months reduced plasma levels of ADMA, an endogenous eNOS inhibitor (Raimondi et al. 2005). Rats fed with high-fructose diet exhibited endothelial dysfunction that was prevented by upregulation of eNOS expression, following dietary inclusion of n-3 PUFAs (Nyby et al. 2005). Likewise in nephrectomized rats and ApoE KO mice, an elevated aortic expression of eNOS and NO production was reported following inclusion of n-3 PUFA-rich diet (Casós et al. 2010; Zanetti et al. 2017). Clinical studies have also validated these findings; for example, chronic treatment of EPA in patients with coronary artery disease led to

improvements of both NO-dependent and -independent vasodilation (Tagawa et al. 1999). Furthermore, acute treatment (4 h) with n-3 PUFAs prevented high fat meal-induced impairment of flow mediated dilation, a measure of NO-dependent relaxation, in the brachial artery of healthy volunteers (Fahs et al. 2010). Most of the animal studies indicated that n-3 PUFA-induced elevation of NO production in the aortic vasculature (Table 1.1), resulting in the reversal of endothelial dysfunction. Although large conduit arteries are not involved in the regulation of mean arterial blood pressure, NO-mediated vascular relaxation of aorta has been reported to reduce arterial stiffness and central blood pressure, as discussed previously in section 1.2.1.i (Kampus et al. 2011; Zhou et al. 2014). Furthermore, it is possible that n-3 PUFAs might also enhance NO production in other vessels, therefore, highlighting the necessity of investigating this pathway in conduit and resistance arteries.

1.3.3.ii Effects of n-3 PUFAs in K_{ATP}-induced vasodilation

There is also evidence indicating the involvement of K_{ATP} channels with n-3 PUFA-induced vasodilation. For example, in rat aorta pre-constricted with noradrenaline and high concentration of potassium (80 mM), EPA-induced relaxation was sensitive to blockade of COX and K_{ATP} channels (Engler et al. 2000). The author suggested that COX metabolites of EPA were possibly involved in K_{ATP} activation. Furthermore, there is some evidence indicating that n-3 PUFA supplementation (28 days) can alter prostanoid production in humans (Chin et al. 1993). n-3 PUFAs were found to attenuate noradrenaline- and angiotensin II-induced vasoconstriction of human forearm resistance vessels which was sensitive to COX inhibition.

A recent study also reported that DHA might be involved in the activation of K_{ATP} channels in rat aorta (Sato et al. 2014). In contrast to the earlier study, this relaxation persisted following inhibition of COX and endothelium removal, perhaps indicating a

direct role of DHA in K_{ATP} activation. However, CYP metabolite of DHA, 16, 17-EDP, was also involved in K_{ATP}-dependent relaxation of rat aorta (Sato et al. 2014). Another interesting observation in this study was the presence of remaining residual relaxation following CYP inhibition and the additional blockade of K_{ATP} channels (Sato et al. 2014). Therefore, it is essential to conduct further investigations to fully elucidate these unknown mechanisms involved with n-3 PUFA-mediated relaxation.

1.3.3.iii Effects of n-3 PUFAs in K_{Ca}-induced vasodilation

The EDH response involves activation of K_{Ca} channels which hyperpolarize vascular SMCs resulting in vasodilation. AA and its metabolites have been reported to regulate the EDH response via K_{Ca} channels. Currently there is no evidence indicating the role of SK_{Ca} and IK_{Ca} in n-3 PUFA-mediated vasodilation. However, there is one study that has investigated the modulation of IK_{Ca} by DHA (Kacik et al. 2014). Their findings demonstrated that PUFAs including DHA, AA and EETs were involved in the inhibition of human IK_{Ca} channels expressed in human embryonic kidney (HEK) cells (Kacik et al. 2014). Therefore, further studies are required to investigate whether this inhibition is also observed in intact arteries and if EPA has a similar effect.

As discussed earlier, AA-derived EETs can activate BK_{Ca} channels present in vascular SMCs mainly derived from resistance arteries confirming their role as EDH factors (72,73). CYP epoxygenase metabolites of DHA, EDPs, have also been reported to activate BK_{Ca} channels resulting in hyperpolarization of vascular SMCs derived from porcine coronary arteries (Ye et al. 2002). Similarly, DHA mediated a concentration-dependent increase in BK_{Ca} channel currents in SMCs derived from rat coronary artery (Lai et al. 2009). In isolated rat coronary arterial tissues, the blockade of BK_{Ca} channels completely abolished DHA-induced vasodilation (Wang et al. 2011). The underlying mechanism involved the release of calcium from sarcoplasmic reticulum mediated by 16,

17-EDPs in rat coronary arteries, resulting in subsequent activation of BK_{Ca} channels. This was further confirmed in a recent study involving patients with idiopathic pulmonary arterial hypertension and BK_{Ca} KO mice (Nagaraj et al. 2016). DHA was reported to enhance BK_{Ca} currents in pulmonary arterial SMCs derived from these patients. In BK_{Ca} KO mice, DHA-induced relaxation in pulmonary artery was significantly attenuated compared to the control mice (Nagaraj et al. 2016).

CYP enzymes can oxygenate EPA into 17(R), 18(S)-epoxyeicosatetraenoic acids (17R, 18S-EPETEs) which were reported to activate BK_{Ca} channels in rat cerebral arteries (Hercule et al. 2007). Supporting this, 17R, 18S-EPETEs were unable to activate BK_{Ca} channels in SMCs extracted from the cerebral arteries of KO mice lacking the BK_{Ca} alpha subunit (BK $\alpha^{-/-}$). Consistently, 17R, 18S-EPETEs mediated a concentration-dependent relaxation in mesenteric arteries derived from wild type mice which was significantly impaired in BK $\alpha^{-/-}$ arteries. Therefore, the authors from this study suggested a direct interaction between 17R, 18S-EPETEs and the alpha subunit of BK_{Ca} channels, since this phenomenon was not dependent upon the intracellular levels of calcium and sarcoplasmic reticulum-induced calcium events.

Lipoxygenase metabolites of n-3 PUFAs, especially DHA, are also implicated in the regulation of BK_{Ca} channels. 15- and 5-lipoxygenase metabolite of DHA, 17S-Hydroxy DHA (17S-HDHA), was reported to activate BK_{Ca} channels (Li et al. 2011). Whole cell patch clamp with SMCs extracted from bovine coronary arteries revealed that 17S-HDHA treatment enhanced outward potassium currents. Application of 17S-HDHA into the extracellular side of inside-out patches of these SMCs, led to the enhancement of BK_{Ca} currents suggesting a direct activation of the BK_{Ca} channel (Li et al. 2011). Furthermore, 17S-HDHA was also reported to cause relaxation in bovine coronary arteries which was significantly inhibited through lipoxygenase blockade and

endothelium removal (Li et al. 2011). A residual relaxation was also observed following blockade of BK_{Ca} channels indicating that other mechanisms are also involved.

Both n-3 PUFAs, especially DHA, have also been associated with direct activation of BK_{Ca} channels (Toshinori Hoshi, Wissuwa, et al. 2013). An increase in BK_{Ca} channel currents following the application of DHA was demonstrated in mice aortic SMCs and cell-free patches derived from HEK cells (Toshinori Hoshi, Wissuwa, et al. 2013). This effect persisted when DHA was applied to both extracellular and intracellular sides of the patches. These cell-free patches lacked intracellular signalling proteins and therefore a direct binding of DHA to BK_{Ca} channels was mentioned as a possible explanation for the channel activation. EPA was also found to activate BK_{Ca} but less potently compared to DHA. In contrast to earlier studies, inhibiting CYP had no effect in DHA-induced activation of BK_{Ca} channels in HEK cells. Intravenous administration of DHA into wild type mice led to a transient drop in arterial blood pressure which was absent in BK_{Ca} KO mice (BK $\alpha^{-/-}$) (Toshinori Hoshi, Wissuwa, et al. 2013). This was also confirmed by a recent study that investigated the effects of DHA in mice with hypoxia-induced hypertension (Nagaraj et al. 2016). Injection of DHA into the central vein of the mice led to reduction in pulmonary pressure and returned the right ventricular systolic pressure to normal levels (Nagaraj et al. 2016). This finding is important as clinical studies have also indicated blood pressure lowering effects of n-3 PUFAs and therefore activation of BK_{Ca} channels could be one of the mechanisms involved (Mori 2014). In agreement with this suggestion, a study involving human coronary arteries demonstrated an increase in outward potassium currents in DHA-treated SMCs (Wu et al. 2007). DHA was also shown to inhibit phasic constrictions in these arteries. Although the potassium channels involved were not characterized, BK_{Ca} channels could be possibly associated with these outward currents based on the studies reviewed earlier.

1.3.3.iv Justification for the study

The findings discussed in this section; firstly validates the role of n-3 PUFAs in improving vasodilation through hyperpolarization of arteries and most studies indicate that BK_{Ca} channels are involved, secondly they demonstrate the complexity and variability in the mechanisms of n-3 PUFAs and its metabolites in eliciting vasodilation, and thirdly they highlight the need for an investigation of the vasorelaxant mechanisms that still remain unexplained. For example, the role of other K_{Ca} channels and as yet unidentified endothelium-independent mechanisms demonstrated by the presence of residual relaxation in some studies. Therefore, this study aimed at fully characterizing the vasodilation mechanisms of both n-3 PUFAs, DHA and EPA, in conduit (aorta) and resistance arteries (mesenteric).

Table 1.1 Summary of the major findings from vascular studies investigating the role of n-3 PUFAs and its metabolites in the regulation of vasodilation. Majority of the studies indicate activation of BK_{Ca} channels by n-3 PUFAs and its metabolites. ADMA = asymmetric dimethylarginine, BK_{Ca} = large conductance K_{Ca}, COX = cyclooxygenase, CYP = cytochrome P450, DHA = docosahexaenoic acid, ECs = endothelial cells, EDPs = epoxydocosapentaenoic acids, EETs = epoxyeicosatrienoic acids, eNOS = endothelial nitric oxide synthase, EPETEs = epoxyeicosatetraenoic acid, EPA = eicosapentaenoic acid, HDHA = hydroxy-docosahexaenoic acid, HETEs = hydroxyeicosatetraenoic acids, IK_{Ca} = intermediate conductance K_{Ca}, K_{Ca} = calcium activated potassium channels, NO = nitric oxide and SMCs = smooth muscle cells.

Species	**Type of Artery**	**Cell**	**Constrictor**	**Type of n-3 PUFA**	**Concentration of n-3 PUFA**	**Effect**	**Ref.**
Bovine	Coronary	ECs	U46619	EPA	30-60 µM	Improved NO production	(Omura et al. 2001)
	Coronary	SMCs	U46619	17S-HDHA	0.1-1 µM	Direct activation of BK_{Ca} channels	(Li et al. 2011)
Mouse	Aorta	ECs	-	EPA & DHA	-	Enhanced eNOS levels	(Casós et al. 2010)
	Aorta	SMCs	-	DHA	3 µM	Activation of BK_{Ca} channels	(Toshinori Hoshi, Wissuwa, et al. 2013)
	Cerebral	SMCs	U46619	17R, 18S-EPETEs	100 nM	α subunit dependent BK_{Ca} activation	(Hercule et al. 2007)
	Mesenteric	SMCs	U46619	17R, 18S-EPETEs	100 nM	α subunit dependent BK_{Ca} activation	(Hercule et al. 2007)

	Pulmonary	-	U46619	DHA	0.3-100 µM	Activation of BK_{Ca} channels	(Nagaraj et al. 2016)
Porcine	Coronary	SMCs	-	13, 14-EDPs	EC_{50} (2.2 ± 0.6 pM)	Activation of BK_{Ca} channels	(Ye et al. 2002)
Rats	-	-	-	EPA & DHA	1 g/kg/day	Reduced ADMA levels	(Raimondi et al. 2005)
	Aorta	ECs	-	EPA & DHA	50g/kg	Enhancement of eNOS levels	(López et al. 2004)
	Aorta	-	Phenylephrine	DHA & EPA	200mg/g (DHA) & 300mg/g (EPA)	Enhancement of eNOS levels	(Zanetti et al. 2017)
	Aorta	SMCs	High KCl & Noradrenaline	COX metabolites of EPA	3-100 µM	Activation of K_{ATP} channels	(Engler et al. 2000)
	Aorta	SMCs	-	DHA	3-30 µM	Enhanced IL-1β induced NO production	(Hirafuji et al. 2002)
	Aorta	SMCs	U46619	16, 17-EDPs	1 µM	Activation of K_{ATP} channels	(Sato et al. 2014)
	Cerebral	SMCs	U46619	17R, 18S-EPETEs	100 nM	Activation of BK_{Ca} channels	(Hercule et al. 2007)
	Coronary	SMCs	-	DHA	EC_{50} (37.53±1.65 µM)	Activation of BK_{Ca} channels	(Lai et al. 2009)
	Coronary	SMCs	Endothelin-1	16, 17-EDPs	EC_{50} (19.7 ± 2.8 nM)	Calcium sparks mediated BK_{Ca} activation	(Wang et al. 2011)
Human	Coronary	VSMCs	PGF2α, Ouabain & High KCl	DHA	1-30 µM	Enhanced outward potassium currents	(Wu et al. 2007)
	-	HEK	-	DHA	EC_{50} value of 500nM	Activation of BK_{Ca} channels	(Toshinori Hoshi,

							Wissuwa, et al. 2013)
	-	HEK	-	DHA	10 µM	Inhibition of IK_{Ca} channels	(Kacik et al. 2014)
	Pulmonary	SMCs	-	DHA	10 µM	Activation of BK_{Ca} channels	(Nagaraj et al. 2016)

Table 1.2 Summary of the major findings from studies investigating potassium channels in human arteries. Through the use of molecular biology, electrophysiology and myograph, functional potassium channels have been reported to regulate vascular tone, especially in resistance arteries. BK_{Ca} = large conductance K_{Ca}, IK_{Ca} = intermediate conductance K_{Ca}, K_{ATP} = adenosine triphosphate-sensitive potassium channel, K_{Ca} = calcium activated potassium channels, K_v7 = potassium voltage-gated channel subfamily Q member, mRNA = messenger ribonucleic acid, PCR = polymerase chain reaction, qPCR = quantitative PCR, Ref. = reference, RT-PCR = reverse transcription-PCR and SK_{Ca} = small conductance.

Type of ion channel	Type of blood vessel	Techniques used	Summary of key findings	Ref.
SK_{Ca} and IK_{Ca}	Coronary artery	Organ bath video-microscopy, PCR, western blot and whole cell patch-clamp	Confirmation of both SK_{Ca} and IK_{Ca} channel currents, expressions and their role in vasodilation	(Feng et al. 2008; Takai et al. 2013)
	Myometrial and omental artery	Wire myograph	Involvement of both channels in vasodilation	(Gillham et al. 2007)
	Skeletal muscle arterioles	Organ bath video-microscopy and western blot	Confirmation of both SK_{Ca} and IK_{Ca} expression and its role in vasodilation	(Liu et al. 2008)
	Mesenteric artery	Immunohistochemistry and pressure myograph	Only IK_{Ca} channels were expressed and involved in vasodilation	(Chadha et al. 2011)
BK_{Ca}	Adipose artery	Immunofluorescence, inside-out patch-clamp, pressure myograph and western blot	Confirmation of BK_{Ca} channel currents, expression and its role in vasodilation	(Nieves-Cintrón et al. 2017)
	Aorta	Hybridization probe and sanger sequencing	Confirmation of BK_{Ca} nucleotide sequence	(McCobb et al. 1995)
	Coronary artery	Immunocytochemistry, patch-clamp, western blot	Confirmation of BK_{Ca} channel currents and expression	(Tanaka et al. 1997; Marijic et al. 2001)

	Mesenteric artery	Whole cell patch-clamp, real time RT-PCR and western blot	Confirmation of BK_{Ca} channel currents and expression	(Yang et al. 2013)
K_{ATP}	Coronary artery	Immunoprecipitation, RT-PCR and western blot	Confirmation of Kir6.1 and SUR2 expression	(Yoshida et al. 2004)
	Meningeal artery	RT-PCR and qPCR	Detection of Kir6.1 and SUR2B mRNA transcripts	(Ploug et al. 2008)
	Pulmonary artery	RT-PCR and patch-clamp	Confirmation of K_{ATP} channel currents and detection of Kir6.1 and SUR2B mRNA	(Cui et al. 2002)
K_v7	Adipose artery	Immunohistochemistry, qPCR, whole cell patch-clamp, and wire myograph	Confirmatiion of $K_v7.1$ & $K_v7.3$-5 expression, channel currents and their role in vasodilation	(Ng et al. 2011)
	Mesenteric artery	qPCR, and wire myograph	Confirmatiion of $K_v7.1$ & $K_v7.3$-5 mRNA and their role in vasodilation	(Ng et al. 2011)

1.4 Aims of this project

Numerous studies have demonstrated the benefits of fish oil intake and as a result it is currently one of the most used dietary supplements in the market. The complex mechanisms of fish oil-induced vasodilation can range from enhancement in NO production to regulation of BK_{Ca} channels (Table 1.1). However, most of these studies are limited to a certain type of vascular bed and n-3 PUFA. Furthermore, a significant amount of residual relaxation was reported indicating the presence of other unknown vasodilation mechanisms. Due to findings from previous studies indicating the role of BK_{Ca} channels, we hypothesised that other vascular potassium channels were possibly involved in n-3 PUFA-induced vasodilation. Therefore, my project was initially focused on fully characterizing the vasodilation pathways of both DHA and EPA using rat aorta (a conduit artery) and rat mesenteric artery (a resistance artery). These previously unidentified pathways were then investigated to determine whether a direct activation by n-3 PUFA was involved. The ultimate goal of this project is to facilitate the development of novel PUFA analogues that can target specific vasodilation pathways involved in providing therapeutic benefits against cardiovascular disorders. Although the use of animal models can bring some uncertainty in the transferability of the acquired data to a clinical setting, there is tremendous evidence demonstrating that the investigated pathways are also involved in the human vasculature. Through the use of different techniques in the field of molecular biology, electrophysiology and myograph, multiple studies with human arteries have demonstrated both the expression and the functional vasoactive role of the potassium channels that were investigated in this project (findings summarized in table 1.2).

Due to the presence of numerous vasodilation pathways that are dependent upon vascular endothelium and/or SMCs, this project was divided into three parts to effectively

characterize the mechanisms involved with n-3 PUFA-mediated vascular relaxation. The first part of the study involved the use of pharmacological inhibitors and wire myograph to:

i. Investigate the role of endothelium in n-3 PUFA-induced relaxation using rat arteries.
ii. Elucidate the endothelium-dependent vasodilation mechanisms of n-3 PUFAs in rat arteries.

Using patch clamp and myograph techniques, multiple studies have demonstrated the role of BK_{Ca} in both DHA and EPA mediated vasodilation (Hercule et al. 2007; Wang et al. 2011). Studies also indicate the role of BK_{Ca} in EET-induced vascular relaxation and most of these findings report an indirect stimulation of BK_{Ca} (Imig et al. 1999; Fukao et al. 2001; Dimitropoulou et al. 2007). One of these pathways includes the TRPV4 channel, which is also involved in the activation of SK_{Ca} and IK_{Ca}. Therefore, the second part of this study examined whether TRPV4 was directly modulated by n-3 PUFAs and my main aims were to;

i. Generate a stable cell line that allowed inducible expression of TRPV4.
ii. Determine whether the inducible expression system was functional.
iii. Verify whether n-3 PUFAs modulate TRPV4 channels expressed in the stable cell line.

It is evident that depending upon the type of vascular bed, n-3 PUFAs and their metabolites can act through diverse mechanisms (Table 1.1). It is also evident that these mechanisms are not always endothelium-dependent. A lot of the studies indicate the role of hyperpolarization, mostly through BK_{Ca}, in n-3 PUFA-mediated relaxation. Therefore, in the final part of my study, my aims were to:

i. Investigate the role of hyperpolarization-induced by potassium channels and characterize the channels involved in the relaxation mediated by n-3 PUFAs using wire myograph.

ii. Generate a stable cell line expressing the target potassium channel and verify its expression.

iii. Assess if the target potassium channel is directly modulated by n-3 PUFAs using whole cell patch clamp.

Chapter 2

Materials and Methods

2.1 Materials

2.1.1 Animal

Male Wistar Kyoto rats (WKY, 8-12 weeks, 200-300 g) were obtained from Harlan (Envigo) and were kept in a room inside the Bioresource Unit at the University of Reading with a 12h:12h dark:light cycle at 21°C with the humidity of 50±10% and ad libitum access to food and water.

2.1.2 Cell lines

Table 2.1 List of cell lines. *DMEM = Dulbecco's modified eagle's medium, FBS = foetal bovine serum and HEK = human embryonic kidney cells.

Cell line	Source	Medium
HEK* Flp-In T-REx-293	Invitrogen	DMEM*, FBS* (10% v/v), 5 μg/ml of blasticidin, 100 μg/ml of zeocin
HEK Flp-In T-REx-293 pcDNA5/FRT/TO (HEK_{VO})	See chapter 2, 2.3	DMEM, FBS (10% v/v), 200 μg/ml of hygromycin, 5 μg/ml of blasticidin
HEK Flp-In T-REx-293 pcDNA5/FRT/TO+TRPV4- HA (HEK_{TRPV4})	See chapter 2, 2.3	DMEM, FBS (10% v/v), 200 μg/ml of hygromycin, 5 μg/ml of blasticidin
HEK Flp-In-293	Invitrogen	DMEM, FBS (10% v/v)
HEK Flp-In-293 pcDNA5/FRT (HEK_{VC})	See chapter 2, 2.4	DMEM, FBS (10% v/v), 200 μg/ml of hygromycin,
HEK Flp-In-293 pcDNA5/FRT+SUR2B (HEK_{SUR2B})	See chapter 2, 2.4	DMEM, FBS (10% v/v), 200 μg/ml of hygromycin,
LentiX 293T	Clontech	DMEM, FBS (10% v/v)
HEK Flp-In-293 pcDNA5/FRT+ pLenti6.3/FRT/MCS (HEK_{VC1})	See chapter 2, 2.4	DMEM, FBS (10% v/v), 200 μg/ml of hygromycin, 10 μg/ml of blasticidin
HEK Flp-In-293 pcDNA5/FRT+SUR2B+ pLenti6.3/FRT/MCS+Kir6.1 (HEK_{KATP})	See chapter 2, 2.4	DMEM, FBS (10% v/v), 200 μg/ml of hygromycin, 10 μg/ml of blasticidin

2.1.3 Pharmacological agents

Table 2.2 List of pharmacological agents. *DDW = distilled deionised water and DMSO = dimethyl sulfoxide. Ref = reference for studies that investigated the potency of the pharmacological agents.

Chemical	Bath concentration	EC_{50}/IC_{50}	Diluent	Mechanism of action	Supplier	Cat. No.	Ref.
Acetylcholine	1 nM - 3 µM	35 nM	DDW*	M_3 receptor agonist	Sigma	A6625	(Cheng et al. 2002)
Apamin	50 nM	8 nM	DDW	SK_{Ca} blocker	Sigma	A9459	(Kohler et al. 2003)
Clotrimazole	1 µM	5 µM	DMSO	CYP inhibitor	Sigma	C6019	(Oyekan et al. 1991; Lischke et al. 1995)
DHA	10 nM - 30 µM	0.9-3.8 µM	Ethanol	Multiple	Sigma	D8768	-
EPA	10 nM - 30 µM	2.5-5.1 µM	Ethanol	Multiple	Sigma	E2011	-
Glibenclamide	1 µM	86 nM	DMSO	K_{ATP} blocker	Sigma	G0639	(Russ et al. 1997)
GSK1016790A	3 nM	10 nM	DMSO	TRPV4 activator	Sigma	G0798	(Willette et al. 2008)
HC-067047	1 µM	133 nM	DMSO	TRPV4 antagonist	Sigma	SML0143	(Everaerts et al. 2010)
Indometacin	10 µM	0.25 µM	DMSO	COX inhibitor	Sigma	I7378	(Kassab et al. 2017)
L-NAME	300 µM	3.1 µM	DDW	NOS inhibitor	Sigma	N5751	(Rees et al. 1990)
NONOate	1 nM – 3 µM	0.1 µM	DMSO	NO donor	Sigma	Sigma	(Hrabie et al. 1993)
TRAM-34	1 µM	20 nM	DMSO	IK_{Ca} blocker	Sigma	T6700	(Wulff et al. 2000)
Paxilline	1 µM	17 nM	DMSO	BK_{Ca} inhibitor	Sigma	P2928	(Sanchez and McManus 1996)
PNU37883A	300 nM - 3 µM	1 µM	DMSO	K_{ATP} blocker	Tocris	2095	(Wellman et al. 1999)
RN-1734	10-30 µM	3.2 µM	DMSO	TRPV4 blocker	Sigma	R0658	(Vincent et al. 2009)
U46619	5-100 nM	35 nM	DMSO	TP receptor agonist	abcam	ab144540	(Abramovitz et al. 2000)
XE991	1-30 µM	0.63 µM	DDW	Kv7 inhibitor	Tocris	2000	(Schroeder et al. 2000; Søgaard et al. 2001)

2.1.4 Antibodies

Table 2.3 List of primary and secondary antibodies. Antibody stocks were diluted in glycerol (50%, v/v) and stored at - 20 ℃. The extra dilution due to the glycerol was taken into consideration when diluting the antibodies. *HA = human influenza hemagglutinin, ICC = immunocytochemistry, IgG = immunoglobulin G, HRP = horseradish peroxidase, Kir6.1 = inward-rectifier potassium channel 6.1, SUR2B = sulfonylurea receptor 2B and WB = western blot.

Type	Antibody	Host	Dilution		Supplier	Cat No.
			WB*	ICC*		
Primary	β-actin	Mouse	1/10,000	-	Sigma	A5441
	HA*	Mouse	1/5000	1/500	Bioscience	901514
	Kir6.1*	Rabbit	1/1000	1/200	Sigma	P0874
	SUR2B*	Mouse	1/1000	1/200	Novus Biologicals	MABN511
Secondary	Goat anti-mouse-IgG*-AlexaFluor488	Donkey	-	1/1000	Invitrogen	A-21202
	Mouse-IgG-HRP*	Goat	1/10,000	-	Stratech	43C-CB1569-FIT
	Rabbit-IgG-HRP	Goat	1/10,000	-	Stratech	111-035-144-JIR
	Rabbit-IgG-Rhodamine Red-X	Donkey	-	1/1000	Stratech	711-295-152-JIR

2.1.5 Plasmid DNA

Table 2.4 List of plasmid DNA involved in creating stable cell lines expressing TRPV4 and K_{ATP} channels along with their respective controls (containing just the plasmid vector without the insert). Plasmids were stored at - 20℃. pLenti6.3/FRT/MCS (Roux et al. 2017), pcDNA5/FRT+HA and pcDNA5/FRT/TO+TRPV4 were kindly provided as gifts by Dr Graeme Cottrell (Hopkins building, University of Reading). pcDNA3+SUR2B and pcDNA3.1/Zeocin+ Kir6.1 were kindly sent as gifts by professor Andrew Tinker (William Harvey Heart Centre, Queen Mary University of London).

Ion channel	Plasmid	Selectable Marker	Source
TRPV4	pOG44	-	Invitrogen
	pcDNA5/FRT/TO	Hygromycin	Invitrogen
	pcDNA5/FRT+HA	Hygromycin	Dr Graeme Cottrell
	pcDNA5/FRT/TO+TRPV4	Hygromycin	Dr Graeme Cottrell
	pcDNA5/FRT/TO+TRPV4-HA	Hygromycin	See chapter 4, 2.2
K_{ATP}	pcDNA5/FRT	Hygromycin	Invitrogen
	pcDNA3+SUR2B	Neomycin	Andrew Tinker
	pcDNA5/FRT+SUR2B	Hygromycin	See chapter 5, 2.3
	pLenti6.3/FRT/MCS	Blasticidin	Dr Graeme Cottrell
	pcDNA3.1/Zeocin+ Kir6.1	Zeocin	Andrew Tinker
	pLenti6.3/FRT/MCS+ Kir6.1	Blasticidin	See chapter 5, 2.4

2.1.6 Competent bacterial cells

Mach1 and Stbl3 cells were purchased from Invitrogen. These cells were made competent using the protocol described by Inoue et al. (Inoue et al. 1990) and stored at – 80 ℃.

2.2 Wire Myograph

2.2.1 Dissection of rat aorta and mesenteric artery

Normal male WKY rats (250-300 g) were used for these experiments as studies have reported impairment of various vasodilation pathways in disease models; for example, reduction in the expression of BK_{Ca} channels and eNOS in SHR (Chou et al. 1998; Amberg and Santana 2003). Due to these findings, it is possible that additional unreported vasodilation pathways may also be impaired in disease models. Since my project was focussed on characterizing the mechanisms involved in n-3 PUFA-induced relaxation using a pharmacological approach, the presence of functional vasodilation pathways in the extracted arteries was essential as it allowed assessment of any significant modifications in n-3 PUFA-induced vasodilation before and after pharmacological treatment(s), using the same arterial segment. Therefore, due to this approach, healthy rats were used as the preferred mammalian model for the characterization of the relaxation response of n-3 PUFAs.

WKY rats were killed in accordance with the schedule one of the Animals (Scientific Procedures) Act 1986 and thus waived by the University of Reading Animal Welfare and Ethical Review Board. This procedure involved an inhaled overdose of isoflurane by the animal followed by an immediate cervical dislocation to ensure death. The fur and skin were then removed from either the abdominal (mesenteric artery) and/or thoracic area (aorta) depending on the type of arteries required for the experiment. For aorta, an incision was made along the upper section of the abdomen allowing removal of the rib cage and providing access to the inner organs. This was followed by the careful removal of the inner organs and oesophagus found on top of the thoracic aorta. The aorta was gently removed and immediately placed in ice-cold isotonic Krebs solution (Table 2.5).

For mesenteric artery, the intestines were carefully removed and immediately kept in ice-cold Krebs.

Table 2.5 Composition of Krebs buffer. Components were dissolved in DDW.

Chemical	Final concentration (mM)
$CaCl_2$ (1 M solution)	2.5
Glucose	11
KCl	3.6
KH_2PO_4	1.2
$MgSO_4.7H_2O$	1.2
NaCl	118
$NaHCO_3$	24

2.2.2 Selection of mounting supports and measurement of tension

Mulvany-Halpern wire myograph (Danish MyoTechnology, 620M) was used to examine arterial tension following application of different vasoactive compounds (Mulvany and Halpern 1976; Mulvany and Halpern 1977). Each myograph chamber was composed of two mounting supports each connected to a force transducer and a micrometer. These supports were initially adjusted depending upon the type of artery under investigation. For aorta, 200 µm pins were used as the mounting supports whereas for the mesenteric artery, myograph jaws were attached that enable the use of gold-plated tungsten wire (diameter: 25 µm). Measurement of tension was conducted using isometric force transducer connected to PowerLab (ML846; AD Instruments) and a computer with Labchart 7 software (AD Instruments). The force transducer was then calibrated using the step-wise force calibration procedure accessed from the myograph interface, whilst the signals were recorded using LabChart. The recorded signals were then converted from volts to millinewtons for each channel using the units conversion feature of LabChart.

2.2.3 Mounting of vessels

The tissue was then pinned in a dissection dish coated with silicone elastomer (Sylgard, World Precision Instruments) for removal of any surrounding connective and perivascular adipose tissue using fine forceps and micro surgical scissors under the microscope (Olympus SZX10, OLYMPUS). It was imperative that the blood vessels were not excessively stretched to avoid any damage to the inner walls.

2.2.3.i Aorta

The chambers were initially filled with fresh Krebs solution (5 ml) and the support pins were brought closer using the micrometer to facilitate the mounting. Approximately 2 mm segments of aorta were cut and carefully mounted onto the 200 µm pins. A small amount of tension (~1 mN) was applied to the vessels to prevent any detachment from the pins and vessels were washed (3x) with Krebs solutions. The vessels were then bubbled with 95% O2/5% CO_2 throughout the experiment and then subjected to zero tension followed by equilibration at 37ºC for 20 min.

2.2.3.ii Mesenteric artery

Following removal of the vein and adipose tissue surrounding the third order mesenteric arteries, a partial cut was made at a 45º angle on top of the vessel near the proximal end. The tungsten wire (length: ~2.2 cm) was then cannulated and the vessel was excised towards the distal end ensuring that approximately 2 mm of the arterial segment was obtained; once the vessel rested on the middle of the wire, the proximal end of the vessel was then carefully excised. The mounting jaws were then moved apart using the micrometer and the cannulated tissue was then transferred into the chamber filled with fresh Krebs solution. The wire was then secured (clockwise) to one of the mounting jaws using the screws on top. The jaws were then brought closer such that there was just

enough space to fit the wire. Another piece of wire (length: 2.2 cm) was then carefully cannulated into the vessel and fastened in the clockwise direction to the other mounting jaw. The jaws were then moved apart ensuring that there was minimal to no tension on the vessel. This allowed the wires to be aligned in parallel to each other and the screws were further tightened. Tissue was washed (3x) with Krebs solutions and bubbled with 95% O2/5% CO_2 throughout the experiment. It was then subjected to zero tension followed by equilibration at 37ºC for 20 min.

2.2.4 Normalisation

The DMT normalization module in Labchart 7 was then used to pre-stretch the arteries to an internal circumference (IC_{100}) that mimics the physiological transmural pressure of 100 mm Hg or 13.3 kPa in rats (Hansen and Bohr 1975; Mulvany and Halpern 1977; Danish Myo Technology 2017). Due to the length/tension relationship, arterial segments can be stretched to an internal circumference which allows the optimum interaction between actin and myosin filaments, generating the maximum response to vasoactive agents (Mulvany and Halpern 1977). Therefore, this procedure is important in not only standardizing experimental conditions but also in enhancing vascular reactivity (McPherson 1992). To achieve this, recording was initially started in Labchart and the channel of interest was selected, opening the DMT normalization window. The tissue endpoint values for the length of the arterial segment were then added (a1 = 0 and a2 = ~2 mm). The appropriate values for the wire diameter and micrometer reading were also added to the normalization window which allowed recording of the first data point. Small stepwise increase in tension was applied to the tissue using the micrometer to collect additional data points. A graph with the resting wall tension vs internal circumference was then plotted by Labchart 7 using the measured force and micrometer settings applied. The position of the micrometer required to achieve IC_{100} was then predicted using the

length/tension relationship that can be mathematically expressed with La Place's equation ;

Effective pressure = $\frac{2.\pi.Wall\ tension}{Internal\ circumference}$

The predicted setting was then applied which subsequently stretched the tissues to a standardized tension within the range of 7-13 mN (aorta) and ~3 mN (mesenteric artery). The tissue was then allowed to stabilize for 20 min.

2.2.5 Experimental protocol

Before starting any experiments, arteries were initially tested for functional endothelium by preconstricting the arteries with TXA_2 receptor (TP) agonist, U46619 (5-100 nM) followed by exposure to acetylcholine (ACh, 1 µM) to elicit arterial relaxation. Arteries demonstrating >90% of the maximum relaxation were used for subsequent myograph experiments. U44619 was preferred over other vasoconstrictors such as phenylephrine, as it elicited a robust sustained contraction of the arterial segment. Furthermore, an increased production of TXA_2 has also been reported in patients with pulmonary hypertension indicating its role in cardiovascular disorders (Christman et al. 1992), which further justified the use of U46619 in my experiments. U46619 (5-100 nM) was added to elicit a stable sub-maximal tone (~ 50-80% of maximum) to ensure that there was enough stimulation to achieve a stable sustained tone and at the same time to limit any physiological antagonism that could attenuate the relaxation effects of n-3 PUFAs. Cumulative addition with increasing concentrations of n-3 PUFA (10 nM - 30 µM) was used to investigate vascular relaxation. In most experiments, control concentration response curves to n-3 PUFAs were initially obtained which ensured that each experimental group had an internal control to compare various treatments. Although

randomisation of experimental group may be reduced by this approach, it lowers sampling error/variance as the tissue is its own control.

2.2.5.i Removal of endothelium from the arteries

To assess the role of endothelium in n-3 PUFA mediated relaxation, some experiments involved removal of the endothelium. A control response curve was initially obtained by preconstricting the artery with U46619 and relaxing it with n-3 PUFA. Using the same tissue, the inner arterial layer was gently rubbed with either a stainless-steel wire (diameter: 250 µm) (aorta) or gold-plated tungsten wire (diameter: 25 µm) (mesenteric artery). Due to the nature of this procedure, there was a risk of damaging and impairing the viability of the arterial segments; as a result, vessels had to demonstrate ≥90% of the original contractile tone to be selected for further experiments. Functional removal of endothelium was demonstrated in arteries with <10% relaxation to ACh (1 µM). The tissue was then constricted with U46619 to reach a stable sub-maximal tone followed by relaxation using n-3 PUFA

2.2.5.ii Pre-treatment of the arteries with pharmacological agents and high KCl Krebs:

The role of various vasodilation pathways in n-3 PUFA mediated relaxation of rat arteries were assessed using pharmacological agents (see table 2.2) and high KCl Krebs (30 mM, for inhibition of hyperpolarization mediated by potassium channels). The final potassium ion concentration of 30 mM was achieved via alligation, which involved the use of high KCl Krebs and normal Krebs. High KCl Krebs was prepared by replacing NaCl (118 mM) with KCl resulting in an overall potassium ion concentration of 122.8 mM [taking into account the additional presence of KCl (3.6 mM) and KH_2PO_4 (1.2 mM) in the buffer]. Appropriate volumes of high KCl Krebs (1.07 ml) and normal Krebs (3.93 ml) were then calculated using the following matrix setup and equations.

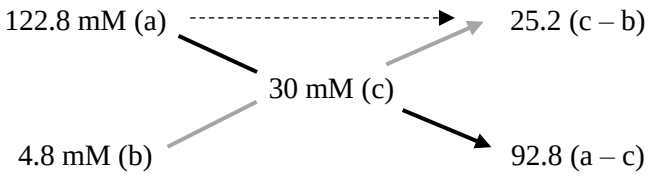

a = potassium concentration of high KCl Krebs

b = potassium concentration of normal Krebs

c = final desired concentration of potassium in the organ bath

Total parts of potassium ions = 25.2 + 92.8 = 118

Therefore, the volume of high KCl Krebs required to achieve a final potassium concertation of 30 mM in an overall volume of 5 ml = $5 \, x \, \frac{25.2}{118}$ = 1.07 ml.

Arterial segments preconstricted with U46619 were relaxed using n-3 PUFA to initially obtain a control response curve. Pharmacological agents were then incubated with the same arterial tissue for 20 min. The pre-treatment concentration for each agent was determined by its IC_{50} value, generally a starting concentration of 10x IC_{50} was used (Table 2.2). However, for some of the drugs due to problems with selectivity and its effect on the maintenance of contractile tone, the pre-treatment concentration had to be reduced. Arteries were then constricted with U46619 to a similar level of tone (~50-80% of maximum) as was achieved in the control experiment by adjusting the concentration of U46619, if necessary, followed by relaxation with n-3 PUFA. Multiple incremental pre-treatments were conducted using the same arterial segment as it allowed the same experiments to be ran in parallel using multiple wire myograph channels. This approach further validated the reproducibility of findings from each experimental group.

2.2.5.iii Pre-treatment of the mesenteric artery with DHA:

The effect of DHA on endothelium-dependent (ACh) and -independent (NONOate) vasodilation pathways were assessed using rat mesenteric artery. Control response curves

were initially obtained by relaxing the U44619 pre-constricted artery with either ACh (1 nM–3 µM) or NONOate (1 nM–3 µM). DHA (300 nM) was then incubated with the same arterial tissue for 1 hour. The tissue was then constricted with U46619 to a similar level of tone, as observed in the control experiment, and cumulatively relaxed with either NONOate or ACh.

2.2.6 Data analysis and statistical procedures

Results from the myograph experiments were expressed as mean±SEM of n experiments, where n refers to the number of biological repeats each acquired from a different rat. Data was processed using Microsoft excel (Office 365) and graphically presented using GraphPad Prism 5 (v5.0, GraphPad Software). Relaxation was expressed as percentage reduction of U46619-induced stable tone. Statistical analysis of the curves was carried out using two-way analysis of variance (ANOVA) and Bonferroni post-hoc test in GraphPad Prism 5. P-value of < 0.05 was considered as being statistically significant.

Potency (EC_{50}) and maximal relaxation (E_{max}) values were obtained for each experimental group using standard variable slope least squares fit based on the hill equation in GraphPad Prism 5. However, the maximal response was not always adequately defined as the highest concentration of n-3 PUFAs that could be achieved without solubility or vehicle effects was 30 µM, as a result, curve estimation was prone to error. To assess if there was an overall difference in either potency (EC_{50}) or maximum response (E_{max}) between DHA and EPA, pooled control curve data from both aorta and mesenteric artery were obtained and analysed using two-tailed t-test. P value of < 0.05 indicated a significant difference from DHA in the artery studied.

2.3 Generation and maintenance of HEK Flp-In T-REX-293 cells expressing TRPV4

2.3.1 Molecular cloning

2.3.1.i Generation of a 3' end DNA segment of TRPV4 without the stop codon using PCR

To enable the expression of the HA epitope tag which was added at the end of the TRPV4 gene, it was crucial to remove the stop codon present in the TRPV4 DNA sequence. I used polymerase chain reaction (PCR) to generate a DNA segment at the 3' end of the TRPV4 sequence without the stop codon using the forward and reverse primers shown in table 2.6. The PCR reaction mix was prepared according to table 2.7 The mix was then transferred into a MJ Mini thermal cycler (Bio-Rad) and the following settings were then used for the PCR reaction:

Steps	Temperature	Time	
1	98 ℃	3 min	
2	98 ℃	30 s	25 cycles, steps 2-4
3	55 ℃	30 s	
4	72 ℃	30 s	
5	72 ℃	10 min	

The first step of the PCR reaction is initialization which involves heat (98 ℃) activation of the DNA polymerase (New England Biolabs 2019). DNA is then denatured into two single strands by breaking the hydrogen bonds in the second step (Gibbs 1990; New England Biolabs 2019). The temperature of the reaction was then lowered to 55 ℃ to allow annealing of the primers to the denatured DNA strands. The temperature was then increased to 72 ℃ which enhances activity of DNA polymerase to synthesise new complementary DNA strands from the primer bound region. The PCR steps (2-4) were then repeated for 25 cycles to amplify the production of the DNA fragments. The final step of the PCR reaction allowed full elongation of any remaining denatured DNA

strands. The DNA obtained from the PCR reaction was then separated by gel electrophoresis and purified as described in section 2.3.1.iv and 2.3.1.v.

Table 2.6 Forward and reverse primer used to generate the 3' end DNA segment of TRPV4. Primers were obtained from Sigma and stored at -20 ℃.

Gene	Primers		Product size (base pair)
TRPV4	Forward	5'-TCATCCTCACCTTTGTGCTG-3'	506 bp
	Reverse	5'-GAGCGGGGCGTCATCAGT-3'	

Table 2.7 Composition of PCR mix. PCR reagents were obtained from New England Biolabs (NEB). *dNTPs = deoxyribonucleotide triphosphate.

Components	Final Concentration	Volume (µl)
DDW	-	31.5
5x reaction buffer (Q5)	1x	10
DNA template	20 ng	2
5 mM dNTPs*	200 µM	2
Forward primer (Table 2.6)	20 pM	2
Reverse primer (Table 2.6)	20 pM	2
DNA polymerase (Q5)	0.02 U/µl	0.5

2.3.1.ii Sanger sequencing

The obtained DNA was analysed using sanger sequencing which is a method that involves the use of dideoxynucleotides, which are nucleotides without the 3' hydroxyl group that involved in 5'-to-3' DNA synthesis (Sanger et al. 1977; L. M. Smith et al. 1985; Smith et al. 1986). Each dideoxynucleotide is uniquely labelled with a different fluorescent marker. Similar to the PCR reaction; nucleotides, primers and DNA polymerase are used in sanger sequencing to synthesise complementary DNA from the target sequence, however the addition of a dideoxynucleotide terminates this elongation process. This allows formation of DNA fragments of every possible length which are subsequently separated using capillary gel electrophoresis and the sequences of

nucleotides is determined by generating a chromatogram, via the detection of fluorescence emitted by dideoxynucleotides following laser-excitation. Therefore, this technique was an important tool in verifying whether the recombinant DNA contained the correct sequence of nucleotides. 20 µl aliquot of the sample DNA (100 ng/µl) was sent to "Source BioScience" for sequencing. The required information about the DNA including the forward and reverse primers were also provided. The chromatogram data was then analysed using SnapGene Viewer (version 4.1.9).

2.3.1.iii Restriction digest

Table 2.8 Composition of the mix for digestion by RE(s). For multiple digestion, the volume of different RE was altered such that it ensured the same level of activity for each enzyme. To prevent star activity the total volume of RE was kept at a maximum of 1µl in 20 µl (5% glycerol). *BSA = bovine serum albumin and RE = restriction enzyme.

Components	Final amount	Volume (µl)
DDW	-	Until 20
10x buffer [depending upon RE*(s) used]	1x	2
10x BSA* (1 mg/ml)	0.1 mg/ml	2
RE(s)	Varied	1 (Total)
DNA	1 µg for insert and 200 ng for vector	Varied

The full cDNA sequence of the plasmids were obtained and analysed using UniProt (an online resource for DNA sequence) (Anon 2018) and ExPASy translate (an online bioinformatics resource tool that allows the detection of the open reading frame) (ExPASy 2018). Restriction enzyme (RE) sites were identified using NEBcutter V2.0 (online resource tool for identifying RE sites) (New England BioLabs 2018). The optimal RE sites were selected by ensuring that: the sites flanked the insert in the correct

orientation, the size of the fragments was significantly different, RE shared similar buffer and incubation temperatures. The restriction digest mix (Table 2.8) was incubated overnight at 37 ℃. The following REs were used to obtain the required DNA fragments for the plasmid, pcDNA5/FRT/TO+TRPV4-HA (Table 2.4):

a) TRPV4 fragment = *Bam* HI and *Kpn* I

b) 3' end DNA segment of TRPV4 = *Kpn* I

c) HA fragment = *Eco* RV and *Xho* I

d) pcDNA5/FRT/TO fragment = *Xho* I and *Bam* HI

2.3.1.iv Separation (DNA electrophoresis)

1% agarose gel was made using 0.5 g of agarose and 50 ml of 1x Tris-acetate-ethylenediaminetetraacetic acid (TAE) buffer (Table 2.9).

Table 2.9 Composition of 50x TAE buffer dissolved in DDW. The 50x TAE was further diluted in DDW to make 1x solution.

Components	Final concentration
Tris/HCl	2 M
Glacial acetic acid	2 M
EDTA (0.5 M pH 8)	50 mM

This solution was microwaved for 1-2 min and swirled in 30 s intervals until the agarose completely dissolved. Subsequently, the solution was allowed to cool down for 3-5 min and 2 µl of the gel DNA stain, SYBR Safe (Invitrogen), was then added to the mix. Following levelling of the gel tray, the solution was poured and the appropriate comb was then clamped into the tray. The solution was left to solidify for 30 min. Whilst waiting the digested DNA was prepared by mixing it with the loading buffer (Table 2.10).

Table 2.10 Composition of 10x DNA loading buffer dissolved in DDW.

Components	Final amount
Xylene cyanol FF	0.25% (w/v)
Bromophenol blue	0.25% (w/v)
Glycerol	50% (v/v)
DDW	50%

The comb was then gently removed and placed into the electrophoresis unit filled with TAE buffer, ensuring that the gel was completely submerged. The DNA samples and the DNA ladder (NEB) were then loaded into the appropriate wells. The gel was ran at 80 V for approximately 1 h. The bands were then compared and analysed using the reference DNA ladder. Images of the DNA fragments were then captured using U:Genius 3 (Syngene) gel imaging system and U:Genius imaging software (version 3.0.7.0, Syngene).

2.3.1.v Gel extraction

DNA bands of interest were excised from the gel using a clean razor blade. Gel pieces were weighed and DNA was extracted using a QIAquick gel extraction kit according to the manufacturer's guidelines (QIAGEN 2015). Briefly, gel pieces were solubilized by adding it to buffer QG and heating it in a waterbath (50°C) for 10 mins. Buffer QG contains guanidine thiocyanate which is a chaotropic salt that facilitates the binding of DNA to the silica membrane present in the spin column (Shi et al. 2015). Isopropanol (1 gel volume) was then added and the mix was transferred into QIAquick spin column followed by centrifugation for 1 min at 17,000 *g*. Isopropanol and ethanol is used to precipitate the DNA from solution and further enhance binding to the column (Green and Sambrook 2017). The supernatant was then discarded and the column was centrifuged with buffer QG and subsequently with buffer PE for 1 min at 17,000 *g*. Buffer PE contains

ethanol which facilitates the removal of any excess salt (Green and Sambrook 2016). DNA was then eluted into a clean microcentrifuge tube using DDW.

2.3.1.vi Ligation of DNA fragments

Ligation experiments were conducted using 1:3 (plasmid:insert) ratio by volume as shown in table 2.11. The reaction was ran in parallel with a negative control containing the digested vector without the DNA insert at 14 ℃ for 4 h.

Table 2.11 Composition of the DNA ligation mix. For each ligation reaction, a negative control was ran in parallel. Ligation reagents were obtained from NEB.

Components	Final amount	Volume (µl)
DDW	-	Until 5
10x T4 DNA ligase buffer	1x	0.5
DNA (Plasmid:insert)	Ratio by volume of 1:3	Varied
T4 DNA ligase	1.5 Weiss U/µl	0.25

2.3.1.vii Bacterial transformation

Bacterial agar (1.5%, w/v) was added to 250 ml of bacterial growth medium super optimal broth (SOB) (Table 2.12) and the solution was sterilized using autoclaving. Using aseptic techniques sterile solutions of $MgCl_2$ (Final conc. 10 mM) and ampicillin (Final conc. 100 µg/ml) were then added to the agar solution next to a flame. The solution was then gently swirled and poured into bacterial plates (~12 plates). The plates were left to set for 30 min. Any moisture inside the plates was removed by incubating them at 37 ℃ for an hour, this was facilitated by placing the plates upside down with the lids partially opened. Plates were sealed with parafilm and stored at 4 ℃ until further use.

Table 2.12 Composition of SOB buffer dissolved in DDW. Buffer was sterilized through autoclaving.

Components	Final concentration
Tryptone	2% (w/v)
Yeast extract	0.5% (w/v)
NaCl	8.56 mM
KCl	2.5 mM

The water bath was initially set to 42 ℃ and the frozen stock of competent Mach1 (section 2.1.6) bacterial cells were placed in ice to allow thawing (~30 min). To reduce the sheer stress of pipetting, P200 pipette tips were cut to leave a wider bore. Competent cells (50 µl) were pipetted in a pre-chilled microcentrifuge tube. The ligation mixes (5 µl) were then gently added to the cells followed by gentle flicking of the tubes. The mix was left in ice for 30 min. Cells were then heat shocked by placing them in the water bath for 30 s and were immediately placed in ice for 5 min. Using aseptic condition that required working near a flame, 950 µl of SOB with catabolite repression (SOC) (Table 2.13) was added to the cells. Cells were then incubated at 37 ℃ for 1 h with shaking (250 RPM).

Table 2.13 Composition of SOC buffer dissolved in DDW. Buffer was sterilized through autoclaving.

Components	Final concentration
Tryptone	2% (w/v)
Yeast extract	0.5% (w/v)
NaCl	8.56 mM
KCl	2.5 mM
Glucose	20 mM

The transformed cells were then centrifuged at 3000 *g* for 3 min. The cell spreader was then sterilized by submerging it in ethanol and quickly passing it to through the flame. The spreader was then allowed to cool down. The excess supernatant was discarded by

tipping the tube. Cell pellet was resuspended in the remaining supernatant and pipetted onto the agar plate. Cells were then gently spread and the plates were incubated upside down at 37°C overnight. Plates were analysed the following morning and were sealed using parafilm and stored at 4°C until required.

2.3.1.viii Colony PCR

Table 2.14 Composition of colony PCR mix.

Components	Final Concentration	Volume (µl)
DDW	-	13.55
10x Taq buffer (Qiagen)	1x	2
Bacterial colony	-	2
5mM dNTPs (NEB)	0.1 µM	0.4
TRPV4 forward primer (Table 2.6)	0.5 µM	1
BGH reverse primer (Sigma)	0.5 µM	1
Taq polymerase (Qiagen)	$1.25x10^{-3}$ U/µl	0.05

The single colonies were initially labelled with a number at the bottom of the plate and picked by gently touching it with a P10 tip for screening using colony PCR. Each bacterial colony was then resuspended with DDW (10 µl) in a microfuge tube. A mix for colony PCR was prepared as described in table 2.14. 2 µl of the single colony was added to a PCR tube containing the colony PCR mix (18 µl).

The samples were then transferred into a MJ Mini thermal cycler (Bio-Rad) and the following settings were then used for the PCR reaction:

Steps	Temperature	Time	
1	94 °C	10 min	
2	94 °C	30 s	35 cycles, steps 2-4
3	55 °C	30 s	
4	72 °C	30 s	
5	72 °C	1 min	
6	10 °C	Forever	

As described earlier, sagner sequencing (3.1.ii) and gel electrophoresis (3.1.iv) were then used to analyse each sample. Using aseptic conditions, the remaining 8 µl of each positive clone was then inoculated in a sterile tube containing 5 ml of sterile SOB with $MgCl_2$

(Final conc. 10 mM) and ampicillin (Final conc. 100 µg/ml), and grown overnight (37 ℃, 250 RPM).

2.3.1.ix Bacterial glycerol stocks

1 ml of the overnight culture was transferred into a cryovial labelled with the name of the DNA, bacterial species, antibiotic resistance and date. 250ul of glycerol was then added and gently mixed. The stocks were stored at -80°C.

2.3.1.x Small scale plasmid preparation

Using the remaining bacterial culture, the DNA was extracted and purified with QIAprep Spin Miniprep Kit (Qiagen) according to the manufacturer's guidelines (QIAGEN 2012b). Briefly, the culture was centrifuged at 3500 *g* for 10 min and the supernatant was discarded. The bacterial pellet was initially resuspended in buffer P1 (250 µl) which contains ethylenediaminetetraacetic acid (EDTA) and ribonuclease A that are involved in the inhibition of deoxyribonuclease activity and degradation of RNA, respectively (Zhou et al. 1997). Buffer P2 (250 µl) was then added to elicit alkaline lysis which involves solubilization of the cell membrane and denaturation of DNA, via the action of sodium dodecyl sulfate (SDS) and sodium hydroxide respectively (Zhou et al. 1997). Subsequently, buffer N3 (350 µl) which contains potassium acetate was then added to neutralize the alkaline pH, facilitating renaturation of the single stranded DNA and precipitation of contaminants such as genomic DNA and cellular proteins (Zhou et al. 1997). The mix was then centrifuged for 10 min at 17,000 *g* and the supernatant was transferred into a QIAprep spin column followed by centrifugation for 1 min. The spin column was then washed with buffer PB (500 µl) and subsequently with buffer PE (750 µl) through centrifugation for 1 min/wash. These buffers contain isopropanol and ethanol which are used to precipitate the DNA from solution and enhance binding to the silica column (Green and Sambrook 2017). The residual ethanol was then removed by

centrifuging the column in an empty tube for 1 min. The column was then placed in a clean microcentrifuge tube and the DNA was eluted using sterile DDW. The purified DNA was then screened using restriction digest (3.1.iii) and DNA electrophoresis (3.1.iv) as described earlier.

2.3.1.xi Large scale plasmid preparation

250 ml culture was inoculated from the glycerol stock (3.1.ix) and transferred into 250 ml of sterile SOB with $MgCl_2$ (Final conc. 10 mM) and ampicillin (Final conc. 100 µg/ml). The culture was incubated overnight with shaking at 37 ℃, 250 RPM. DNA was then purified from the culture with EndoFree Plasmid Maxi Kit (Qiagen) according to the manufacturer's guidelines (QIAGEN 2012a).

Briefly, the culture was centrifuged at 5000 *g* for 20 min and the bacterial pellet was resuspended initially in buffer P1 (10 ml) followed by buffer P2 (10 ml with 5 min incubation) and subsequently in buffer P3 (10 ml). The mix was then centrifuged for 5 min at 5000 *g* and the supernatant was filtered using a QIAfilter cartridge. The supernatant was then incubated on ice with buffer ER (2.5 ml) for 30 min. Following equilibration of Qiagen-tip 500 with buffer QBT (10 ml), the supernatant was then added to the Qiagen-tip and purified using gravity flow. Buffer QBT contains the detergent triton-x-100 for further permeabilization of the cell membrane and sodium chloride along with isoprapanol facilitates the precipitation and binding of the DNA to the silica column (Green and Sambrook 2017). The Qiagen-tip was then washed (2x) with buffer QC (30 ml) and subsequently the DNA was then eluted using buffer QN (15 ml). Isopropanol (10.5 ml) was subsequently added to the eluted DNA. Both buffer QC and QN contain contain sodium chloride and isopropanol. The mix was centrifuged for 1 h at 4 ℃ and 5000 *g*. The pellet was then washed with endotoxin-free 70% ethanol (5 ml) followed by centrifugation at 5000 *g* for 10 min. The pellet was air-dried and resuspended in DDW

followed by centrifugation at 17,000 *g* for 1 min. The supernatant was then transferred into a clean tube and the DNA was analysed using the techniques described in 3.1.iii and 3.1.iv.

2.3.2 Cell culture

2.3.2.i Revival of frozen mammalian cells

Following removal of the frozen cells from liquid nitrogen, the cryovial was cleaned with 70% ethanol and inside a microbiological safety cabinet, the lid of the vial was partially loosened and retightened to release any pressure. The vial was immediately placed into a water bath (37 ℃) and allowed to thaw completely before the cells were added to sterile tube containing 9 ml of the appropriate warm culture medium (see table 2.1) and centrifuged at 100 *g* for 5 min. Cells were resuspended in 10 ml of medium and transferred into a labelled sterile T75 flask.

2.3.2.ii Culturing protocol

Cells were cultured in Dulbecco's Modified Eagle's medium (Sigma) at 37 ℃ in a humidified 95% (v:v) air/5% (v:v) CO_2. Every 2-3 days, the older medium was removed and disinfected. Fresh medium (10 ml) was then immediately added to the T75 flask. Flasks were then transferred into an incubator. Once the cells were approximately 90% confluent, the medium was removed and cells were washed with PBS without Ca^{2+} and Mg^{2+} (5 ml). Trypsin-EDTA (5 ml) was then added to the flask to detach the cells. The cells were incubated at 37 ℃ for 5 min. Cells were then resuspended in medium (5 ml) to neutralize trypsin. This mix was then transferred into a sterile tube and centrifuged at 100 *g* for 5 min. The pellet was resuspended in medium (10 ml) and cells were split at 1:5 ratio. The flask was then labelled with the new passage number and date prior to incubation. Cells were cultured for a maximum of 35 passages.

2.3.2.iii Cryopreservation of cells

Cells were counted and then resuspended in 90% FBS+10% DMSO at 1.2 x 10^6 cells/ml following passaging of the cells. 1 ml aliquots were then transferred into cryovials labelled with the passage number, date, culture medium used and the detailed description of cells. To ensure controlled freezing, the vials were then transferred into an isopropanol freezing container (Fisher scientific) and incubated overnight at -80 ℃. The vials were then stored in liquid nitrogen the following day and all the details regarding its location were recorded.

2.3.3 Stable transfection using PEI

Human embryonic kidney cells (HEK) Flp-In T-REx-293 were used to create stable cell lines expressing the TRPV4 channels. The Flp-In T-REx system allowed tetracycline-inducible expression of TRPV4. These cells contained Flp recombination target (FRT) sites which allowed integration of the expression vector, pcDNA5/FRT/TO (Invitrogen), into its genome as shown in Fig 2.1 (ThermoFisher 2010) (O'Gorman et al. 1991). The methods used to create this stable cell line are further explained below.

Cells were initially plated at approximately 1.5 x 10^6 cells per 35 mm well in antibiotic-free DMEM medium (10% FBS, v/v) resulting in 90% confluency the following day. Cells were divided into two groups which included a control group that was transfected with just the empty plasmid vector, pcDNA5/FRT/TO, (HEK_{VO}) and another group transfected with the vector containing the gene of interest or the insert, pcDNA5/FRT/TO+TRPV4-HA (HEK_{TRPV4}). The following day, medium was replaced with 1.5 ml of fresh antibiotic-free medium (10% FBS, v/v), 2 h prior to transfection. Whilst waiting, the transfection mix was prepared at 3:1 ratio of PEI (9 µg/well) and pOG44+DNA (3 µg/well). Polyethylenimine (PEI) is a cationic polymer that can form positively charged complexes with DNA and can subsequently bind to the anionic

structures of the cell surface, ultimately resulting in DNA internalization via endocytosis (Boussif et al. 1995). pOG44 is a vector that contains the gene for FLP recombinase which mediates integration of the plasmid into the cell genome using the FRT sites (Fig 2.1) (Buchholz et al. 1996; ThermoFisher 2012). The pOG44/DNA was prepared in 9:1 ratio (2.7 µg of pOG44:0.3 µg of either pcDNA5/FRT/TO or pcDNA5/FRT/TO+TRPV4-HA). pOG44 and DNA were initially added to 200 µl of DMEM medium (without antibiotics and FBS)/well followed by a 5 min incubation at room temperature. PEI was then added and the mix was allowed to incubate for 20 min at room temperature. The transfection mix (200 µl) was then slowly added in drops to each well. Cells were subsequently incubated for 2-3 days and transferred into 5x 10 cm dishes for each 3x wells from a 6 well plate. Cells were then selected using medium containing the appropriate antibiotics (Table 2.1) which was replaced every 2-3 days for 2-3 weeks.

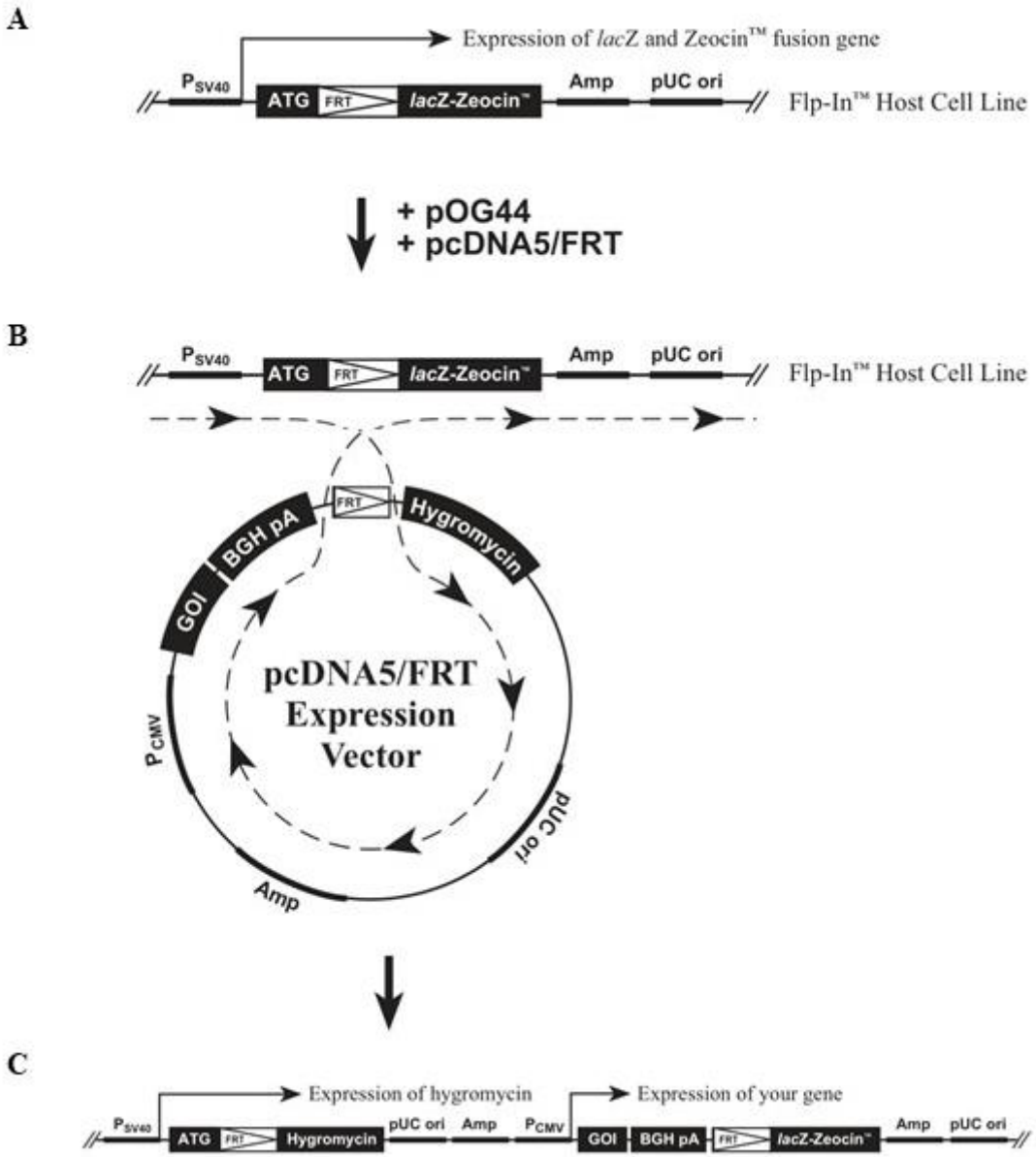

Fig 2.1 Flp-In System (**A**) The host mammalian cells were stably transfected with pFRT/*lacZeo* confering resistance to zeocin. (**B**) These cells were then cotransfected with pOG44 and the expression vector (pcDNA5/FRT) with the gene of interest (GOI). (**C**) The expression vector is integrated into the genome of the host cell due to homologous recombination between the FRT sites catalyzed by Flp recombinase expressed from pOG44. This allows expression of the GOI and changes antibiotic resistance of the cells from zeocin to hygromycin. Image taken from (ThermoFisher 2010).

2.3.4 Isolation of single mammalian cell colonies

Following selection of the transfected cells in antibiotics, some single cell colonies were identified under the microscope after 2-3 weeks. The colonies were labelled underneath the dish and prepared to be picked once enough cells were observed per colony, provided they were well separated from other colonies. A cloning cylinder was created by chopping the top part (accounting for 1/3 of the tube) of a sterile 500 µl tube and removing the lid. The top rim of the cloning cylinder was then coated with sterile vacuum grease. The 10 cm dish was then gently tilted freeing the cell colony from the medium, which allowed the formation of a tight seal around the cells once the cloning cylinder was placed on top of it. 80 µl of trypsin was then added to the cylinder and cells were incubated at 37 ℃ until complete detachment. Cells were then resuspended with 80 µl of the appropriate medium (Table 2.1) and transferred to a 24 well plate containing an additional 340 µl of medium per well. Clones were transferred to larger culture plates and flasks once they were confluent. After the cells reach confluency in a T25 flask, half of the cells were frozen down (section 2.3.2.iii) immediately whereas the other half remained in culture. Cells were later screened using immunocytochemistry (section 2.5) and western blotting (section 2.6) to detect expression of the protein of interest. Following confirmation of the expression, more stocks of cells were frozen down and the cells were expanded for experimentation.

2.4 Generation and maintenance of HEK Flp-In cells expressing K_{ATP}

The K_{ATP} channel is a hetero-octameric complex composed of four SUR subunits and four Kir6 subunits (Shi et al. 2012). The predominant subunits that form the vascular K_{ATP} isoform are SUR2B and Kir6.1 (Foster and Coetzee 2016). Using molecular cloning the recombinant plasmids for each subunit were initially constructed. Due to the size of the plasmids, a two-step process was used to transfer each plasmid into HEK cells to generate the stable cell line. The first step involved lipofectamine mediated stable transfection of the SUR2B subunit into HEK cells (HEK_{SUR2B}) and the second step involved lentiviral transduction of the Kir6.1 subunit into HEK_{SUR2B}. The detailed protocol is described in the following sections.

2.4.1 Molecular cloning

2.4.1.i Construction of the recombinant plasmids

RE digests were performed using the protocol detailed in section 2.3.1.iii. The following REs were used to obtain the DNA fragments (Table 2.4) for the plasmids, pcDNA5/FRT+SUR2B and pLenti6.3/FRT/MCS+ Kir6.1;

a) pcDNA5/FRT and SUR2B fragments = *Mfe* I and *Xho* I

b) pLenti6.3/FRT/MCS and Kir6.1fragment = *Bam* HI and *Psp* OMI

The DNA fragments were separated using gel electrophoresis (section 2.3.1.iv) and purified using the QIAquick gel extraction kit (section 2.3.1.v). DNA fragments were then ligated using the protocol detailed in section 2.3.1.vi.

2.4.1.ii Bacterial transformation

Bacterial transformation was performed using the protocol described in section 2.3.1.vii, however for experiments with plasmids: pLenti6.3/FRT/MCS and pLenti6.3/FRT/MCS+Kir6.1, the incubation temperature was set to 28 °C resulting in a

3-4 h increase in incubation duration. Due to the presence of 5' and 3' long terminal repeats (LTR) in the lentiviral vector, bacterial cells can utilize these sites to delete the GOI through homologous recombination (Sharan et al. 2009; Im et al. 2014). Proteins that suppress these recombination events are more active at lower temperature, hence these experiments were carried out at 28 ℃ (Personal communication, Dr Graeme S. Cottrell). Furthermore, smaller single colonies of bacteria were preferred to be picked as it was believed that the bigger colonies were likely to have the smaller DNA sequence (without GOI), containing only the ampicillin resistance gene between the two LTR regions which facilitated cell growth. Initial transformation was done using Mach1 cells followed by plasmid purification using QIAprep Spin Miniprep Kit (section 2.3.1.x). The plasmid was then screened with restriction digest (section 2.3.1.iii) and gel electrophoresis (section 2.3.1.iv). The purified plasmid was then transformed into Stbl3 (section 2.1.6) competent cells which are designed to suppress recombination events between LTRs (Al-Allaf et al. 2013). Cells were then spread onto agar plates as described in section 2.3.1.vii.

2.4.1.iii Plasmid preparation

Bacterial glycerol stocks were stored at -80 ℃ as described in section 2.3.1.ix. Both small and large scale plasmid preparation were conducted using the protocols described in section 2.3.1.x and 2.3.1.xi respectively, however Stbl3 cells containing either pLenti6.3/FRT/MCS or pLenti6.3/FRT/MCS+Kir6.1 were initially inoculated (28 ℃) in 5 ml of SOB overnight and further inoculated (28 ℃) in another 250 ml of SOB for 24 h to maximize cell growth.

2.4.2 Cell culture

Cell culture was performed using the protocol described in section 3.2, provided that any materials that came in contact with the virally transduced cells were initially disinfected before discarding.

2.4.3 Stable transfection using lipofectamine

HEK Flp-In-293 cells were used to stably transfect SUR2B subunits. Similar to Flp-In T-REx cells, these cells were also composed of FRT sites which allowed integration of the expression vector, pcDNA5/FRT (Fisher scientific), into the genome of the cells (O'Gorman et al. 1991) (ThermoFisher 2018). Cells were plated using the same protocol as described in section 2.3.3 with antibiotic-free medium. The following day the older medium was aspirated and 1.5 ml of fresh antibiotic-free medium (10% FBS, v/v) was added 2 h prior to transfection. pOG44+DNA (3 µg/well) and lipofectamine (8 µl/well) were incubated into two different tubes containing Opti-MEM (250 µl/tube) for 5 min at room temperature. Lipofectamine is a cationic liposome that is extensively used for the transfection of recombinant DNA. The positively charged head group of the liposome condenses the nucleic acid and facilitates interactions with the anionic cell membrane resulting in the cellular uptake of the target DNA (Dalby et al. 2004). The pOG44/DNA mix was prepared in 9:1 ratio (2.7 µg of pOG44:0.3 µg of DNA). The diluted pOG44/DNA was added to the lipofectamine and were incubated for 20 min at room temperature. This transfection mix was then added to each well in a 6 well plate and the plate was carefully rocked to allow the mix to evenly spread across the well. Following 2-3 days of incubation, cells were trypsinized and transferred to 5x 10 cm dishes for each 3 wells from a 6 well plate. Cells were initially incubated in antibiotics-free medium (10% FBS, v/v) for 6-8 hours and then selected using medium containing the appropriate

antibiotics which was replaced every 2-3 days (Table 2.1). Single colonies of the cells were then picked and screened as described in section 2.3.4.

2.4.4 Lentiviral production

Lentivirus is a subtype of retrovirus and is extensively used as a viral vector for gene delivery due to its high transduction efficiency. Lenti-X 293T cells are subclones of HEK 293 that are transformed with the adenovirus type 5 DNA and allows high-titer lentiviral production (Pear et al. 1993). These cells were transfected using the following viral plasmids which include; (i) pLenti6.3/FRT/MCS, the lentiviral transfer plasmid which contained the GOI (Kir6.1) flanked by two LTRs and a modified 3' LTR with the deletion of U3 region which enabled self-inactivation of the virus following transduction (Thermofisher 2010), (ii) pMDG.1, VSV-G, envelope plasmid which contained the gene for the G protein of the vesicular stomatitis virus (VSV-G) envelope, (iii) pRSV.rev, HIV- 1 Rev, this plasmid contained the gene for Rev transactivating protein and (iv) pMDLg/p.RRE, packaging plasmid which contained genes for viral structural proteins, enzymes and rev response element (RRE) [for detailed review regarding lentiviral production see (Merten et al. 2016)].

Lenti-X 293T cells were initially seeded at about 1.7 x 10^6 cells/dish in 4x 10 cm dishes. Briefly, following detachment of cells (10 ml) from a T75 flask, 8 ml of cells were diluted in 32 ml of antibiotic-free medium and 8 ml of this mix was added to each dish. After the cells were fully confluent, cells were trypsinized and diluted using 80 ml of antibiotic-free medium. The pooled cells were transferred (8ml/dish) to 10x 10 cm dishes coated with poly-D-lysine (Final conc.: 40µg/ml) and incubated overnight. Medium was then replaced with 8 ml of antibiotic free medium containing 4-(2-hydroxyethyl)-1-piperazineethanesulfonic acid (HEPES) and FBS (10% v/v) for each dish 2 h prior to transfection.

Table 2.15 Composition of the transfection mix per 10 cm dish for lentiviral production. (Roux et al. 2017)

Plasmids	Conc.
DNA of interest	9 µg
pMDG.1, VSV-G (envelope)	4.5 µg
pRSV.rev, HIV- 1 Rev	2.25 µg
pMDLg/p.RRE (packaging)	4.5 µg
Total Conc.	**20.25 µg**

Two transfection mixes were prepared according to table 2.15 for pLenti6.3/FRT/MCS (control) and pLenti6.3/FRT/MCS+Kir6.1. The plasmids were incubated in optimem (2ml/dish) for 5 min at room temperature. Based on the 3:1 ratio of PEI:DNA, 60.75 µg of PEI was then added to each mix and allowed to incubate for 20 min at room temperature. 2 ml of this mix was then gently pipetted to each dish and cells were incubated overnight. The medium was then replaced with antibiotic free medium containing HEPES and FBS (10% v/v). Lentivirus was then purified using ViraBind lentivirus purification kit (Cell Biolabs) according to the manufacturer's guidelines (CELL BIOLABS 2017).

Briefly, after 36-48 hours of incubation to facilitate the viral production, the medium was collected and centrifuged for 5 min at 1700 *g*. The supernatant was then filtered through a 0.45 µm syringe filter. The purification filter was then pre-washed with the provided washing buffer and then used for purifying the viral supernatant using gravity flow. The filter was then washed again and the virus was eluted using the elution buffer. 100 µl aliquots of the virus were stored at -80 ℃ following addition of glycerol (10%). These steps were then repeated to get another batch of the purified virus using the same purification filter.

2.4.5 Viral transduction

Stable HEK Flp-In-293 cell lines that were initially transfected with pcDNA5/FRT and pcDNA5/FRT+SUR2B were seeded at 1.5 x 10^6 cells/well in a 6 well plate with overnight incubation. The following day, HEK Flp-In-293 pcDNA5/FRT (control) cells (HEK_{VC}) were virally transduced with pLenti6.3/FRT/MCS (control) whereas HEK Flp-In-293 pcDNA5/FRT+SUR2B cells were virally transduced with pLenti6.3/FRT/MCS+Kir6.1 (HEK_{KATP}). Two different volumes of lentivirus were added to each well, which comprised of 5 µg/µl of polybrene with either 250 µl of lentivirus + 250 µl of antibiotic-free medium or just 500 µl of lentivirus. Cells were then rocked for 30 min at 4 ℃. 1.5 ml of antibiotic-free medium was then added to each well and cells were incubated for 72 h. Cells were then trypsinized and transferred to 2x 10 cm dishes/well containing medium with the appropriate antibiotic (Table 2.1) for selection.

2.4.6 Dilution cloning

In contrast to cationic polymer-based transfection, it was impossible to isolate monoclonal cells directly from the dishes following antibiotic selection due to high efficiency of lentiviral transduction, resulting in an increased survival and close proximity of the cell colonies. As a result, dilution cloning was implemented to obtain single cell colonies. Cells were initially pooled from each dish following trypsinization and using serial dilution approximately 50-100 cells were added to 10 cm dishes. Half of the remaining cells were then cryopreserved whereas the other half remained in culture. After about 2 weeks, single cell colonies were identified, picked and screened using the methods described in section 2.3.4.

2.5 Immunocytochemistry

2.5.1 Preparation of cells, materials and solutions

Glass coverslips (13 mm) were initially placed in 12 well plate and coated with poly-D-lysine (Final conc.: 40µg/ml) for 20 min which facilitated the attachment of cells. The coverslips were then washed with PBS (Phosphate buffered saline) (3x) and 2.5 x 10^5 cells were added to each well. For HEK Flp-In T-REx-293 pCDNA5/FRT/TO and pCDNA5/FRT/TO+TRPV4-HA cells, tetracycline (0.1 ug/ml) was added for overnight incubation to induce protein expression.

The following buffers were prepared before starting the experiment:

2.5.1.i PBS with Ca^{2+} and Mg^{2+} (20 ml)

Table 2.16 Composition of 10x PBS.

Components	Final concentration
NaCl	1.36 M
KCl	27 mM
Na_2HPO_4	101 mM
KH_2PO_4	18 mM

10x PBS, $CaCl_2$ (90 mM) and $MgCl_2$ (49 mM) stock solutions were initially prepared.

Table 2.17 Composition of PBS with Ca^{2+} and Mg^{2+} dissolved in DDW.

Components	Final concentration	Volume (ml)
10x PBS	1x	2
DDW	-	17.6
$MgCl_2$	0.49 mM	0.2
$CaCl_2$	0.90 mM	0.2

2.5.1.ii 4% paraformaldehyde (PFA) solution (100 ml)

A beaker containing 70 ml of DDW was initially microwaved for ~30s and 10 ml of 10x PBS was added. A stir bar was used to mix the solution inside a fume cupboard and 4 g of PFA was added to the solution. pH was increased using 10 M NaOH stock solution which was slowly added in drops until PFA completely dissolved. The solution was then

allowed to cool to room temperature and HCl was slowly added to get to pH 7.4. DDW was then added to make a final volume of 100 ml. Finally, the solution was filtered using 0.2 µm filter.

2.5.1.iii 5x blocking buffer (20 ml)

Table 2.18 Composition of blocking buffer. 2 ml aliquots of the buffer were stored at -20 ℃. Buffer was thawed and diluted to 1x with DDW before use.

Components	Final concentration
10x PBS	5x
Normal Horse Serum	10% (w/v)
Saponin	0.5% (w/v)
DDW	-

2.5.2 Experimental protocol

Cells were initially washed (3x) with PBS (Ca^{2+} and Mg^{2+}), care was taken not to directly pipette onto the cells to prevent cell detachment. Cells were then incubated with either 4% PFA (Anti-HA) or methanol (Anti-Kir6.1 and -SUR2B) for 20 min at 4°C. PFA and methanol are used as fixatives in order to preserve cell morphology and prevent degradation of the samples. Cells were again washed (3x) with blocking buffer for 5 min/wash on the shaker. Coverslips were then transferred to a glass plate covered with parafilm. 50 µl of primary antibody with the appropriate concentration (section 2.1.4, Table 2.3) was gently pipetted to each coverslip. The glass plate was then transferred into a tray with a wet paper towel soaked with DDW at the bottom and the tray was covered with a lid to prevent the coverslips from drying. Cells were then incubated overnight at 4°C. Coverslips were transferred back to the 12 well plate and washed (3x) with blocking buffer (500 µl/well). Whilst waiting for the wash, the appropriate concentration and volume of secondary antibody (section 2.1.4, Table 2.3) was prepared. Care was taken to limit direct exposure of the antibody to light, as this can result in photobleaching. The

coverslips were then transferred to the glass plate covered with parafilm. The secondary antibody (50 µl) was then gently pipetted onto the coverslip and the plate was transferred into the tray containing wet paper towel. Aluminium foil was used to cover the tray to prevent exposure to light and cells were incubated for 2 h at room temperature.

Following incubation, coverslips were again transferred back to the 12 well plate and washed (3x) with blocking buffer whilst rocking for 5 min/wash. To prevent exposure to light the well plate was covered with tin foil. The coverslips were then washed with PBS (3x). Microscope slides were then labelled and a small drop of mounting medium (Vectashield with DAPI, Vector Laboratories) was added to the slide for each coverslip. Coverslips were then gently mounted face down and excess mounting medium was carefully squeezed out using a paper towel. The edge of the coverslips was then sealed with nail polish and was allowed to dry before imaging.

2.5.3 Visualization of the cells using an epifluorescent microscope

Cells were visualized with Axioimager.A1 microscope (Zeiss) and images were acquired using Axiovision 4.6.3 imaging software (Zeiss) with either x20 (Zeiss EC Plan-Neofluar 20X/0.50) or x40 objective lens (Zeiss EC Plan-Neofluar 40X/0.75). The exposure mode was selected as “Fixed” which allowed comparison of the same fluorophore between different samples using the same level of exposure. Therefore, the cells transfected with the target protein DNA were initially used to measure and set the exposure, as these cells had the higher fluorescence compared to the control cells. Images were then processed using Axiovision4.

2.5.4 Visualization of the cells using a confocal microscope

Cells were prepared as described in section 2.5.2 and then visualized using A1-R confocal with resonant scanner microscope (Nikon) and x100 objective lens (Apo TIRF 100x/1.49

∞/0.13-0.20). Images were then processed with NIS Elements AR 4.51.00 (Nikon). Cells were located by selecting the Galvano scan mode in the graphical user interface panel. The zoom was set to 2 units and the image saturation was adjusted by changing the gain settings using a wavelength different from the fluorophore. After setting the focal plane at the centre of the cell, symmetric mode was then selected in the ND acquisition panel to obtain at least five optical sections with 0.5 µm intervals from bottom to top. Images were then processed using NIS Elements AR.

2.6 Western blot

2.6.1 Cell lysis

Table 2.19 Composition of lysis buffer (LB). pH was adjusted to 7.4 using HCl and 10 ml aliquots were stored at -20 ℃. 1 tablet of protease inhibitor (Fisher scientific) was added per 10 ml of LB before use.

Component	Final concentration
Tris base	50 mM
Sodium Fluoride	10 mM
Sodium Pyrophosphate	10 mM
Triton –X-100	0.1%

Western blotting was used to assess the protein expression of the different ion channels in the stable HEK cells following transfection and/or transduction. The experiments were conducted at 4 ℃ to prevent protein degradation. Cells were placed on ice and washed (3x) with PBS. 150µL of lysis buffer (LB) (Table 2.19) was added to each well in a 6 well plate. Cells were then rocked at 4 ℃ for 30 min. Lysed cells were then scraped from the wells and pipetted into a microfuge tube. Cells were then centrifuged for 10 min at 12,000 *g*, 4 ℃. The supernatant was then transferred to a new microfuge tube and kept in ice.

2.6.2 Quantification of protein concentration

Bicinchoninic acid (BCA) protein assay kit (Fisher scientific) was used to measure the protein concentration of our lysate samples. This method utilizes the biuret reaction which involves temperature-dependent reduction of Cu^{+2} to Cu^{+} ions mediated by the peptide bonds present in protein molecules (P. K. Smith et al. 1985). BCA then chelates Cu^{+} ions resulting in the formation of a purple-coloured complex that absorbs light at 540 nm. BSA (1 mg/ml) was used as the protein standard and diluted to different concentrations ranging from 0, 0.2, 0.4, 0.6, 0.8 and 1 ug/well to an overall volume of 10

µl per well in duplicates in a 96 well plate. 2 µl of each lysate sample was added in triplicates to each well with 8 µl of DDW. BCA (Reagent A) and $CuSO_4$ (Reagent B) were mixed in a 50:1 ratio (5 ml of BCA was added to 100 µl $CuSO_4$ which was enough for 24 wells). 200 µl of BCA:$CuSO_4$ mix was added to each well and the plate was incubated at 37 ℃ for 30 min. The absorbance for each well was then measured using Emax plate reader (Molecular Devices) at 540 nm and SoftMax Pro v5 software. Absorbance values were then averaged and subtracted with the value obtained from the blank standard in Microsoft excel. These values vs its concentration in mg/ml were then used to plot a standard curve in GraphPad Prism 5. The protein concentration for the lysate samples were then determined through interpolation of the curve. The samples were aliquoted at 30 µg of total protein and stored at -20°C until required.

2.6.3 Preparation of SDS-PAGE gel and protein lysates

2.6.3.i Assembling the gel apparatus

The front and back (1.5 mm spacers) glass plates were initially washed with DDW followed by acetone. These plates were then carefully inserted into the casting frame with the shorter plate at the front. To prevent any leakage, the frame was then placed on top of a flat surface which allowed the plates to slide down allowing the bottom edges of both plates to become completely parallel. The rubber strips were then placed at the bottom of the casting stand and the frame was tightly secured. DDW was poured in between the glass plates to confirm if there was any leakage. The plates were then drained and dried using paper towel.

2.6.3.ii Separating gel preparation

Polyacrylamide gels are extensively used for the separation and analysis of proteins samples. Tetramethylenediamine (TEMED) is used to catalyse free radical formation from ammonium persulfate which subsequently reacts with acrylamide monomers to

initiate the polymerisation chain reaction (Shi and Jackowski 1998). SDS is a detergent that can solubilise cell membranes and is also added to the gel to ensure that the protein molecules are linearized and have a uniform negative charge throughout electrophoresis (Peters 1991). About 7.5 ml of the separating gel (Table 2.20) was gently pipetted into the glass plates and subsequently 200 µl of water-saturated butanol was pipetted across the surface of the separating gel. This butanol mix was prepared by mixing equal volumes of DDW and butanol which produced two different layers, the top butanol layer was then used. The gel was left to polymerise for 30 min.

Table 2.20 Composition of 8% separating gel. 2.5 µl of TEMED was added in a fume cupboard. *APS = ammonium persulfate.

Component	Volume per 10 ml (8%)
DDW	6.3 ml
1.5 M Tris/HCl pH 8.8	2.5 ml
40% Acrylamide	2.0 ml
10% APS* (w/v)	100µl
10% SDS (w/v)	100 µl

2.6.3.iii Stacking gel preparation

Table 2.21 Composition of 3% stacking gel. 2.5 µl of TEMED was added in a fume cupboard.

Component	Volume per 5 ml (3%)
DDW	3.275 ml
0.5 M Tris/HCl pH 6.8	1.25 ml
40% Acrylamide	0.375 ml
10% APS (w/v)	50µl
10% SDS (w/v)	50 µl

The stacking gel (Table 2.21) was then prepared whilst waiting for the separating gel to set. Upon completion of the gel polymerisation, butanol was washed away using DDW and filter paper was used to gently dry the plates without touching the gel. The stacking gel was then added until it filled the plates and the comb (1.5 mm) was gently inserted

into the plate ensuring that no air bubbles were present. The gel was then left to polymerise for 30 min.

2.6.3.iv Reduction and denaturation of the protein lysates

Table 2.22 Composition of 5x SDS loading buffer. Buffer was filtered using 0.45 μm syringe filter and aliquots of 500μl were stored at -20°C.

Component	Final concentration
0.5 M Tris/HCl pH 6.8	250 mM
Glycerol	50% (v/v)
SDS	10% (w/v)
Bromophenol blue	-

Whilst waiting for the gel to polymerise, 5x SDS loading buffer (Table 2.22) was initially warmed at 37 ℃ and vortexed until the residues completely dissolved. β-mercaptoethanol was then added to the loading buffer in a fume hood to a final concentration of 2.5% (v/v). β-mercaptoethanol is a reducing agent that cleaves disulphide bonds and denatures protein molecules (Peters 1991). Bromophenol blue dye was added to track the migration of the protein sample whereas glycerol was added to increase the density of the buffer which allowed the sample to settle at the bottom of the well. An appropriate volume of 5x loading buffer (Final conc. 1x) was added to the lysate samples and the samples were briefly heated at 90 ℃. The lysates were then placed in ice allowing it to reach room temperature followed by centrifugation for 1 min at 10,000 *g*.

2.6.4 Gel electrophoresis

The electrophoresis works on the principle that glycine can acquire neutral, positive or negative charge states, depending on the pH (Peters 1991). Glycine becomes neutrally charged as it enters the stacking gel (pH 6.8) resulting in slower electrophoretic migration (Peters 1991). In contrast, chloride ions from Tris-HCl migrate at a higher speed and therefore protein molecules with intermediate electrophoretic mobility become

concentrated between glycine and chloride ions. This stacks the protein molecules into tight bands before it enters the running gel (pH 8.8). Due to the increase in pH, glycine then becomes negatively charged in the running gel and migrates at a faster speed, leaving the protein molecules behind to allow separation based on their size. The gel cassette was transferred into the electrode assembly and clamped with another gel or blank cassette on the opposite side. The assembly was then placed into the tank and the combs were carefully removed. Running buffer (Table 2.23) was then used to initially flush the wells to remove any unpolymerized acrylamide and then used to fill the tank. Subsequently, lysate samples and molecular weight markers were carefully pipetted into the appropriate wells. The lid was then secured on top of the tank and the gel was ran at constant current, 20 mA (0.02 A) per gel for about 3 h until the dye front ran to the bottom.

Table 2.23 Composition of 10x running buffer. DDW was added to dissolve the salts by stirring and HCl was used to adjust the pH to 8.3. For 1 litre of 1x running buffer, 10 ml of 10% SDS (w/v) was added to 100 ml of 10x running buffer and the buffer was further diluted with DDW (890 ml).

Component	Final concentration
Tris base	250 mM
Glycine	1.9 M

2.6.5 Transfer to membrane

Table 2.24 Composition of 20x transfer buffer. DDW was added to dissolve the salts by stirring and HCl was used to adjust the pH to 8.3. For 1 litre of final 1x transfer buffer, 200 ml of 100% methanol was added to 50 ml of 20x transfer buffer and the buffer was further diluted with DDW (750 ml).

Component	Final concentration
Tris base	960 mM
Glycine	781 mM
SDS	26 mM

Transfer buffer (Table 2.24) was initially kept in 4 ℃ and about 20 min prior to completion of gel electrophoresis, a 9 x 7.5 cm segment of polyvinylidene fluoride (PVDF) membrane (Immobilon-P, Merck Millipore) was immersed in 100% methanol for 15 s. The membrane was then transferred to DDW for 2 min and subsequently equilibrated by immersing it in transfer buffer for 10 min on a rocker. 2 thick filter papers and 2 fibre pads were soaked in transfer buffer. Following the completion of the electrophoresis, the gel cassette was removed and the glass plates were separated using the gel releaser by gently opening each corner of the plates. Gel was then removed from the plate and equilibrated in transfer buffer for 10 min. In a tray containing transfer buffer, the transfer cassette was initially placed with the clear side at the bottom. 1 fibre pad was placed on top of the cassette followed by a filter paper and the PVDF membrane was added on top. The gel was then placed and a wet filter paper was added onto the gel followed by a wet fibre pad. Using a roller any air bubbles between the PVDF membrane and the gel was removed. The cassette was carefully closed and placed into the mini-trans blot cell (Bio-Rad). A magnetic stirring bar was placed at the bottom and the tank was filled with transfer buffer. The cooling unit filled with dry-ice was transferred into the tank and the mini-trans blot cell was placed on top of a magnetic stirrer. The transfer was carried out at 1 A per cell for 1 h at constant current and the dry ice was replaced every 20 min. Following completion, the membrane was carefully immersed in PBS for 5 min on a rocker. PBS was then replaced with PBST/M (TWEEN 20, 0.1% and non-fat milk powder, 5%) and the membrane was further incubated for 1 h on a rocker. Due to the high affinity of the membrane for proteins, TWEEN 20 was used to prevent non-specific binding of the antibodies and the milk was used to block the free unbound sites of the membrane.

Depending on the size of the membrane (determined by the amount of protein samples used), appropriate concentration of primary antibody (Table 2.3) diluted in PBST/M was added to the membrane. Membrane was incubated overnight using a rocker at 4 °C. The following day, the membrane was washed with PBST for 5 min (6x) on a rocker and was incubated with an appropriate concentration of secondary antibody for 1 h at room temperature. Lastly, membrane was washed with PBST (6x) for 5 min whilst rocking.

2.6.6 Imaging of the membrane

A mix containing 2 ml of each of the enhanced chemiluminescence detection buffers (Clarity Western ECL Substrate, Bio-Rad) were prepared into a vial. The PBST was drained from the membrane by gently touching its edge on a paper tower and was transferred onto a tray. The detection buffer was then pipetted onto the membrane and was incubated for 1 min at room temperature. Tin foil was used to cover the tray to prevent any extra exposure to light. Membranes were then imaged by transferring into ImageQuant LAS 4000 mini (GE Healthcare Life Sciences) and using ImageQuantTM LAS 4000 mini software (version 1.2, GE Healthcare Life Sciences). An image of the protein ladder was initially taken followed by the membrane which was exposed at increasing intervals until the optimum image was obtained without overexposure. Finally, images were then labelled and saved as TIFF files.

2.7 Measurement of changes in $[Ca^{2+}]_i$ using Fluo-4 AM

HEK_{VO} and HEK_{TRPV4} cells were seeded (1 x 10^6 cells/well) onto a 6 well plate with coverslips (22x22 mm) coated with poly-D-lysine (Final conc.: 40 µg/ml). After 24 h, tetracycline (0.1 µg/ml, 16 h) was added to each well containing HEK_{TRPV4} cells. Cells were then washed with 3x PBS (with 1.3 mM $CaCl_2$) and were loaded in the dark with Fluo-4 acetoxymethyl (AM) ester (4 µM, 20 min, 37 °C) using the loading buffer (Table 2.25). Fluo-4 AM is a fluorescent dye that can bind to free $[Ca^{2+}]_i$ ions which results in an increase in its fluorescent intensity and is therefore commonly used for calcium assays (Gee et al. 2000). For some experiments, inhibitors of TRPV4 were also added with the Fluo-4. Cells were then washed 3x with the loading buffer. Furthermore, some experiments involved the initial pre-treatment of the cells with either DHA or EPA (30 µM, 1 h). The coverslips were then broken into smaller fragments using a diamond tipped scribe and the fragments were transferred into a 24 well plate containing the loading buffer.

Table 2.25 Composition of loading buffer. *HBBS = Hank's Buffered Salt Solution

Component	Final concentration
HEPES (Ca^{2+}/Mg^{2+} free) pH 7.4	20 mM
10x HBBS*	1x
BSA-protease free (10%, v/v)	0.1% (v/v)
$CaCl_2$ (1 M)	1.3 mM
DDW	-

Fluorescence was then measured (1.2 s intervals) at 488 nm excitation and 506 nm emission wavelengths using a Nikon Eclipse TE2000-5 inverted microscope with 40x objectives (Nikon Plan Fluor 40x/1.30 ∞/0.17 WD 0.2). Baseline fluorescence was initially measured for 30 s before the drug [n-3 PUFA (30 µM) or GSK1016790A (3 nM, GSK)] was applied and the responses were measured for an additional 370 s prior to the application of ionomycin (10 µM). WinFluor V3.9.1 (University of Strathclyde Glasgow)

was then used to obtain and export the images into TIFF files. Subsequently, ImageJ (1.51j8, National Institutes of Health) was used to analyse the imported images by initially selecting the cells as regions of interest (ROI) using the selection tool. The ROI manager was then opened to add each ROIs and multi measure their fluorescence intensity (mean grey value). Traces were then generated using Microsoft excel (Office 365) as shown in Fig 2.2 and Fig 2.3. The values for the mean baseline fluorescence along with the maximum fluorescence induced by the drug (n-3 PUFA or GSK) and ionomycin were then obtained using the traces. Data was then processed using the following equations:

$a = \frac{b}{c}$ and $d = \frac{e}{c}$

b ($HEK_{TRPV4+Tet}$ cells) = maximum fluorescence induced by GSK – mean baseline fluorescence

c = maximum fluorescence induced by ionomycin – mean baseline fluorescence

e = maximum fluorescence induced by GSK (following treatments) or n-PUFA – mean baseline fluorescence

Values were then expressed as % response,

Therefore, $\frac{d}{a} \times 100$

Fluorescence response for the representative traces were expressed as a % of the maximum response mediated by ionomycin. Results for the bar graph were expressed as mean % response ($\frac{d}{a} \times 100$)±SEM of n experiments, where n refers to each experiment carried out on a different day and data was graphically presented using GraphPad Prism 5. Statistical analysis was carried out using one-way analysis of variance (ANOVA) and Bonferroni post-hoc test in GraphPad Prism 5. P-value of < 0.05 was considered as being statistically significant.

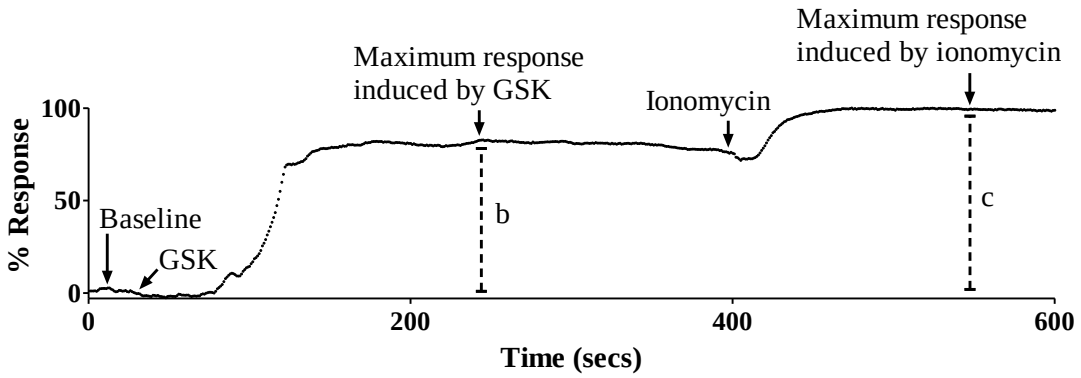

Fig 2.2 Original representative trace demonstrating the effect of GSK and ionomycin in $HEK_{TRPV4+Tet}$ cells. Baseline fluorescence was initially measured for 30 s prior to the application of GSK (3 nM). Ionomycin (10 µM) was applied at 400 s and fluorescence was measured for an additional 200 s to obtain the maximum response. Values for the mean baseline response along with the maximum response induced by GSK and ionomycin were obtained as indicated by the arrows.

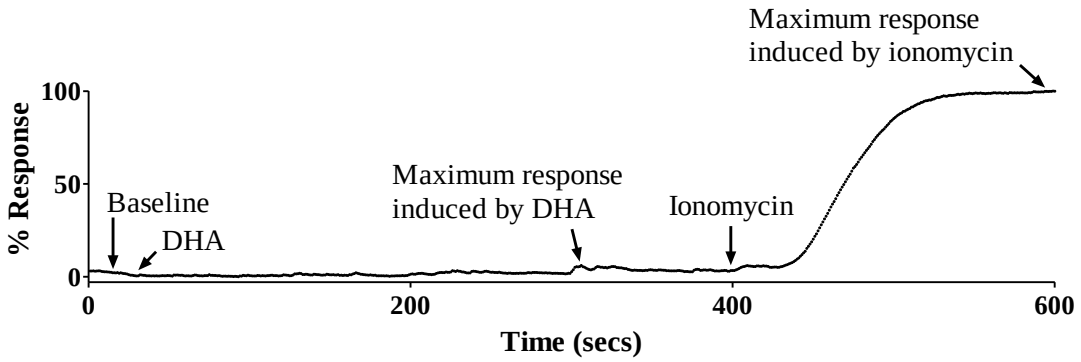

Fig 2.3 Original representative trace demonstrating the effect of DHA and ionomycin in $HEK_{TRPV4+Tet}$ cells. Baseline fluorescence was initially measured for 30 s prior to the application of DHA (30 µM). Ionomycin (10 µM) was applied at 400 s and fluorescence was measured for an additional 200 s. Values for the mean baseline response along with the maximum response induced by DHA and ionomycin were obtained as indicated by the arrows.

2.8 Patch clamp electrophysiology

Table 2.26 Composition of intracellular and extracellular patch clamp buffers. For intracellular buffer: KOH was used to adjust the pH to 7.2 and 1 ml of filtered (0.2 µm) aliquots were stored at -20 ℃. For extracellular buffer: NaOH was used to adjust the pH to 7.4 and buffer was stored at 4 ℃.

Intracellular buffer		**Extracellular buffer**	
Component	**Final concentration (mM)**	**Component**	**Final concentration (mM)**
KCl	110	KCl	4
$MgCl_2 \cdot 6H_2O$	1	$MgCl_2 \cdot 6H_2O$	1
EGTA	10	NaCl	130
HEPES	10	HEPES	10
MgATP	3	D-Glucose	10
NaADP	1	$CaCl_2$	1.8

The activation of K_{ATP} channels by n-3 PUFAs was further investigated using whole cell patch clamp. Depending upon the experimental plan, HEK_{VC} and/or HEK_{KATP} cells were seeded at 2.5 x 10^5 cells/well in a 6 well plate with coverslips and incubated overnight.

2.8.1 Intracellular and extracellular buffers

The intracellular buffer was prepared using the recipe shown in table 2.26. The buffer was then filtered (0.2 µm) and 1 ml aliquots were stored at -20 ℃. The intracellular buffer was thawed in ice prior to use for experiments. 500 ml of the extracellular buffer was prepared using the recipe from table 2.26 and stored at 4 ℃.

2.8.2 Patch pipettes

Glass capillaries (BF150-86-10, Sutter) were vertically pulled using a Narishige PP-830 puller (Narishige Group) to make patch pipettes with a resistance of ~3 MΩ. The double pull setting was incorporated where the first and the second pull were conducted at 62 ℃ and 49 ℃ respectively. Multiple patch pipettes were prepared before starting any experiments.

2.8.3 Acquiring giga seal

Cells were initially transferred into the recording chamber and a single isolated cell was positioned at the centre of the microscope. A patch pipette was filled with the intracellular buffer and was attached to the pipette holder. A light positive pressure was applied by gently attaching a 1ml syringe to the tube connected to the pipette holder. Using the coarse setting, the micromanipulator was used to lower the pipette into the bath until it was just above the cell. A rectangular current response was observed due to the test pulse (10 mV, 100 Hz) along with the resistance of the pipette (~3 MΩ) in pClamp 10.6 software (Molecular devices). The value for the pipette resistance was recorded and the offset was electronically set to zero using the MultiClamp 700B commander software (Molecular devices). The pipette was then lowered using the fine setting of the micromanipulator until the tip touched the cell, which was indicated by a reduction in current and an increase in pipette resistance of not more than 1 MΩ. The syringe was immediately removed to release the positive pressure, facilitating the formation of a giga Ω seal (characterised by increase in resistance to >1 GΩ) and the voltage was held at -40 mV. In some cases, additional application of suction was required to enhance seal formation. This resulted in the cell-attached patch clamp configuration which led to the

production of fast capacitive transients due to the pipette's capacitance. These transients were then electronically cancelled using the MultiClamp 700B commander software.

2.8.4 Whole-cell patch clamp

To achieve the whole cell configuration, a negative pressure was applied to the pipette to break through the membrane, with mouth pipetting using the tube connected to the pipette holder. This resulted in the production of slow capacitive transients due to the formation of a series circuit consisting of the cell capacitance and the series resistance (R_s, pipette resistance + access resistance), also known as the RC circuit. To avoid any detrimental effects of the RC circuit when clamping the voltage, the capacitance and R_s were compensated electronically using MultiClamp 700B commander software. The series resistance was compensated to 70% to avoid any oscillation in the positive feedback (ringing) mediated by a higher R_s compensation (Walz et al. 2002). The values for series resistance and the membrane capacitance were recorded. Whole-cell patch–clamp recordings were performed using MultiClamp 700B amplifier (Molecular devices). Current signals were filtered at 2 kHz and sampled at 10 kHz using Axon Digidata 1550B (Molecular devices). Currents were recorded using a ramp protocol (-150 to +50 mV over 1 s with a holding potential of -80 mV) with pClamp 10.6. Briefly, the ramp protocol was used to initially measure the baseline currents for 10 s. Changes in the current signals were recorded following the initial application of the vehicle followed by the pharmacological agents until the responses plateaued. Finally, an inhibitor in combination with the same agonist was used until maximum reduction in the agonist response was achieved.

2.8.5 Data analysis

Peak current values at +40 mV were obtained from pClamp 10.6 and the mean current-density (pA/pF) was calculated in Microsoft Excel. Graphs were plotted using GraphPad Prism 5. Results were expressed as mean±SEM of n experiments, where n refers to a single individual cell from a separate cover slip. Statistical analysis was carried out using one-way analysis of variance (ANOVA) and Bonferroni post-hoc test in GraphPad Prism 5. P-value of < 0.05 was considered as being statistically significant.

Chapter 3

The role of endothelium in n-3 PUFA-mediated vasodilation

3.1 Introduction

The inner endothelium layer of blood vessels has an important role in the production of various vasodilators including NO, PGI_2 and EDHFs such as EETs (Bunting et al. 1976; Dusting et al. 1977; Chen et al. 1988; Shimokawa et al. 1996; Forstermann and Münzel 2006; Edwards et al. 2010). Stimulation of M_3 receptors can result in subsequent activation of eNOS which can facilitate the production of NO (Marlettaz 1993). NO can then diffuse into the underlying SMCs and enhance PKG activity, leading to the activation of MLCP which subsequently inhibits vasoconstriction (Wu et al. 1996; Lee et al. 1997). The metabolites of AA, such as PGI_2 and EETs, have also been reported to induce vasodilation following enzymatic metabolism by COX and CYP respectively (Silva et al. 2016; Fleming 2016). PGI_2 can activate IP receptors present in SMCs which augments PKA activity resulting in vascular relaxation (Majed and Khalil 2012). CYP-derived EETs are also involved in eliciting relaxation of vascular SMCs through mechanisms that activate potassium channels such as BK_{Ca} channels (Li et al. 2002; Archer et al. 2003; Campbell et al. 2006; Dimitropoulou et al. 2007). n-3 PUFAs can compete with these enzymes to produce metabolites that are also involved in vasodilation, these include the COX-derived series-3 PGs along with CYP-derived EpETEs and EDPs (Arnold, Konkel, et al. 2010; Thomson et al. 2012; Engler et al. 2000; Ye et al. 2002; Hercule et al. 2007).

n-3 PUFAs have been reported to improve the ability of endothelium to induce vasodilation through mechanisms that enhance production of NO and COX metabolites (Tagawa et al. 1999; Engler et al. 2000). Both DHA and EPA have been reported to augment NO production in rat aorta and bovine coronary arteries respectively (Hirafuji et al. 2002; Omura et al. 2001). In aging spontaneously hypertensive and ApoE KO mice, supplementation of n-3 PUFAs also led to enhanced NO production (Raimondi et al.

2005; Casós et al. 2010). These findings were consistent with clinical studies; for example, with patients suffering from coronary artery disease, treatment with EPA led to improvements in NO-dependent vasodilation response (Tagawa et al. 1999). There is also evidence indicating that both DHA- and EPA-mediated relaxations of rat aorta were sensitive to the blockade of COX (Engler et al. 2000; Sato et al. 2014). Furthermore, n-3 PUFA supplementation was reported to attenuate constriction of human forearm resistance arteries via COX-dependent pathway (Chin et al. 1993).

EETs, CYP metabolites of AA, were also reported to induce vasodilation in canine coronary arteries through activation of K_{Ca} channels (Oltman et al. 1998) and it was later confirmed that BK_{Ca} was the subtype involved (Fukao et al. 2001). Similarly, CYP epoxygenase metabolites of DHA, EDPs, were also reported to activate BK_{Ca} channels resulting in hyperpolarization of vascular SMCs derived from porcine coronary arteries (Ye, Zhang et al. 2002). Acute application of DHA was reported to elicit concentration-dependent increase in BK_{Ca} currents in rat coronary vascular SMCs (Lai, Wang et al. 2009). In addition, in isolated rat coronary arterial tissues the blockade of BK_{Ca} channels completely abolished DHA-induced vasodilation (Wang, Chai et al. 2011). The underlying mechanism was reported to involve the release of calcium from sarcoplasmic reticulum mediated by EDPs in rat coronary arteries, resulting in subsequent activation of BK_{Ca} channels. Furthermore, a reduction in the blood pressure was observed following intravenous administration of DHA in wild type mice but not in BK_{Ca} KO mice (Toshinori Hoshi, Wissuwa, et al. 2013).

EDH pathway is another major vasodilation pathway predominantly associated with maintaining resistance arterial tone and involves the K_{Ca} channels, especially SK_{Ca} and IK_{Ca} (Ozkor and Quyyumi 2011; Edwards et al. 2010; Shimokawa et al. 1996). Most of the research demonstrates that DHA and CYP-derived metabolites of both DHA and EPA

are involved in the activation of BK_{Ca} channels (Patterson et al. 2002; Lai et al. 2009; Ye et al. 2002; Hercule et al. 2007), however, currently there is no evidence indicating the involvement of SK_{Ca} and IK_{Ca} channels in n-3 PUFA-mediated relaxation. At present there is only one study that demonstrated DHA-mediated inhibition of IK_{Ca} channels expressed in HEK cells (Kacik et al. 2014).

As indicated by table 1.1 (chapter 1), mechanisms associated with n-3 PUFA-mediated relaxation can differ depending upon factors such as the size of the artery, the type of n-3 PUFAs and its metabolites. However, most of these studies are limited to one type of n-3 PUFA and a specific vascular bed. Therefore, the main aim of this study was to investigate the vasodilation pathways of both n-3 PUFAs, DHA and EPA, using a conduit artery (aorta) and a resistance artery (mesenteric artery), allowing a detailed characterisation and comparison of any heterogeneity involved with the vasodilation mechanisms of each n-3 PUFA.

3.2 Results

3.2.1 Effect of endothelium removal in n-3 PUFA mediated vascular relaxation

The endothelial layer is involved in the regulation of various vasodilation pathways including NO, COX, CYP and EDH (Forstermann and Münzel 2006; Bunting et al. 1976; Dusting et al. 1977; Chen et al. 1988; Shimokawa et al. 1996; Ozkor and Quyyumi 2011; Edwards et al. 2010), therefore I investigated the role of endothelium in n-3 PUFA mediated vascular relaxation. Using wire myograph (chapter 2, section 2.2), the relaxant effect of n-3 PUFAs were recorded before and after the removal of endothelium from the arteries. Arteries demonstrating <10% relaxation to ACh were considered to have functional removal of endothelium. Cumulative administration of DHA and EPA individually led to potent relaxation of both mesenteric artery and aorta. Relaxation was expressed as percentage reduction of U46619-induced stable tone and statistical analysis of the curves was carried out using two-way ANOVA and Bonferroni post-hoc test.

Representative traces demonstrating the effect of endothelium removal in DHA-induced relaxation of rat mesenteric artery and aorta are shown in Fig 3.1 and Fig 3.2 respectively. In rat mesenteric artery, endothelium removal led to partial inhibition of DHA-induced vascular relaxation [Log EC_{50}; -5.79±0.04 (Control) and -5.56±0.05 (Endothelium removed)] (Figs 3.3A) (n=5, $P<0.05$) whereas relaxation mediated by EPA remained unaffected (Figs 3.3B) (n=6). In contrast, endothelium removal attenuated EPA-induced relaxation of rat aorta [Log EC_{50}; -5.25±0.03 (Control) and -5.11±0.05 (Endothelium removed)] (Fig 3.4B) (n=6, $P<0.05$). However, the relaxation elicited by DHA was not modified following removal of the endothelium in rat aorta (Fig 3.4A) (n=7).

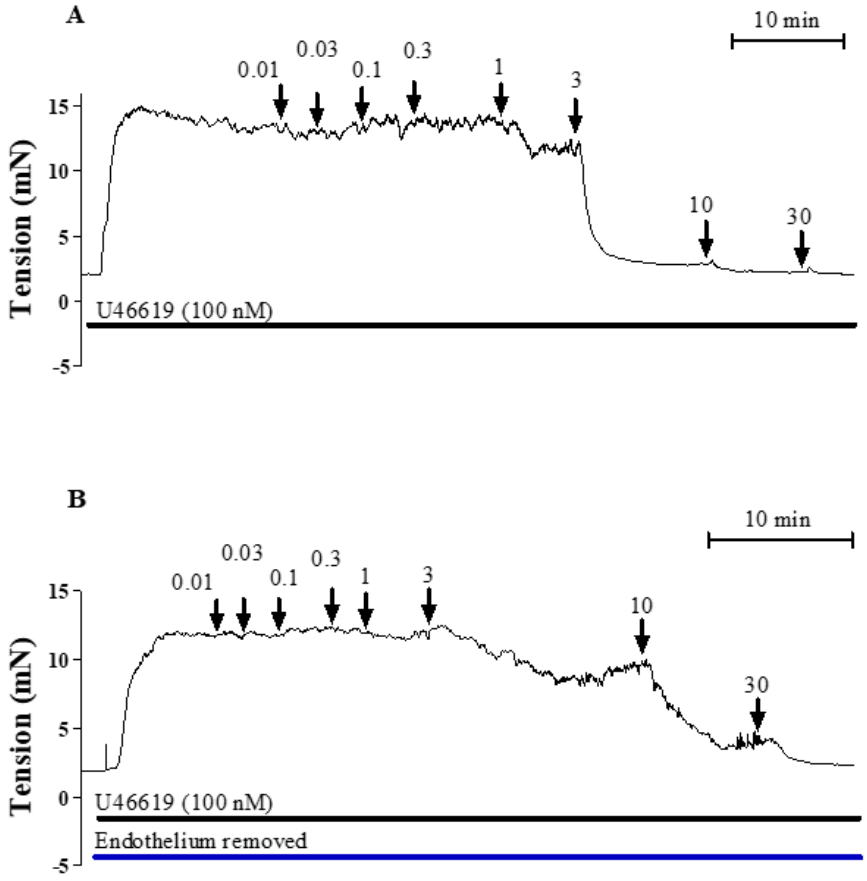

Fig 3.1 Original representative traces demonstrating the effect of endothelium removal in DHA-induced relaxation of rat mesenteric artery. After initially obtaining the control response curve, changes in vascular tone were recorded following removal of the endothelium from the same arterial segment. DHA was cumulatively added (0.01 – 30 μM) to induce vascular relaxation as indicated by the arrows.

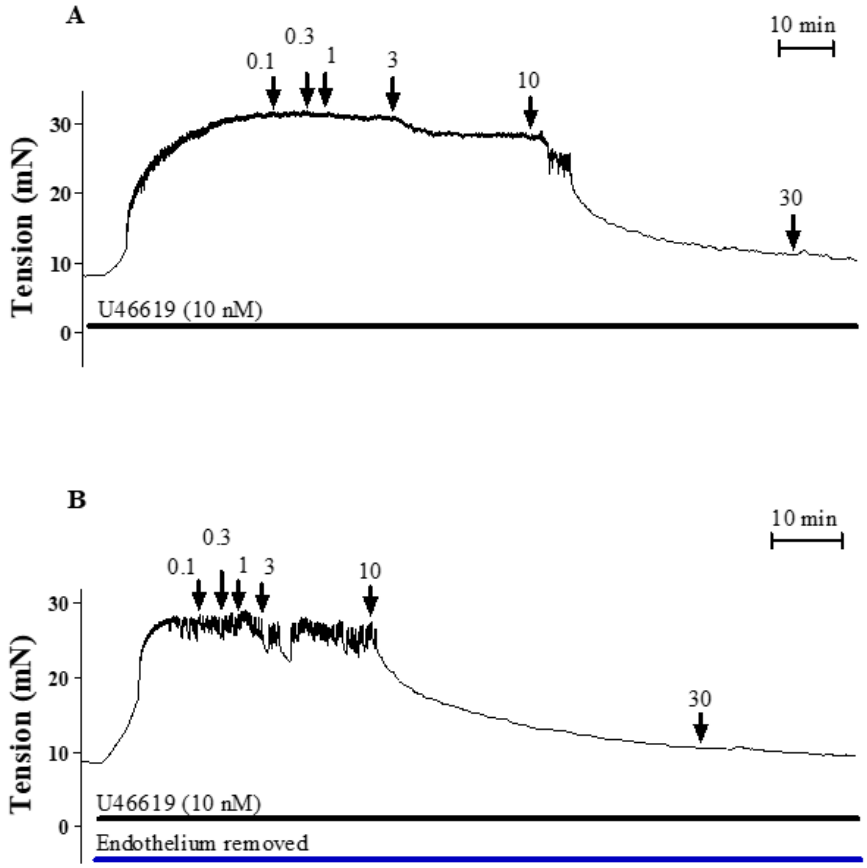

Fig 3.2 Original representative traces demonstrating the effect of endothelium removal in DHA-induced relaxation of rat aorta. After initially obtaining the control response curve, changes in vascular tone were recorded following removal of the endothelium from the same arterial segment. DHA was cumulatively added (0.1 – 30 μM) to induce vascular relaxation as indicated by the arrows.

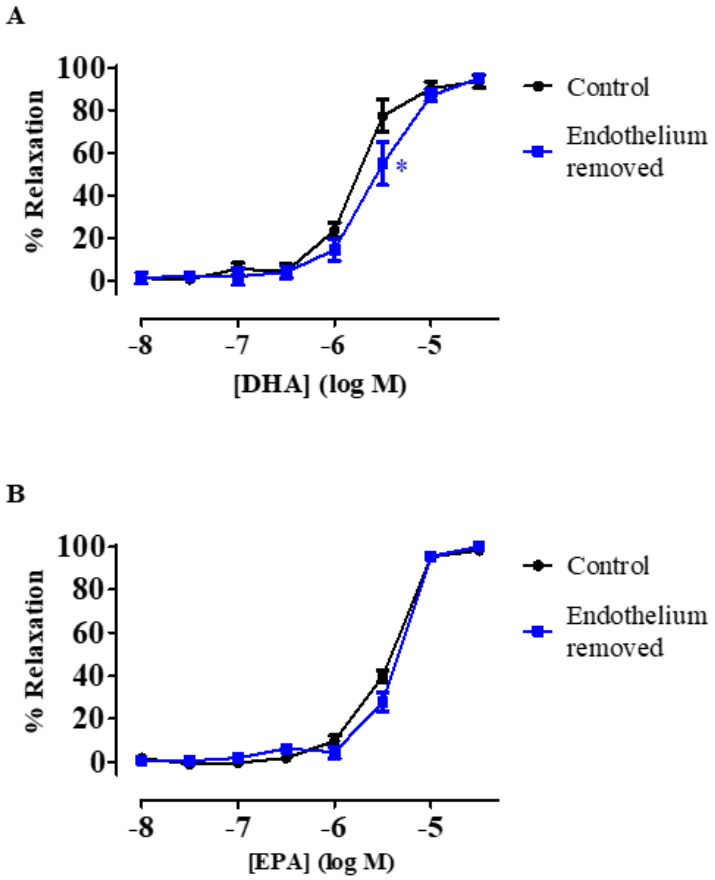

Fig 3.3 Concentration response curves demonstrating relaxation mediated by (A) DHA (*n*=5) and (B) EPA (*n*=6) in rat mesenteric artery before and after the removal of endothelium. Using wire myograph, changes in n-3 PUFA (10 nM – 30 µM) mediated relaxation were recorded by initially obtaining a control response curve followed by endothelium removal from the same arterial segment. Data are expressed as mean±SEM. *P<0.05 indicates significant difference from the control curve as determined using two-way ANOVA with Bonferroni post-test.

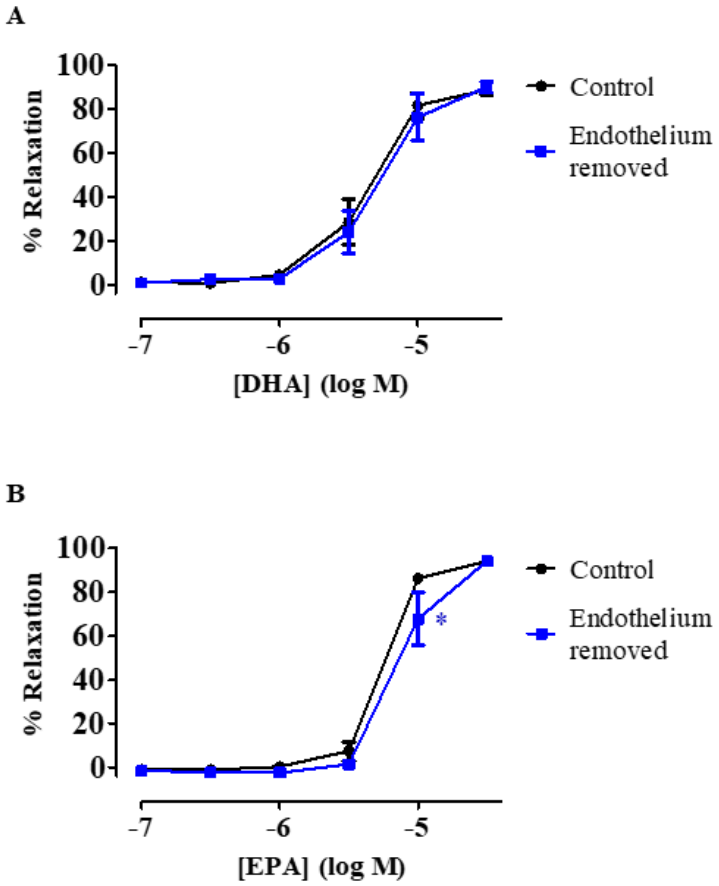

Fig 3.4 Concentration response curves demonstrating relaxation mediated by (A) DHA (*n*=7) and (B) EPA (*n*=6) in rat aorta before and after the removal of endothelium. Using wire myograph, changes in n-3 PUFA (100 nM – 30 µM) mediated relaxation were recorded by initially obtaining a control response curve followed by endothelium removal from the same arterial segment. Data are expressed as mean±SEM. *P<0.05 indicates significant difference from the control curve as determined using two-way ANOVA with Bonferroni post-test.

3.2.2 Effect of NO and COX inhibition in n-3 PUFA mediated vascular relaxation

In the earlier section 3.2.1, I demonstrated that there was a small endothelium-dependent component involved in DHA- and EPA-induced relaxation of rat mesenteric artery along with EPA-induced relaxation of rat aorta. Therefore, the next experiments were designed to characterise these endothelium-dependent pathways that were involved with n-3 PUFA mediated relaxation. The role of NO and COX was initially investigated through the pre-treatment (20 min) of the arteries with L-NAME (300 µM) and indometacin (10 µM). Fig 3.5 and 3.6 shows the representative traces demonstrating the effect of NO and COX inhibition in DHA-induced relaxation of rat mesenteric artery and aorta respectively. The arterial incubation with L-NAME led to inhibition of basal NO production resulting in potentiation of constriction, as a result, U46619 had to be applied at 10x lower concentration to match the tone of the previous control response curve. Additionally, these effects were mostly observed in rat mesenteric arteries as demonstrated by Fig 3.5B. Pre-treatment with L-NAME followed by the additional inhibition of COX using indometacin failed to modify both DHA- and EPA-mediated relaxation in rat mesenteric artery (Figs 3.7A and 3.7B) (n=5). Consistently, pre-treatment of rat aorta with L-NAME and indometacin also failed to modify both DHA- and EPA-induced relaxation (Figs 3.8A and 3.8B) (n=5).

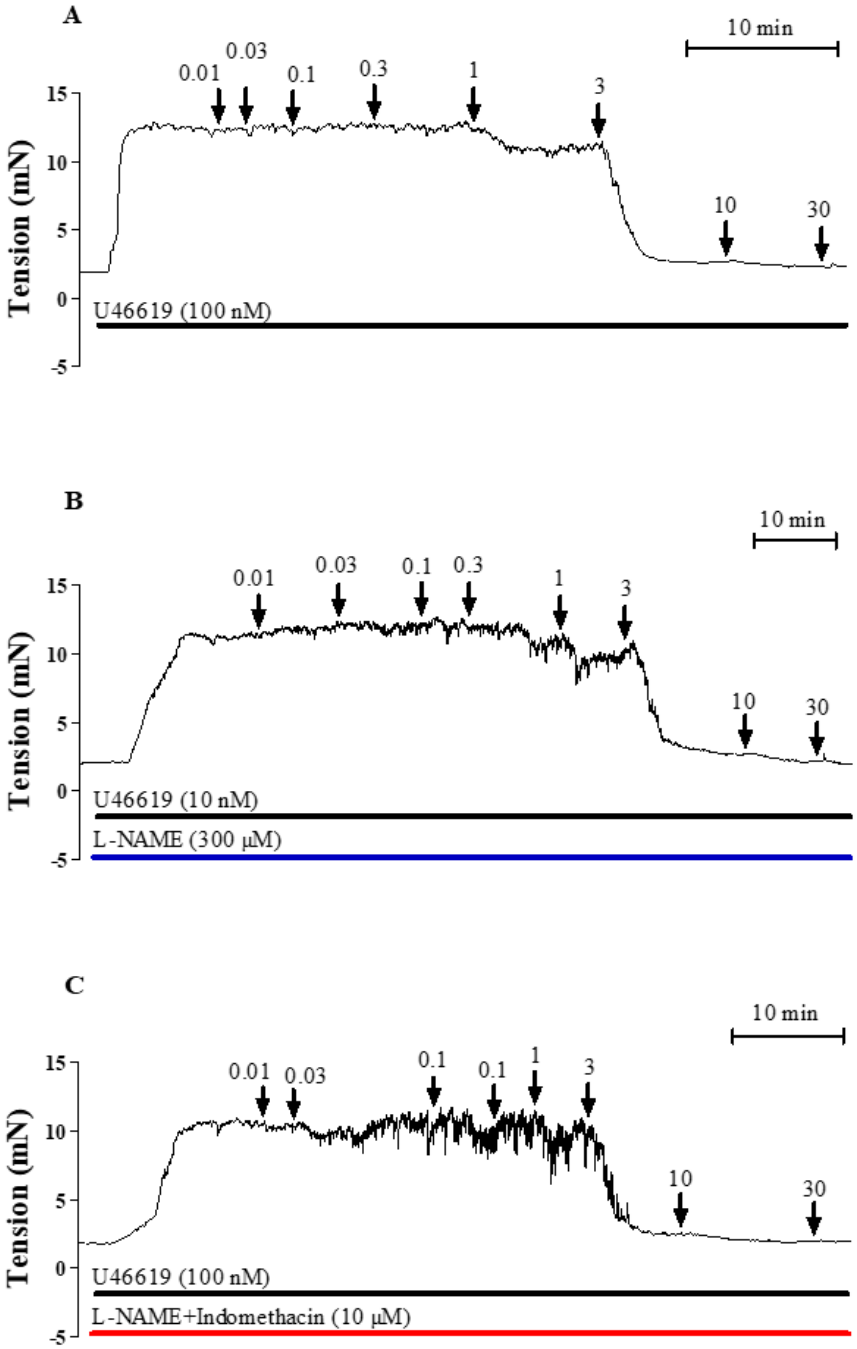

Fig 3.5 Original representative traces demonstrating the effect of L-NAME (300 µM) and indometacin (10 µM) in DHA-induced relaxation of rat mesenteric artery. After initially obtaining the control response curve, changes in vascular tone were recorded following successive incremental treatments of the same arterial segment with L-NAME to inhibit eNOS and additional treatment with indometacin to inhibit COX. DHA was cumulatively added (0.01 – 30 µM) to induce vascular relaxation as indicated by the arrows.

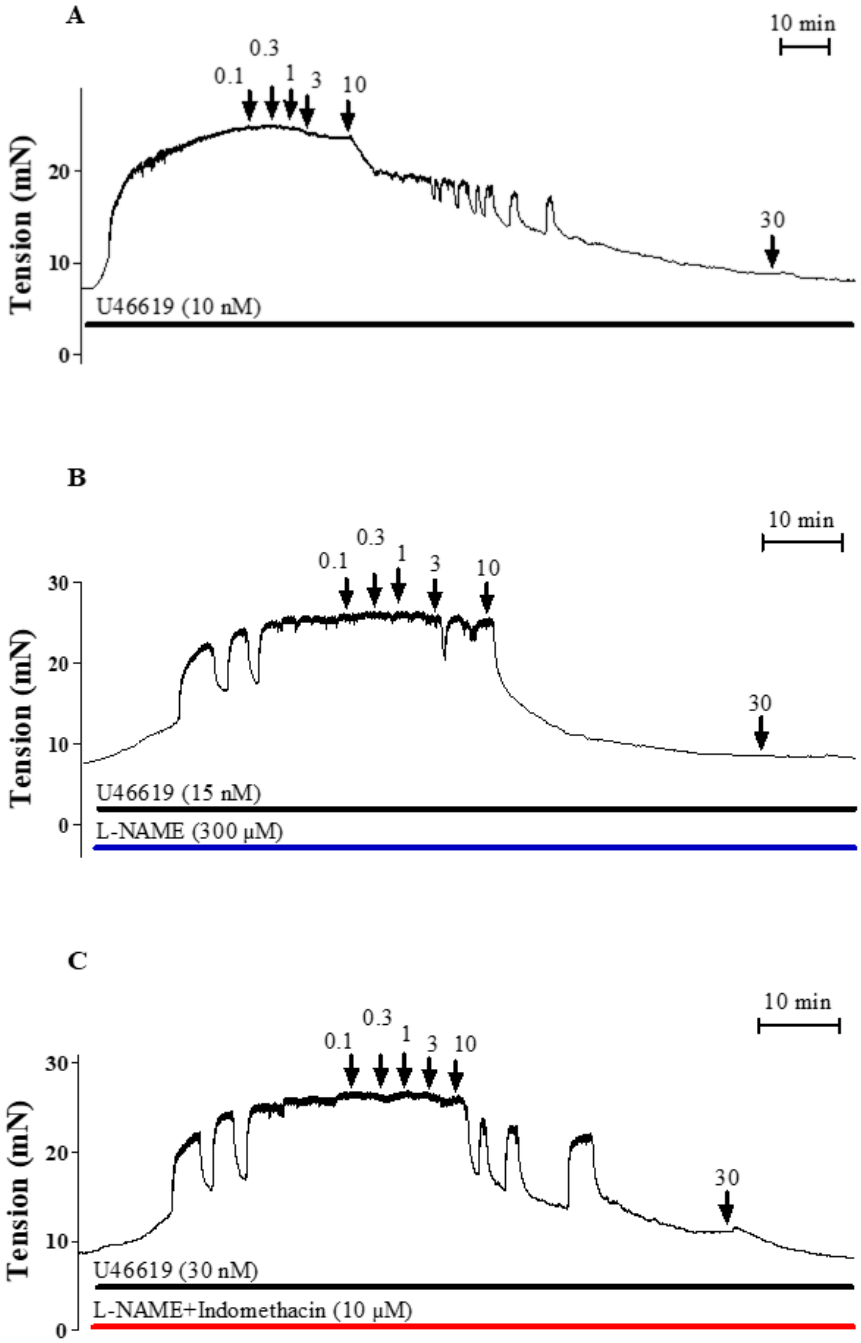

Fig 3.6 Original representative traces demonstrating the effect of L-NAME (300 µM) and indometacin (10 µM) in DHA-induced relaxation of rat aorta. After initially obtaining the control response curve, changes in vascular tone were recorded following successive incremental treatments of the same arterial segment with L-NAME to inhibit eNOS and additional treatment with indometacin to inhibit COX. DHA was cumulatively added (0.1 – 30 µM) to induce vascular relaxation as indicated by the arrows.

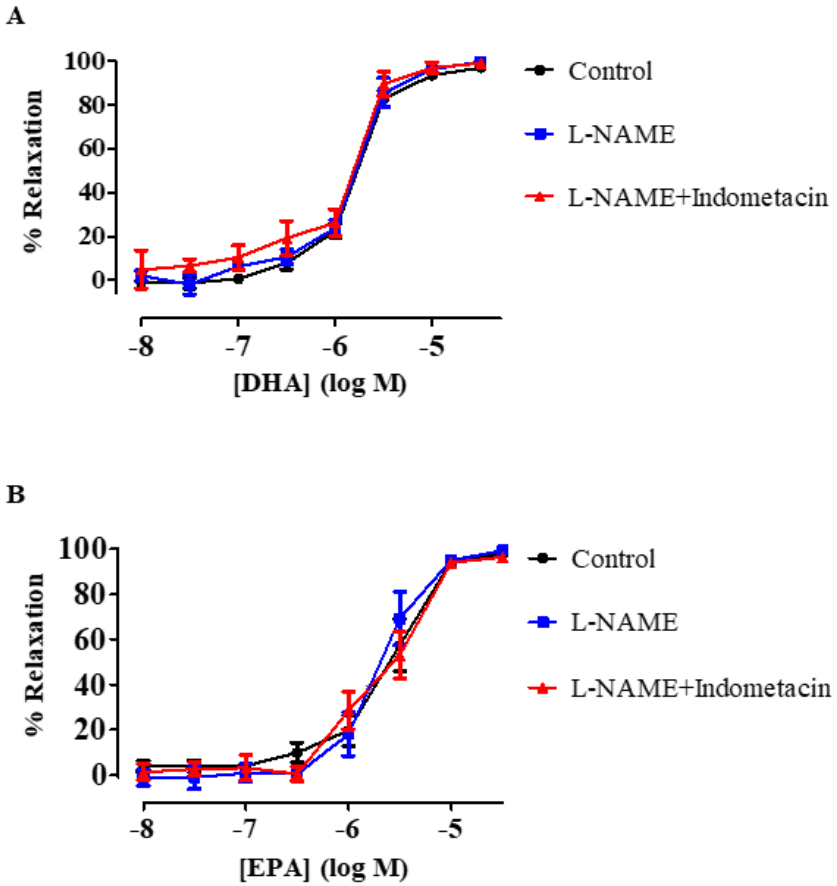

Fig 3.7 Concentration response curves demonstrating relaxation mediated by (A) DHA (*n*=5) and (B) EPA (*n*=5) in rat mesenteric artery following inhibition of eNOS with L-NAME (300 µM) and indometacin (10 µM). Using wire myograph, changes in n-3 PUFA (10 nM – 30 µM) mediated relaxation were recorded by initially obtaining a control response curve followed by pre-treatment of the same arterial segment with the inhibitors (20 min). Data are expressed as mean±SEM. *P<0.05 indicates significant difference from the control curve as determined using two-way ANOVA with Bonferroni post-test.

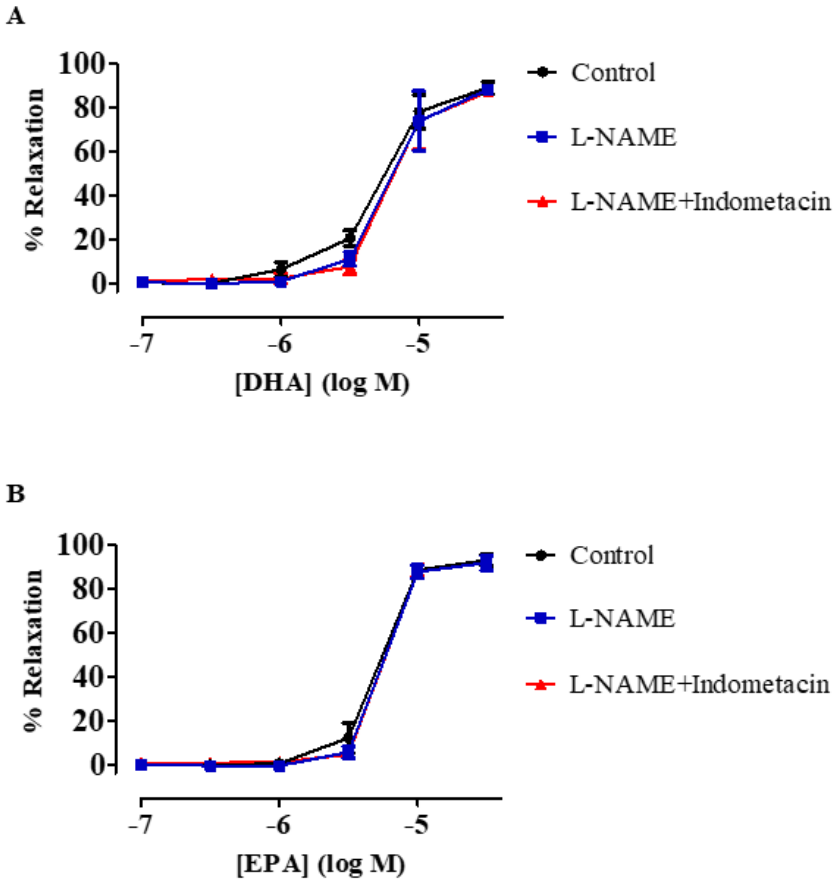

Fig 3.8 Concentration response curves demonstrating relaxation mediated by (A) DHA (*n*=5) and (B) EPA (*n*=5) in rat aorta following inhibition of eNOS with L-NAME (300 µM) and indometacin (10 µM). Using wire myograph, changes in n-3 PUFA (100 nM – 30 µM) mediated relaxation were recorded by initially obtaining a control response curve followed by pre-treatment of the same arterial segment with the inhibitors (20 min). Data are expressed as mean±SEM. *P<0.05 indicates significant difference from the control curve as determined using two-way ANOVA with Bonferroni post-test.

3.2.3 Effect of n-3 PUFAs on ACh- and NONOate-mediated vasodilation in n-3 PUFA-mediated vascular relaxation

As demonstrated in the previous sections 3.2.1 and 3.2.4, endothelium removal only partially attenuated relaxation elicited by acute application of n-3 PUFAs. Most of the research demonstrating the role of NO in the n-3 PUFA-induced vasodilation involves chronic supplementation with n-3 PUFAs. Therefore, the next objective was to investigate the effects of the pre-treatment of rat mesenteric artery with DHA in ACh-induced vasodilation. NONOate, which is a NO donor that can cause endothelium-independent relaxation, was also used to investigate the effect of DHA at the level of SMCs. The protocol (chapter 2, section 2.2.5.iii) involved preincubation of rat mesenteric artery with a low concentration of DHA (300 nM) for 1 h, followed by pre-constriction with U46619 and subsequent vasodilation using either ACh (endothelium dependent) or NONOate (endothelium independent). Fig 3.9 and 3.10 shows the representative traces demonstrating the effect of DHA in ACh- and NONOate-induced relaxation of rat mesenteric artery respectively. Pre-treatment of mesenteric artery with DHA did not modify the ACh-induced vascular relaxation (1 nM–3 µM) (Fig 3.11A) (n=6). However, significant potentiation in NONOate-induced relaxation (1 nM – 3 µM) of mesenteric artery was observed following arterial incubation with DHA [Log EC_{50}; -6.96±0.09 (Control) and -7.46±0.10 (300 nM DHA)] (Fig 3.11B) (n=7, $P<0.05$).

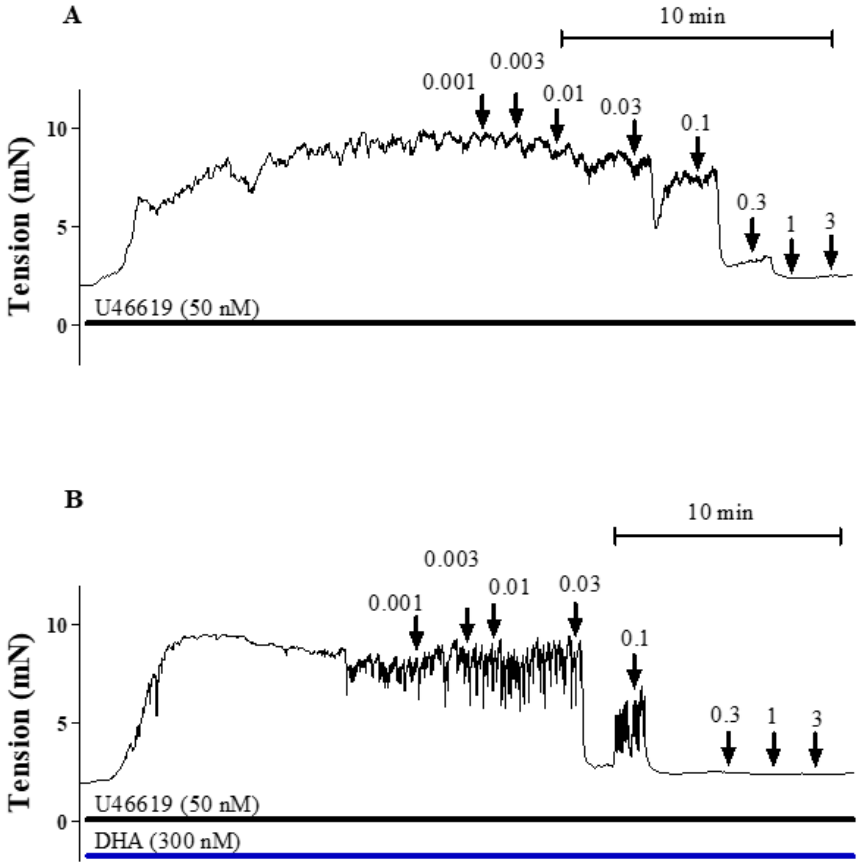

Fig 3.9 Original representative traces demonstrating the effect of DHA in ACh-induced relaxation of rat mesenteric artery. After initially obtaining the control response curve, changes in vascular tone were recorded following treatment of the same arterial segment with DHA (300 nM) for 1 h. ACh was cumulatively added (0.001 – 30 μM) to induce vascular relaxation as indicated by the arrows.

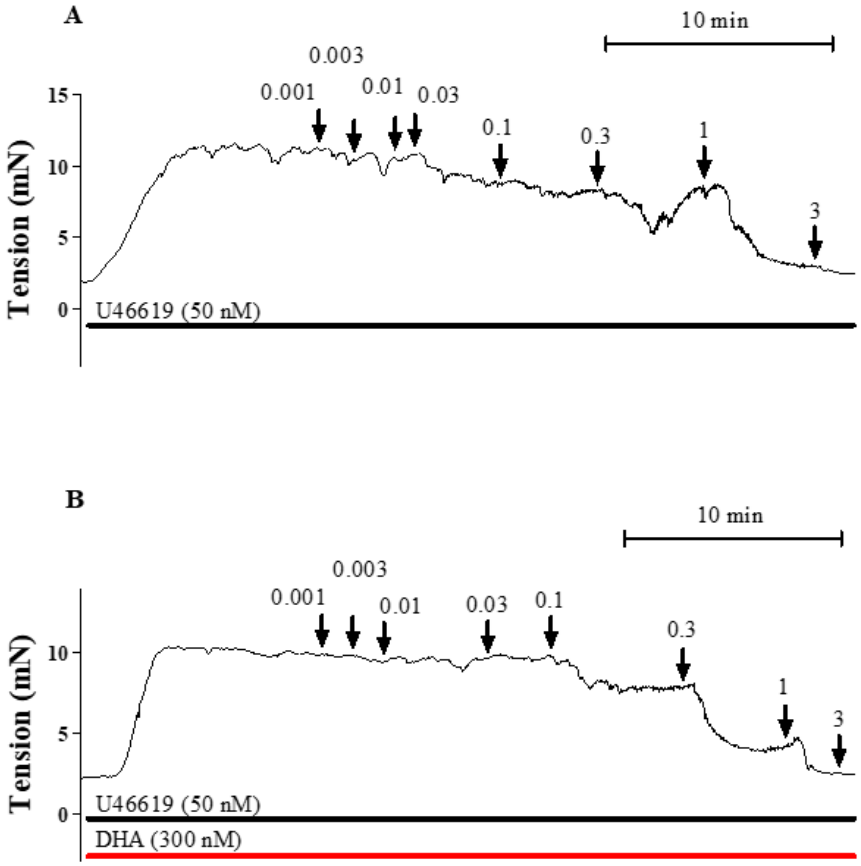

Fig 3.10 Original representative traces demonstrating the effect of DHA in NONOate-induced relaxation of rat mesenteric artery. After initially obtaining the control response curve, changes in vascular tone were recorded following treatment of the same arterial segment with DHA (300 nM) for 1 h. NONOate was cumulatively added (0.001 – 30 μM) to induce vascular relaxation as indicated by the arrows.

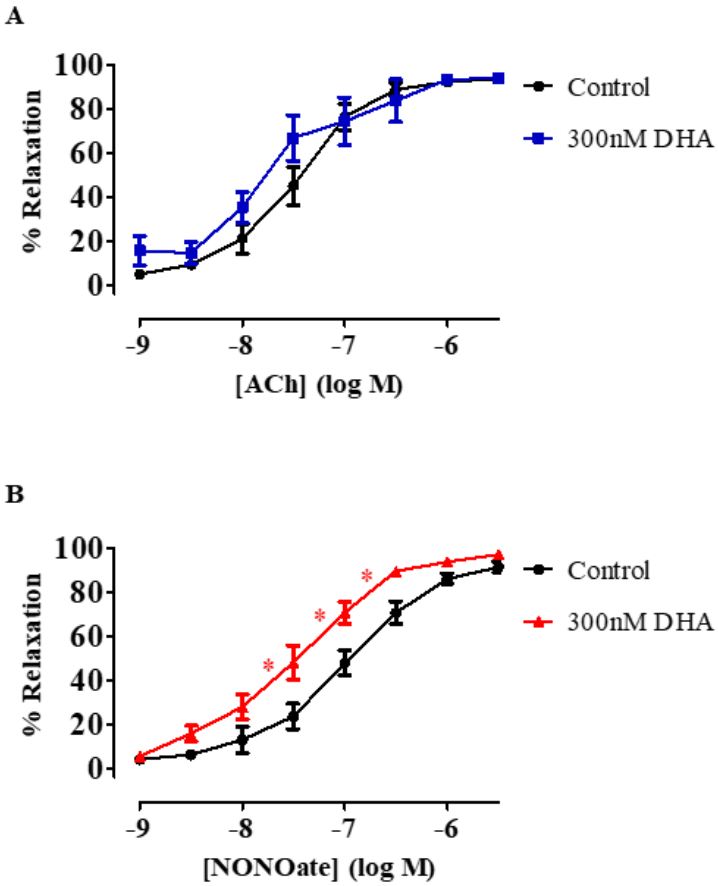

Fig 3.11 Concentration response curves demonstrating relaxation mediated by (A) ACh (*n*=6) and (B) NONOate (*n*=7) in rat mesenteric artery following treatment of the arteries with DHA (300 nM) for 1 h. Using wire myograph, changes in either ACh or NONOate (10 nM – 30 µM) mediated relaxation were recorded by initially obtaining a control response curve followed by pre-treatment of the same arterial segment with DHA. Data are expressed as mean±SEM. *Indicates P<0.05, significant difference from control curve assessed by two-way ANOVA followed by Bonferroni post-test.

3.2.4 Effect of CYP epoxygenase inhibition in n-3 PUFA mediated vascular relaxation

The endothelium-dependent component observed with n-3 PUFA-induced vasodilation was not associated with the NO and COX pathway in both rat mesenteric artery and aorta, therefore I investigated CYP epoxygenase which is also found in the endothelium. Multiple electrophysiological studies have reported that acute application of CYP-derived metabolites of n-3 PUFAs can directly activate BK_{Ca} channels present in vascular SMCs (Patterson et al. 2002; Hercule et al. 2007; Ye et al. 2002; Qian et al. 2018). Therefore, n-3 PUFA mediated relaxation of U46619 constricted arteries were recorded before and after the treatment of the arteries with clotrimazole (1 µM, 20 min) for the non-selective inhibition of CYP. Representative traces demonstrating the effect of inhibiting CYP in DHA-induced relaxation of rat mesenteric artery and aorta are shown in Fig 3.12 and Fig 3.13 respectively. DHA-induced relaxation was unaffected following inhibition of CYP epoxygenase in both rat mesenteric artery and aorta (Figs 3.14A and 3.15A) (n=6 and 5, respectively). However, EPA-mediated relaxation was partially attenuated in both rat mesenteric artery [Log EC_{50}; -6.20±0.03 (Control) and -5.56±0.06 (Clotrimazole)] and aorta [Log EC_{50}; -5.00±0.06 (Control) and -4.93±0.44 (Clotrimazole)] following inhibition of CYP (Figs 3.14B and 3.15B) (n=5, $P<0.05$). Although the responses to EPA in rat aorta did not plateau, there was a rightward shift of the response curve following clotrimazole pre-treatment (Fig 3.15B) which was consistent with the mesenteric data (Fig 3.14B), further indicating the role of CYP40 in EPA-induced relaxation. Log EC_{50} and maximal relaxation (E_{max}) values for each experimental group are summarized in table 3.1.

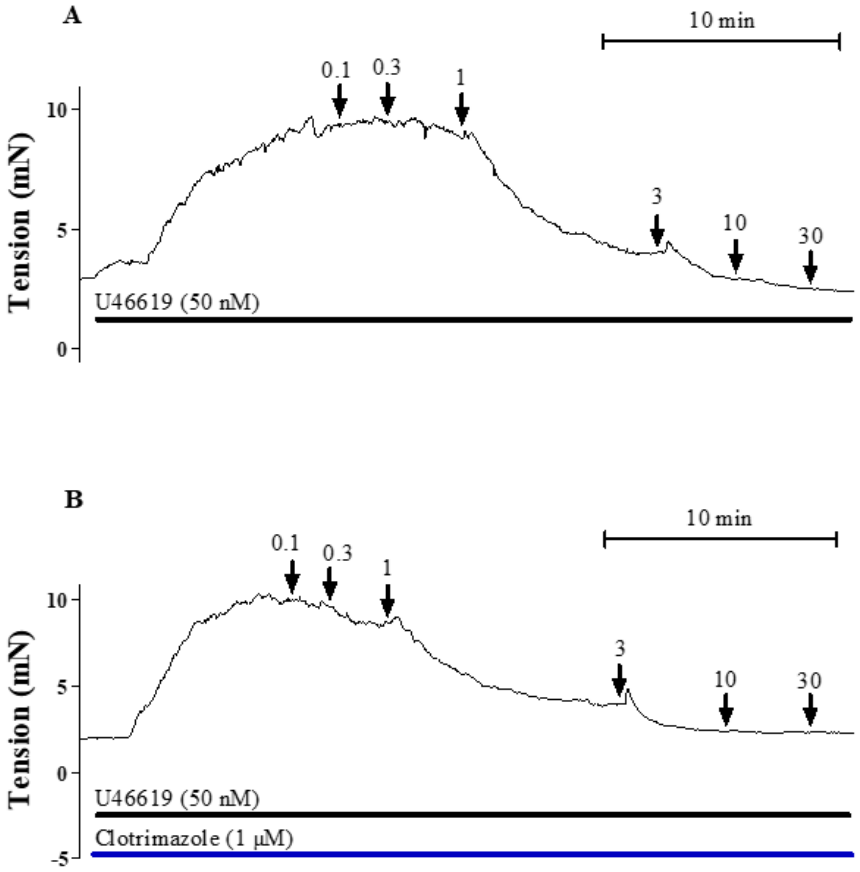

Fig 3.12 Original representative traces demonstrating the effect of clotrimazole in DHA-induced relaxation of rat mesenteric artery. After initially obtaining the control response curve, changes in vascular tone were recorded following treatment of the same arterial segment with clotrimazole (1 μM) to inhibit CYP epoxygenase. DHA was cumulatively added (0.1 – 30 μM) to induce vascular relaxation as indicated by the arrows.

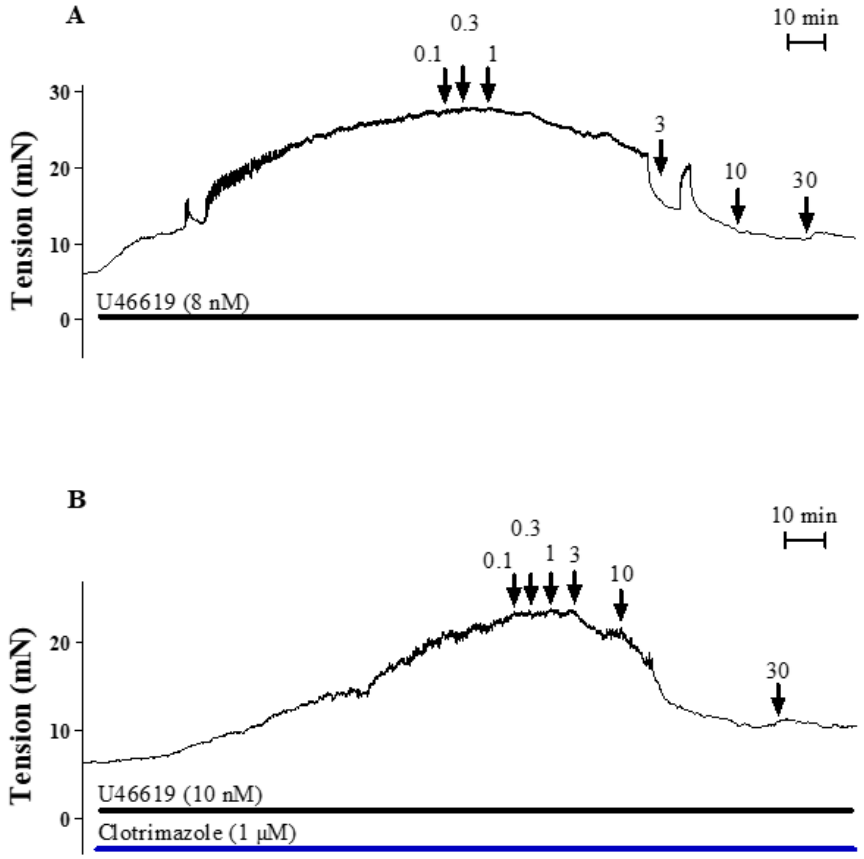

Fig 3.13 Original representative traces demonstrating the effect of clotrimazole in DHA-induced relaxation of rat aorta. After initially obtaining the control response curve, changes in vascular tone were recorded following treatment of the same arterial segment with clotrimazole (1 μM) to inhibit CYP epoxygenase. DHA was cumulatively added (0.1 – 30 μM) to induce vascular relaxation as indicated by the arrows.

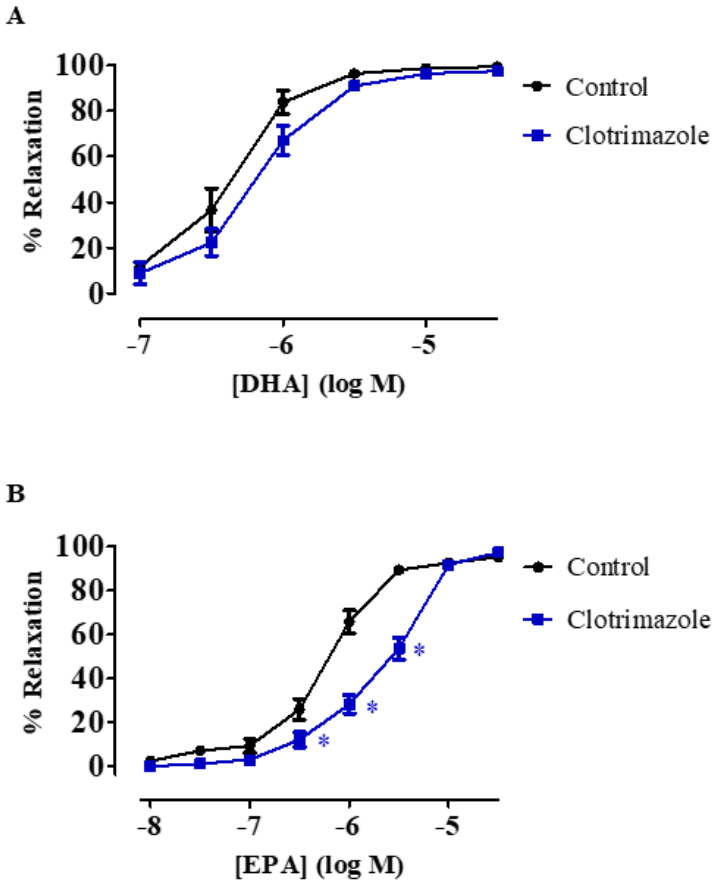

Fig 3.14 Concentration response curves demonstrating relaxation mediated by (A) DHA (*n*=5) and (B) EPA (*n*=6) in rat mesenteric artery before and after the treatment of the arteries with clotrimazole (1 µM). Using wire myograph, changes in n-3 PUFA (10 nM – 30 µM) mediated relaxation were recorded by initially obtaining a control response curve followed by pre-treatment of the same arterial segment with clotrimazole (20 min). Data are expressed as mean±SEM. *P<0.05 indicates significant difference from the control curve as determined using two-way ANOVA with Bonferroni post-test.

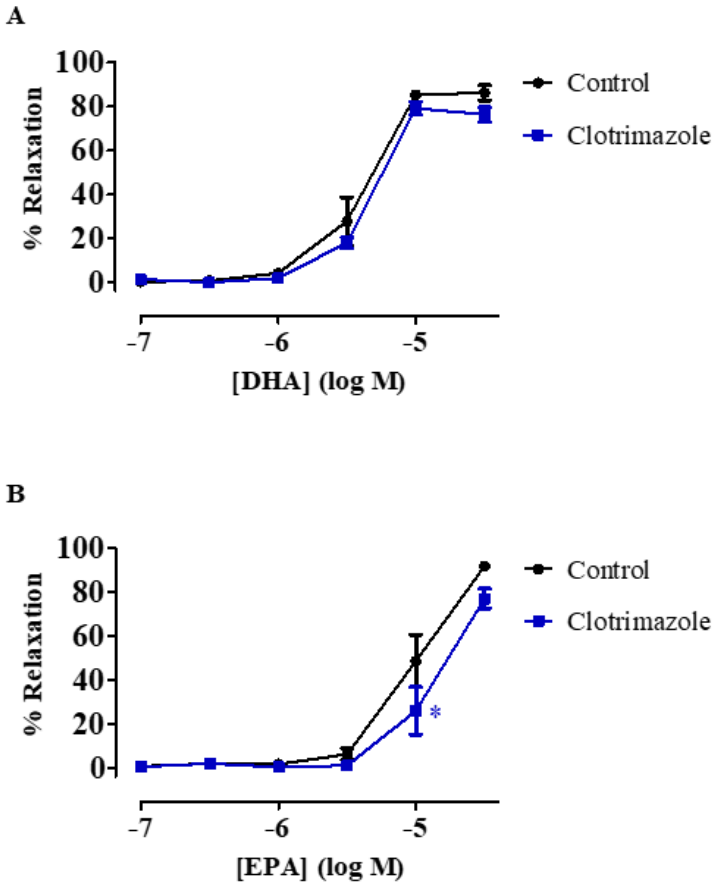

Fig 3.15 Concentration response curves demonstrating relaxation mediated by (A) DHA (*n*=5) and (B) EPA (*n*=5) in rat aorta before and after the treatment of the arteries with clotrimazole (1 µM). Data are expressed as mean±SEM. Using wire myograph, changes in n-3 PUFA (100 nM – 30 µM) mediated relaxation were recorded by initially obtaining a control response curve followed by pre-treatment of the same arterial segment with clotrimazole (20 min). *P<0.05 indicates significant difference from the control curve as determined using two-way ANOVA with Bonferroni post-test.

3.2.5 Effect of SK_{Ca}, IK_{Ca} and BK_{Ca} inhibition in n-3 PUFA mediated vascular relaxation

In the previous section 3.2.3, I demonstrated that the endothelium-dependent component of EPA-induced vasodilation involved the CYP epoxygenase. BK_{Ca} has been reported to be activated both directly by DHA and indirectly through CYP-derived metabolites of both n-3 PUFAs (Patterson et al. 2002; Lai et al. 2009; Ye et al. 2002; Hercule et al. 2007). Therefore, to investigate whether the n-3 PUFA-mediated vasodilation involved activation of K_{Ca} channels, arteries were pre-treated in successive increments with L-NAME (300 µM), apamin (50 nM, SK_{Ca} inhibitor), TRAM-34 (1 µM, IK_{Ca} inhibitor) and paxilline (1 µM, BK_{Ca} inhibitor) for 20 min. The relaxant effects of n-3 PUFAs were then assessed following constriction with U46619.

3.2.5.i. Rat mesenteric artery

Fig 3.16 shows the representative traces demonstrating the effect of K_{Ca} inhibition in DHA-induced relaxation of rat mesenteric artery. DHA-induced relaxation was unaffected following incubation of L-NAME (300 µM) and apamin (50 nM). However, partial attenuation in relaxation was observed with the additional inhibition of IK_{Ca} with TRAM-34 (1 µM) (Fig 3.17A) (n=5, $P<0.05$) and further reduction in relaxation was observed following subsequent addition of paxilline (1 µM) [Log EC_{50}; -5.87±0.04 (Control) and -5.37±0.06 (L-NAME+Apamin+TRAM-34+Paxilline)] (Fig 3.17A) (n=5, $P<0.05$). EPA-induced relaxation was also assessed in rat mesenteric artery, however, attenuation in relaxation was only observed via the inhibition of BK_{Ca} channels by paxilline [Log EC_{50}; -5.41±0.02 (Control) and -5.11±0.07 (L-NAME+Apamin+TRAM-34+Paxilline)] (Fig 3.17B, n=5, $P<0.05$). Since these experiments involved five consecutive concentration response curves that were acquired using the same piece of

tissue, additional experiments were conducted to confirm that these effects were real and exclusive to the action of n-3 PUFAs. Time control groups were ran in parallel with the test group using segments from the same piece of mesenteric artery to assess changes in the contractile tone. Although the concentration of U46619 had to be increased to match the original tone of the control curve, especially for the last concentration response curve (Fig 3.16B); there was no difference between the first and the fourth time control curve (Fig 3.18A and 3.18C respectively), demonstrating that a similar stable contractile tone could be achieved. Furthermore, randomizing the pre-treatments by individually inhibiting the BK_{Ca} channels with L-NAME and paxilline immediately after obtaining the first control response curve, also led to significant attenuation of DHA-induced relaxation [Log EC_{50}; -6.34±0.05 (Control) and -5.89±0.06 (L-NAME+Paxilline)]. This is consistent with my previous findings and further confirms the role of BK_{Ca} channels in DHA-induced vasodilation. Another experiment was also conducted with the additional blockade of SK_{Ca} and IK_{Ca} channels using a single pre-treatment (consisting of L-NAME, apamin, TRAM-34 and Paxilline) immediately after the first control curve. The findings from this experiment demonstrated further enhancement in the inhibition of DHA-induced relaxation [Log EC_{50}; -6.25±0.07 (Control) and -5.57±0.07 (L-NAME+Apamin+TRAM-34+Paxilline)] (Fig 3.19B), confirming the additional role of IK_{Ca} channels as indicated before (Fig 3.17A). Moreover, multiple incremental pre-treatments with the K_{Ca} inhibitors did not modify EPA-induced relaxation of rat aorta (Fig 3.21B), further validating that the reported effects were elicited entirely due to the action of n-3 PUFAs rather than due to changes in the tissue's responsiveness to n-3 PUFAs.

3.2.5.ii. Aorta

Studies indicate that the role of EDH as the predominant vasodilation mechanism increases as the arterial size decreases (Shimokawa et al. 1996). Consistent with these studies, my findings also demonstrate that IK_{Ca} and BK_{Ca} are involved in both DHA- and EPA-induced relaxation of rat mesenteric artery. Therefore, the next experiments focussed on investigating whether there was heterogeneity in the EDH component of n-3 PUFAs between the conduit and resistance arteries. Rat aorta was examined using the same protocol as described earlier (see section 3.2.5). Representative traces demonstrating the effect of K_{Ca} inhibition in DHA-induced relaxation of rat aorta are shown in Fig 3.20. DHA-induced relaxation was unaffected following inhibition of eNOS with L-NAME (300 µM) and SK_{Ca} with apamin (50 nM) (Fig 3.21A). Similar to rat mesenteric artery, additional inhibition of IK_{Ca} with TRAM-34 (1 µM) partially attenuated DHA-induced relaxation (n=5, $P<0.05$) and subsequent inhibition of BK_{Ca} with paxilline (1 µM) led to further attenuation of relaxation [Log EC_{50}; -5.25±0.04 (Control) and -5.07±0.08 (L-NAME+Apamin+TRAM-34+Paxilline)] (n=5, $P<0.05$). In contrast to DHA, EPA-induced relaxation of rat aorta was unaffected following the blockade of eNOS and K_{Ca} channels (Fig 3.21B) (n=5). A summary of log EC_{50} and maximal relaxation (E_{max}) values for each experimental group can be found in table 3.1.

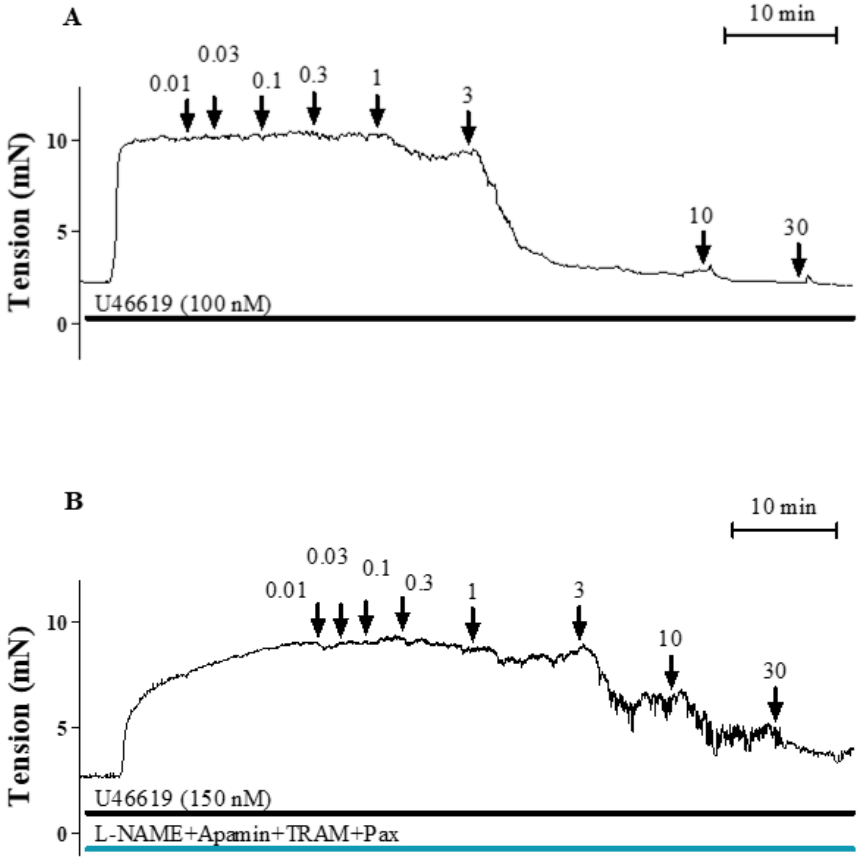

Fig 3.16 Original representative traces demonstrating the effect of inhibiting K_{Ca} in DHA-induced relaxation of rat mesenteric artery. After initially obtaining the control response curve, changes in vascular tone were recorded following treatment (20 min) of the same arterial segment with L-NAME (300 µM) to inhibit eNOS, apamin (50 nM) to inhibit SK_{Ca}, TRAM-34 (1 µM) to inhibit IK_{Ca} and paxilline (1 µM) to inhibit BK_{Ca}. DHA was cumulatively added (0.01 – 30 µM) to induce vascular relaxation as indicated by the arrows. TRAM = TRAM-34 and Pax = paxilline.

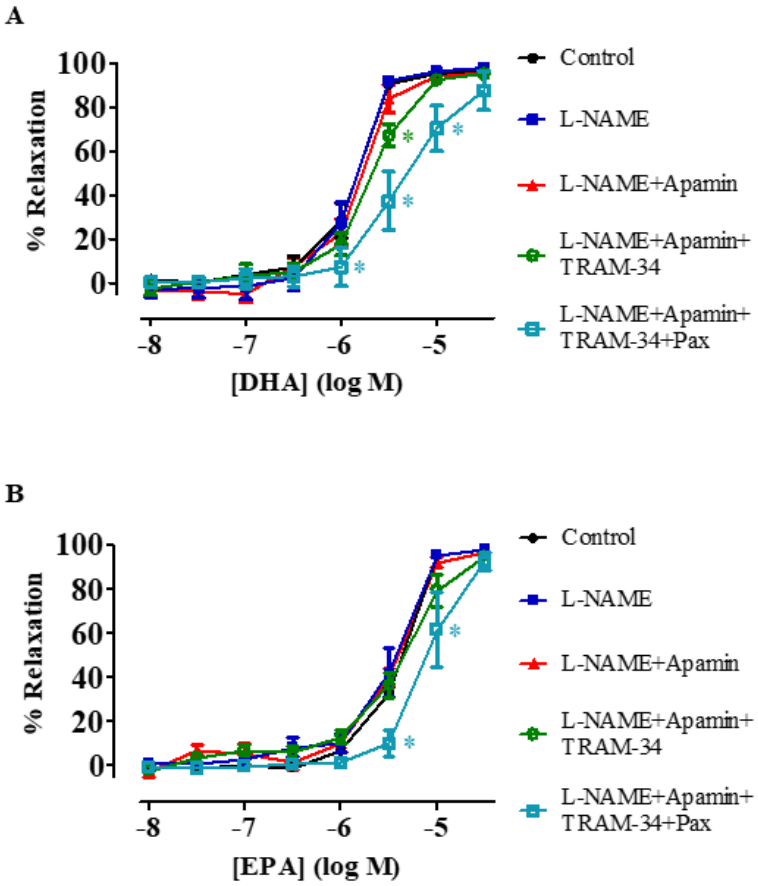

Fig 3.17 Concentration response curves demonstrating relaxation mediated by (A) DHA and (B) EPA in rat mesenteric artery following inhibition of eNOS with L-NAME (300 µM), SK_{Ca} with apamin (50 µM), IK_{Ca} with TRAM-34 (1 µM) and BK_{Ca} with paxilline (Pax, 1 µM) (*n*=5). Using wire myograph, changes in n-3 PUFA (10 nM – 30 µM) mediated relaxation were recorded by initially obtaining a control response curve followed by pre-treatment of the same arterial segment with K_{Ca} inhibitors (20 min). Data are expressed as mean±SEM. *Indicates $P<0.05$, significant difference from control curve assessed by two-way ANOVA followed by Bonferroni post-test. Pax = paxilline.

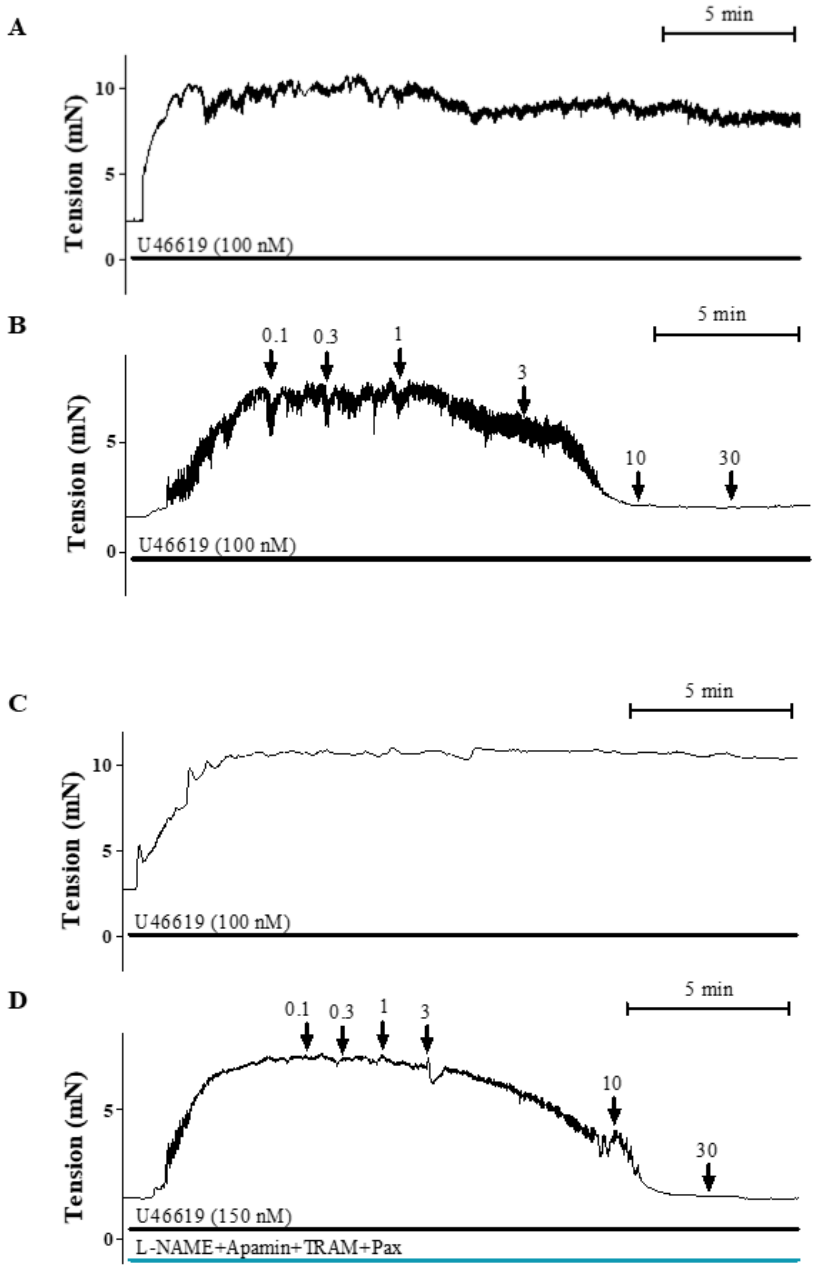

Fig 3.18 Original representative traces demonstrating time control and DHA response curves. Two segments derived from the same rat mesenteric artery were used in parallel to initially obtain (A) time- and (B) DHA-control response curves. (C) Stable constriction with U46619 was observed in the fourth concentration response experiment as demonstrated by the time control group whereas (D) inhibition in relaxation was observed with the other tissue following pre-treatment (20 min) with L-NAME (300 µM), apamin (50 nM), TRAM-34 (1 µM) and paxilline (1 µM). DHA was cumulatively added (0.01 – 30 µM) to induce vascular relaxation as indicated by the arrows. TRAM = TRAM-34 and Pax = paxilline.

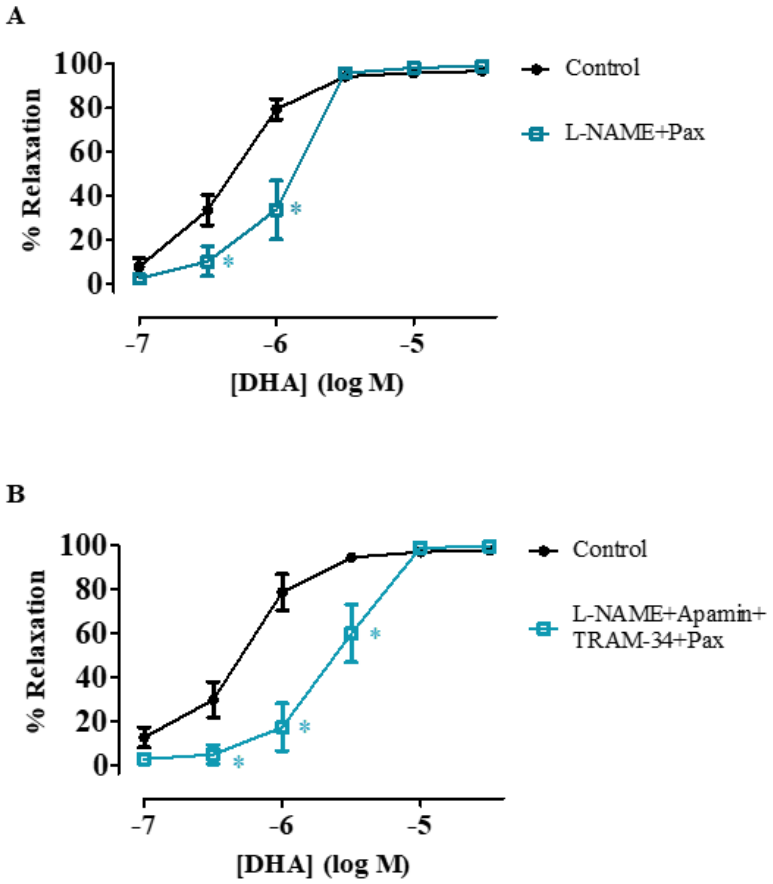

Fig 3.19 Concentration response curves demonstrating relaxation mediated by DHA in rat mesenteric arteries following pre-treatment with (A) L-NAME (300 µM) + paxilline (Pax, 1 µM) and (B) L-NAME + apamin (50 µM) + TRAM-34 (1 µM) + paxilline (*n*=4). Using wire myograph, changes in DHA (100 nM – 30 µM) mediated relaxation were recorded by initially obtaining a control response curve followed by the subsequent pre-treatment of the same arterial segment with L-NAME+K_{Ca} inhibitor(s) (20 min). Data are expressed as mean±SEM. *Indicates $P<0.05$, significant difference from control curve assessed by two-way ANOVA followed by Bonferroni post-test. Pax = paxilline.

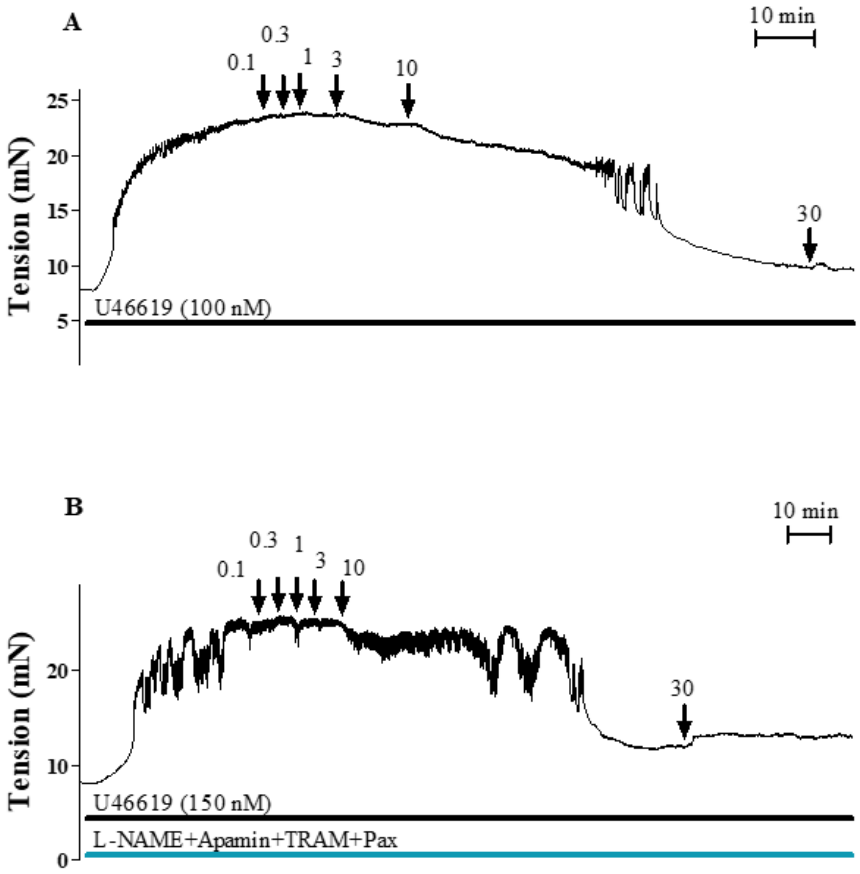

Fig 3.20 Original representative traces demonstrating the effect of inhibiting K_{Ca} in DHA-induced relaxation of rat aorta. After initially obtaining the control response curve, changes in vascular tone were recorded following treatment (20 min) of the same arterial segment with L-NAME (300 µM) to inhibit eNOS, apamin (50 nM) to inhibit SK_{Ca}, TRAM-34 (1 µM) to inhibit IK_{Ca} and paxilline (1 µM) to inhibit BK_{Ca}. DHA was cumulatively added (0.1 – 30 µM) to induce vascular relaxation as indicated by the arrows. TRAM = TRAM-34 and Pax = paxilline.

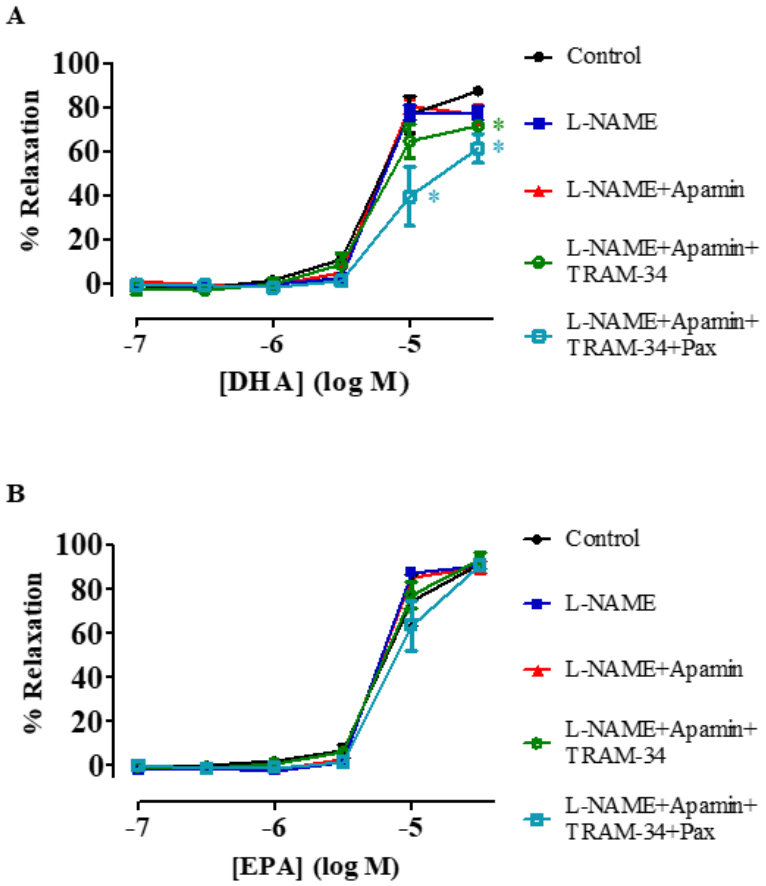

Fig 3.21 Concentration response curves demonstrating relaxation mediated by (A) DHA and (B) EPA in rat aorta following inhibition of eNOS with L-NAME (300 µM), SK_{Ca} with apamin (50 µM), IK_{Ca} with TRAM-34 (1 µM) and BK_{Ca} with paxilline (Pax, 1 µM) (*n*=5). Using wire myograph, changes in n-3 PUFA (100 nM – 30 µM) mediated relaxation were recorded by initially obtaining a control response curve followed by pre-treatment of the same arterial segment with K_{Ca} inhibitors (20 min). Data are expressed as mean±SEM. *Indicates $P<0.05$, significant difference from control curve assessed by two-way ANOVA followed by Bonferroni post-test. Pax = paxilline.

Table 3.1 Summary of log EC_{50} and maximal relaxation (E_{max}) values for each experimental group. Values were obtained using standard variable slope least squares fit based on the hill equation in GraphPad Prism 5. N.D. indicates not determined as GraphPad could not produce an optimal curve fit due to nature of the data points, resulting in ambiguity for the values obtained. L-N = L-NAME, TRAM = TRAM-34 and Pax = paxilline.

Experiment	Type of artery	n-3 PUFA	Experimental Condition	Log EC_{50}		E_{max} (%)	
				Log EC_{50}	SEM (±)	E_{max} (%)	SEM (±)
Endothelium removed	Mesenteric artery	DHA *n=5*	Control	-5.79	0.04	92.71	2.77
			Endothelium removed	-5.56	0.05	95.80	4.56
		EPA *n=6*	Control	-5.43	0.02	100.60	2.11
			Endothelium removed	-5.37	0.03	100.30	2.31
	Aorta	DHA *n=7*	Control	-5.37	0.06	89.52	5.28
			Endothelium removed	-5.30	0.07	91.33	7.03
		EPA *n=6*	Control	-5.25	0.03	94.19	2.13
			Endothelium removed	-5.11	0.05	94.72	5.18
L-NAME, Indometacin	Mesenteric artery	DHA *n=5*	Control	-5.80	0.03	95.89	1.93
			L-N	-5.79	0.04	98.59	2.79
			L-N+ Indometacin	-5.80	0.06	98.36	4.11
		EPA *n=5*	Control	-5.56	0.06	101.10	5.43
			L-N	-5.68	0.06	99.46	4.99
			L-N+ Indometacin	-5.58	0.08	102.40	7.35
	Aorta	DHA *n=5*	Control	-5.30	0.05	90.08	4.29
			L-N	-5.22	0.07	89.00	5.98
			L-N+ Indometacin	-5.20	0.07	87.54	5.74
		EPA *n=5*	Control	-5.31	0.05	93.34	3.03
			L-N	-5.27	0.04	92.13	2.12
			L-N+ Indometacin	-5.25	0.03	92.41	1.32

Acetylcholine	Mesenteric artery	*n=6*	Control	-7.46	0.07	94.25	3.33
			300 nM DHA	-7.72	0.17	92.11	5.53
NONOate	Mesenteric artery	*n=7*	Control	-6.96	0.09	95.32	5.60
			300 nM DHA	-7.46	0.10	100.2	4.50
Clotrimazole	Mesenteric artery	DHA *n=5*	Control	-6.34	0.06	98.90	2.81
			Clotrimazole	-6.16	0.06	96.84	2.76
		EPA *n=5*	Control	-6.20	0.03	94.80	1.94
			Clotrimazole	-5.56	0.06	106.70	5.41
	Aorta	DHA *n =5*	Control	-5.41	0.08	86.80	4.73
			Clotrimazole	**N.D.**	**N.D.**	77.76	2.07
		EPA *n=5*	Control	-5.00	0.06	97.05	9.89
			Clotrimazole	-4.93	0.44	77.89	24.04
L-NAME, Apamin, TRAM-34, Paxilline	Mesenteric artery	DHA *n=5*	Control	-5.87	0.04	96.66	2.72
			L-N	-5.88	0.04	97.65	3.36
			L-N+ Apamin	-5.82	0.04	96.34	3.10
			L-N+Apamin +TRAM	-5.68	0.04	96.19	3.04
			L-N+Apamin +TRAM+Pax	-5.37	0.06	91.20	5.31
		EPA *n=5*	Control	-5.41	0.02	99.13	1.72
			L-N	-5.44	0.04	100.2	4.77
			L-N+ Apamin	-5.43	0.03	98.31	3.38
			L-N+Apamin +TRAM	-5.34	0.06	99.94	6.06
			L-N+Apamin +TRAM+Pax	-5.11	0.07	96.29	8.59
		DHA *n=5*	Control	-5.25	0.04	87.82	3.60
			L-N	**N.D.**	**N.D.**	77.73	2.10
			L-N+ Apamin	**N.D.**	**N.D.**	78.76	2.72
			L-N+Apamin +TRAM	-5.28	0.06	71.98	4.28
			L-N+Apamin +TRAM+Pax	-5.07	0.08	62.20	6.75

	Aorta	EPA *n=5*	Control	-5.19	0.06	91.54	5.08
			L-N	-5.25	0.03	90.74	1.29
			L-N+ Apamin	-5.24	0.03	89.89	1.56
			L-N+Apamin +TRAM	-5.19	0.03	93.41	3.12
			L-N+Apamin +TRAM+Pax	-5.10	0.05	91.16	4.72

3.3 Summary

There is evidence indicating that the endothelium-dependent vasodilation pathways are involved in the n-3 PFUA-mediated relaxation (Table 1.1). Consistent with these findings, my myograph experiments revealed that there was minor but a significant role of the endothelium in DHA mediated relaxation of rat mesenteric artery (Fig 3.3A-B) and EPA mediated relaxation in rat aorta (Fig 3.4B), demonstrating heterogeneity in the vasodilation mechanisms of n-3 PUFAs. Relaxation mediated by the acute application of both n-3 PUFAs did not involve NO and COX pathways (Fig 3.7-3.8). A postprandial study reported that enhancement in the vascular reactivity of healthy men was observed within few hours of consuming a fish oil rich meal (Jackson et al. 2009). Therefore, I investigated the effects of the pre-treatment of rat mesenteric arteries with DHA for 1 h. My findings indicated that the pre-treatment was associated with potentiation of NONOate-induced relaxation (Fig 3.11A). In contrast to NONOate, ACh-induced relaxation (Fig 3.11B) was unaffected by DHA, indicating that improvements in NO-mediated relaxation perhaps occurs at the level of SMCs. In agreement with my findings, the *in vivo* human study involving n-3 PUFA supplementation also demonstrated that sodium nitroprusside (NO donor) was more potent in enhancing vascular reactivity compared to ACh (Jackson et al. 2009). It is possible that these effects are only observed during chronic exposure to n-3 PUFAs. In fact most of the studies that demonstrated the

role of NO in n-3 PUFA-induced relaxation, investigated the effects of n-3 PUFA supplementation lasting more than a week (Omura et al. 2001; Hirafuji et al. 2002; López et al. 2004; Raimondi et al. 2005). Indeed acute studies conducted using rat arterial tissue indicated an absence of NO component in relaxation elicited by both DHA and EPA, consistent with my findings (Fig 3.7 and 3.8) (Engler et al. 2000). Due to the current evidence, it is logical to suggest that the acute vascular relaxation observed with n-3 PUFAs does not involve the endothelial production of NO, and any improvements in this component possibly requires chronic exposure to n-3 PUFAs.

CYP epoxygenase is expressed in vascular ECs and can produce metabolites of DHA and EPA (EDPs and EPETEs respectively) that have been reported to elicit vasodilation, in various vascular beds such as mouse cerebral artery (Hercule et al. 2007), mouse mesenteric artery (Hercule et al. 2007), rat cerebral (Hercule et al. 2007) and rat coronary arteries (Wang et al. 2011) (Table 1.1). As a result, to further characterise the endothelium-dependent vasodilation pathways of n-3 PUFAs, I investigated the role of CYP epoxygenase. My findings demonstrate that CYP epoxygenase was only associated with EPA-induced relaxation of both arteries (Fig 3.14-3.15), indicating heterogeneity in vasodilation mechanism that can depend upon the type of n-3 PUFA. This also suggests that CYP-derived metabolites of EPA may be involved in activation of K_{Ca} channels as indicated by a previous study (Hercule et al. 2007). As a result, my next objective was to investigate the EDH pathway.

Based on my findings, SK_{Ca} channels were not involved in n-3 PUFA-induced relaxation. Some studies have reported TP receptor-mediated inhibition SK_{Ca} channels in rat cerebral (McNeish and Garland 2007) and mesenteric arteries (Crane and Garland 2004). Therefore, it is possible that any potential SK_{Ca} component of n-3 PUFA-mediated vasodilation was lost due to the TP receptor-mediated pre-constriction of the arteries with

U46619. My findings demonstrated a novel role of the endothelial IK_{Ca} channels which was only observed with DHA-induced relaxation of both arteries (Fig 3.17A and 3.21A). Similarly, BK_{Ca} was also involved in DHA mediated vasodilation of both vascular beds (Fig 3.17A and 3.21A) and EPA mediated relaxation of the mesenteric artery (Fig 3.17B), further indicating heterogeneity in the mechanisms depending upon both the type of n-3 PUFA and vascular bed. A summary of log EC_{50} and maximal relaxation (E_{max}) values for each experimental group can be found in table 3.1 for comparison. An interesting finding from the above experiments is the large residual relaxation that remained following blockade of the K_{Ca} channels, indicating the presence of other endothelium-independent mechanisms. Therefore, my next objective was to characterise these unidentified pathways in rat mesenteric artery and aorta.

Chapter 4

The role of TRPV4 in n-3 PUFA mediated vasodilation

4.1 Introduction

TRPV4 is a non-selective cation channel with six transmembrane domains that is expressed in vascular ECs and SMCs (Everaerts and Owsianik 2010). It is involved in different physiological processes throughout the body including osmoregulation, thermoregulation and vasodilation (Everaerts and Owsianik 2010). An increased influx of Ca^{2+} into the endothelium is one of the main mechanisms involved in initiating a cascade of vasodilation pathways including EDH which involves K_{Ca} channels (Edwards et al. 2010). Therefore, different mechanisms have been reported to be involved with TRPV4 mediated vasodilation including EDH and NO pathways following local Ca^{2+} influx via TRPV4 (Filosa et al. 2013; Sukumaran et al. 2013; Cabral and Garvin 2014). PUFAs such as AA have been reported to directly activate TRPV4 in human coronary arteries, resulting in vasodilation through activation of endothelial SK_{Ca} and IK_{Ca} channels (Zheng et al. 2013). EETs were also reported to activate TRPV4 present in mice mesenteric arteries through a similar mechanism involving the SK_{Ca} and IK_{Ca}, resulting in hyperpolarization and relaxation of adjacent vascular SMCs (Sonkusare et al. 2012). Furthermore, in rat cerebral (Earley et al. 2005) and mouse mesenteric arteries (Earley, Pauyo, et al. 2009), EETs were found to activate TRPV4 present in vascular SMCs resulting in the intracellular release of Ca^{2+} from SR and subsequent activation of BK_{Ca}. n-3 PUFAs have also been reported to activate other TRP channels such as transient receptor potential cation channel subfamily V member 1 (TRPV1) (Matta et al. 2007) and transient receptor potential cation channel, subfamily A, member 1 (TRPA1) (Motter and Ahern 2012). Futhermore, PUFAs with the greater amount of unsaturation and an n-3 double bond were indicated to be more potent in activating PKC-phosphorylated TRPV1 channels (Matta et al. 2007). Both DHA and EPA were also reported to directly

activate TRPA1 channels expressed in HEK cells, using patch-clamp electrophysiology (Motter and Ahern 2012).

My findings reported in chapter 3 demonstrated the role of IK_{Ca} and BK_{Ca} in DHA-induced relaxation of both rat aorta and mesenteric artery along with EPA-induced relaxation of the rat mesenteric artery. Although there is evidence indicating TRPA1 mediated vasodilation via K_{Ca} activation (Earley, Gonzales, et al. 2009; Sinha et al. 2015), current studies indicate that the expression of TRPA1 in the vasculature is limited to ECs present in cerebral arteries (Earley 2012). In contrast to TRPA1, TRPV4 channels have been reported to be expressed in both ECs and SMCs found in various arteries (Filosa et al. 2013). Furthermore, numerous studies indicate that TRPV4 can activate both BK_{Ca} and IK_{Ca} present in the vasculature and as a result, it is possible that TRPV4 channels may be the initial target of n-3 PUFAs resulting in subsequent activation of the downstream vasodilation signalling cascade involving the K_{Ca}. Based on these findings, the next experiments focused on investigating whether n-3 PUFAs could directly stimulate TRPV4 to activate K_{Ca} resulting in vasodilation. I initially used wire myograph (chapter 2, section 2.2) to investigate whether vascular relaxation mediated by both n-3 PUFAs were modified following inhibition of TRPV4. I then created a stable cell line with inducible expression of TRPV4 (chapter 2, section 2.3) and used Fluo-4 AM based calcium imaging (chapter 2, section 2.7) to investigate whether the n-3 PUFAs directly modulated TRPV4 activity. Results obtained from each experiment are described in the following sections.

4.2 Results

4.2.1 Effect of TRPV4 inhibition in n-3 PUFA mediated vascular relaxation

As indicated earlier, TRPV4 is expressed in the vasculature and regulates vasodilation through different mechanisms including modulation of K_{Ca}. As my findings from chapter 3 (section 3.2.5) demonstrated a component of EDH is involved with n-3 PUFA mediated vasodilation, I initially investigated whether n-3 PUFAs were indirectly modulating K_{Ca} through TRPV4 using wire myograph. Experimental protocol for wire myograph has been described in detail in chapter 2 (section 2.2). Briefly, the relaxant effect of n-3 PUFAs were recorded before and after the incubation of arteries with a TRPV4 antagonist, either RN-1734 (10 – 30 µM) or HC-067047 (1 µM), for 20 min. Results were expressed as mean±SEM of n experiments and statistical analysis was carried out using two-way ANOVA and Bonferroni post-hoc test.

Representative traces from Fig 4.1 and Fig 4.2 demonstrate the effect of RN-1734 in DHA-induced relaxation of rat mesenteric artery and aorta respectively. In rat mesenteric artery, RN-1734 (30 µM) led to partial inhibition of DHA-induced vascular relaxation [Log EC_{50}; -6.39±0.04 (Control) and -6.09±0.08 (RN-1734)] (Fig 4.3A) (n=6, $P<0.05$). Both DHA- and EPA-induced relaxation were unaffected following treatment of rat aorta with RN-1734 (Figs 4.3B-C, n=4-5, $P<0.05$). Additional experiments were not conducted using a higher cocentraiton of RN-1734 as it disrupted the maintenance of the contractile tone. This is possibly due to problems with the selectivity of blocker since it has been reported to inhibit other ion channels such as TRPV1 (IC_{50} > 100 µM) (Vincent et al. 2009).

Experiments with HC-067047 (1 μM) were only conducted in rat aorta as it affected the stability of U46619-constricted tone in rat mesenteric artery. Representative traces from Fig 4.4 demonstrates the effect of HC-067047 in DHA-induced relaxation of rat aorta. Both DHA- and EPA-induced relaxation were unaffected by HC-067047 in rat aorta (Figs 4.5A-B, n=5, $P<0.05$). A summary of log EC_{50} and maximal relaxation (E_{max}) values for each experimental group can be found in table 4.1 for comparison.

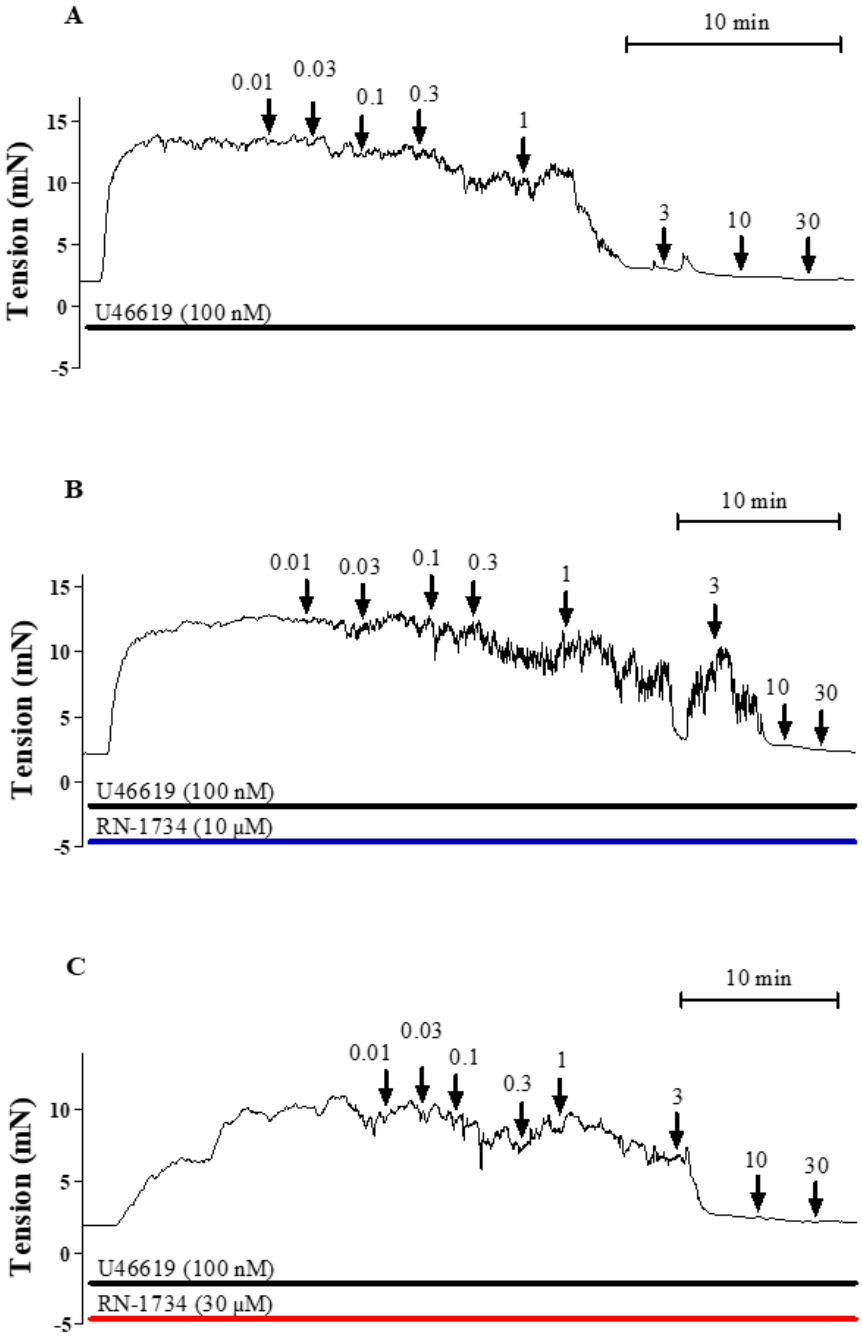

Fig 4.1 Original representative traces demonstrating the effect of RN-1734 (10 µM – 30 µM) in DHA-induced relaxation of rat mesenteric artery. After initially obtaining the control response curve using wire myograph, changes in the vascular tone were recorded following treatment of the same arterial segment with RN-1734 (20 min) to inhibit TRPV4. DHA was cumulatively added (0.01 – 30 µM) to induce vascular relaxation as indicated by the arrows.

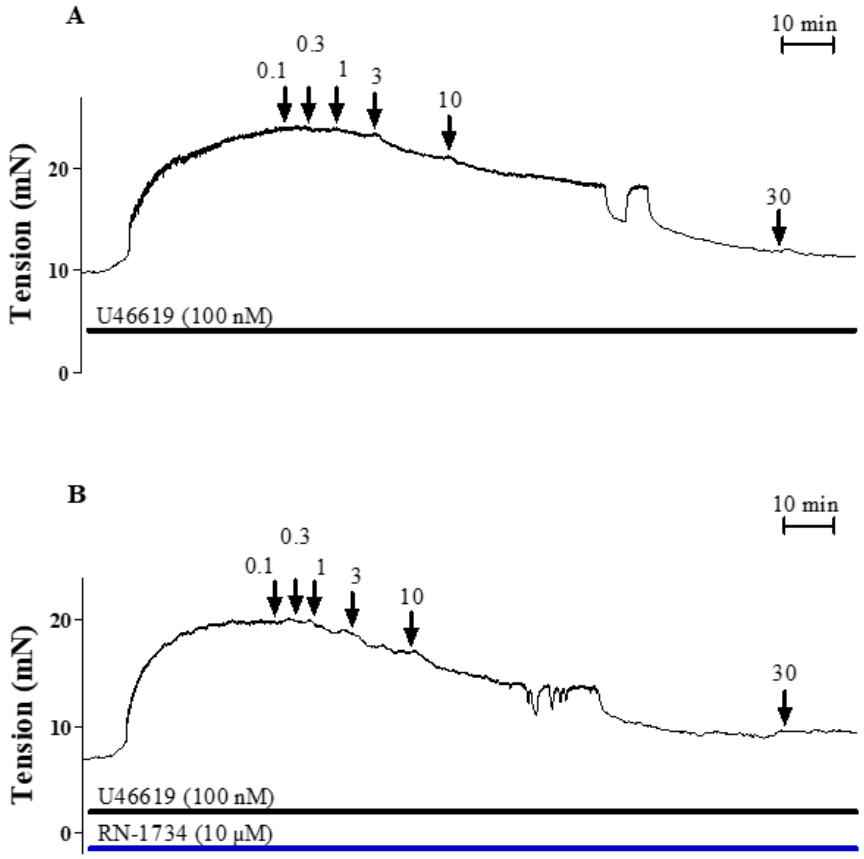

Fig 4.2 Original representative traces demonstrating the effect of RN-1734 (10 µM) in DHA-induced relaxation of rat aorta. After initially obtaining the control response curve using wire myograph, changes in the vascular tone were recorded following treatment of the same arterial segment with RN-1734 (20 min) to inhibit TRPV4. DHA was cumulatively added (0.1 – 30 µM) to induce vascular relaxation as indicated by the arrows.

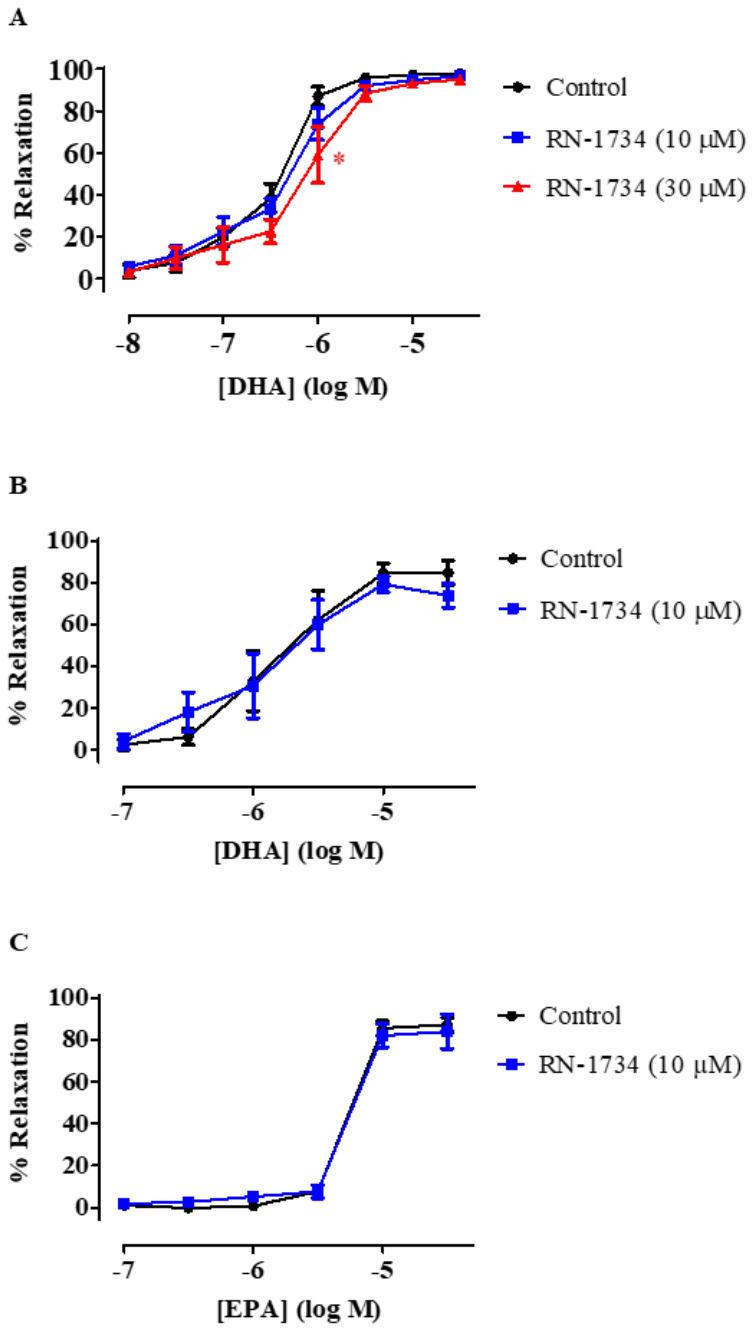

Fig 4.3 Concentration response curves demonstrating the effect of RN-1734 (10 – 30 µM), a TRPV4 inhibitor, in relaxation mediated by (A) DHA in rat mesenteric artery (*n*=6), (B) DHA in rat aorta (*n*=5) and (C) EPA in rat aorta (*n*=4). Using wire myograph, changes in n-3 PUFA (10 nM – 30 µM) mediated relaxation were recorded by initially obtaining a control response curve followed by consecutive pre-treatments of the same arterial segment with RN-1734 (20 min). Data are expressed as mean±SEM. *P<0.05 indicates significant difference from the control curve as determined using two-way ANOVA with Bonferroni post-test.

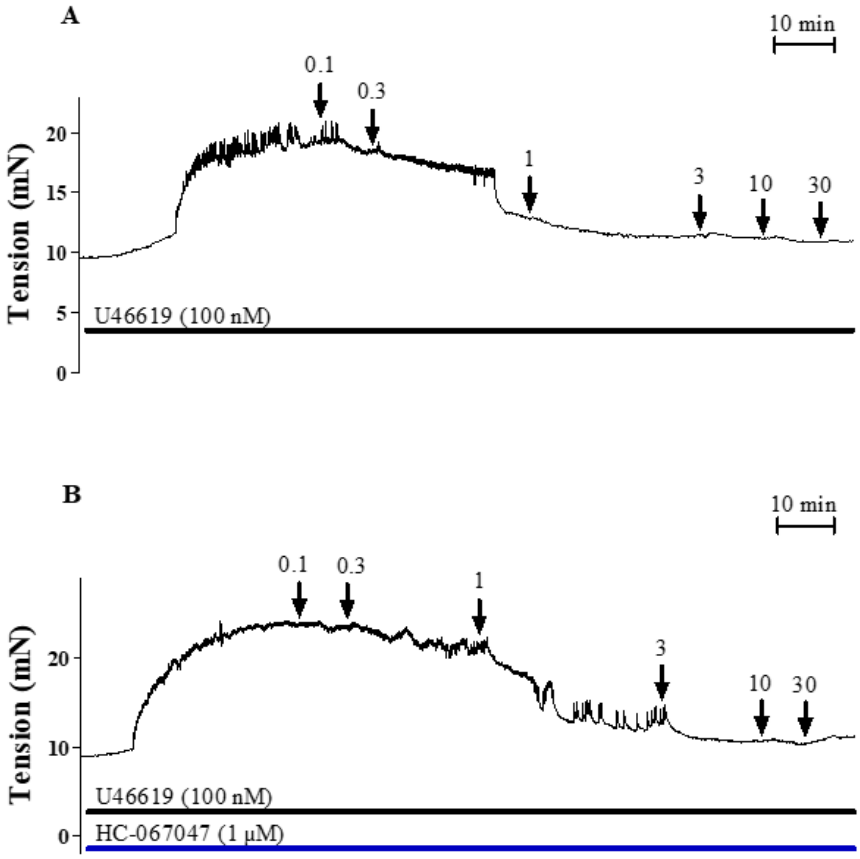

Fig 4.4 Original representative traces demonstrating the effect of HC-067047 (1 µM) in DHA-induced relaxation of rat aorta. After initially obtaining the control response curve using wire myograph, changes in the vascular tone were recorded following treatment of the same arterial segment with HC-067047 (20 min) to inhibit TRPV4. DHA was cumulatively added (0.1 – 30 µM) to induce vascular relaxation as indicated by the arrows.

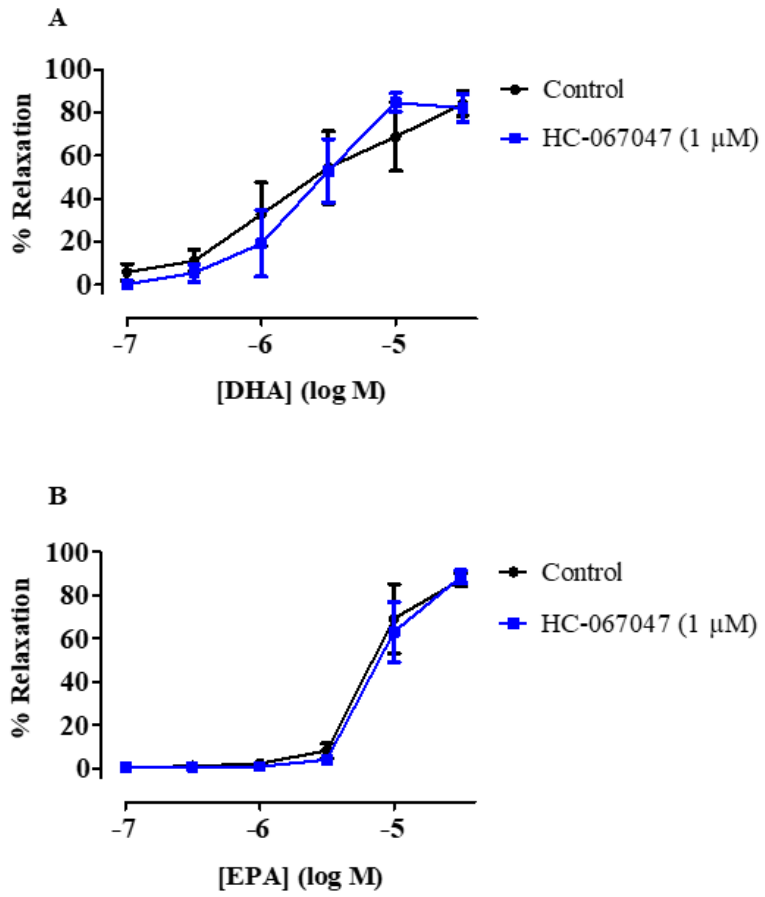

Fig 4.5 Concentration response curves demonstrating relaxation mediated by (A) DHA- and (B) EPA-induced relaxation of rat aorta (*n*=5) following inhibition of TRPV4 with HC-067047 (1 µM). Using wire myograph, changes in n-3 PUFA (100 nM – 30 µM) mediated relaxation were recorded by initially obtaining a control response curve followed by pre-treatment of the same arterial segment with HC-067047 (20 min). Data are expressed as mean±SEM. *P<0.05 indicates significant difference from the control curve as determined using two-way ANOVA with Bonferroni post-test.

Table 4.1 Summary of log EC_{50} and maximal relaxation (E_{max}) values from each myograph experiments that were conducted to investigate the effects of TRPV4 inhibition. Values were obtained using standard variable slope least squares fit based on the hill equation in GraphPad Prism 5.

Experiment	Type of artery	n-3 PUFA	Experimental Condition	Log EC_{50}		E_{max} (%)	
				Log EC_{50}	SEM (±)	E_{max} (%)	SEM (±)
RN-1734	Mesenteric artery	DHA *n=6*	Control	-6.39	0.04	98.24	2.43
			RN-1734 (10 µM)	-6.27	0.06	97.11	3.28
			RN-1734 (30 µM)	-6.09	0.08	95.54	4.73
	Aorta	DHA *n=5*	Control	-5.82	0.15	87.26	9.24
			RN-1734 (10 µM)	-5.84	0.19	78.55	9.69
		EPA *n=4*	Control	-5.31	0.06	87.08	2.28
			RN-1734 (10 µM)	-5.28	0.12	83.82	4.13
HC-067047	Aorta	DHA *n=5*	Control	-5.70	0.42	92.38	34.54
			HC-067047	-5.64	0.13	86.27	9.28
		EPA *n=5*	Control	-5.18	0.08	87.82	7.08
			HC-067047	-5.11	0.06	89.30	5.93

4.2.2 Generation of HEK Flp-In T-REx-293 pcDNA5/FRT/TO and pcDNA5/FRT/TO+TRPV4-HA cell lines

My myograph results indicated that TRPV4 was involved with DHA-induced relaxation in rat mesenteric artery. Therefore, the next step was to investigate whether n-3 PUFAs could directly activate TRPV4 channels. To this aim, I began by generating a stable cell line expressing the ion channel and using Fluo-4 AM based calcium imaging assay to examine channel activity. Methods used for creating the stable cell line has been described in detail in chapter 2, section 2.3.

4.2.2.i Construction of recombinant plasmids: pcDNA5/FRT+TRPV4-HA

PCR (chapter 2, section 2.3.1.i) was used to generate a 3' end DNA segment of the TRPV4 gene without the stop codon to enable fusion of TRPV4 to the HA epitope tag present in the plasmid. The amplified DNA fragment was then analysed using sanger sequencing (chapter 2, section 2.3.1.ii). Restriction digests (chapter 2, section 2.3.1.iii) were then performed to generate the DNA fragments required for the construction of pcDNA5/FRT+TRPV4-HA plasmid (Fig 4.6). The following REs and plasmids were used to obtain the necessary fragments (chapter 2, table 2.4):

a) pcDNA5/FRT/TO+TRPV4 (required fragment expected at 2663 bp) = *Bam* HI and *Kpn* I
b) 3' end DNA segment of TRPV4 (required fragment expected at 138 bp) = *Kpn* I
c) pcDNA5/FRT+HA (required fragment expected at 4876 bp) = *Eco* RV and *Bam* HI

The digested DNA was then loaded on an agarose gel and the fragments were separated using gel electrophoresis (chapter 2, section 2.3.1.iv). The required DNA fragments were

then excised from the gel and purified using QIAquick gel extraction kit (chapter 2, section 2.3.1.v) and subsequently ligated (chapter 2, section 3.1.vi). The ligated DNA was then used to transform Mach1 competent cells (chapter 2, section 2.3.1.vii) and the cells were spread onto agar plates. Single bacterial colonies were then screened by colony PCR (chapter 2, section 2.3.1.viii) using the primers, TRPV4 forward primer and BGH reverse. PCR samples were then analysed using gel electrophoresis and positive clones were identified in lanes 8 and 14 as shown in Fig 4.7A, indicated by single bands representing the PCR amplified DNA (604 bp). The clones were then inoculated overnight in 5 ml of sterile SOB with $MgCl_2$ and ampicillin. After preparing a glycerol stock (chapter 2, section 2.3.1.ix) from the overnight culture, plasmid DNA was purified using QIAprep Spin Miniprep Kit (chapter 2, section 2.3.1.x). The purified plasmid DNA was then screened by restriction digest using *Bam* HI and *Xho* I followed by gel electrophoresis. Bands for the TRPV4+3' end DNA segment-HA (predicted size, 2663 bp) fragment and the remaining of the pcDNA5/FRT vector (predicted size, 5014 bp) were observed as shown in Fig 4.7B. The glycerol stock obtained from one of the positive clones was then used to inoculate a 250 ml culture and the DNA was purified using EndoFree Plasmid Maxi Kit (chapter 2, section 2.3.1.xi). DNA was screened again using sanger sequencing and restriction digest followed by gel electrophoresis. Bands for TRPV4+3' end DNA segment-HA (predicted size, 2663 bp) fragment and the remaining of the pcDNA5/FRT vector (predicted size, 5014 bp) were observed (Fig 4.7C).

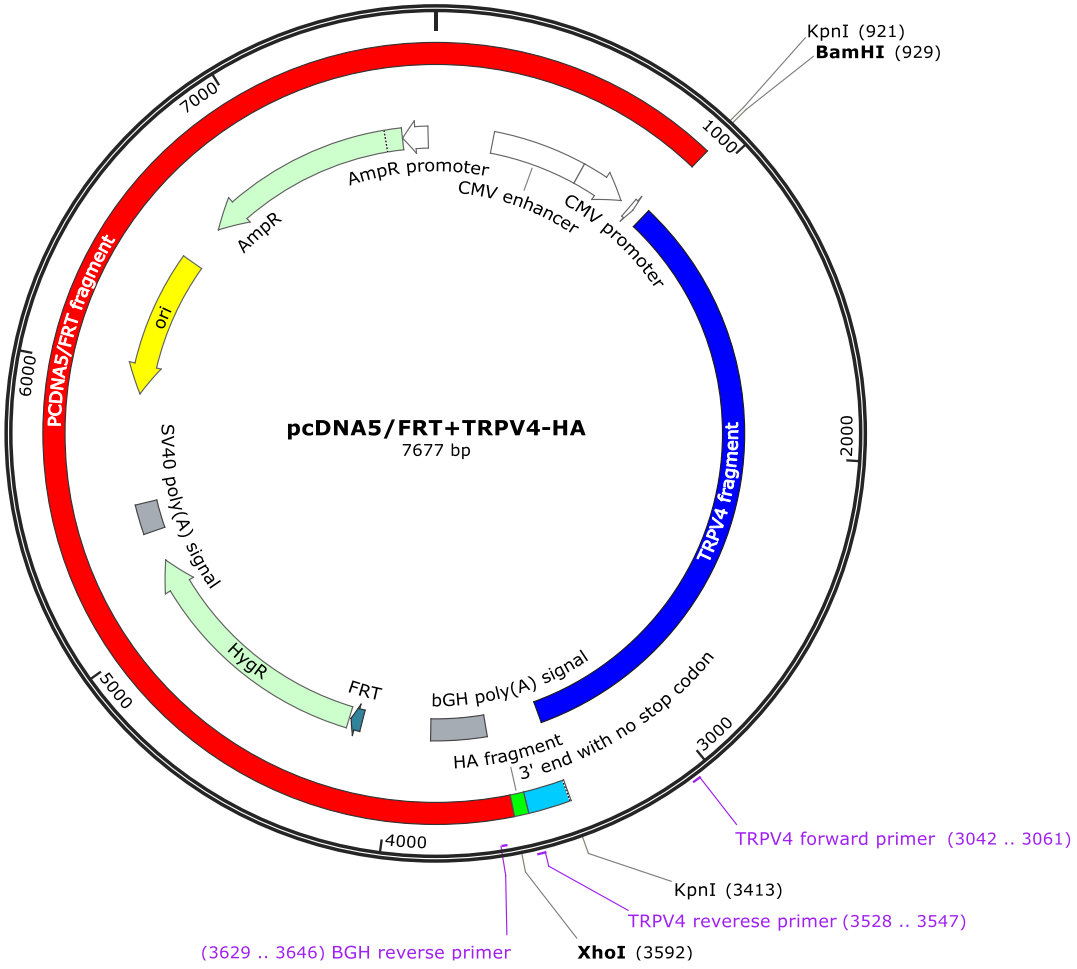

Fig 4.6 Vector map of the recombinant plasmid pcDNA5/FRT+TRPV4-HA. Primers (TRPV4 forward, TRPV4 reverse and BGH reverse), restriction enzyme sites (*Bam* HI, *Kpn* I and *Xho* I) and the different fragments (TRPV4, 3' end with no stop codon and pcDNA5/FRT-HA) involved in the construction and analysis of the plasmid have been indicated. Figure was created using SnapGene 4.1.9.

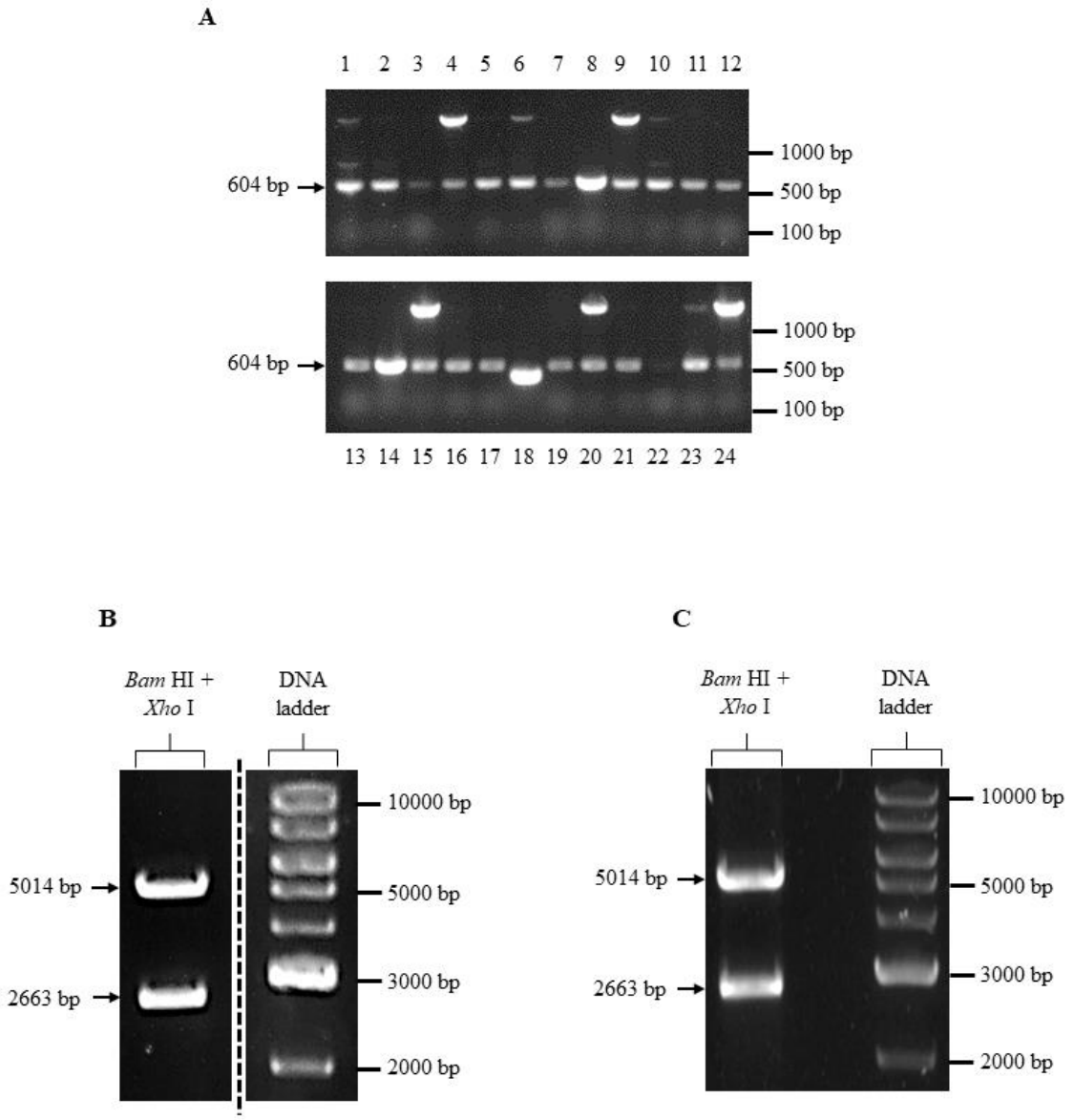

Fig 4.7 Analysis of the recombinant plasmid pcDNA5/FRT+TRPV4-HA using agarose gel electrophoresis. (**A**) Colony PCR was used to identify single colonies of transformed Mach1 cells with DNA containing the correct inserts. Positive clones were identified in lane 8 and 14 indicated by single bands representing the PCR-amplified DNA (604 bp). Restriction digest with *Bam* HI and *Xho* I was used to analyse the plasmid following (**B**) small scale and (**C**) large scale plasmid preparation. Bands for the pcDNA5/FRT vector (expected at 5014 bp) and TRPV4+3' end DNA segment-HA (expected at 2663 bp) fragment were observed.

4.2.2.ii Construction of recombinant plasmids: pcDNA5/FRT/TO+TRPV4-HA

My aim was to create a stable cell line that allowed inducible expression of the TRPV4 channels following tetracycline administration. Therefore, this required re-insertion of the HA tagged TRPV4 sequence without the stop codon into the pcDNA5/FRT/TO vector containing the *tet* operator 2 regions that allowed tetracycline-induced protein expression. The following REs and plasmids were used to obtain the necessary fragments (Fig 4.8) (chapter 2, table 2.4):

a) pcDNA5/FRT+TRPV4-HA (required fragment expected at 2663 bp) = *Bam* HI and *Xho* I

b) pcDNA5/FRT/TO (required fragment expected at 5081 bp) = *Xho* I and *Bam* HI

The DNA fragments were initially separated using gel electrophoresis (chapter 2, section 2.3.1.iv), extracted with QIAquick gel extraction kit (chapter 2, section 2.3.1.v) and subsequently ligated (chapter 2, section 2.3.1.vi). The ligated DNA was then used to transform Mach1 competent cells (chapter 2, section 2.3.1.vii) and the cells were spread onto agar plates. Colony PCR (chapter 2, section 2.3.1.viii) was then used to screen single bacterial colonies. DNA samples from each colony were analysed using gel electrophoresis. Positive clones were identified in lane 1 and 3 as shown by the single bands for the PCR-amplified DNA (predicted size, 604 bp) in Fig 4.9A. A 5 ml bacterial culture was then inoculated overnight for each clone and 1 ml of the inoculated culture was used for glycerol stocks (chapter 2, section 2.3.1.ix). The remaining culture was then used to purify the DNA using QIAprep Spin Miniprep Kit (chapter 2, section 2.3.1.x). The purified DNA was then screened through restriction digest followed by gel electrophoresis. The correct bands were observed for TRPV4+3' end DNA segment-HA fragment (predicted size, 2663 bp) and the remaining of the pcDNA5/FRT/TO vector

(predicted size, 5081 bp) as shown in Fig 4.9B. The glycerol stock was then used to inoculate a 250 ml culture and the DNA was purified using EndoFree Plasmid Maxi Kit (chapter 2, section 2.3.1.xi). Single and double RE digest along with a control (undigested plasmid) was then used to assess the size and quality of the purified plasmid followed by gel electrophoresis (Fig 4.9C). Double RE digest with *Bam* HI and *Xho* I produced bands with the correct predicted sizes as described earlier. Single digest of the plasmid with either of the RE produced a single band confirming the presence of a single restriction site for each RE. The uncut plasmid produced three different bands each representing nicked circular, linear and supercoiled (highest intensity) plasmid from top to bottom (Fig 4.9C).

4.2.2.iii Detection of the expression of TRPV4-HA following PEI mediated stable transfection of the plasmids

Using the techniques described in chapter 2 (section 2.3.2 and 2.3.3), PEI was used to stably transfect HEK Flp-In T-REx-293 cells with the recombinant plasmids generated in the earlier section. The Flp-In T-REx system allowed inducible expression of the gene of interest following exposure to tetracycline. Briefly, cells were plated in antibiotic-free DMEM medium (10% FBS, v/v) and divided into two groups which included a control group (HEK_{VO}) that was transfected with just the plasmid vector, pcDNA5/FRT/TO, and another group transfected with the vector containing the gene of interest (HEK_{TRPV4}), pcDNA5/FRT/TO+TRPV4-HA. The following day, the transfection mix was prepared at 3:1 ratio of polyethylenimine (PEI) (9 µg/well) and pOG44+DNA (3 µg/well). The pOG44/DNA was prepared in 9:1 ratio (2.7 µg of pOG44:0.3 µg of either pcDNA5/FRT/TO or pcDNA5/FRT/TO+TRPV4-HA). The transfection mix was then added to each well and cells were incubated for 2-3 days. Cells were then selected using medium containing the appropriate antibiotics (chapter 2, table 2.1) which was replaced

every 2-3 days for 2-3 weeks. Single colonies of the cell line were then isolated (chapter 2, section 2.3.4) and transferred into a 12 well plate. The clones were transferred to larger culture plates and flasks once they were confluent. Immunocytochemistry (chapter 2, section 2.5) and western blotting (chapter 2, section 2.6) were then used to detect the expression of TRPV4-HA following treatment of HEK_{VO} and HEK_{TRPV4} with (+) and without tetracycline (0.1 µg/ml, 16 h). Using epifluorescent microscopy, TRPV4-HA immunoreactivity was undetectable in most of the uninduced HEK_{TRPV4} cells; however, few of these cells demonstrated some TRPV4-HA expression, indicating a possible leakage in the tetracycline-inducible expression system (Figure 4.10A). Other studies have also reported a similar leakage with the T-REx system (Liu et al. 2011; Cachat et al. 2014). Significant expression of TRPV4-HA was detected in $HEK_{TRPV4+Tet}$ cells (Fig 4.10A) indicating that the expression system was functional. In addition, results from the western blot also revealed an immunoreactive band at approximately 98 kDa, the predicted molecular weight of TRPV4-HA, for $HEK_{TRPV4+Tet}$ cells only (Fig 4.10B). TRPV4-HA expression was undetectable in HEK_{VO+Tet} and uninduced HEK_{TRPV4}, further confirming the specificity of detection and a functional tetracycline inducible system in the HEK_{TRPV4} cells. Although expression of TRPV4 was not detected in the uninduced HEK_{TRPV4} cells using western blot, images obtained with immunocytochemistry revealed a possible leakage with the T-REx system, resulting in lower levels of TRPV4 expression. Immunocytochemistry is a technique that allows the visual detection of the target protein expression in a single cell and as a result is more sensitive compared to western blot. Therefore, it is possible that due to the lower levels of TRPV4 expression in the uninduced HEK_{TRPV4}, western blot was not sensitive enough to detect any expression of these channels. In addition, some antibodies can only bind to the target proteins that are either in their denatured structure or in their native tertiary structure (Willingham 1999).

The conditions used for western blot results in denaturation of the protein molecules whereas proteins are fixed and are closer to their native structure with immunocytochemistry, therefore it is possible that this might have affected the antigen binding affinity of the primary antibody. However, tetracycline induction of $HEK_{TRPV4+Tet}$ cells clearly demonstrated TRPV4 expression with western blot and therefore the observed discrepancy was most likely due to the reduced protein levels of TRPV4 in the uninduced HEK_{TRPV4} cells.

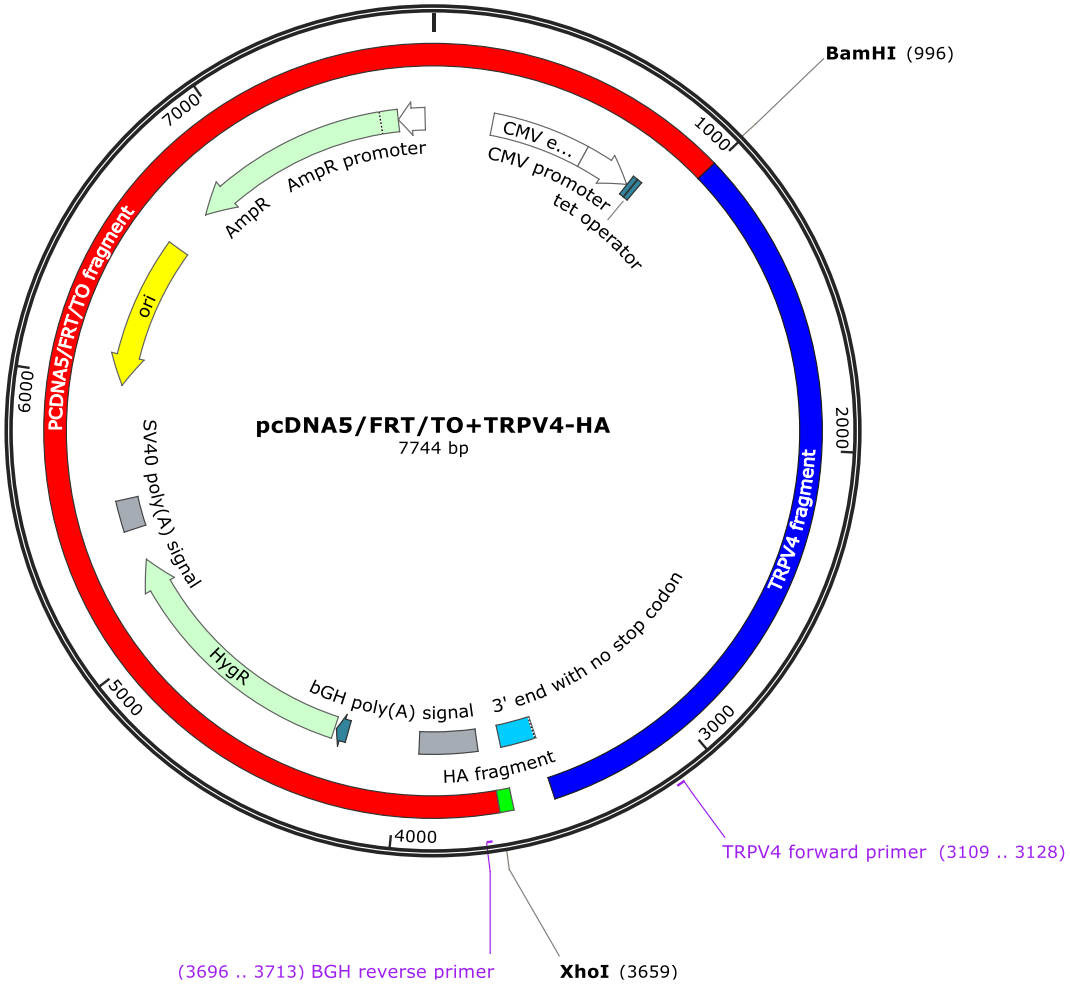

Fig 4.8 Vector map of the recombinant plasmid pcDNA5/FRT/TO+TRPV4-HA. Primers (TRPV4 forward and BGH reverse), restriction enzyme sites (*Bam* HI and *Xho* I) and the different fragments (TRPV4+3' end with no stop codon-HA and pcDNA5/FRT/TO) involved in construction of the plasmid have been indicated. Figure was created using SnapGene 4.1.9.

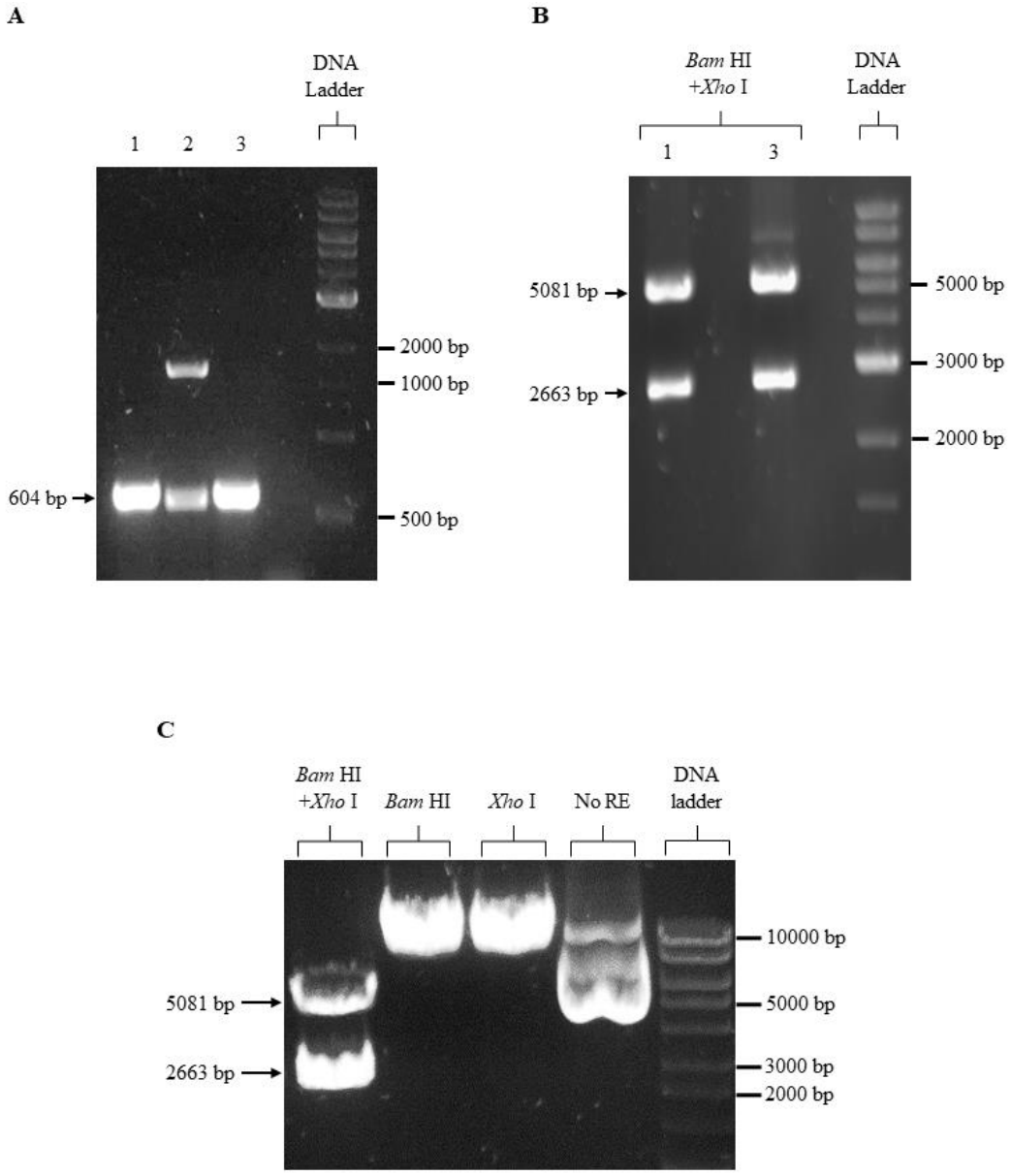

Fig 4.9 Analysis of the recombinant plasmid pcDNA5/FRT/TO+TRPV4-HA using agarose gel electrophoresis. (**A**) Using colony PCR, positive clones of transformed Mach1 cells were identified in lane 1 and 3 indicated by single bands representing the PCR-amplified DNA (604 bp). Restriction digest was used to analyse the plasmid following (**B**) small scale and (**C**) large scale plasmid preparation. Bands for the pcDNA5/FRT/TO vector (expected at 5081 bp) and TRPV4+3' end DNA segment-HA (expected at 2663 bp) fragment were observed following double restriction digest with *Bam* HI and *Xho* I. Single bands were observed following digestion with either of the enzymes. The undigested plasmid was separated into three fragments that represent nicked circular, linear and supercoiled DNA.

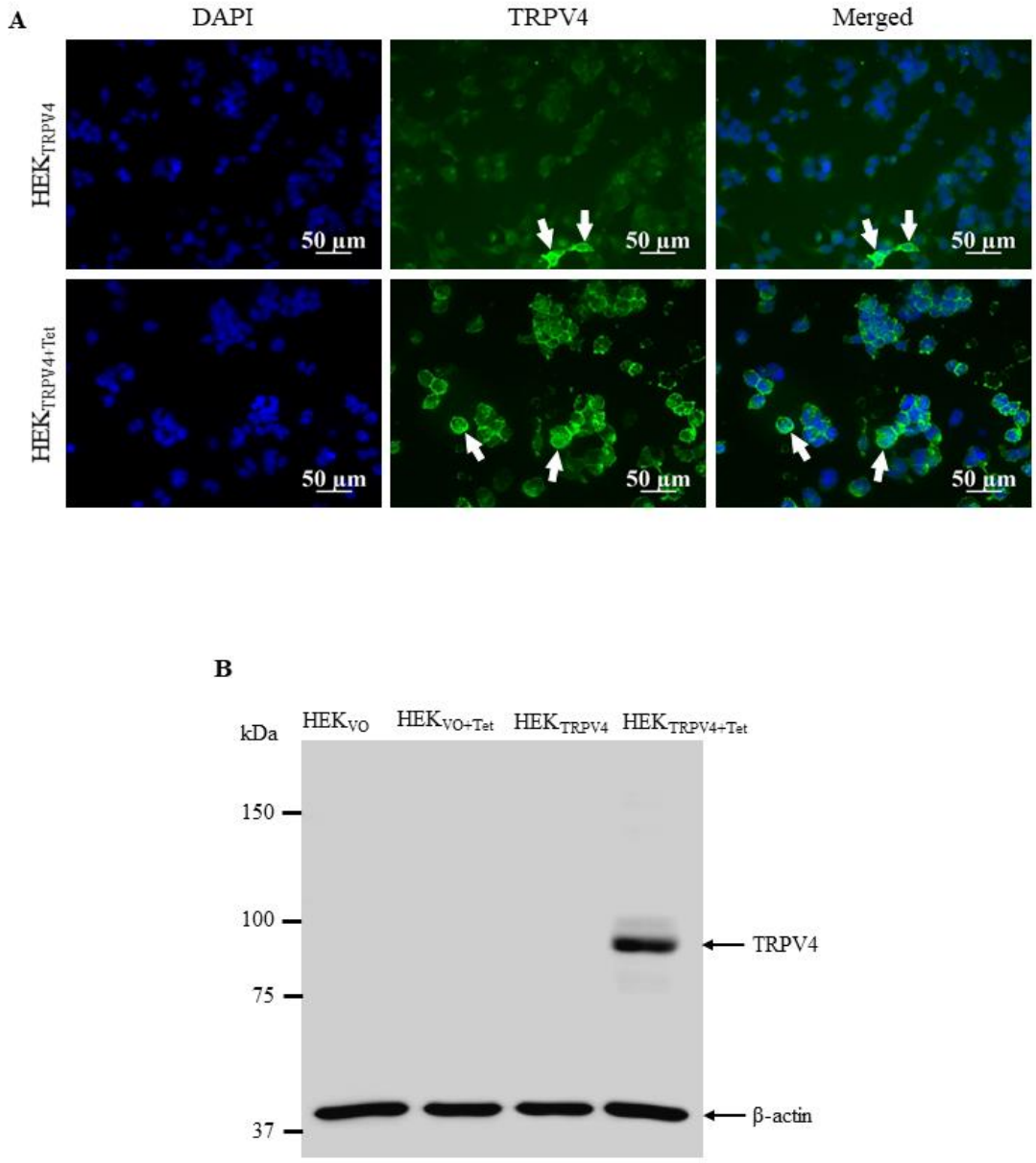

Fig 4.10 The effect of tetracycline on TRPV4-HA expression. Immunofluorescence and epifluorescent microscopy (20x objectives) of HEK_{TRPV4} cells using anti-HA antibody (green) and nuclear stain DAPI (blue), (**A**) TRPV4 signals were mostly absent in HEK_{TRPV4} cells (although TRPV4 signals were detected in a few cells, arrows). Significant expression of TRPV4 (arrows) was detected in tetracycline (0.1 µg/ml) induced $HEK_{TRPV4+Tet}$ cells. Scale bar, 50 µm. (**B**) Western blot analysis for TRPV4-HA expression in HEK_{TRPV4} and HEK_{VO} cells with (+) and without tetracycline. The immunoreactive band at ~98 kDa indicates expression of TRPV4 in induced $HEK_{TRPV4+Tet}$ cells. Bands were absent in HEK_{VO} or HEK_{TRPV4} cells.

4.2.3 TRPV4 is not directly modulated by n-3 PUFAs

PUFAs such as AA and EETs have been reported to directly activate TRPV4, resulting in subsequent activation of K_{Ca} that can lead to vasodilation (Zheng et al. 2013; Sonkusare et al. 2012; Earley et al. 2005; Earley, Pauyo, et al. 2009). My myograph results indicate the role of IK_{Ca} and BK_{Ca} along with TRPV4 in n-3 PUFAs, notably DHA mediated vascular relaxation. Therefore, I investigated whether the TRPV4 channels were directly modulated by n-3 PUFAs using the fluorescent calcium indicator, Fluo-4 AM. As described in chapter 2 (section 2.7), HEK_{VO} and HEK_{TRPV4} cells were initially seeded onto a 6 well plate with poly-D-lysine and the following day tetracycline (0.1 µg/ml, 16 h) was added to each well containing HEK_{TRPV4} cells. Cells were then washed and loaded in the dark with Fluo-4 AM (4 µM, 20 min, 37 °C). For some experiments HC-067047 (1 µM), an inhibitor of TRPV4, was also added together with the Fluo-4 AM whereas some experiments involved the initial pre-treatment of the cells with either DHA or EPA (30 µM, 1 h). Cells were then washed and the coverslips were transferred into a 24 well plate to enable visualisation under the microscope. Baseline fluorescence was initially measured for 30 s prior to the administration of the drug [either n-3 PUFA (30 µM) or GSK (3 nM)] and the subsequent responses were measured for an additional 370 s followed by the application of ionomycin (10 µM, responses were measured for another 200 s). GSK failed to elicit any significant changes in $[Ca^{2+}]_i$ with HEK_{VO} cells (Fig 4.11A and 4.12A-B), prior to the application of ionomycin. In uninduced HEK_{TRPV4} cells, GSK led to a significant increase in $[Ca^{2+}]_i$ which was about half of the response generated by ionomycin (Fig 4.11B and 4.12A-B), confirming the presence of some leakage in the tetracycline-inducible expression system as mentioned earlier (Fig 4.10A). In tetracycline induced $HEK_{TRPV4+Tet}$ cells, GSK elicited significant increase in $[Ca^{2+}]_i$ that was comparable to the ionomycin response (Fig 4.11C, 4.12A-B). However, these

responses were completely abolished following treatment of $HEK_{TRPV4+Tet}$ cells with the HC-067047 (Fig 4.11D and 4.12A-B), indicating the presence of functional of TRPV4 channels. The presence of n-3 PUFA-mediated activation of TRPV4 was then investigated with $HEK_{TRPV4+Tet}$ cells. Application of the vehicle (ethanol) used for the dilution of n-3 PUFAs along with DHA and EPA failed to elicit any significant increase in $[Ca^{2+}]_i$, as indicated by Fig 4.13 and Fig 4.14. Pre-treatment of the $HEK_{TRPV4+Tet}$ cells with either of the n-3 PUFA for 1h, also did not induce any significant changes in GSK-induced calcium influx, as demonstrated by Fig 4.15 and 4.16.

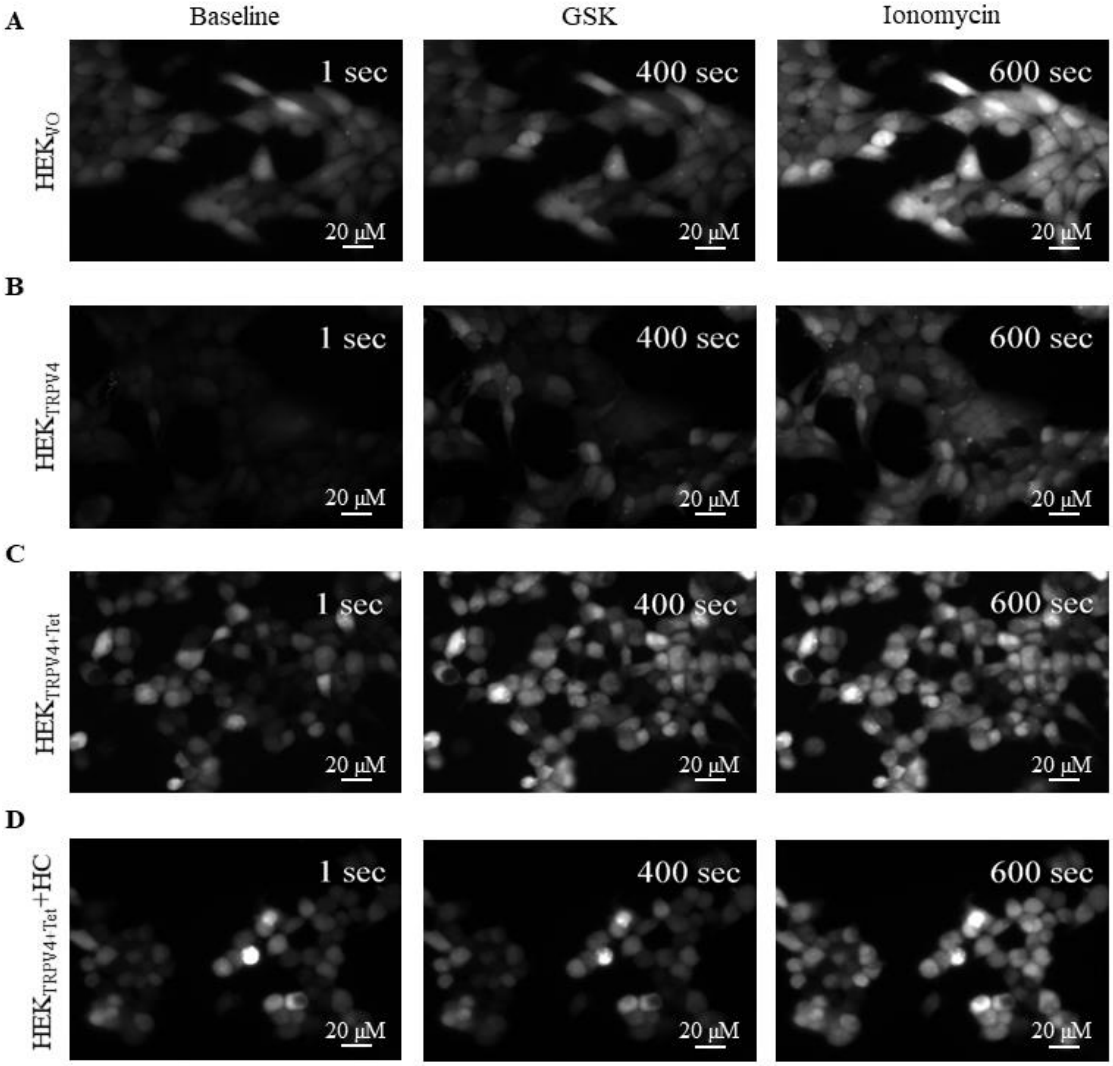

Fig 4.11 Representative images of HEK_{VO} and HEK_{TRPV4} cells loaded with Fluo-4 AM demonstrating the changes in $[Ca^{2+}]_i$ at different time points, following acute application of GSK. Images indicate baseline fluorescence (1 sec), maximum fluorescence induced by GSK (GSK1016790A) (3 nM, 400 sec) and maximum fluorescence induced by ionomycin (10 µM, 600 sec) in; (**A**) HEK_{VO}, (**B**) HEK_{TRPV4}, (C) $HEK_{TRPV4+Tet}$ and (**D**) $HEK_{TRPV4+Tet}$ pre-treated with HC-067047 (HC) (1 µM, 20 min). $HEK_{TRPV4+Tet}$ cells were pre-incubated with tetracycline (0.1 µg/ml, 16 h) to induce TRPV4 expression. Fluorescence was measured with 40x objective lens using excitation and emission wavelengths of 488 nm and 506 nm respectively.

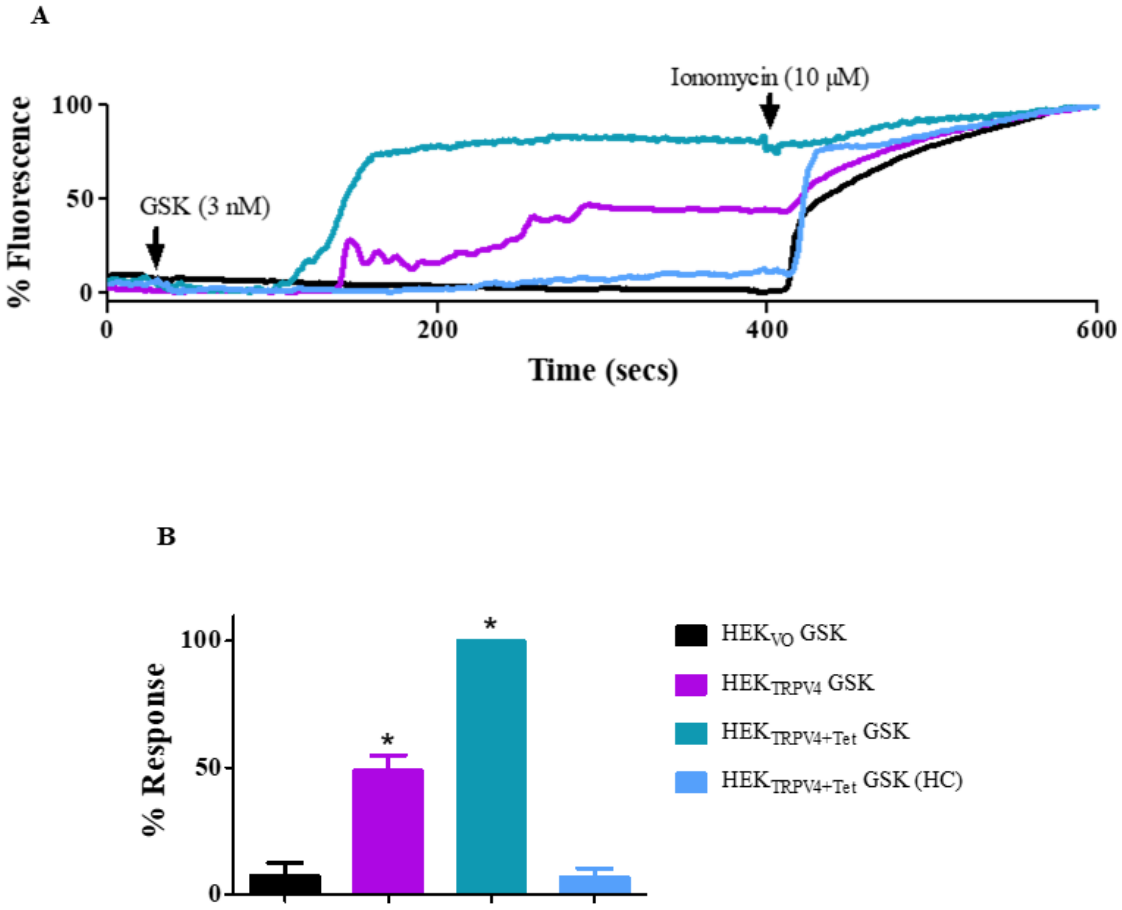

Fig 4.12 HEK$_{TRPV4+Tet}$ cells express functional TRPV4 channels. (**A**) Original traces and (**B**) bar graph demonstrating the changes in $[Ca^{2+}]_i$ following the acute application of GSK (GSK1016790A) (3 nM) in HEK$_{VO}$, HEK$_{TRPV4}$ and HEK$_{TRPV4+Tet}$ cells pre-treated with or without HC-067047 (HC) (1 µM, 20 min). GSK and ionomycin (10 µM) were applied at 30 and 400 s respectively, as indicated by the arrows. Tetracycline (0.1 µg/ml, 16 h) was used to induce TRPV4 expression in HEK$_{TRPV4+Tet}$ cells. *P<0.05 indicates significant difference from the GSK response in HEK$_{VO}$ cells as determined using one-way ANOVA with Bonferroni post-test (*n*=3).

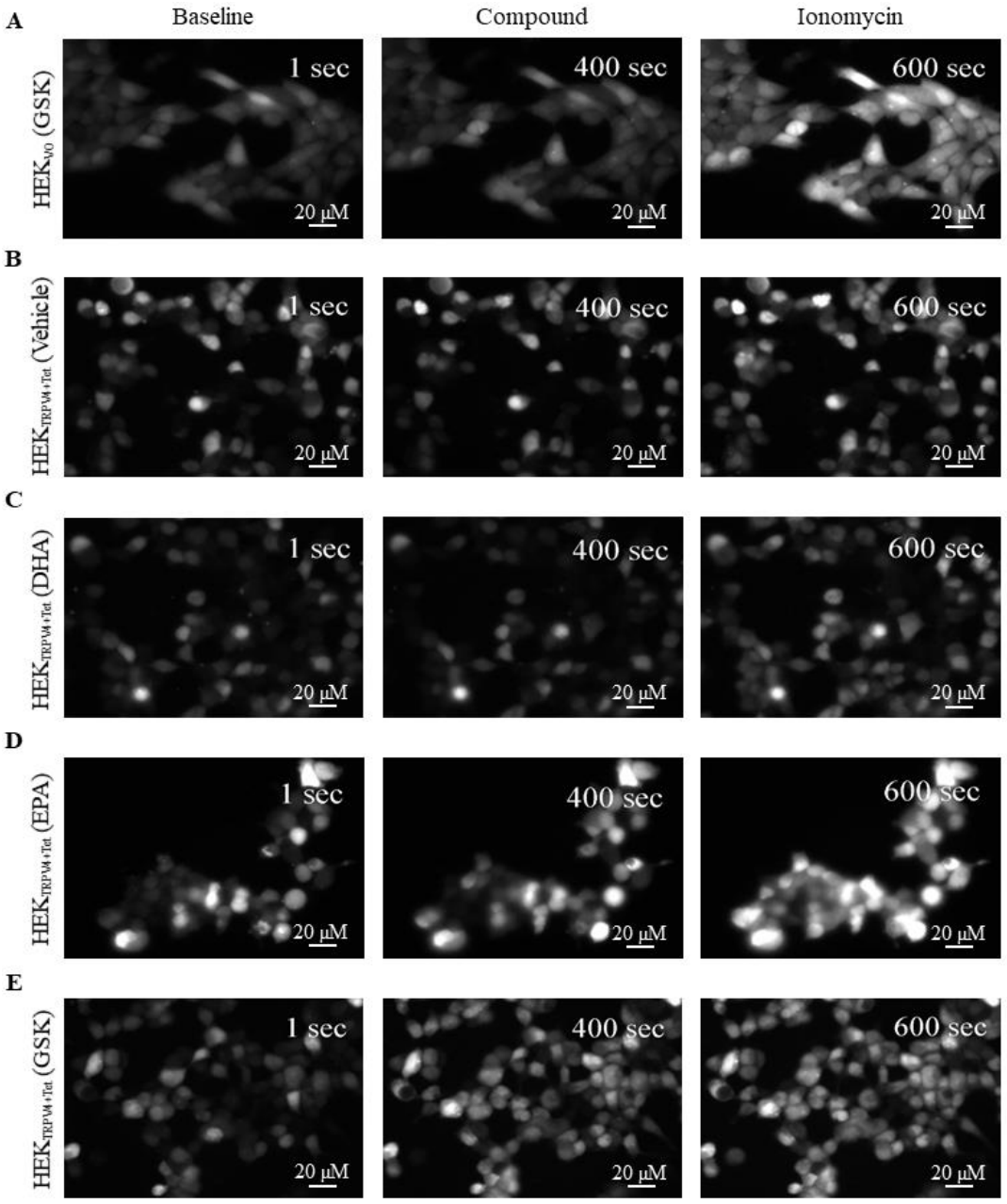

Fig 4.13 Representative images demonstrating changes in $[Ca^{2+}]_i$ at different time points. Images indicate baseline fluorescence (1 sec) and maximum fluorescence (400 sec) induced by (**A**) GSK (GSK1016790A) (3 nM) in HEK_{VO} cells (control) and by (**B**) vehicle (ethanol), (**C**) DHA (30 µM), (**D**) EPA (30 µM) and (**E**) GSK in $HEK_{TRPV4+Tet}$ cells. The third column of images represents maximum fluorescence elicited by ionomycin (10 µM, 600 sec). $HEK_{TRPV4+Tet}$ cells were pre-incubated with tetracycline (0.1 µg/ml, 16 h) to induce TRPV4 expression. Fluorescence was measured with 40x objective lens using excitation and emission wavelengths of 488 nm and 506 nm respectively.

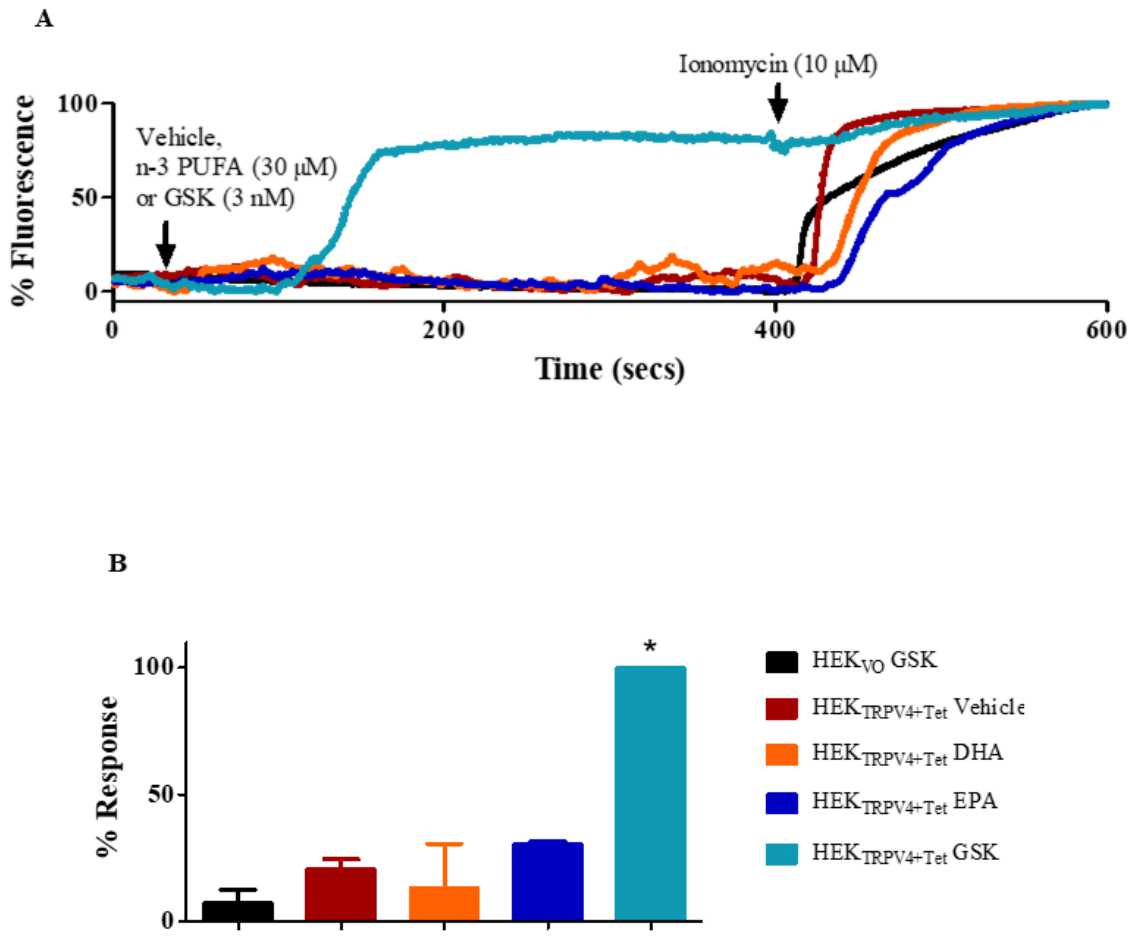

Fig 4.14 Acute application of n-3 PUFAs did not elicit any significant changes in $[Ca^{2+}]_i$. (**A**) Original traces and (**B**) bar graph demonstrating the changes in $[Ca^{2+}]_i$ following the acute application of GSK (GSK1016790A) (3 nM) in HEK_{VO} cells along with vehicle (ethanol), DHA (30 µM), EPA (30 µM) and GSK in $HEK_{TRPV4+Tet}$ cells. Compounds and ionomycin (10 µM) were applied at 30 and 400 s respectively, as indicated by the arrows. Tetracycline (0.1 µg/ml, 16 h) was used to induce TRPV4 expression in $HEK_{TRPV4+Tet}$ cells. *P<0.05 indicates significant difference from the GSK response in HEK_{VO} cells as determined using one-way ANOVA with Bonferroni post-test (*n*=3).

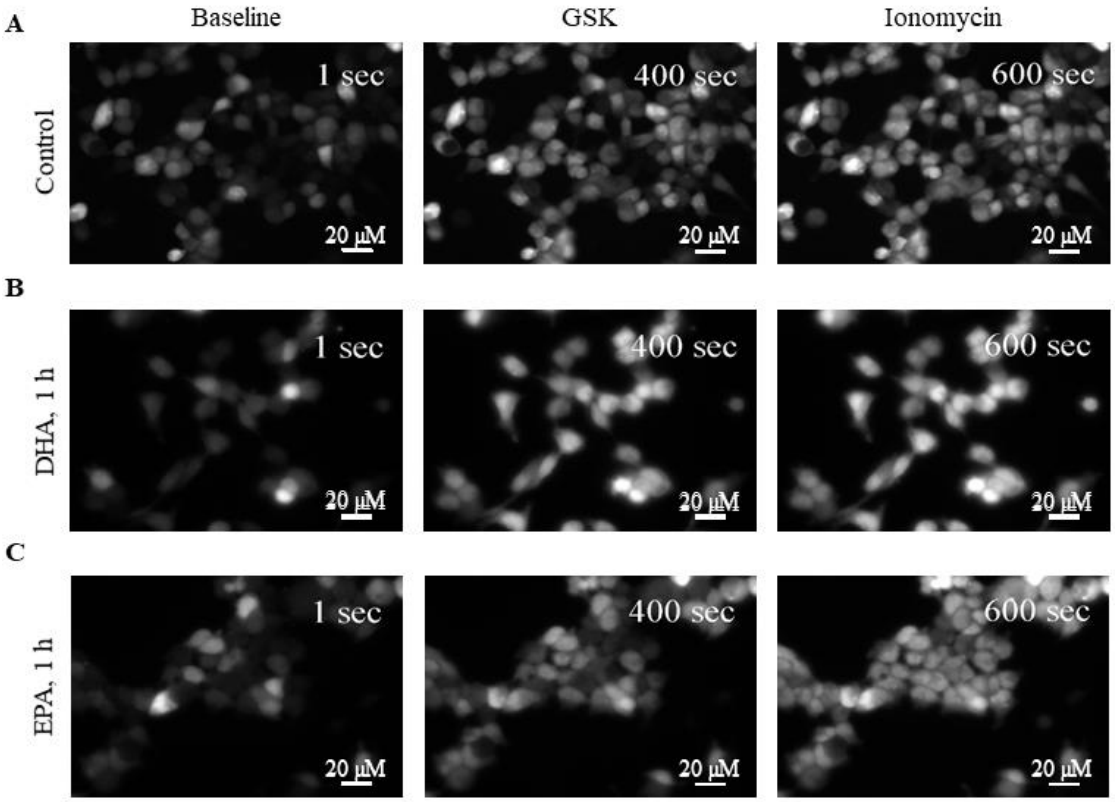

Fig 4.15 Representative images of $HEK_{TRPV4+Tet}$ cells pre-treated with or without n-3 PUFAs demonstrating the changes in $[Ca^{2+}]_i$ at different time points. Images indicate baseline fluorescence (1 sec), maximum fluorescence (400 sec) induced by GSK (GSK1016790A) (3 nM); in $HEK_{TRPV4+Tet}$ cells (**A**) without any pre-treatments (control) and with the pre-treatment of (**B**) DHA (30 µM, 1 h) and (**C**) EPA (30 µM, 1 h), followed by maximum fluorescence induced by ionomycin (10 µM, 600 sec). $HEK_{TRPV4+Tet}$ cells were pre-incubated with tetracycline (0.1 µg/ml, 16 h) to induce TRPV4 expression. Fluorescence was measured with 40x objective lens using excitation and emission wavelengths of 488 nm and 506 nm respectively.

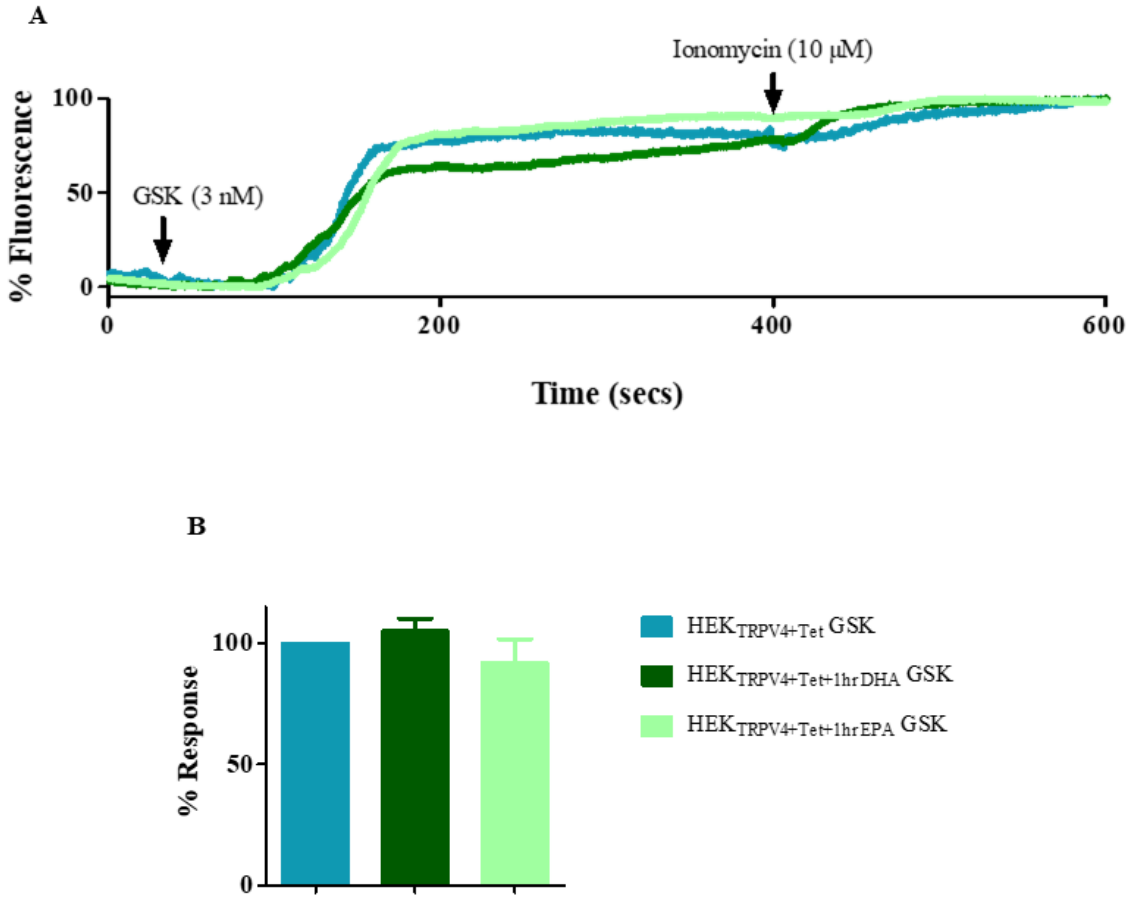

Fig 4.16 Pre-treatment of $HEK_{TRPV4+Tet}$ cells with n-3 PUFAs did not alter GSK-mediated response. (**A**) Original traces and (**B**) bar graph demonstrating changes in $[Ca^{2+}]_i$ following the acute application of GSK (GSK1016790A) (3 nM) in $HEK_{TRPV4+Tet}$ cells pre-treated with or without n-3 PUFA (30 µM, 1 h). GSK and ionomycin (10 µM) were applied at 30 and 400 s respectively, as indicated by the arrows. Tetracycline (0.1 µg/ml, 16 h) was used to induce TRPV4 expression in $HEK_{TRPV4+Tet}$ cells. *P<0.05 indicates significant difference from the GSK response in HEK_{VO} cells as determined using one-way ANOVA with Bonferroni post-test (*n*=3).

4.3 Summary

Multiple studies have reported that PUFAs such as AA and EETs can stimulate TRPV4 to subsequently activate K_{Ca} channels resulting in hyperpolarization and relaxation of vascular SMCs (Earley et al. 2005; Earley, Pauyo, et al. 2009; Zheng et al. 2013; Sonkusare et al. 2012). In chapter 3 (section 3.2.5), the role of IK_{Ca} and BK_{Ca} channels were demonstrated in DHA-mediated relaxation of both rat aorta and mesenteric artery along with EPA-mediated relaxation of the rat mesenteric artery. Therefore, the next experiments focussed on investigating whether TRPV4 was initially stimulated by n-3 PUFAs which subsequently led to the activation of K_{Ca} channels resulting in relaxation of rat arteries. My myograph findings demonstrate that DHA-induced vascular relaxation was partially attenuated through the inhibition of TRPV4 with RN-1734 in rat mesenteric artery (Fig 4.3A), and the magnitude of inhibition appeared to be similar to the IK_{Ca} component observed previously (Fig 3.17A). However, RN-1734 did not affect both DHA- and EPA-induced relaxation of rat aorta (Figs 4.3B and 4.3C), indicating heterogeneity in the vasodilation mechanisms depending upon the vascular bed. Similarly, another TRPV4 blocker, HC-067047, also did not affect both DHA- and EPA-induced relaxation of rat aorta (Figs 4.5A-B).

To assess whether n-3 PUFAs were involved in the modulation of TRPV4, a stable cell line that allowed inducible expression of TRPV4 was generated using molecular cloning and PEI-mediated transfection of the recombinant plasmids (Fig 4.6-4.9). Epifluorescent microscopy and western blot was then used to confirm the expression of TRPV4-HA in $HEK_{TRPV4+Tet}$ cells (Fig 4.10). Using the calcium indicator, Fluo-4 AM, I then investigated whether the TRPV4 channels were functional and if the n-3 PUFAs could influence channel activity. In my negative control, HEK_{VO} cells, GSK failed to evoke any changes in $[Ca^{2+}]_i$ as shown in Fig 4.11A and 4.12. In uninduced HEK_{TRPV4} cells,

application of GSK led to some increase in $[Ca^{2+}]_i$ as demonstrated by Fig 4.11B and 4.12, indicating the presence of some leakage in the tetracycline-inducible expression system. In tetracycline-induced $HEK_{TRPV4+Tet}$ cells, application of GSK led to significant calcium influx compared to HEK_{VO} cells and this effect was completely abolished following additional treatment with HC067047 (Fig 4.11C-D and 4.12A). This demonstrated that the TRPV4 channels expressed in the stable cell line were functional. The effects of n-3 PUFAs were then investigated via acute application of both DHA and EPA. Both n-3 PUFAs failed to activate TRPV4 channels in $HEK_{TRPV4+Tet}$ cells (Fig 4.13C-D and 4.14B). Pre-treatment of these cells with either of the n-3 PUFA for 1 h also did not elicit any significant changes in GSK-induced calcium influx (Fig 4.15 and 4.16). My myograph finding demonstrated that the blockade of TRPV4 can result in partial inhibition of DHA-induced relaxation in rat mesenteric artery. However, in $HEK_{TRPV4+Tet}$ cells, n-3 PUFAs failed to elicit any increase in $[Ca^{2+}]_i$. There is a possibility that TRPV4 maybe indirectly modulated by metabolites of n-3 PUFA, similar to AA-derived EETs. Furthermore, the microdomains such as the localization of IK_{Ca} and TRPV4 in myoendothelial projections reported in native vascular ECs are not present in the stable HEK cells. There is also evidence indicating that n-3 PUFAs can only activate TRPV1 channels following initial phosphorylation by PKC (Matta et al. 2007). Studies indicate that the opening of TRPV1 to certain stimuli such as heat, capsaicin and anandamide can be potentiated by PKC-mediated channel phosphorylation (Vellani et al. 2001). As a result, it can be speculated that the stable cells may lack these necessary microdomains and intracellular machinery required to observe any changes in $[Ca^{2+}]_i$, with the acute application of n-3 PUFAs. Consistent with my findings, a recent electrophysiological study also demonstrated that the acute application of EPA does not activate TRPV4 channels expressed in HEK cells (Caires et al. 2017). However, an indirect interaction

between TRPV4 and n-3 PUFA was indicated, as overnight supplementation of vascular ECs with EPA was reported to enhance TRPV4 currents, due to an increase in cell membrane fluidity (discussed in chapter 6, section 6.3). To summarize, my findings along with other studies indicate that DHA does not directly affect the activity of TRPV4 channels and the TRPV4 component of DHA-mediated relaxation, observed in rat mesenteric artery (Fig 4.3A), possibly involves an indirect activation of these channels.

Chapter 5

The role of K_{ATP} in n-3 PUFA mediated vasodilation

5.1 Introduction

Omega-6 PUFAs such as AA have been reported to induce vasodilation through different molecular mechanisms including activation of potassium channels. Studies using patch clamp electrophysiology have demonstrated that AA can directly activate BK_{Ca} channels present in SMCs derived from rabbit pulmonary artery (Kirber et al. 1992; Clarke et al. 2002). Furthermore, numerous studies have indicated that CYP metabolites of AA (EETs) can also directly activate BK_{Ca} expressed in various mammalian arteries such as rabbit carotid artery (Dong et al. 1997), rat mesenteric artery (Adeagbo 1997), rat renal arteries (Zou et al. 1996), guinea pig coronary artery (Eckman et al. 1998), bronchial SMCs (Dumoulin et al. 1998) and bovine coronary arteries (Harder et al. 1984).

There is also evidence indicating that EETs can activate other types of potassium channels including K_{ATP} (Ye et al. 2005; Ye et al. 2006). These channels are hetero-octameric complexes composed of Kir6 and SUR subunits (Inagaki et al. 1995; Inagaki et al. 1996; Seino 1999). Expression of these channels has been reported in different types of cells including pancreatic, skeletal muscle, vascular endothelial and SMCs (Ashcroft et al. 1984; Spruce et al. 1985; Janigro et al. 1993; Dart and Standen 1993). K_{ATP} is involved in various physiological processes such as insulin secretion, cardiac arrhythmia (Ye et al. 2005; Ye et al. 2006; Lu et al. 2006) and vasodilation (Ashcroft and Rorsman 1990; Tinker et al. 2014; Blanco-Rivero et al. 2008; Standen et al. 1989). Most of the studies investigating the effect of PUFAs on vascular K_{ATP} have been conducted using CYP-derived metabolites of AA (EETs). Depending upon the type of tissue, EETs have been reported to activate K_{ATP} through two different mechanisms; for example in cardiac myocytes, EETs can directly bind to the Kir6 subunit present in cardiac K_{ATP} resulting in reduction of channel sensitivity to ATP (Lu, Hoshi, et al. 2001; Lu et al. 2005), whereas

in rat mesenteric artery, EETs indirectly activate vascular K_{ATP} through PKA-dependent pathway (Ye et al. 2005; Ye et al. 2006; Lu et al. 2006).

Similar to AA and EETs, n-3 PUFAs have also been reported to elicit vasodilation through activation of potassium channels. Studies demonstrate a direct activation of BK_{Ca} present in mouse aortic (Toshinori Hoshi, Wissuwa, et al. 2013) and rat coronary (Lai et al. 2009) SMCs by DHA. Furthermore, CYP metabolites of DHA (EDPs) also activate BK_{Ca} in porcine (Ye et al. 2002) and rat coronary arteries (Wang et al. 2011). Studies also indicate that CYP-derived metabolites of EPA (EpETEs) can activate BK_{Ca} present in SMCs derived from rat cerebral and mouse mesenteric arteries (Hercule et al. 2007). There is also some evidence indicating that both DHA (Sato et al. 2014) and EPA (Engler et al. 2000) can relax rat arteries through activation of the K_{ATP} channels. Myograph data from these studies demonstrated an inhibition in n-3 PUFA- and EDP-induced relaxation of rat aorta following blockade of K_{ATP} (Engler et al. 2000). However, there is currently no evidence in the literature indicating a direct modulation of these channels by n-3 PUFAs.

K_v7 channels have also been reported to be modulated by fatty acids such as AA and n-3 PUFAs. These are voltage-gated potassium channels composed of five α subunits, $K_v7.1$-7.5, that form homomeric and heteromeric complexes (Greene and Hoshi 2017). They are involved in the regulation of vascular tone and current evidence suggests that most of the α-subunits, excluding $K_v7.2$, are expressed in blood vessels (Ng et al. 2011). Studies have demonstrated that 12-lipoxygenase metabolites of AA can enhance M currents (Villarroel 1994; Yu 1995), which mainly involve $K_v7.2$ and $K_v7.3$ heteromers (Brown and Passmore 2009). Cardiac I_{Ks} channel which is composed of $K_v7.1$ and *KCNE1* subunits was also reported to be modulated by n-3 PUFAs (Osteen et al. 2010). DHA was found to enhance I_{Ks} currents in *Xenopus* oocytes which was dependent upon the presence

of *KCNE1* subunit (Doolan et al. 2002). Another study also reported that dietary inclusion of n-3 PUFAs enhanced I_{Ks} currents in porcine ventricular myocytes (Verkerk et al. 2006). In-depth studies revealed that acute administration of both n-3 PUFAs was involved in facilitating activation of I_{Ks} in guinea pig cardiomyocytes (Moreno et al. 2015). Negatively charged n-3 PUFAs were also reported to enhance M currents in Xenopus oocytes by promoting channel opening (Liin et al. 2016). On the contrary, chronic administration of n-3 PUFAs could not enhance I_{Ks} currents and also attenuated the expression of $K_v7.1$ in COS7 cells (Moreno et al. 2015).

My myograph data from the earlier experiments (chapter 3, section 3.2.1 and 3.2.5) revealed that a significant amount of residual relaxation remained, following removal of endothelium and inhibition of K_{Ca}, indicating the presence of other endothelium-independent vasodilation mechanism(s) that still allowed full relaxation of the arteries. Hyperpolarization of SMCs through opening of the potassium channels is one of the most important vasodilation mechanisms especially in resistance arteries, therefore the next set of experiments focussed on investigating this pathway. I initially used wire myograph (chapter 2, section 2.2) to investigate the effect of non-selective inhibition of potassium channels-induced hyperpolarization in n-3 PUFA mediated relaxation of both rat aorta and mesenteric artery. To characterise the potassium channels involved, I then investigated the role of K_{ATP} channels in n-3 PUFA mediated relaxation with wire myograph, using a K_{ATP} selective inhibitor (PNU37883A). To further investigate whether n-3 PUFAs could directly modulate K_{ATP}, I initially created a stable cell line expressing the Kir6.1 and SUR2B subunits (chapter 2, section 2.4). These stable cells were then used for whole cell patch clamp (chapter 2, section 2.8) to examine K_{ATP} channel activity. Finally, I also examined the role of K_v7 channels in n-3 PUFA mediated relaxation with wire myograph using a non-selective K_v7 inhibitor (XE991).

5.2 Results

5.2.1 Effect of inhibiting potassium channel-induced hyperpolarization in n-3 PUFA mediated vascular relaxation

Potassium channels have an important role in inducing vasodilation through hyperpolarization of vascular smooth muscle cells. Findings from the earlier experiments revealed that a significant amount of residual relaxation remained following removal of endothelium and inhibition of K_{Ca} with n-3 PUFA-induced relaxation (chapter 3, section 3.2.1 and 3.2.5). Therefore, the next experiments focussed on characterising these unknown vasodilation mechanisms. High KCl Krebs (30 mM) can be used to alter the reversal potential for potassium ions which can lead to inhibition of intracellular potassium efflux, resulting in subsequent inhibition of hyperpolarization at physiological membrane potentials. As a result, I initially investigated the effect of high KCl Krebs (30 mM) in n-3 PUFA mediated vasodilation using wire myograph (protocol described in chapter 2, section 2.2.5.ii). The relaxant effect of n-3 PUFAs was recorded before and after the incubation of arteries with high KCl Krebs for 20 min. Representative traces from Fig 5.1 and Fig 5.2 demonstrate the effects of high KCl Krebs in DHA-induced relaxation of rat mesenteric artery and aorta respectively. In rat mesenteric artery, incubation of high KCl Krebs led to significant inhibition and reduction of the efficacy of DHA to induce vascular relaxation [(30µM DHA; 96±0.9% (Control) and 35±7.6% (High KCl Krebs)] (Fig 5.3A) (n=6, $P<0.05$). Similarly, high KCl Krebs also inhibited EPA-induced relaxation of rat mesenteric artery although to a lesser extent [30µM EPA; 98.2±0.26% (Control) and 69.3±4.4% (High KCl Krebs)] (Fig 5.3B) (n=5, $P<0.05$). DHA-induced relaxation was completely abolished following incubation with high KCl Krebs in rat aorta [30µM DHA; 89.4±2.3% (Control) and 2.6±3.2% (High KCl Krebs)]

(Figs 5.4A) (*n*=5, P<0.05). Similarly, EPA-induced relaxation was also abrogated following pre-treatment with high KCl Krebs [30µM EPA; 92.9±2.4% (Control) and 9.4±4.1% (High KCl Krebs)] (Figs 5.4B) (*n*=5, P<0.05)

5.2.2 Effect of K_{ATP} inhibition on n-3 PUFA mediated vascular relaxation

The robust reduction and abrogation of n-3 PUFA mediated relaxation in rat mesenteric artery and aorta respectively, following pre-incubation with high KCl Krebs, strongly indicates that potassium channels are involved. As I have already demonstrated the role of IK_{Ca} and BK_{Ca} in n-3 PUFA-induced relaxation, I investigated K_{ATP} channels to further characterise the potassium channels involved using wire myograph (chapter 2, section 2.2.5.ii). Experiments were initially conducted with glibenclamide, however, application of this inhibitor disrupted the maintenance of arterial tone. This was not surprising as previous studies have indicated that glibenclamide can act as a TP receptor antagonist (Cocks et al. 1990). Fig 5.5 and Fig 5.6 shows representative traces demonstrating the effect of PNU37883A (3 µM) in DHA-induced relaxation of rat mesenteric artery and aorta respectively. In rat mesenteric artery, PNU37883A caused significant inhibition of n-3 PUFA-induced relaxation that was more potent with DHA [30µM DHA; 91.9±0.9% (Control) and 54.3±12.3% (PNU37883A)] in comparison to EPA [30µM EPA; 92.2±1.7% (Control) and 84.6±2.7% (PNU37883A)] (Fig 5.7A-B) (*n*=5, P<0.05). Similarly in rat aorta, PNU37883A-induced inhibition was also more potent with DHA-mediated relaxation [30µM DHA; 86.8±1.5% (Control) and 12.2±3.7% (PNU37883A)] (Fig 5.8A) (*n*=5, P<0.05) when compared to the relaxant effects of EPA [30µM EPA; 89.6±1.8% (Control) and 40±13.8% (PNU37883A)] (Fig 5.8B) (*n*=5, P<0.05). A detailed

summary of log EC_{50} and maximal relaxation (E_{max}) values for each experimental group can be found in table 5.1.

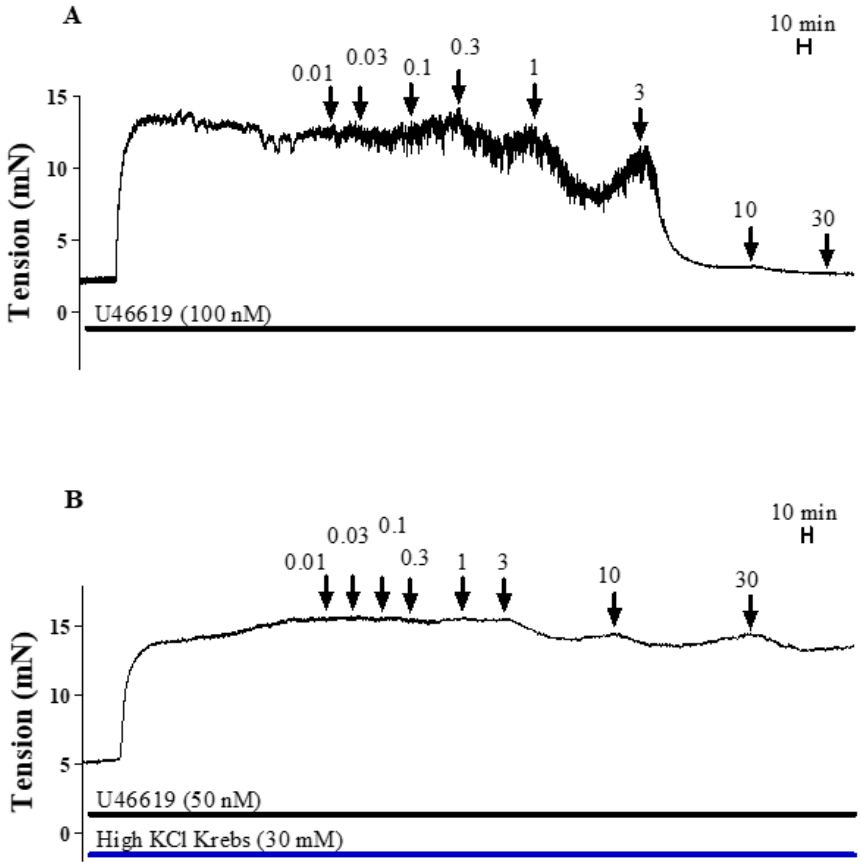

Fig 5.1 Original representative traces demonstrating the effect of high KCl Krebs (30 mM) in DHA-induced relaxation of rat mesenteric artery. After initially obtaining the control response curve using wire myograph, changes in the vascular tone were recorded following treatment of the same arterial segment with high KCl Krebs (20 min) to inhibit hyperpolarization induced by potassium channels. DHA was cumulatively added (0.01 – 30 μM) to induce vascular relaxation as indicated by the arrows.

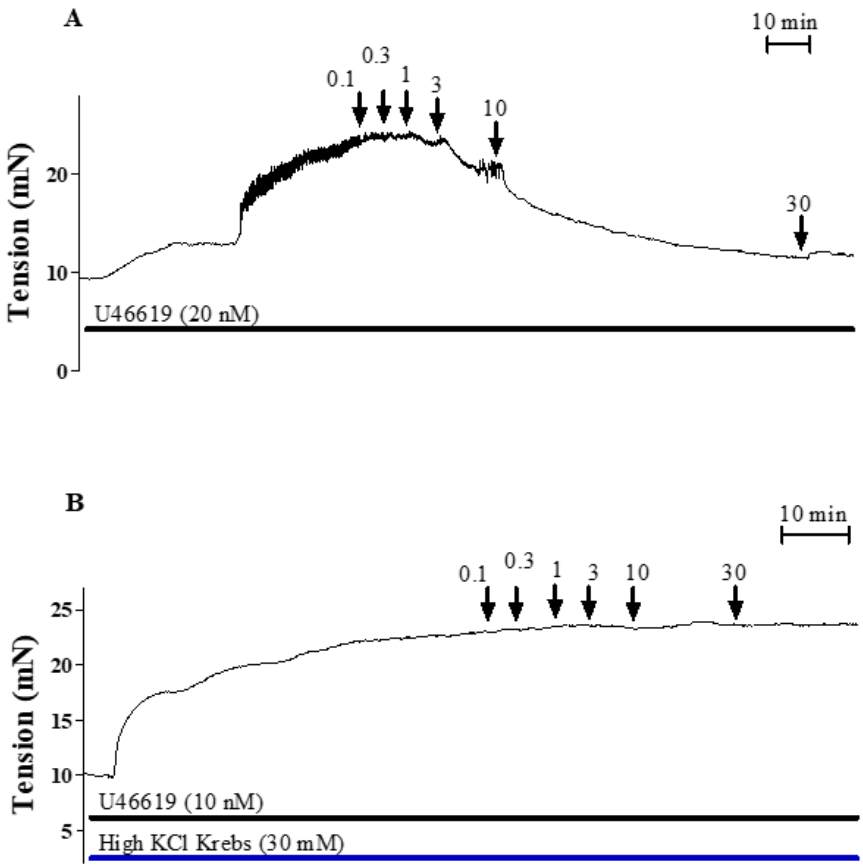

Fig 5.2 Original representative traces demonstrating the effect of high KCl Krebs (30 mM) in DHA-induced relaxation of rat aorta. After initially obtaining the control response curve using wire myograph, changes in the vascular tone were recorded following treatment of the same arterial segment with high KCl Krebs (20 min) to inhibit hyperpolarization induced by potassium channels. DHA was cumulatively added (0.1 – 30 µM) to induce vascular relaxation as indicated by the arrows.

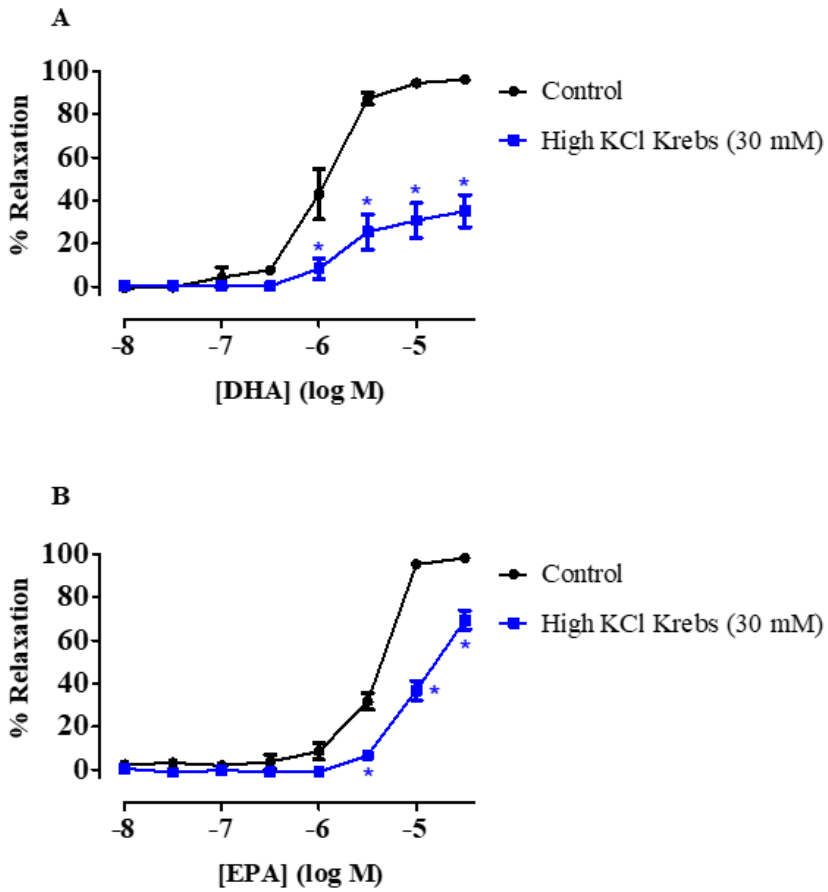

Fig 5.3 Concentration response curves demonstrating relaxation mediated by (A) DHA (*n*=6) and (B) EPA (*n*=5) in rat mesenteric artery following inhibition of hyperpolarization mediated by potassium channels with high KCl Krebs (30 mM). Using wire myograph, changes in n-3 PUFA (10 nM – 30 µM) mediated relaxation were recorded by initially obtaining a control response curve followed by pre-treatment of the same arterial segment with high KCl Krebs (20 min). Data are expressed as mean±SEM. *P<0.05 indicates significant difference from the control curve as determined using two-way ANOVA with Bonferroni post-test.

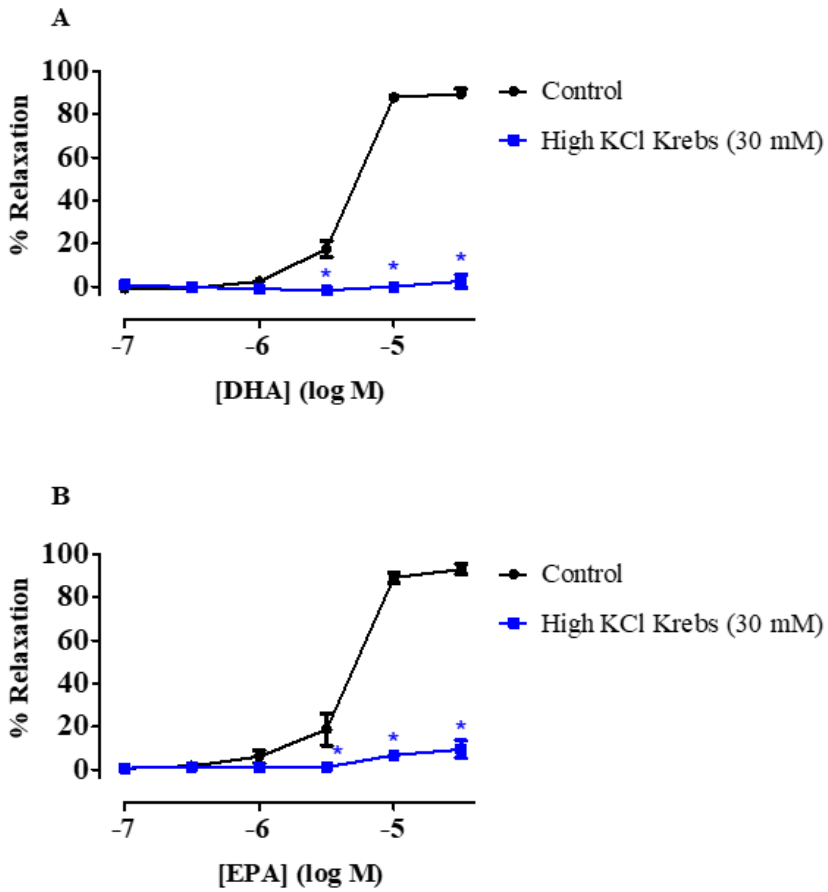

Fig 5.4 Concentration response curves demonstrating relaxation mediated by (A) DHA (*n*=5) and (B) EPA (*n*=5) in rat aorta following inhibition of hyperpolarization mediated by potassium channels with high KCl Krebs (30 mM). Using wire myograph, changes in n-3 PUFA (100 nM – 30 µM) mediated relaxation were recorded by initially obtaining a control response curve followed by pre-treatment of the same arterial segment with high KCl Krebs (20 min). Data are expressed as mean±SEM. *P<0.05 indicates significant difference from the control curve as determined using two-way ANOVA with Bonferroni post-test.

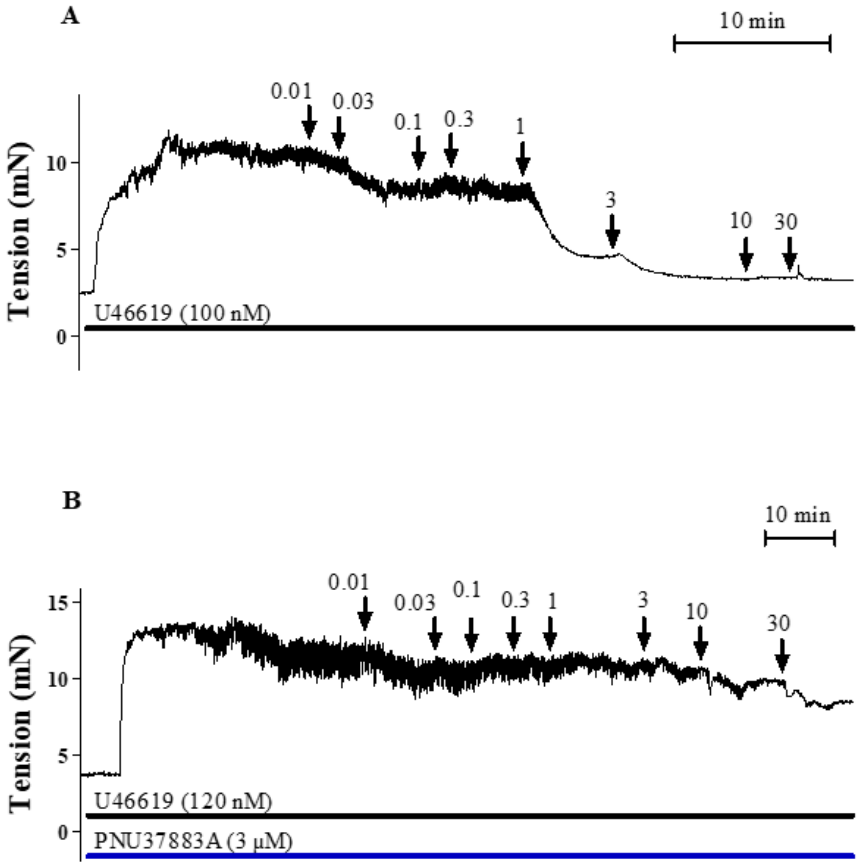

Fig 5.5 Original representative traces demonstrating the effect of PNU37883A (3 µM) in DHA-induced relaxation of rat mesenteric artery. After initially obtaining the control response curve using wire myograph, changes in the vascular tone were recorded following treatment of the same arterial segment with PNU37883A (20 min) to inhibit K_{ATP} channels. DHA was cumulatively added (0.01 – 30 µM) to induce vascular relaxation as indicated by the arrows.

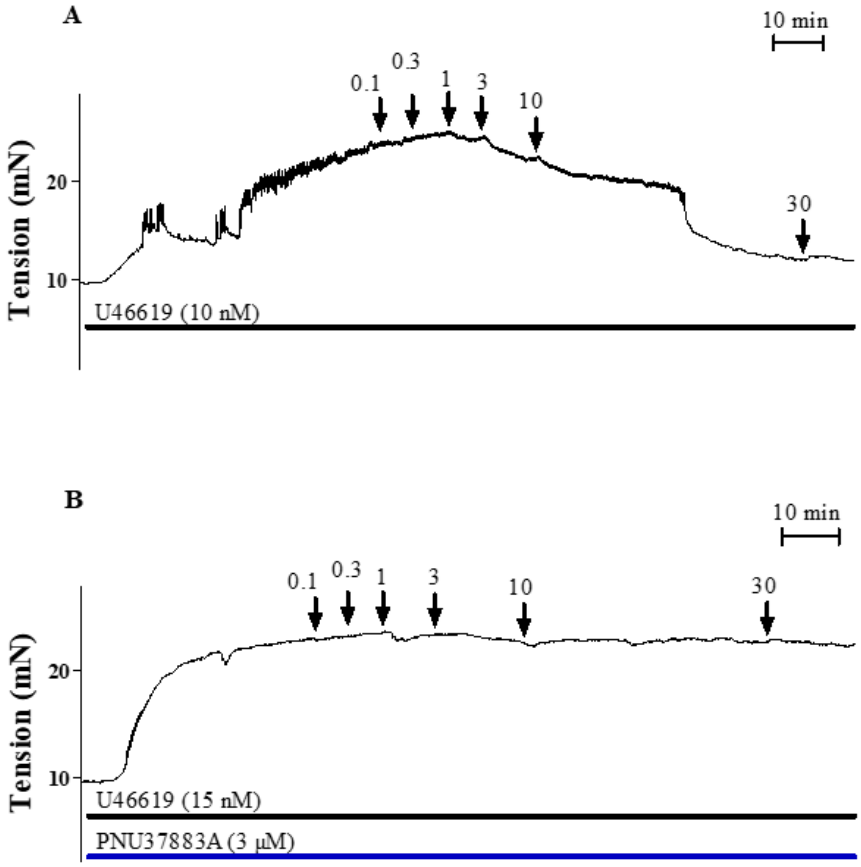

Fig 5.6 Original representative traces demonstrating the effect of PNU37883A (3 μM) in DHA-induced relaxation of rat aorta. After initially obtaining the control response curve using wire myograph, changes in the vascular tone were recorded following treatment of the same arterial segment with PNU37883A (20 min) to inhibit K_{ATP} channels. DHA was cumulatively added (0.1 – 30 μM) to induce vascular relaxation as indicated by the arrows.

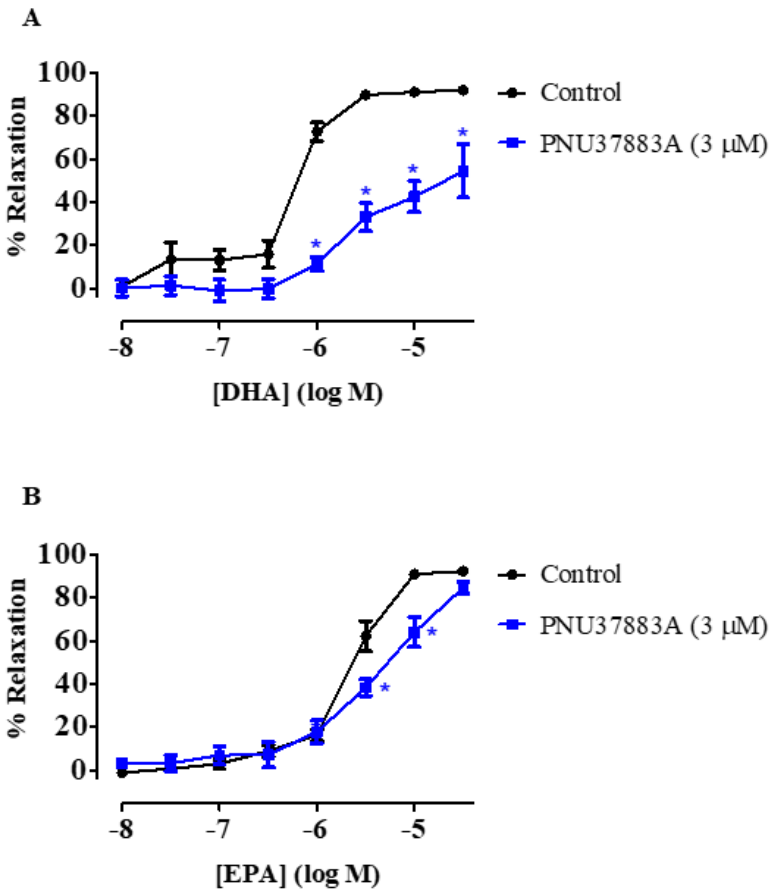

Fig 5.7 Concentration response curves demonstrating relaxation mediated by (A) DHA (*n*=5) and (B) EPA (*n*=5) in rat mesenteric artery following inhibition of K_{ATP} channels with PNU37883A (3 µM). Using wire myograph, changes in n-3 PUFA (10 nM – 30 µM) mediated relaxation were recorded by initially obtaining a control response curve followed by pre-treatment of the same arterial segment with PNU37883A (20 min). Data are expressed as mean±SEM. *P<0.05 indicates significant difference from the control curve as determined using two-way ANOVA with Bonferroni post-test.

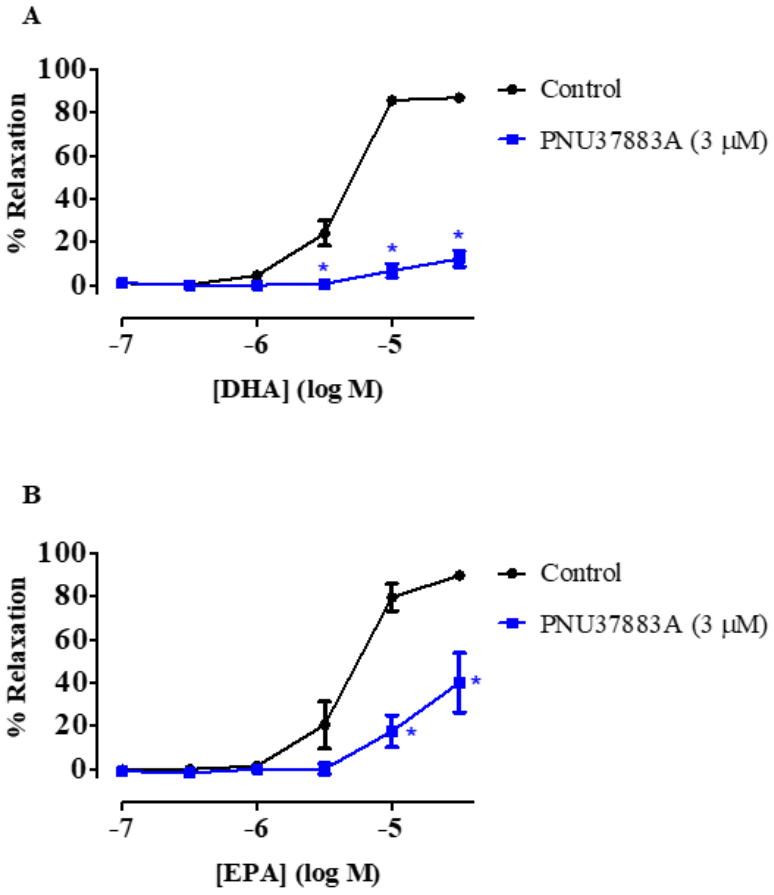

Fig 5.8 Concentration response curves demonstrating relaxation mediated by (A) DHA (*n*=5) and (B) EPA (*n*=5) in rat aorta following inhibition of K_{ATP} channels with PNU37883A (3 µM). Using wire myograph, changes in n-3 PUFA (100 nM – 30 µM) mediated relaxation were recorded by initially obtaining a control response curve followed by pre-treatment of the same arterial segment with PNU37883A. Data are expressed as mean±SEM. *P<0.05 indicates significant difference from the control curve as determined using two-way ANOVA with Bonferroni post-test.

Table 5.1 Summary of log EC_{50} and maximal relaxation (E_{max}) values from each myograph experiments that were conducted to investigate the effects of high KCl Krebs and PNU37883A. Values were obtained using standard variable slope least squares fit based on the hill equation in GraphPad Prism 5. N.D. indicates not determined as GraphPad could not produce an optimal curve fit due to nature of the data points, resulting in ambiguity for the values obtained.

Experiment	Type of artery	n-3 PUFA	Experimental Condition	Log EC_{50}		E_{max} (%)	
				Log EC_{50}	SEM (±)	E_{max} (%)	SEM (±)
High KCl Krebs	Mesenteric artery	DHA *n=6*	Control	-5.95	0.04	95.98	3.43
			High KCl Krebs	-5.74	0.16	33.75	4.25
		EPA *n=5*	Control	-5.39	0.03	99.02	2.66
			High KCl Krebs	-4.98	0.05	77.45	5.84
	Aorta	DHA *n=5*	Control	-5.37	0.05	89.54	2.17
			High KCl Krebs	**N.D.**	**N.D.**	**N.D.**	**N.D.**
		EPA *n=5*	Control	-5.33	0.05	93.11	3.59
			High KCl Krebs	-5.08	0.21	9.48	2.00
PNU37883A	Mesenteric artery	DHA *n=5*	Control	-6.17	0.05	91.12	2.65
			PNU37883A	-5.60	0.18	53.61	8.17
		EPA *n=5*	Control	-5.64	0.04	94.10	2.83
			PNU37883A	-5.24	0.18	99.30	15.38
	Aorta	DHA *n=5*	Control	-5.39	0.05	87.07	2.62
			PNU37883A	-5.01	0.11	12.39	3.03
		EPA *n=5*	Control	-5.31	0.06	90.11	5.55
			PNU37883A	-5.00	0.20	41.90	16.44

5.2.3 Generation of HEK Flp-In-293 pcDNA5/FRT and pcDNA5/FRT+SUR2B cell lines

Using wire myograph, I have demonstrated that activation of potassium channels is perhaps the main mechanism that determines the vasodilation effect of n-3 PUFAs especially in rat aorta (Fig 5.4), likely via a hyperpolarisation mechanism. Further investigation of the potassium channels revealed that K_{ATP} has a major role in n-3 PUFA-induced relaxation (Figs 5.7-5.8). Therefore, the next step was to investigate whether n-3 PUFAs could directly modulate K_{ATP}. The K_{ATP} channel is a complex composed of four sulfonylurea receptor (SUR) subunits and four Kir6 subunits (Fig 1.10) (Shi et al. 2012). Most studies indicate that the vascular K_{ATP} channels, present in both ECs and SMCs, are mainly composed of Kir6.1 and SUR2B (Foster and Coetzee 2016). To this aim, I generated a stable cell line in a two-step process where the initial step involved the construction and transfection of one of the subunits, SUR2B, followed by construction and lentiviral transduction of Kir6.1. Detailed description of the methods used for creating the stable cell line can be found in chapter 2, section 2.4.

5.2.3.i Construction of recombinant plasmids: pcDNA5/FRT and pcDNA5/FRT+SUR2B

Restriction digests (chapter 2, section 2.3.1.iii) were performed to obtain the DNA fragments required for the construction of pcDNA5/FRT+SUR2B plasmid (Fig 5.9). The following REs and plasmids were used to obtain the necessary fragments (chapter 2, table 2.4):

a) pcDNA5/FRT (required fragment expected at 4246 bp) = *Mfe* I and *Xho* I
b) pcDNA3+SUR2B (required fragment expected at 7069 bp) = *Mfe* I and *Xho* I

The digested DNA was then loaded on an agarose gel and the fragments were separated using gel electrophoresis (chapter 2, section 2.3.1.iv). The required DNA fragments were then excised from the gel and purified using QIAquick gel extraction kit (chapter 2, section 2.3.1.v) and subsequently ligated (chapter 2, section 2.3.1.vi). The ligated DNA was then used to transform Mach1 competent cells (chapter 2, section 2.3.1.vii). Plasmid DNA from five individual bacterial colonies was prepared using QIAprep Spin Miniprep Kit (chapter 2, section 2.3.1.x) from overnight cultures. After preparing glycerol stocks (chapter 2, section 2.3.1.ix) from the overnight cultures, plasmid DNA was then screened by restriction digest using *Mfe* I and *Xho* I, followed by gel electrophoresis. All clones produced the correct bands for the pcDNA5/FRT vector (predicted size, 4246 bp) fragment and the pcDNA3+SUR2B (predicted size, 7069 bp) fragment as shown in Fig 5.10A. The glycerol stock obtained from one of the clones was then used to inoculate a 250 ml culture and the plasmid DNA was purified using EndoFree Plasmid Maxi Kit (chapter 2, section 2.3.1.xi). Plasmid DNA was screened again using restriction digest followed by gel electrophoresis. Bands for the pcDNA5/FRT vector (predicted size, 4246 bp) fragment and the pcDNA3+SUR2B (predicted size, 7069 bp) fragment were observed with *Mfe* I and *Xho* I (Fig 5.10B). An additional restriction digest with *Afl* II also produced the correct bands for the two fragments predicted at around 3528 and 7786 bp.

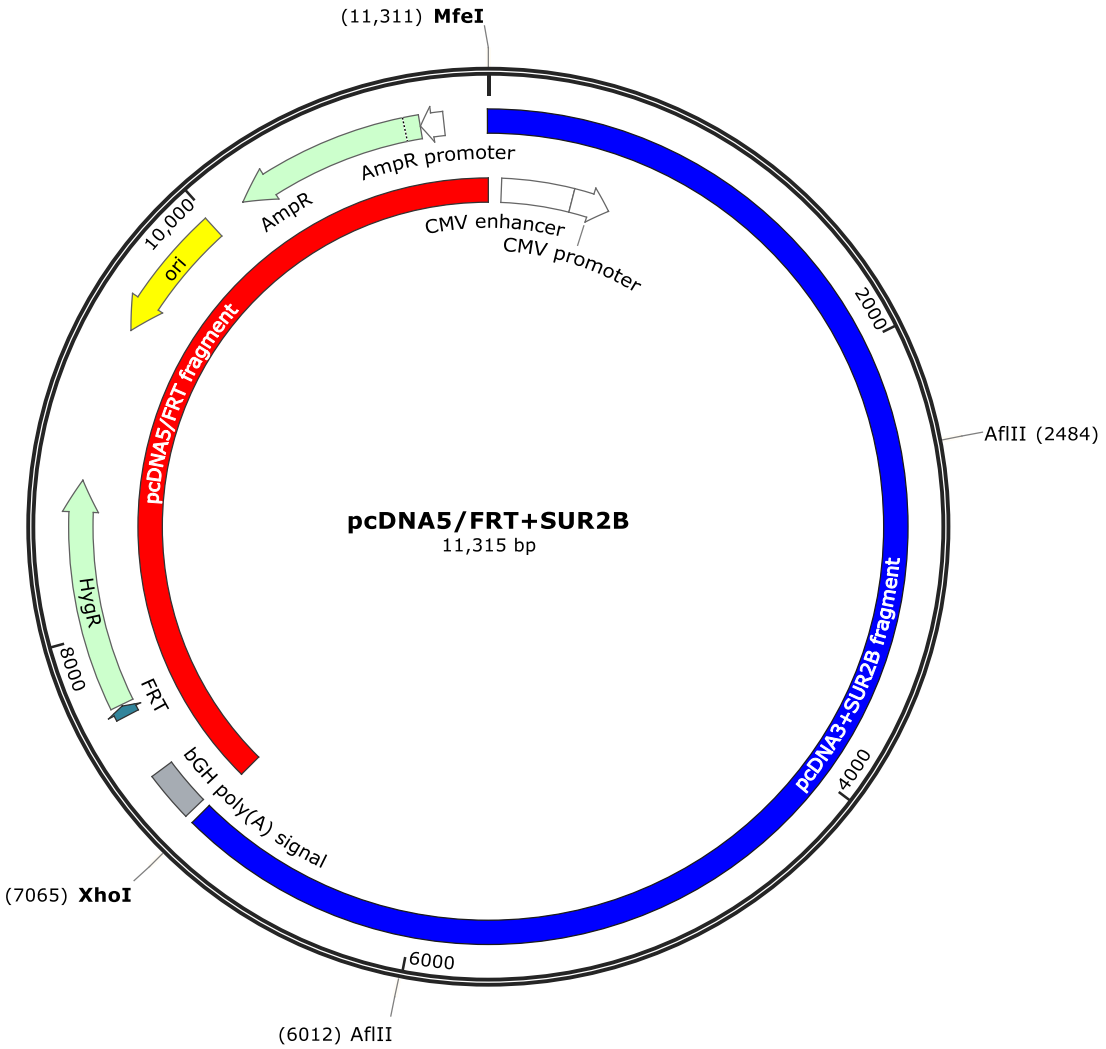

Fig 5.9 Vector map of the recombinant plasmid pcDNA5/FRT+SUR2B. Restriction enzyme sites (*Afl* II, *Mfe* I and *Xho* I) and the different fragments (pcDNA3+SUR2B and pcDNA5/FRT) involved in the construction and analysis of the plasmid have been indicated. Figure was created using SnapGene 4.1.9.

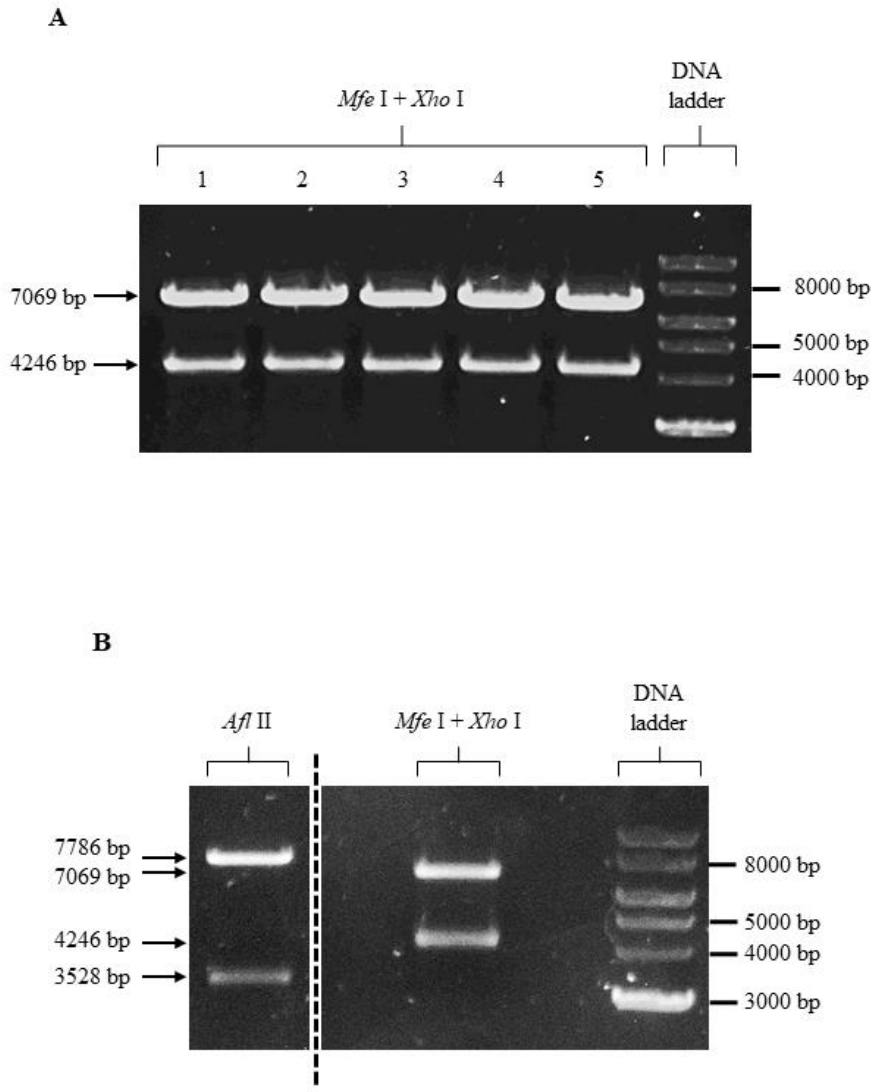

Fig 5.10 Analysis of the recombinant plasmid pcDNA5/FRT+SUR2B using agarose gel electrophoresis. Single restriction digest with *Afl* II and double digest with *Mfe* I and *Xho* I was used to analyse the plasmid following (**A**) small scale and (**B**) large scale plasmid preparation. *Mfe* I and *Xho* I produced two bands representing the pcDNA5/FRT vector (expected at 4246 bp) and pcDNA3+SUR2B (expected at 7069 bp) fragments. *Afl* II also produced two fragments that were expected at 3528 and 7786 bp.

5.2.3.ii Detection of the expression of SUR2B following lipofectamine mediated stable transfection of the plasmids

As described in chapter 2 (section 2.4.3), lipofectamine was used to stably transfect HEK Flp-In-293 cells with the recombinant plasmids generated in the earlier section. Briefly, cells were plated in antibiotic-free DMEM medium (10% FBS, v/v) and divided into two groups which included a control group (HEK_{VC}) that was transfected with the empty plasmid vector, pcDNA5/FRT, and another group (HEK_{SUR2B}) transfected with the vector containing the gene of interest, pcDNA5/FRT+SUR2B (+POG44), as described in chapter 2, section 2.4. Following antibiotic selection, single clones of SUR2B were expanded and then analysed for expression by immunocytochemistry (chapter 2, section 2.5) and western blotting (chapter 2, section 2.6). Using epifluorescent microscopy, SUR2B expression was absent in HEK_{VC} cells whereas immunoreactivity was detected in HEK_{SUR2B} cells (Fig 5.11A). Furthermore, western blot also confirmed the expression of SUR2B in HEK_{SUR2B} cells (Fig 5.11B) whereas immunoreactive signals were absent in HEK_{VC} cells. However, the immunoreactive band for SUR2B was observed at a higher molecular weight compared to the expected size of 174 kDa, indicating the involvement of either a post-translational modification or an SDS-resistant oligomer of SUR2B.

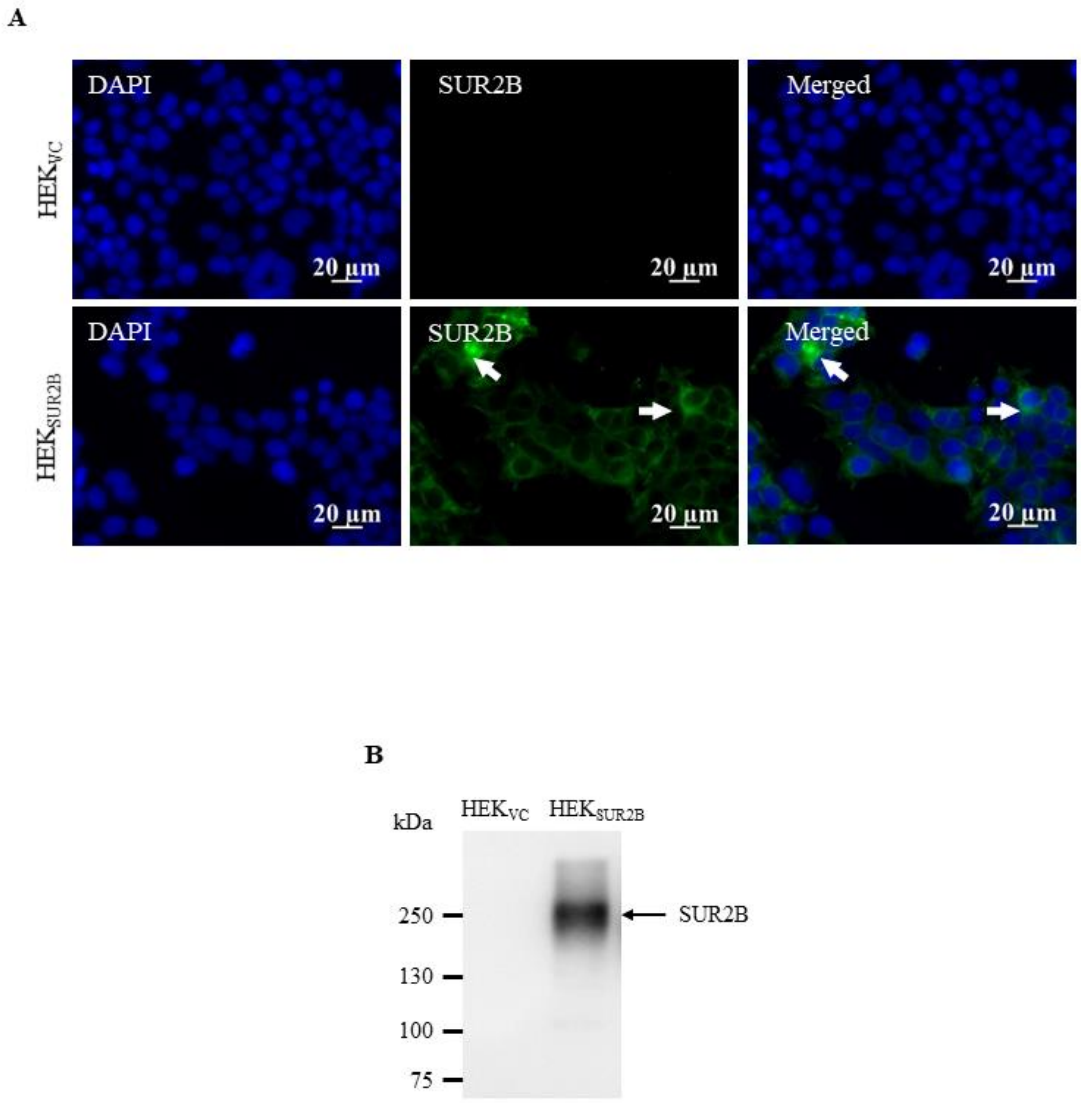

Fig 5.11 Expression of SUR2B subunits in HEK$_{SUR2B}$. (**A**) Immunofluorescence and epifluorescent microscopy (40x objectives) were used to investigate HEK$_{VC}$ and HEK$_{SUR2B}$ cells using nuclear stain DAPI (blue) and anti-SUR2B antibody (green). Significant expression of SUR2B (arrows) was detected in HEK$_{SUR2B}$ cells whereas these signals were absent in HEK$_{VC}$ cells. Scale bar, 20 µm. (**B**) Western blot analysis for SUR2B expression in HEK$_{VC}$ and HEK$_{SUR2B}$ cells. The immunoreactive band indicates expression of SUR2B in HEK$_{SUR2B}$ cells.

5.2.4 Generation of HEK Flp-In-293 pcDNA5/FRT+pLenti6.3/FRT/MCS and pcDNA5/FRT+SUR2B+pLenti6.3/FRT/MCS+Kir6.1 cell line

There is evidence indicating that EETs can activate potassium channels such as K_{ATP} channels present in the vasculature, resulting in vasodilation (Ye et al. 2005; Ye et al. 2006; Lu et al. 2006). Based on the findings from the myograph experiments, I demonstrated that K_{ATP} channels have a major role in n-3 PUFA-induced relaxation (Figs 5.7-5.8). Therefore, the next step was to investigate whether n-3 PUFAs could directly modulate K_{ATP}. To this aim I generated a stable cell line expressing K_{ATP} channels (HEK_{KATP}). As the vascular K_{ATP} isoform is composed of the SUR2B and Kir6.1 subunits, this experiment of generating the HEK_{KATP} cell line was divided into a two-step process. As demonstrated in the earlier section, the initial step involved the generation of a stable cell line expressing the SUR2B subunit. Therefore, my next objective was to virally transduce the other subunit, Kir6.1, into HEK_{SUR2B} stable cells to enable the formation of the K_{ATP} channel complex in these cells. The detailed description of the methods can be found in chapter 2, section 2.4.

5.2.4.i Construction of recombinant plasmids: pLenti6.3/FRT/MCS and pLenti6.3/FRT/MCS+Kir6.1

The DNA fragments required for the construction of pLenti6.3/FRT/MCS+Kir6.1 plasmid (Fig 5.12) were obtained using restriction digests (chapter 2, section 2.3.1.iii). The following REs and plasmids were used to obtain the necessary fragments (chapter 2, table 2.4):

a) pLenti6.3/FRT/MCS (required fragment expected at 7639 bp) = *Bam* HI and *Psp* OMI

b) pcDNA3.1/Zeocin+ Kir6.1 (required fragment expected at 2200 bp) = *Bam* HI and *Psp* OMI

The digested DNA was separated using gel electrophoresis (chapter 2, section 2.3.1.iv) and the necessary DNA fragments were then excised from the gel and purified using QIAquick gel extraction kit (chapter 2, section 2.3.1.v) followed by ligation (chapter 2, section 2.3.1.vi). Mach1 competent cells were then transformed using the ligated DNA (chapter 2, section 2.4.1.ii). Plasmid DNA from four individual bacterial colonies was prepared using QIAprep Spin Miniprep Kit (chapter 2, section 2.3.1.x). After preparing glycerol stocks (chapter 2, section 2.3.1.ix) from the overnight cultures, plasmid DNA was then screened by restriction digest using *Afl* II followed by gel electrophoresis. Only one of the clones (Lane 2) produced the correct bands representing the fragments of pLenti6.3/FRT/MCS+Kir6.1 plasmid with the predicted size of 2315, 3656 and 3936 bp as shown in Fig 5.13A. The purified DNA from the positive clone was then transformed into Stbl3 competent cells (chapter 2, section 2.4.1.ii) and plasmid DNA from two individual bacterial clones was purified using QIAprep Spin Miniprep Kit. After preparing the glycerol stocks from the overnight cultures, plasmid DNA was then analysed using restriction digest (*Afl* II) and gel electrophoresis that revealed the presence of the correct bands as described earlier (Fig 5.13B). The glycerol stock obtained from the positive clone was then used to inoculate an initial 5ml culture followed by a 250 ml culture at 28 ℃ and the plasmid DNA was purified using EndoFree Plasmid Maxi Kit (chapter 2, section 2.3.1.xi). Finally, screening of the DNA with restriction digest (*Afl* II) and gel electrophoresis revealed the presence of the correct bands for both bacterial clones (Fig 5.13C).

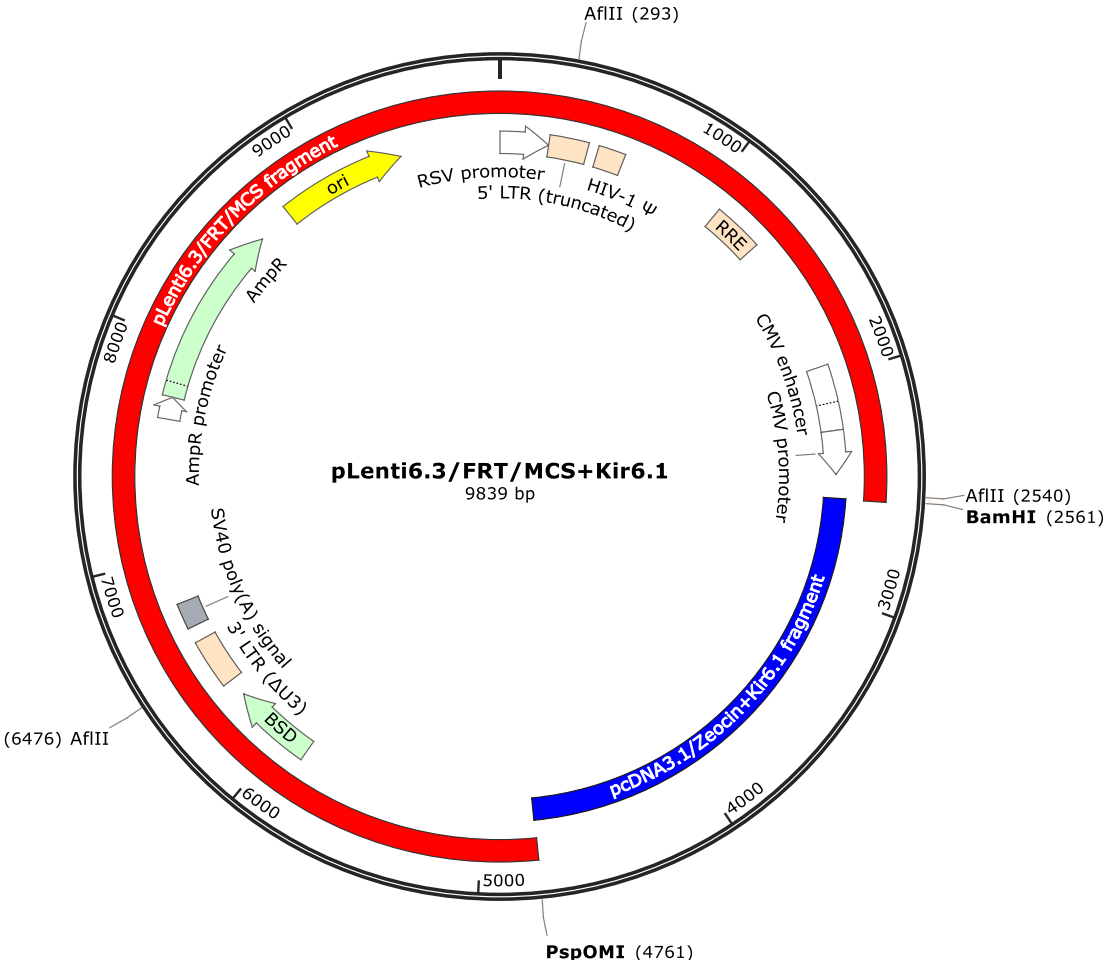

Fig 5.12 Vector map of the recombinant plasmid pLenti6.3/FRT/MCS+Kir6.1. Restriction enzyme sites (*Afl* II, *Bam* HI and *Psp* OMI) and the different fragments (pLenti6.3/FRT/MCS and pcDNA3.1/Zeocin+Kir6.1) involved in the construction and analysis of the plasmid have been indicated. Figure was created using SnapGene 4.1.9.

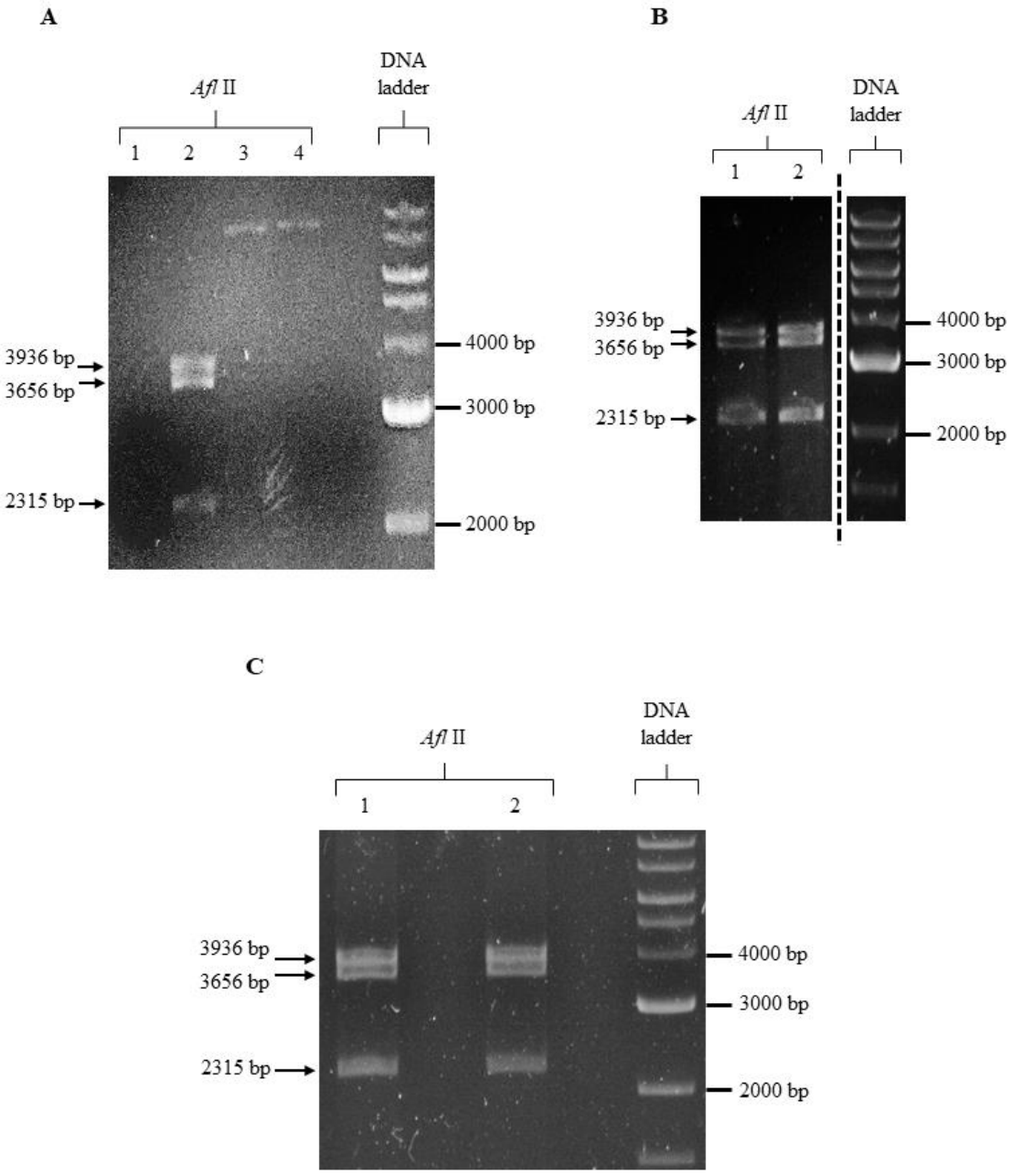

Fig 5.13 Analysis of the recombinant plasmid pLenti6.3/FRT/MCS+Kir6.1 using agarose gel electrophoresis. Restriction digest with *Afl* II was used to analyse the plasmid following (**A**) small scale (Mach1 culture), (**B**) small scale (Stbl3 culture) and (**C**) large scale (Stbl3 culture) plasmid preparation. Bands for the pLenti6.3/FRT/MCS+Kir6.1 vector were expected at 2315, 3656 and 3936 bp.

5.2.4.ii Detection of the expression of Kir6.1 following lentiviral transduction of the plasmids

The detailed protocol for lentiviral production and transduction of HEK_{SURB} cells with Kir6.1 has been described in chapter 2 (section 2.4.4-2.4.5). Briefly, the Lenti-X 293T cells were initially seeded in 10 cm dishes coated with poly-D-lysine using antibiotic-free DMEM medium (10% FBS, v/v). The cells were then divided into two groups to perform transfection with the recombinant plasmids, pLenti6.3/FRT/MCS (control) and pLenti6.3/FRT/MCS+Kir6.1 respectively. Based on the 3:1 ratio of PEI:plasmid DNA, the transfection mix was prepared in optimem and gently pipetted onto the cells followed by overnight incubation. The medium was then replaced with antibiotic free medium containing HEPES and FBS (10% v/v). Lentivirus was then purified using ViraBind lentivirus purification kit (Cell Biolabs) according to the manufacturer's guidelines.

HEK_{VC} and HEK_{SUR2B} cells were seeded in a 6 well plate and lentivirally transduced with the plasmid vector, pLenti6.3/FRT/MCS (HEK_{VC1}) and pLenti6.3/FRT/MCS+Kir6.1 (HEK_{KATP}) respectively. Cells were then incubated in antibiotic-free medium for 72 h and transferred to 2x 10 cm dishes/well containing medium with the appropriate antibiotic (chapter 2, table 2.1) for selection. Dilution cloning (chapter 2, section 2.4.6) which involved serial dilution of the cells, resulting in the presence of 50-100 cells per 10 cm dish, was used to obtain single colonies of the cell line. The clones were transferred to larger culture plates and flasks once they were confluent. Immunocytochemistry (chapter 2, section 2.5) and western blotting (chapter 2, section 2.6) were then used to detect the expression of Kir6.1. Confocal microscopy (chapter 2, section 2.5.4) revealed the presence of both Kir6.1 and SUR2B immunoreactivity in HEK_{KATP} (Fig 5.14A). However, the expression of both K_{ATP} subunits were completely absent in HEK_{VC1} as shown in Fig 5.14A. Western blot also affirmed the expression of Kir6.1 in HEK_{KATP} (Fig

5.14B) which was completely absent in HEK_{VC1} cells further confirming that the viral transduction was successful. However, the smeared immunoreactive band for Kir6.1 was observed at a considerably higher molecular weight compared to the expected size of 48 kDa, indicating the involvement of either a post-translational modification or an SDS-resistant oligomer of the subunit(s). As HEK_{KATP} cells were transfected and transduced with both K_{ATP} subunits, it is possible that these oligomers could be made up of either Kir6.1 or SUR2B+Kir6.1 subunits.

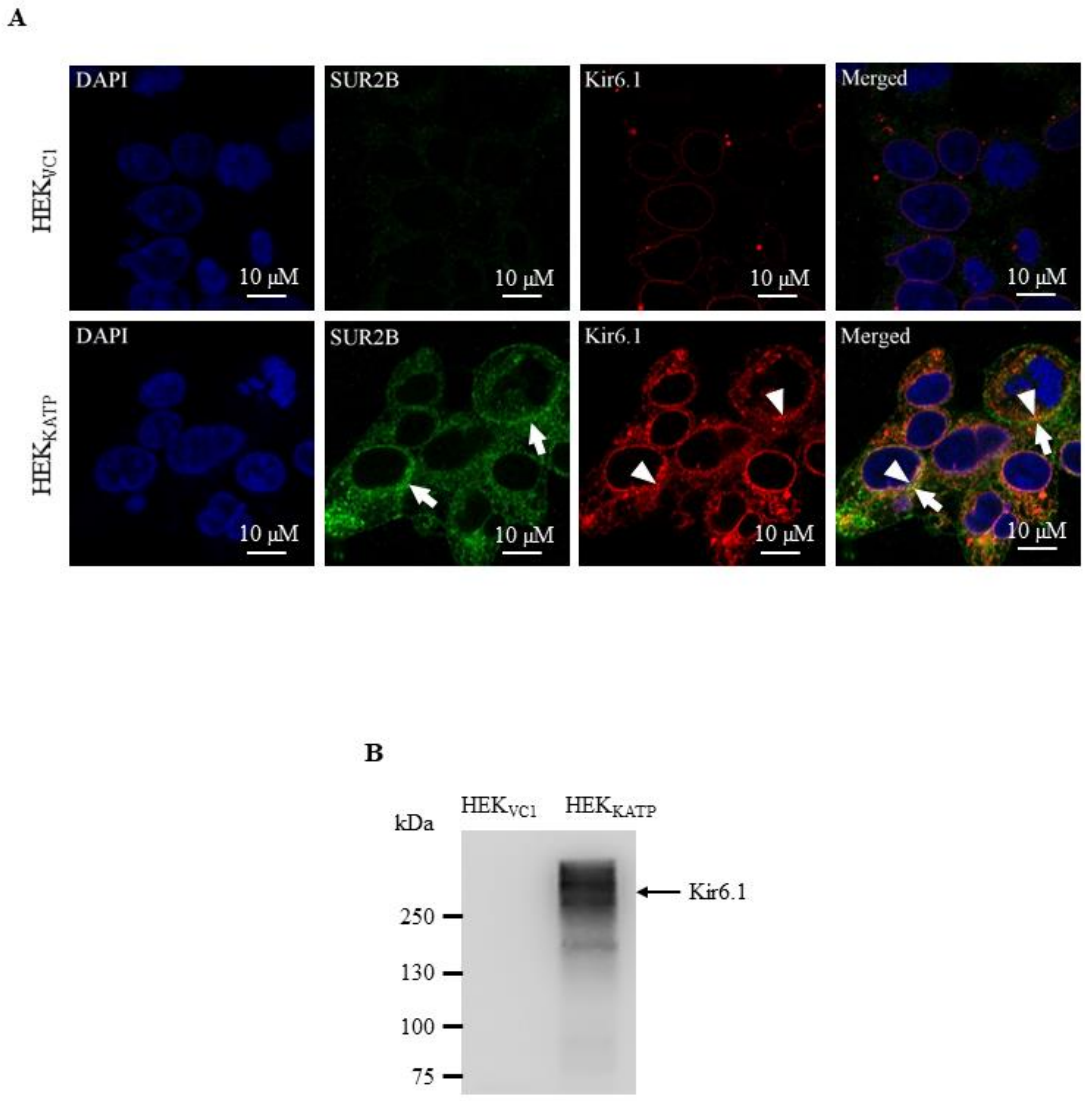

Fig 5.14 Expression of K_{ATP} channels in HEK_{KATP}. (**A**) Immunofluorescence and confocal microscopy (100x objectives) of HEK_{VC1} and HEK_{KATP} cells using nuclear stain DAPI (blue), anti-SUR2B antibody (green) and anti-Kir6.1 antibody (red). Significant expression of SUR2B (arrows) and Kir6.1 (arrow heads) was detected in HEK_{KATP} cells whereas these signals were absent in HEK_{VC1} cells. Scale bar, 10 µm. (**B**) Western blot analysis for Kir6.1 expression in HEK_{VC1} and HEK_{KATP} cells. The immunoreactive band indicates expression of Kir6.1 in HEK_{SUR2B} cells.

5.2.5 K_{ATP} is not directly modulated by n-3 PUFAs

My myograph experiments indicated a significant role of K_{ATP} channels in the relaxation mediated by both DHA and EPA in rat aorta and mesenteric artery (Fig 5.7-5.8). However, a direct modulation of K_{ATP} channels by n-3 PUFAs is yet to be reported. Therefore, I investigated whether the K_{ATP} channels could be directly activated by n-3 PUFAs. This study involved the use of patch clamp electrophysiology with the stable cell line expressing K_{ATP} channels (HEK_{KATP}).

The protocol used for the patch clamp technique has been described in chapter 2, section 2.8. Briefly, HEK_{KATP} cells were seeded in 6 well plates and incubated overnight. Using the microscope and the micromanipulator, pipette was lowered until it was just above a single cell. After recording the pipette resistance, giga Ω seal was formed and negative pressure was applied using mouth pipetting to achieve the whole cell configuration. The currents were recorded using a ramp protocol (-150 to +50 mV over 1 s with a holding potential of -80 mV). Following initial recording of the baseline currents for 10 s, pharmacological agents or n-3 PUFAs were applied until responses plateaued.

Although ethanol was used for diluting n-3 PUFAs in the myograph experiments, perfusion of this solvent generated a biphasic response characterised by an increase and subsequent irreversible reduction in whole cell currents (data not shown). As a result, DMSO was the vehicle used for dissolving the pharmacological agents along with n-3 PUFAs and therefore, it was essential to initially investigate the effects of DMSO on K_{ATP} channel activity. Application of DMSO (0.3 %) failed to elicit any changes in current density as indicated by the representative current density-voltage traces (Fig 5.15A) and time course traces (Fig 5.15B). K_{ATP} openers such as levcromakalim (10 μM) and pinacidil (10 μM), were then used to investigate whether the K_{ATP} channels expressed by the stable cell line were functional. Levcromakalim evoked significant increase in current

density compared to DMSO and this effect was inhibited following additional application of PNU37783A (3 µM) (Fig 5.15A-B). Similarly, pinacidil also activated K_{ATP} channels as indicated by the enhanced current density whereas additional administration of PNU377883A significantly reduced this effect (Fig 5.15C-D). Following confirmation of the presence of functional K_{ATP} channels in the stable cells, direct modulation of K_{ATP} activity by DHA (30 µM) was then investigated. DHA failed to directly activate K_{ATP} channels (n=4, $P<0.05$) (Fig 15 E-F) and significant increase in K_{ATP} currents were only achieved following additional application of either levcromakalim (n=2, $P<0.05$) or pinacidil (n=4, $P<0.05$) (Fig 5.15G).

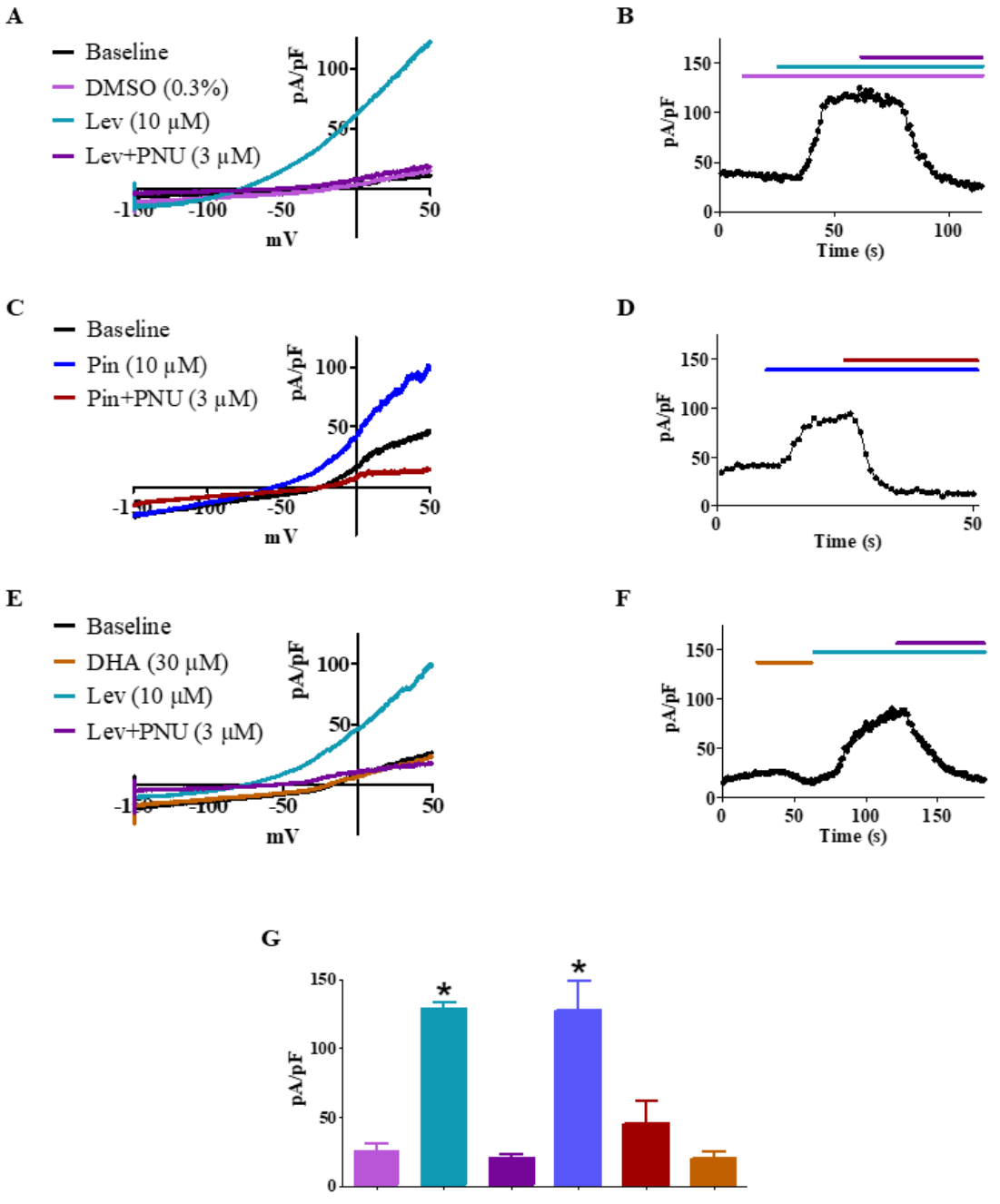

Fig 5.15 DHA is not involved in the direct modulation of K_{ATP} channels. Whole cell current density-voltage traces and current density time course traces at +40 mV, indicating the effects of the acute application of (**A**) (**B**) DMSO (0.3%), Lev (10 µM), Lev+PNU (3 µM), (**C**) (**D**) Pin (10 µM), Pin+PNU and (**E**) (**F**) DHA (30 µM), Lev, Lev+PNU. Currents were recorded using a ramp protocol (-150 to +50 mV) over 1 s with a holding potential of -80 mV. After recording the baseline currents for 10 s, the effects of n-3 PUFA/pharmacological agonist were then recorded until the responses plateaued. An inhibitor in combination with the agonist was then used until

maximum inhibition was achieved. (**G**) Bar graph indicating the mean current densities of HEK_{KATP} at +40 mV. Values were taken from the peak current obtained following application of DMSO (0.3 %) (*n*=4), Lev (10 µM) (*n*=2), Lev+PNU (3 µM) (*n*=2), Pin (10 µM) (*n*=4), Pin+PNU (*n*=4) and DHA (30 µM) (*n*=4). Current density values were obtained by dividing the peak current (mV) at +40 mV by cell capacitance (pF). Data are expressed as mean±SEM. *P<0.05 indicates significant difference from DMSO-induced response as determined using one-way ANOVA with Bonferroni post-test.

5.2.6 Effect of K_v7 inhibition in n-3 PUFA mediated vascular relaxation

Previous myograph experiments demonstrated that high KCl Krebs was marginally more effective compared to PNU37883A in inhibiting n-3 PUFA-induced relaxation, especially with EPA (Fig 5.1-5.8). This indicated that the other potassium were also involved besides K_{ATP}. Studies have demonstrated that n-3 PUFAs can directly activate K_v7 channels present in cardiac and neuronal cells (Doolan et al. 2002; Verkerk et al. 2006; Moreno et al. 2015; Liin et al. 2016). Therefore, I investigated the role of these channels in n-3 PUFA-induced relaxation of rat aorta and mesenteric artery using wire myograph (protocol described in chapter 2, section 2.2).

Concentration dependent relaxation produced by n-3 PUFAs were significantly inhibited following pre-treatment with the K_v7 channel blocker, XE991 (1 µM). Representative traces demonstrating the effect of XE991 in DHA-induced relaxation of rat mesenteric artery and aorta can be found in Fig 5.16 and Fig 5.17. In rat mesenteric artery, XE991 partially attenuated DHA-induced relaxation (Fig 5.18A) (n=5, P<0.05). Similarly, EPA-induced relaxation was also partially inhibited following pre-treatment with XE991 (Fig 5.18B) (n=5, P<0.05). In rat aorta, pre-treatment with XE991 elicited significant inhibition of relaxation that was more potent with DHA [30µM DHA; 80.2±6.1% (Control) and 24.2±8.8% (XE991)] (Fig 5.19A) (n=6, P<0.05) in comparison to EPA [30µM EPA; 87.4±2.2% (Control) and 55.2±17.7% (XE991)] (Fig 5.19B) (n=5, P<0.05). A detailed summary of log EC_{50} and maximal relaxation (E_{max}) values for each experimental group can be found in table 5.2.

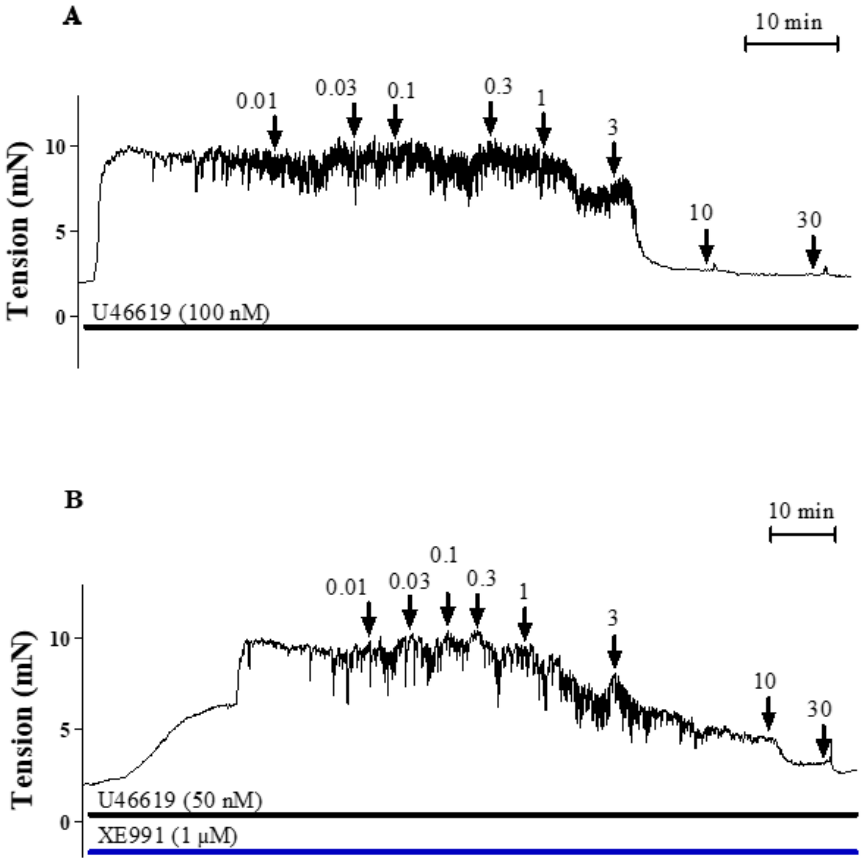

Fig 5.16 Original representative traces demonstrating the effect of XE991 (1 μM) in DHA-induced relaxation of rat mesenteric artery. After initially obtaining the control response curve using wire myograph, changes in the vascular tone were recorded following treatment of the same arterial segment with XE991 (20 min) to non-selectively inhibit K_v7 channels. DHA was cumulatively added (0.01 – 30 μM) to induce vascular relaxation as indicated by the arrows.

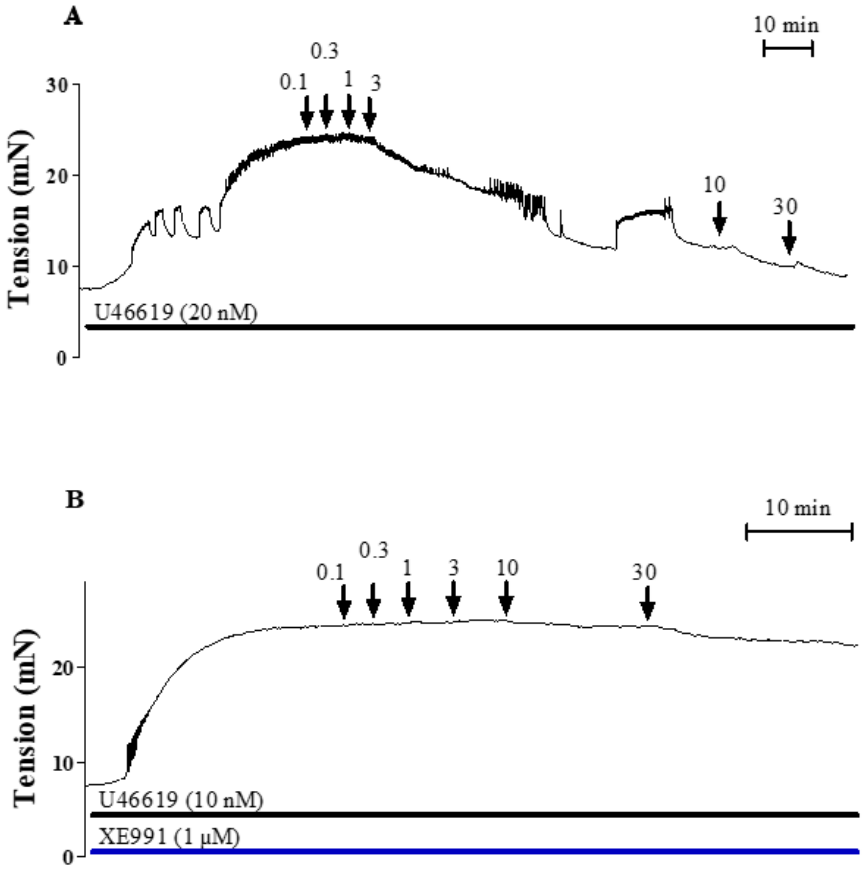

Fig 5.17 Original representative traces demonstrating the effect of XE991 (1 µM) in DHA-induced relaxation of rat aorta. After initially obtaining the control response curve using wire myograph, changes in the vascular tone were recorded following treatment of the same arterial segment with XE991 (20 min) to inhibit non-selectively K_v7 channels. DHA was cumulatively added (0.1 – 30 µM) to induce vascular relaxation as indicated by the arrows.

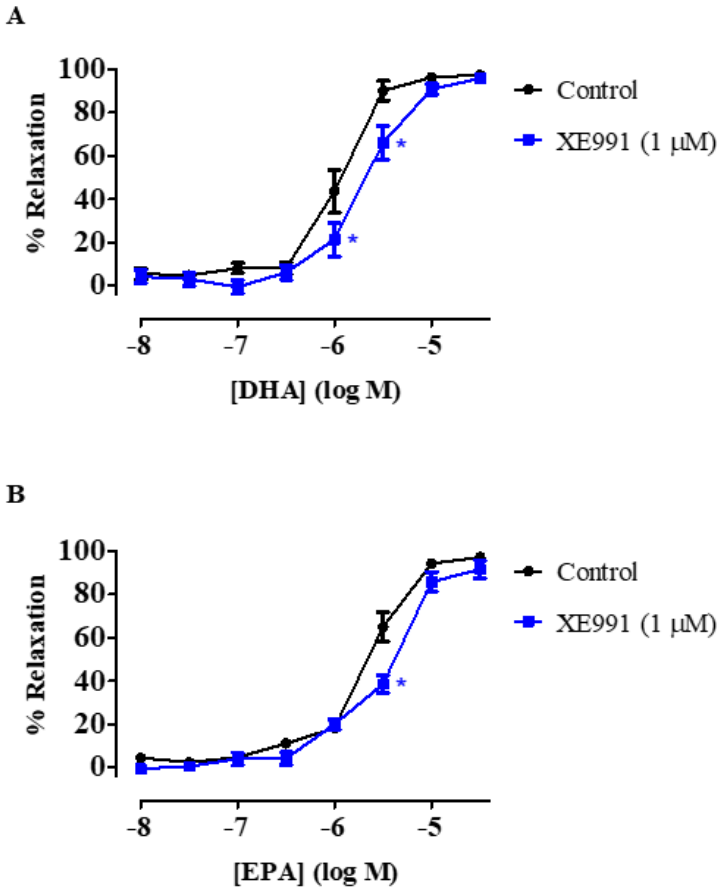

Fig 5.18 Concentration response curves demonstrating relaxation mediated by (A) DHA (*n*=5) and (B) EPA (*n*=5) in rat mesenteric artery following non-selective inhibition of K_v7 channels with XE991 (1 µM). Using wire myograph, changes in n-3 PUFA (10 nM – 30 µM) mediated relaxation were recorded by initially obtaining a control response curve followed by pre-treatment of the same arterial segment with XE991 (20 min). Data are expressed as mean±SEM. *P<0.05 indicates significant difference from the control curve as determined using two-way ANOVA with Bonferroni post-test.

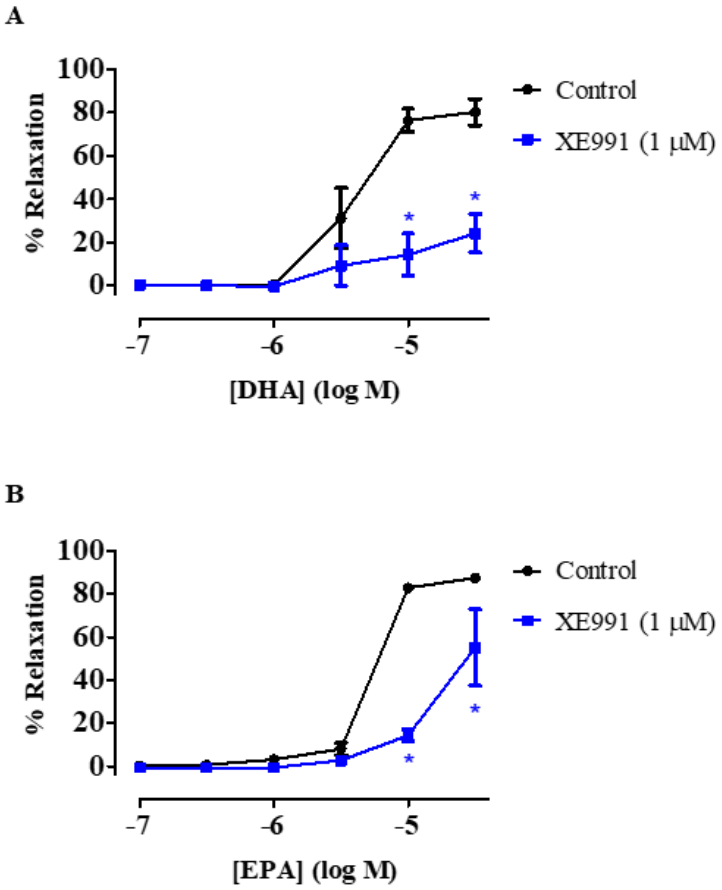

Fig 5.19 Concentration response curves demonstrating relaxation mediated by (A) DHA (*n*=6) and (B) EPA (*n*=5) in rat aorta following non-selective inhibition of K_v7 channels with XE991 (1 µM). Using wire myograph, changes in n-3 PUFA (100 nM – 30 µM) mediated relaxation were recorded by initially obtaining a control response curve followed by pre-treatment of the same arterial segment with XE991 (20 min). Data are expressed as mean±SEM. *P<0.05 indicates significant difference from the control curve as determined using two-way ANOVA with Bonferroni post-test.

Table 5.2 Summary of log EC_{50} and maximal relaxation (E_{max}) values from each myograph experiments that were conducted to investigate the effects of K_v7 inhibition. Values were obtained using standard variable slope least squares fit based on the hill equation in GraphPad Prism 5. N.D. indicates not determined as GraphPad could not produce an optimal curve fit due to nature of the data points, resulting in ambiguity for the values obtained.

Experiment	Type of artery	n-3 PUFA	Experimental Condition	Log EC_{50}		E_{max} (%)	
				Log EC_{50}	SEM (±)	E_{max} (%)	SEM (±)
XE991	Mesenteric artery	DHA *n=5*	Control	-5.94	0.04	96.88	2.91
			XE991	-5.68	0.05	96.22	4.07
		EPA *n=5*	Control	-5.63	0.03	98.35	2.50
			XE991	-5.43	0.06	98.60	5.40
	Aorta	DHA *n=6*	Control	-5.44	0.07	80.03	6.46
			XE991	-4.98	1.41	32.30	47.45
		EPA *n=5*	Control	-5.37	0.08	89.16	6.34
			XE991	**N.D.**	**N.D.**	26.51	10.53

5.3 Summary

My initial myograph findings demonstrated that the endothelial component of n-3 PUFA mediated relaxation involved CYP and IK_{Ca} channels. Subsequent characterization of the endothelium independent mechanisms revealed that BK_{Ca} channels were associated with n-3 PUFA mediated relaxation, consistent with previous studies (Ye et al. 2002; Hercule et al. 2007; Toshinori Hoshi, Wissuwa, et al. 2013). The residual relaxation that remained indicated the presence of other compensatory mechanisms that led to full relaxation of rat arteries by n-3 PUFAs.

Numerous studies have indicated that PUFAs can modulate potassium channels such as BK_{Ca}, K_{ATP} and K_v7 (Ye et al. 2005; Ye et al. 2006; Liin et al. 2014; Moreno et al. 2015; Liin et al. 2016), therefore, the next objective was to investigate the role of hyperpolarization mediated by potassium channels in n-3 PUFA-induced relaxation using high KCl Krebs. The high KCl Krebs changes the reversal potential of potassium ions resulting in inhibition of potassium efflux and hyperpolarization at physiological membrane potentials. High KCl Krebs completely abolished n-3 PUFA-mediated relaxation in rat aorta (Fig 5.4) and in rat mesenteric artery, it led to significant attenuation in the vasodilation effect of n-3 PUFAs, especially with DHA, resulting in the reduction of the maximum relaxation response (Fig 5.3). My findings from previous myograph experiments demonstrated the role of BK_{Ca} and IK_{Ca} channels (Fig 3.17A-B and 3.21A) in the vasodilation effects of n-3 PUFAs, however in contrast to high KCl Krebs a large residual relaxation remained following blockade of these channels indicating the involvement of other potassium channels. Therefore, I investigated whether vascular K_{ATP} channels were also involved as there is some evidence indicating the role of these channels in n-3 PUFA-induced relaxation (Engler et al. 2000; Sato et al. 2014). Similar to high KCl Krebs, inhibition of K_{ATP} by PNU37883A also resulted in almost complete

abolishment and significant reduction of n-3 PUFA-mediated relaxation in rat aorta (Fig 5.7A-B) and mesenteric artery (Fig 5.8A-B) respectively. Furthermore, the inhibitory effect of PNU37883A was more profound with relaxation mediated by DHA compared to EPA, indicating heterogeneity in vasodilation mechanisms of n-3 PUFAs.

Due to evidence from the myograph experiments, my next objective was to investigate whether K_{ATP} channels were directly activated by n-3 PUFAs. Therefore, a stable cell line expressing K_{ATP} channels was generated by initially transfecting with SUR2B and subsequently transducing with Kir6.1 subunit. Using whole cell patch clamp, my findings demonstrated that both levcromakalim (Fig 5.15A-B) and pinacidil (Fig 5.15C-D) elicited significant increase in current density that was inhibited following additional administration of PNU37883A. This verified the presence of functional K_{ATP} channels in the stable cell line and therefore, the acute effects of DHA on K_{ATP} channel activity was then investigated. DHA failed to evoke any changes in K_{ATP} currents (Fig 5.15E-F), indicating an indirect modulation of K_{ATP} in n-3 PUFA-mediated relaxation. There is evidence demonstrating that activation of K_{ATP} by EETs initially involves the stimulation of $G\alpha_s$ protein and PKA dependent signalling in rat mesenteric SMCs (Ye et al. 2006). Therefore, it is possible that the HEK_{KATP} stable cells lack these intracellular machineries required for K_{ATP} activation by n-3 PUFAs and as a result, future electrophysiological studies should involve the use of native vascular cells, to fully confirm whether n-3 PUFAs indirectly modulate K_{ATP} channel activity.

The findings from the myograph experiments (Fig 5.1-5.8) indicate that high KCl Krebs was marginally more effective compared to PNU37883A, in inhibiting the n-3 PUFA-mediated relaxation, especially involving EPA. Furthermore, inhibition of K_{ATP} channels led to significant attenuation of EPA-induced relaxation, however there was still some residual relaxation that remained. Recent studies have indicated that K_v7 channels can be

directly activated by n-3 PUFAs (Liin et al. 2014; Moreno et al. 2015; Liin et al. 2016), however, there are no studies at the moment that have investigated whether these channels are involved in the relaxation effects of n-3 PUFAs. Therefore, I investigated the role of K_v7 channels in n-3 PUFA-mediated relaxation of rat aorta and mesenteric artery. Similar to the earlier myograph experiments, inhibition of K_v7 by XE991 led to significant attenuation of n-3 PUFA-induced relaxation that was more profound in rat aorta compared to the mesenteric artery (Fig 5.18-5.19). Furthermore, consistent with high KCl Krebs and PNU37883A data, XE991-mediated inhibition of relaxation was more profound with DHA compared to EPA. A detailed discussion regarding these findings can be found in chapter 6, section 6.5.

Findings from my myograph experiments demonstrate the important role of potassium channels in vasodilation mediated by n-3 PUFAs. One of the most interesting findings from these experiments is the heterogeneity in the vasodilation mechanisms, as potassium channels seem to completely regulate n-3 PUFA-induced relaxation only in the rat aorta but not in the mesenteric artery. This is the first study to comprehensively investigate the role of K_{ATP} channels in conduit and resistance rat arteries using both DHA and EPA. Furthermore, my findings indicate that the vasodilation effect of n-3 PUFAs probably involves an indirect activation of K_{ATP} channels. This is also the first study to demonstrate the role of K_v7 channels in the n-3 PUFA-mediated relaxation of rat arteries. To summarize, potassium channels have an important role in the vasodilation effect of n-3 PUFAs especially in the conduit rat aorta and my findings indicate that it mainly involves the K_{ATP} and K_v7 channels.

Chapter 6

Discussion

6.1 Overview

In 2015, CVDs were the cause of 31% of total deaths around the world which accounts for 17.7 million people, making it the leading cause of mortality (WHO 2017). There are many risk factors that are associated with CVDs such as hypertension, dyslipidaemia, obesity and endothelial dysfunction (Stewart et al. 2017). Endothelial dysfunction involves the impairment of endothelial vasodilation mechanisms resulting in an enhanced contractile state of the blood vessels. Both DHA and EPA have been reported to improve endothelial function and cardiovascular health especially in people suffering from CVDs (Mori 2014); and one of the mechanisms associated with these protective effects is the vasodilation of blood vessels. However, currently there is a gap in the literature as most studies only investigate one type of vascular bed and n-3 PUFA (see Table 1.1 for summary of these studies). In addition, there is extensive evidence indicating that vasodilation mechanisms can vary depending upon the size of blood vessels. For example, EDH has been reported to be more predominant in the smaller resistance arteries whereas NO is the main pathway involved in conduit arteries (Shimokawa et al. 1996; Sandow and Hill 2000; Hilgers et al. 2006).

Endothelial dysfunction can occur in both conduit and resistance arteries due to cardiovascular risk factors such as aging (Blackwell et al. 2004; Csiszar et al. 2007; Lesniewski et al. 2009). As previously mentioned, resistance arteries are mainly involved in the regulation of mean blood pressure as these vessels provide the greatest vascular resistance in systemic circulation (Pocock et al. 2013). In clinical practice, peripheral blood pressure is commonly measured by assessing the brachial artery and it has been extensively used as a predictor of CVDs. Although large conduit arteries, such as aorta, do not elicit moment to moment control of the overall mean arterial pressure, there is evidence indicating that the central aortic pressure might be the better indicator of

cardiovascular risk compared to peripheral pressure (McEniery et al. 2014). This is perhaps justified by the predominance of aortic over brachial pressure in major organs such as heart, kidney and brain (McEniery et al. 2014). Furthermore, central rather than peripheral pressure was reported to have a higher correlation with CVD surrogate markers such as left ventricular mass by various studies (Covic et al. 2000; Wang et al. 2009; Roman et al. 2010). Central pressure can be elevated via inhibition of NO production resulting in the subsequent enhancement of arterial stiffness in conduit arteries such as aorta (Wilkinson et al. 2002; Wilkinson et al. 2004). The largest dampening of pulsatile ventricular pressure in the circulatory system is observed in the aorta (Marchais et al. 1993) and therefore, aortic stiffness has been reported to be the most reliable predictor (blood pressure-independent) of CVDs compared to other conduit arteries (Laurent et al. 2007). This is not surprising as stiffening of the aorta results in the reduction of vascular compliance and enhances the propagation speed of forward and reflected pulse pressure in arteries; this subsequently increases systolic central blood pressure, pulse pressure and cardiac afterload (Chen et al. 2017). These effects can be detrimental as it can promote ventricular hypertrophy (Yucel et al. 2015) and can damage the smaller peripheral arteries (Van Sloten et al. 2015). Multiple studies have demonstrated that aortic stiffening rather than elevated peripheral resistance is involved in isolated systolic hypertension (Wallace et al. 2007; McEniery et al. 2009). In addition, both structural and functional changes, such as aortic calcification and endothelial dysfunction respectively, were reported to enhance vascular stiffness (Wallace et al. 2007; McEniery et al. 2009). Multiple studies have indicated the role of vasodilation in the reduction of arterial stiffness in major arteries. Nebivolol, a β-blocker that induces vasodilation, was reported to reduce arterial stiffness of large conduit arteries and this effect was inhibited following the blockade of eNOS (McEniery et al. 2004).

Furthermore, studies were conducted to compare the therapeutic efficacy of nebivolol against other non-vasodilating β-blockers. Nebivolol was found to be more effective in reducing aortic pulse pressure, central blood pressure and left ventricular wall thickness in patients with isolated systolic and untreated hypertension (Dhakam et al. 2006; Kampus et al. 2011). These studies reported that the improved effectiveness of nebivolol was due to its additional ability of eliciting NO-dependent vasodilation. Similarly, a nonselective α/β-blocker, arotinolol, was also reported to induce eNOS phosphorylation and NO-dependent vasodilation in aorta, resulting in the subsequent reduction of central blood pressure and aortic stiffness in spontaneously hypertensive rats (SHR) (Zhou et al. 2014). Although resistance arteries are predominantly involved in the regulation of peripheral resistance and the overall mean blood pressure, these findings clearly demonstrate the therapeutic potential of reducing central aortic pressure and aortic stiffness via activation of vasodilation pathways. Therefore, my PhD project involved the use of both conduit (rat aorta) and resistance arteries (rat mesenteric artery) for the characterization of the mechanisms underlying DHA- and EPA-mediated vasodilation. To make the study physiologically relevant, relaxation to n-3 PUFA was elicited at concentrations of free fatty acid (100nM - 30 μM) that are attainable in human plasma following n-3 PUFA rich meal (~70 μM) (Conquer and Holub 1998; Newens et al. 2011).

6.2 The role of endothelium in n-3 PUFA-mediated vasodilation

The endothelium is an important inner layer of the blood vessels and are involved in the release of various vasoactive factors that regulate the vascular tone. As described in chapter 1, section 1.2, different vasodilation mechanisms involving NO, PGI_2, EETs and EDH are dependent upon the presence of endothelial layer. As a result, my initial experiments aimed at investigating the role of endothelium in n-3 PUFA-induced relaxation of rat aorta and mesenteric arteries using wire myograph (chapter 2, section 2.2). In rat mesenteric artery, endothelium removal led to partial attenuation of DHA-mediated relaxation (Fig 3.3A). EPA-induced relaxation was also partially attenuated in the rat aorta (Fig 3.4B). These findings are consistent with multiple studies that have indicated the role of endothelium-dependent mechanisms in the vasodilation effect of n-3 PUFAs (Omura et al. 2001; López et al. 2004; Raimondi et al. 2005). Results from my experiments demonstrate two interesting characteristics of n-3 PUFA-mediated relaxation which are; 1) endothelium removal could only partially attenuate relaxation mediated by n-3 PUFAs and therefore, a substantial amount of remaining residual relaxation indicates that the mechanisms are primarily endothelium-independent and 2) endothelial removal did not affect vasodilation mediated by EPA in rat mesenteric artery and DHA in rat aorta, indicating heterogeneity in the pathways involved that depended upon the type of artery and n-3 PUFA.

As my experiments indicated that endothelium is involved in n-3 PUFA-mediated relaxation, I then characterized these mechanisms by initially investigating the NO pathway. Both animal and human studies have demonstrated that n-3 PUFAs can improve NO-mediated relaxation (Geleijnse et al. 2002; López et al. 2004; Raimondi et al. 2005). Different mechanisms have been reported such as upregulation of eNOS expression and reduction of ADMA (endogenous eNOS inhibitor), especially in rat aorta (López et al.

2004; Raimondi et al. 2005). However, my findings demonstrate that both DHA- and EPA-induced relaxation remained unaffected following eNOS inhibition in rat mesenteric artery and aorta (Fig 3.7-3.8). There is extensive evidence indicating the role of NO in the vasodilation effects of n-3 PUFAs, however, most of these murine studies have investigated the long-term effects of n-3 PUFA supplementation (Omura et al. 2001; Hirafuji et al. 2002; López et al. 2004; Raimondi et al. 2005). The shortest n-3 PUFA treatment that was used in these studies was 24 h, whilst most of them lasted for more than a week (Hirafuji et al. 2002). Furthermore, these chronic murine studies were conducted using vascular cells rather than arterial tissue and therefore lacked functional evidence. My project focused on investigating the acute vasodilation effects of n-3 PUFAs in rat arteries and therefore, the duration of n-3 PUFA exposure could possibly explain the discrepancy. Similar to my findings, Engler *et al* (2000) also reported that NO was not involved in relaxation of rat aorta mediated by both DHA and EPA when acutely applied.

A postprandial study conducted in the University of Reading demonstrated that vascular reactivity (examined via the use of sodium nitroprusside and ACh) of healthy men was immediately improved within few hours of consuming a fish oil rich meal (Jackson et al. 2009). Furthermore, these effects were reported to be more potent with sodium nitroprusside (a NO donor) compared to ACh (Jackson et al. 2009). Based on the findings from this study, I investigated the endothelium dependent and independent vasodilation effects of ACh and NONOate (a NO donor) respectively, following pre-treatment of rat mesenteric artery with DHA for 1 h. Similar to the postprandial study, my findings also demonstrated that the relaxation mediated by NONOate was significantly potentiated following pre-treatment with DHA for 1 h (Fig 3.11B). However, ACh-induced relaxation was not affected with the same pre-treatment protocol (Fig 3.11B). These

findings suggest that the acute effects of n-3 PUFAs mostly involve the activation of endothelium independent vasodilation pathways. Therefore, it is plausible to suggest that any significant improvements in NO-mediated vasodilation requires chronic administration of n-3 PUFAs. Based on the supplementation studies, the shortest n-3 PUFA treatment that led to enhancement of NO production was 24 h (Hirafuji et al. 2002). Therefore, it would be interesting to examine the effects of a 24 hr treatment of rat arteries with n-3 PUFAs. However, preliminary data from our lab demonstrated significant changes in the vascular tone and relaxation of rat aorta from the original response, following 24 hr culture of the arterial segments in normal medium (DMEM) (Personal communication, Dr Alister McNeish). As a result, experiments involving longer pre-treatments were not conducted. These findings indicate that perhaps an *in vivo* approach involving dietary supplementation with n-3 PUFAs, which was beyond the scope of my PhD, would be more suitable for investigating the chronic effects of these fatty acids in rat arteries.

There is also evidence indicating that an increase in NO production following DHA supplementation can only be observed in conditions where the bioavailability of NO is compromised (Villalpando et al. 2015). For example, an elevated NO production with DHA was reported in orchidectomized rats, with significantly lower levels of NO, however, this was not observed with normal healthy rats (Villalpando et al. 2015). Furthermore, a meta-analysis also reported that the reduction of blood pressure due to n-3 PUFAs was only observed in hypertensive patients and not in the healthy volunteers (Morris et al. 1993). Therefore, the findings from my experiments indicate that relaxation mediated by the acute application of n-3 PUFAs does not involve endothelial NO and different factors such as the type of animal models and duration of the treatment can influence the effects of n-3 PUFAs. It is possible that any significant improvements in

the NO pathway by these fatty acids can only be observed in patients with compromised NO-mediated vasodilation but not in healthy individuals.

The endothelium is involved in the production of other vasoactive factors including COX metabolites of AA (PGI_2) that can elicit vasodilation (chapter 2, section 2.2). n-3 PUFAs can compete with AA for endothelial enzymes such as COX and there is evidence indicating that supplementation with n-3 PUFAs can alter prostanoid production resulting in inhibition of noradrenaline- and angiotensin II-induced constriction of human forearm vasculature (Chin et al. 1993). Engler *et al* (2000) demonstrated that both DHA- and EPA-induced relaxations of rat aorta were sensitive to COX inhibition. However, my findings demonstrate that COX-derived metabolites are not involved in the relaxation mediated by both n-3 PUFAs in rat mesenteric artery and aorta (Fig 3.7-3.8). This disparity could be explained by the methodological differences between our studies, these include; the use of a different vasoconstrictor (noradrenaline) along with considerably larger and older WKY rats used by the Engler group (16–17 weeks, 355±11 g). Aging is a risk factor for CVDs and has been reported to promote endothelial dysfunction through different mechanisms such as impairment of NO production and PGI_2-mediated relaxation (Nicholson et al. 2009; Seals et al. 2011). Similar to the discussion regarding the NO pathway, it is possible that any significant improvements in the production of COX-derived metabolites of n-3 PUFAs can only be observed, following an impairment of this pathway. Another interesting difference between our studies was the potency of EPA-induced relaxation. The Engler *et al* (2000) study demonstrated that 30 µM of EPA could only elicit 30±4% relaxation of the contractile tone induced by noradrenaline, whereas in my experiments EPA normally mediated >80% relaxation in rat aorta [E_{max}; 92.60±1.08 (Control) (n=30] (Table 6.1). Surprisingly, their findings also demonstrated that EPA could evoke concentration dependent contractile effects following pre-

treatment of the aorta with indometacin whereas none of the treatments in my experiments led to n-3 PUFA-induced constriction. It is possible that this discrepancy in the potency of EPA is perhaps due to the difference in the vasoconstrictors that were used. However, our preliminary experiments with phenylephrine-constricted arteries demonstrated near maximal relaxation with DHA [30 μM; 89.53±4.32], similar to what we observed with U46619-induced constriction (Fig 6.1). Although we had problems with the stability of the phenylephrine mediated contractile tone as mentioned previously, in some experiments we were able to achieve sustained contraction and therefore data from Fig 6.1 were taken from these experiments. Furthermore, there is evidence indicating that n-3 PUFAs are involved in the inhibition of PGI_2 production and COX-2 expression in human ECs (Dudley et al. 1995; Lee et al. 2009), suggesting that perhaps COX-2 metabolites of n-3 PUFAs are probably not involved in vasodilation. In agreement with my findings, a study conducted with rats of the same age and weight as used in my experiments, demonstrated that DHA-induced relaxation of U46619-constricted rat aorta was insensitive to the combined inhibition of COX with indometacin and eNOS via endothelium removal (Sato et al. 2014). As a result, it is important to consider that the type of vasoconstrictor and the age of the animal used in any investigation may significantly influence the mechanisms underlying n-3 PUFA mediated relaxation.

In the endothelium, n-3 PUFAs compete with AA as substrates for another enzyme, the CYP epoxygenase(s), resulting in the production of DHA-derived EDPs and EPA-derived EPETEs (22, 25, 60). Both EDPs and EPETEs have been reported to mediate vasodilation through activation of BK_{Ca} channels in various vascular beds such as mouse cerebral artery (Hercule et al. 2007), mouse mesenteric artery (Hercule et al. 2007), porcine coronary arteries (Ye et al. 2002), rat cerebral (Hercule et al. 2007) and rat

coronary arteries (Wang et al. 2011) (Table 1.1). Therefore, to characterize endothelium-dependent mechanisms involved with n-3 PUFA-induced relaxation, I investigated the role of CYP epoxygenase in rat mesenteric artery and aorta. DHA-induced relaxation was not affected following inhibition of CYP in both arteries (Fig 3.14A and 3.15A respectively). However, EPA-induced relaxation was partially attenuated by CYP inhibition in rat aorta and mesenteric artery (Figs 3.14B and 3.15B). There is evidence indicating that the production of EETs can occur within 30 min of AA preincubation in cultured bovine coronary arterial ECs and canine coronary arteries (Rosolowsky et al. 1990; Rosolowsky and Campbell 1996). Furthermore, studies report that the CYP enzymes have similar or even higher catalytic activities for n-3 PUFAs compared to AA (Arnold, Markovic, et al. 2010). Therefore, it is highly likely that CYP was involved in the production of EPETEs in our myograph experiments, since the tissues were exposed to n-3 PUFAs for more than 30 min. Furthermore, these findings also demonstrate the heterogeneity in the vasodilation mechanisms depending upon the type of n-3 PUFA, since clotrimazole-mediated inhibition was only observed with the relaxation elicited by EPA (Fig 6.2). The large residual relaxation with EPA following inhibition of CYP, indicates that other mechanisms are also involved. Therefore, results from these experiments demonstrate that the presence of CYP epoxygenase is not necessary to induce full vascular relaxation by n-3 PUFAs and is consistent with the previous myograph data (Fig 3.3-3.4) demonstrating minimal contribution of endothelium. As a result, my next objective was to investigate endothelium-independent pathways, I started by examining the role of BK_{Ca} channels in n-3 PUFA-mediated relaxation of rat aorta and mesenteric artery.

Table 6.1 Summary of log EC_{50} and maximal relaxation (E_{max}) values obtained from pooled control data for DHA and EPA in aorta and mesenteric arteries. These values were acquired using standard variable slope least squares fit based on the hill equation in GraphPad Prism 5. Data were analysed using two-tailed t-test. *P<0.05 indicates a significant difference from DHA in the artery studied.

Type of artery	**n-3 PUFA**	**Log EC_{50}**		**E_{max} (%)**	
		Log EC_{50}	**SEM (±)**	**E_{max} (%)**	**SEM (±)**
Mesenteric artery	DHA *n=40*	-6.03	0.04	96.54	0.49
	EPA *n=35*	-5.61*	0.05	97.90	0.59
Aorta	DHA *n=35*	-5.42	0.04	90.14	1.00
	EPA *n=30*	-5.30*	0.03	92.60	1.08

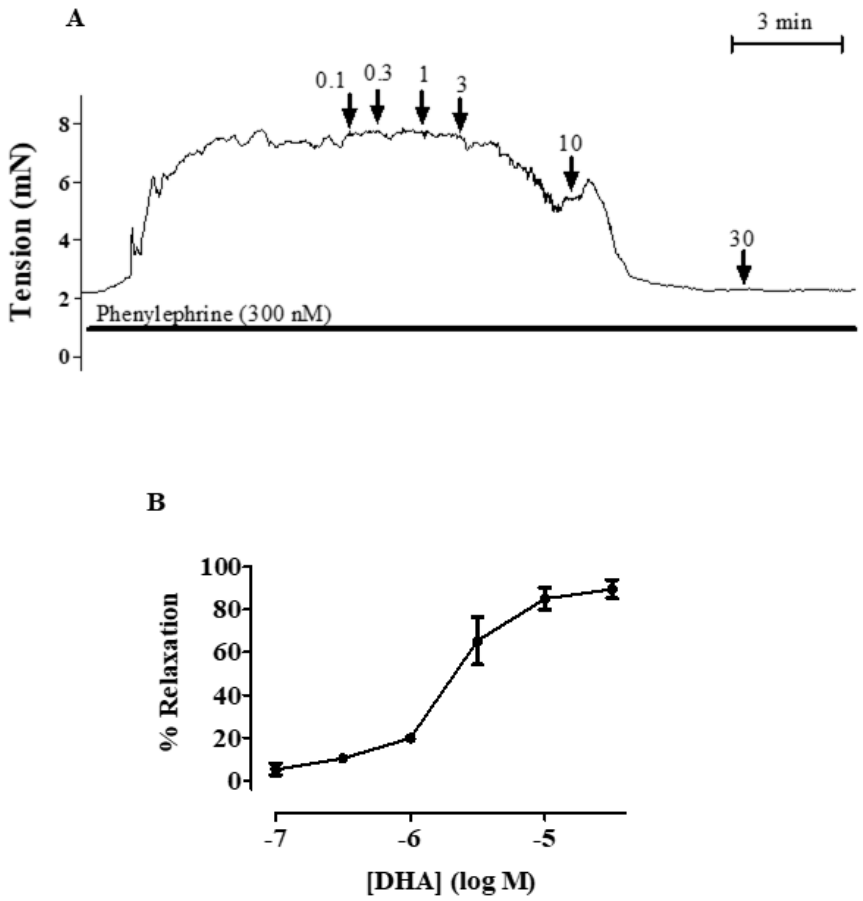

Fig 6.1 (A) Original representative trace and (B) concentration response curves demonstrating relaxation mediated by DHA (*n*=5) in rat mesenteric artery preconstricted with phenylephrine. DHA was cumulatively added (0.1 – 30 μM) to induce vascular relaxation as indicated by the arrows. Data are expressed as mean±SEM and were taken from experiments with stable contractile tone.

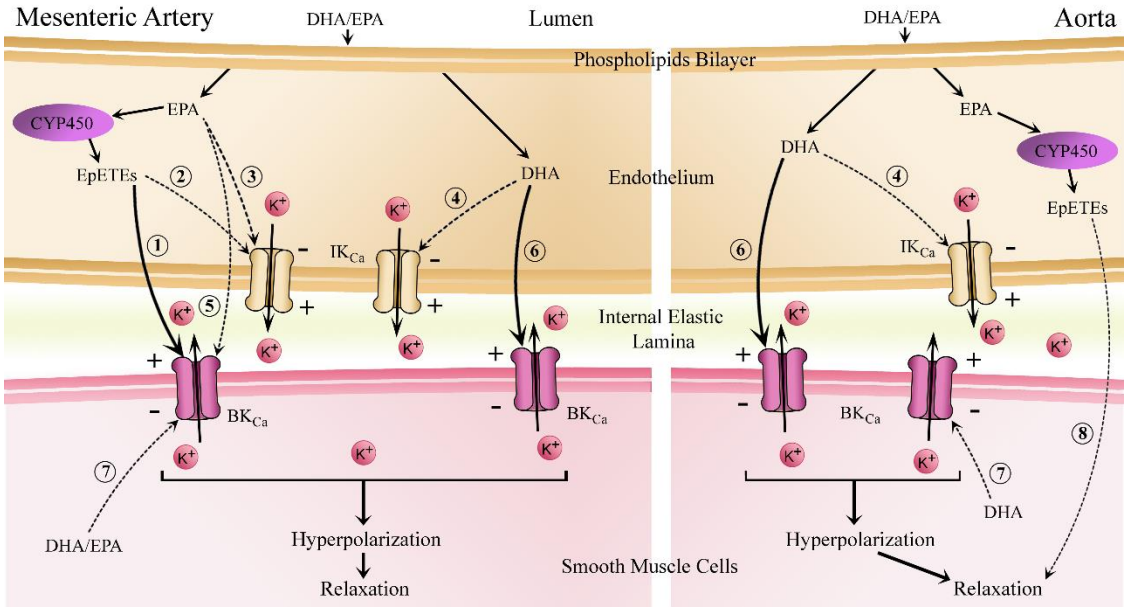

Fig 6.2 Summary of the potential vasodilation mechanisms involved in n-3 PUFA-mediated relaxation of rat mesenteric artery and aorta preconstricted with U46619. Pathways that have been previously reported are indicated by the solid arrows whereas dotted arrows represent hypothetical pathways based on my findings. n-3 PUFAs can enter the cytosol of the endothelium either through diffusion from the plasma or from the phospholipid bilayer via the activity of phospholipase A2 (PLA_2); (**1**) CYP epoxygenase can convert EPA into EpETEs, activating BK_{Ca}. IK_{Ca} may be potentially activated by (**2**) EpETEs, (**3**) EPA and (**4**) DHA. (**5**) Similar to EpETEs, EPA might also directly activate BK_{Ca} channels. (**6**) DHA is involved in the direct activation of BK_{Ca} (Toshinori Hoshi, Wissuwa, et al. 2013). (**7**) Both n-3 PUFAs may enter the cytosol of vascular SMCs via diffusion or release from the phospholipid bilayer due to the activity of PLA_2 and directly activate BK_{Ca}. (**8**) EpETEs may elicit arterial relaxation through K_{Ca}-independent mechanisms which could involve other potassium channels such as K_{ATP} and K_v7. BK_{Ca} = large conductance calcium activated potassium channels, DHA = docosahexaenoic acid, EPA = eicosapentaenoic acid, EpETEs = epoxyeicosatetraenoic acids and IK_{Ca} = intermediate conductance calcium activated potassium channels. (Limbu et al. 2018)

Various endothelial factors such as EETs and NO can activate BK_{Ca} channels expressed in SMCs resulting in subsequent hyperpolarization and vasodilation (Dimitropoulou et al. 2007; Félétou and Vanhoutte 2009) (chapter 1, section 2.5). As mentioned earlier, there is extensive evidence indicating that CYP-derived metabolites of n-3 PUFAs are involved in activation of BK_{Ca} channels present in SMCs. Furthermore, EDPs were reported to be 1000 times more potent in activating BK_{Ca} channels compared to AA-derived EETs (Ye et al. 2002). Both DHA and EPA (to a lesser extent) were reported to directly activate BK_{Ca} channels in cell-free patches, using path clamp electrophysiology (Toshinori Hoshi, Wissuwa, et al. 2013). Therefore, I investigated the role of BK_{Ca} channels in DHA- and EPA-mediated relaxation of rat aorta and mesenteric artery. Consistent with previous studies, inhibition of BK_{Ca} led to significant attenuation in the relaxation effect of DHA in both rat mesenteric artery and aorta (Figs 3.17A and 3.21A respectively). Furthermore, DHA might be directly activating these channels as CYP metabolites were not involved (Fig 3.14A and 3.15A). However, there is also a possibility that lipoxygenase metabolites of DHA such as 17S-HDHA could be involved in the activation of BK_{Ca} channels (Li et al. 2011). The vasodilation effect of EPA was also investigated, and my findings demonstrate that the relaxation was sensitive to the blockade of BK_{Ca} channels in rat mesenteric artery (Fig 3.17B), whereas relaxation in rat aorta was unaffected. As CYP was associated with the vasodilation effect of EPA in rat mesenteric artery (Fig 3.14B), it is possible that EPETEs are involved in the activation of BK_{Ca} channels. Therefore, my findings indicate that BK_{Ca} is associated with DHA-induced relaxation in both arteries. However, with EPA-induced relaxation it was only involved in the mesenteric artery, indicating heterogeneity in the vasodilation pathway that can depend upon the type of artery and n-3 PUFA (Fig 6.2). Studies indicate that n-3 PUFAs can activate BK_{Ca} channels by binding to the S5 and S6 pore forming segments

of the α subunits (Toshinori Hoshi, Xu, et al. 2013). Additionally, the first transmembrane segment and the N-terminus present in the β subunits of the BK_{Ca} channel complex are also involved in n-3 PUFA binding (T. Hoshi et al. 2013). Using PUFAs with various acyl chain lengths and double bonds, a study demonstrated that DHA elicited the largest enhancement of BK_{Ca} currents (Toshinori Hoshi, Xu, et al. 2013). EPA and AA were less effective compared to DHA, however both PUFAs evoked similar levels of amplification of the BK_{Ca} currents (Toshinori Hoshi, Xu, et al. 2013). Although EPA (C20:5) is composed of an additional double bond compared to AA (C20:4), both PUFAs are made up of 20-carbon chains; suggesting that the increased effectiveness of DHA (C22:6) was due to its longer acyl length and not due to the additional double bond. This is consistent with our data since the blockade of BK_{Ca} with paxilline was more effective in inhibiting relaxation induced by DHA compared to EPA in both arteries (Fig 3.17 and 3.21). Depending upon the cardiovascular disorder and the type of artery, alteration of BK_{Ca} expression has been reported by various studies. For example, a decrease in the expression of BK_{Ca} α subunit was reported in pulmonary artery derived from rats with pulmonary hypertension (Bonnet et al. 2003). However, in mesenteric arteries, which is involved in regulation of blood pressure, an enhancement of β1 subunit expression of the BK_{Ca} channels was reported in SHR (Chang et al. 2006). Furthermore, this study also demonstrated that an increase in expression was only observed once the animals were hypertensive and the reduction of blood pressure with captopril (an angiotensin-converting enzyme inhibitor) was able to reverse this effect. These findings suggest that the BK_{Ca} channels may have an important role as a compensatory vasodilation mechanism in hypertension and therefore the blood pressure lowering effects reported with n-3 PUFAs in hypertensive patients, possibly involves n-3 PUFA mediated

activation of these channels (Geleijnse et al. 2002; Campbell et al. 2013; Miller et al. 2014).

The EDH response can be initiated by an increase in $[Ca^{2+}]_i$ that activates SK_{Ca} and IK_{Ca} channels, resulting in hyperpolarization of ECs which can electrically spread to SMCs, via myoendothelial gap junctions, eventually causing vasodilation (Chapter 1, section 1.2.3). Currently, there are no studies demonstrating the role of SK_{Ca} and IK_{Ca} channels in n-3 PUFA-mediated relaxations. My findings demonstrate that SK_{Ca} channels are not involved in the relaxation effect of both DHA and EPA in rat aorta and mesenteric artery (Fig 3.17 and 3.21). There is evidence indicating that TP receptors can inhibit SK_{Ca} channels in rat cerebral (McNeish and Garland 2007) and mesenteric arteries (Crane and Garland 2004). This was further confirmed by subsequent studies demonstrating that the inhibitory mechanism involved activation of Rho/ROCK signalling by TP receptors (McNeish et al. 2012; Gauthier et al. 2014). As my myograph experiments involved initial preconstriction of rat arteries with a TP receptor agonist (U46619), it can be speculated that any potential SK_{Ca} component of n-3 PUFA-induced relaxation was disguised due to the agonist. I also investigated IK_{Ca} channels using both n-3 PUFAs in rat arteries. My findings demonstrate an IK_{Ca} component in DHA-induced relaxation of both rat mesenteric artery and aorta (Figs 3.17A and 3.21A respectively). This is a novel finding that not only demonstrates the role of IK_{Ca} in the vasodilation effect of DHA, but also heterogeneity in the vasodilation mechanisms, as IK_{Ca} was not involved in EPA-mediated relaxation (Fig 6.2). In contrast to my findings which investigated arterial tissues, DHA has been reported to inhibit IK_{Ca} channel activity in human embryonic kidney (HEK) cells (Kacik et al. 2014). This discrepancy might have occurred due to the restriction of arterial IK_{Ca} channels to signalling microdomains in the endothelium, where activation of associated channels such as TRPV4 regulates IK_{Ca}-mediated

hyperpolarization (Sonkusare et al. 2012); it is possible that HEK cells lack these microdomains and the intracellular machinery, therefore the effects observed are perhaps due to an indirect stimulation of IK_{Ca} channels by DHA in the native tissue.

Depending upon the type of CVD, there is evidence indicating that some vasodilation pathways are significantly impaired whereas other pathways can act as compensatory mechanisms; for example, a study with SHRs demonstrated that an increased cholesterol intake enhanced the production of EDHF-like factors whereas NO production was inhibited (Kagota et al. 1999). Furthermore, EDH-like response was also reported to have a compensatory role that prevented the development of hypertension in eNOS/COX KO mice (Scotland et al. 2005). Studies indicate that the expression of endothelial K_{Ca} channels increases with decreasing arterial size in rats (Sandow and Hill 2000; Hilgers et al. 2006). This has also been validated by human studies that have demonstrated the expression and the functional role of SK_{Ca} and IK_{Ca} channels in smaller vascular beds such as skeletal muscle arterioles (Liu et al. 2008), coronary (Feng et al. 2008; Takai et al. 2013) and mesenteric arteries (Chadha et al. 2011) (Table 1.2). Therefore, these findings indicate that the K_{Ca} channels perhaps have an important role in the regulation of resistance arterial tone and blood pressure. Furthermore, in IK_{Ca} KO mice, significant impairment in endothelial and smooth muscle hyperpolarization was demonstrated, resulting in subsequent inhibition of ACh-induced relaxation of carotid and cremaster arteries (Si 2006). It was also indicated that the deletion of these channels led to significant augmentation of blood pressure and left ventricular hypertrophy (Si 2006). Similar to the BK_{Ca} channels, the EDH pathway has been reported to act as a compensatory vasodilation mechanism in various CVDs such as hypertension. Therefore, based on my findings (Fig 3.17 and 3.21) it is possible that the therapeutic effects

observed with DHA probably involves activation of both IK_{Ca} and BK_{Ca} channels (Geleijnse et al. 2002; Campbell et al. 2013; Miller et al. 2014).

6.3 The role of TRPV4 in n-3 PUFA mediated vasodilation

TRPV4 is a non-selective cation channel expressed in various types of cells including vascular ECs and SMCs (chapter 1, section 1.2.3.iii) (Filosa et al. 2013). PUFAs such as EETs, CYP-derived metabolites of AA, have been reported to activate TRPV4 channels resulting in vascular relaxation of SMCs (Earley et al. 2005). Although it was initially thought that EETs were involved in the direct modulation of BK_{Ca} channels, subsequent electrophysiological studies demonstrated that EETs were unable to enhance BK_{Ca} currents in isolated membrane patches (Earley et al. 2005). It was later discovered that EETs activated TRPV4 channels which subsequently led to the opening of BK_{Ca} in rat cerebral arteries (Earley et al. 2005). A similar mechanism involving the TRPV4 channels was also reported to activate the endothelial SK_{Ca} and IK_{Ca} channels in murine mesenteric arteries (Sonkusare et al. 2012). My findings from chapter 3, section 3.2.5, demonstrated that IK_{Ca} and BK_{Ca} channels are involved in DHA-mediated relaxation of both rat mesenteric artery and aorta whereas BK_{Ca} was involved with EPA-induced relaxation of rat mesenteric artery. Furthermore, TRPV4 has been reported to activate both channels in the vasculature; therefore, using wire myograph I investigated the role of these channels in n-3 PUFA-induced relaxation. My findings demonstrated that inhibition of TRPV4 led to partial attenuation of DHA-mediated relaxation of rat mesenteric artery (Fig 4.3), this was similar to the inhibition observed following blockade of the IK_{Ca} channels (Fig 3.17A). There is evidence demonstrating heterogenous activation of the K_{Ca} channels by TRPV4 depending upon the type of artery; for example, a study conducted in mouse mesenteric artery demonstrated that the relaxation mediated by TRPV4 was completely abolished following inhibition of endothelial K_{Ca} channels

(Sonkusare et al. 2012) and therefore, did not involve the BK_{Ca} channels in contrast to rat cerebral arteries (Earley et al. 2005). Furthermore, it was also reported that IK_{Ca} was predominantly activated by TRPV4 (Sonkusare et al. 2012). Therefore, it is possible that the IK_{Ca} component of DHA-induced relaxation involves the initial activation of TRPV4 channels in rat mesenteric artery.

In rat aorta, TRPV4 was not involved in the vasodilation effect of either n-3 PUFAs (Fig 3B-C and Fig 3A-B). Most studies involving the TRPV4-dependent activation of K_{Ca} have been reported in resistance arteries such as mesenteric (Sonkusare et al. 2012; Ma et al. 2013; Sonkusare et al. 2014; Yap et al. 2014; Ho et al. 2015), cerebral (Earley, Pauyo, et al. 2009) and pulmonary artery (Lin et al. 2015) along with cremaster arterioles (Bagher et al. 2012). Furthermore, there is also evidence indicating the predominance of EDH response in the smaller resistance arteries due to increased expression of K_{Ca} and myo-endothelial gap junctions in comparison to conduit arteries (Shimokawa et al. 1996; Sandow and Hill 2000; Hilgers et al. 2006; Billaud et al. 2014). Therefore, it is possible that these myoendothelial microdomains, that allow interaction between TRPV4 and IK_{Ca} channels, are not present in large conduit arteries like rat aorta.

Metabolites of PUFAs such as EETs, which are derived from AA, act as endogenous agonists of TRPV4 channels that can elicit vasodilation through subsequent activation of K_{Ca} (Sonkusare et al. 2012). My results demonstrated that both TRPV4 and IK_{Ca} were involved in DHA-induced relaxation of rat mesenteric artery and therefore, it was logical to hypothesize that the IK_{Ca} component involves an initial direct activation of TRPV4 by DHA, similar to EETs. To assess these effects, I created a stable cell line that allowed the inducible expression of TRPV4 following tetracycline administration, as described in chapter 4, section 4.2.2. The regulation of TRPV4 channels by DHA and EPA was then investigated. Acute application of both n-3 PUFAs failed to elicit any TRPV4-mediated

changes in $[Ca^{2+}]_i$ levels (Fig 4.13). There is evidence demonstrating that both IK_{Ca} and TRPV4 channels are localized in the myoendothelial projections and together can elicit hyperpolarization in the native vascular cells (Sonkusare et al. 2012; Sonkusare et al. 2014). Furthermore, it was also reported that indirect modulation of TRPV4 by muscarinic receptors was dependent upon the subsequent activation of PKC-anchoring protein, AKAP150, which was also localized in the myoendothelial projections. Using whole cell patch clamp, a recent study also reported that EPA is not involved in the direct activation of TRPV4 channels expressed in HEK cells (Caires et al. 2017). This is consistent with my findings and further indicates that perhaps HEK cells lack the necessary microdomains that are required for the activation of TRPV4 channels with acute application of n-3 PUFAs. Moreover, in human microvascular ECs, overnight supplementation with EPA was reported to enhance TRPV4 currents. This study also indicated the presence of silent TRPV4 channels in ECs that were insensitive to agonist application (Caires et al. 2017). EPA supplementation of these ECs were reported to activate the silent channels. Mechanistic investigation into membrane remodelling demonstrated that the EPA treatment led to an increase in membrane fluidity and reduction in bending stiffness, resulting in the subsequent activation of the silent channels (Caires et al. 2017). My findings from Fig 4.16 demonstrated that TRPV4 activity was not modified following an acute treatment (1 h) of the stable cells with n-3 PUFAs, indicating that perhaps optimum incorporation of these fatty acids into the plasma membrane requires a longer treatment (Fig 4.16). However, it should also be noted that native ECs were used for the overnight supplementation study and therefore, additional experiments are required to fully confirm that these effects are also observed in the stable HEK cells.

6.4 The role of K_{ATP} in n-3 PUFA mediated vasodilation

Based on the findings from my previous myograph experiments, the most potent attenuation of n-3 PUFA-induced relaxation was observed following the combined blockade of IK_{Ca} and BK_{Ca} channels, which are both potassium channels involved in hyperpolarization of vascular SMCs (Fig 3.17 and 3.21). However, a considerable amount of residual relaxation always remained, indicating that the mechanisms of n-3 PUFA-mediated vasodilation was largely endothelium independent. Given that my results indicated the critical role of hyperpolarization, although it was not examined directly, I investigated whether additional potassium channels were also involved in the vasodilation effect of DHA and EPA. Therefore, the subsequent myograph experiments were focussed on investigating the effects of non-selective inhibition of potassium channel-induced hyperpolarization, using high KCl Krebs solution. In the rat mesenteric artery, exposure to high KCl Krebs led to significant attenuation in relaxation which was characterised by reduction in the maximum response, an effect that seemed more profound with DHA compared to EPA (Fig 5.3A-B). Furthermore, the relaxation effect of both DHA and EPA was completely abrogated with high KCl Krebs in rat aorta (Fig 5.4A-B). This is consistent with another study that also demonstrated a similar effect with DHA-induced relaxation in rat aorta (Sato et al. 2014). I believe this is the most compelling evidence indicating the critical role of potassium channels by any vascular study to date, since the relaxation response of both DHA and EPA was completely dependent upon the activation of potassium channels in rat aorta and significant inhibition in n-3 PUFA-induced relaxation was observed with high KCl Krebs in rat mesenteric artery as well. Therefore, the next objective was to characterise the potassium channel(s) involved.

To date most studies have reported the activation of BK_{Ca} channels in n-3 PUFA-mediated relaxation, however there is also some evidence suggesting a possible role for K_{ATP} channels (Engler et al. 2000; Engler and Engler 2000). A more recent study led by Sato *et al*. (2014) indicated that both DHA- and EDP-mediated vasodilation of rat aorta were sensitive to the inhibition of K_{ATP}. Therefore, as my findings have already demonstrated that BK_{Ca} and IK_{Ca} channels are involved in the vasodilation effects of n-3 PUFAs with a large residual relaxation remaining, I investigated the role of K_{ATP} channels in rat mesenteric artery and aorta using wire myograph. Consistent with the findings involving high KCl Krebs (Fig 5.3A-B), inhibition of K_{ATP} with PNU37883A also led to significant attenuation of n-3 PUFA-induced relaxation in rat mesenteric artery, that was more profound with DHA in comparison to EPA. Similarly, in rat aorta, relaxation to DHA was almost completely abrogated whereas EPA-induced relaxation was significantly inhibited following the blockade of K_{ATP} channels. In contrast to the complete abrogation of relaxation observed with high KCl Krebs, some residual relaxation remained with EPA in rat aorta following K_{ATP} inhibition. Furthermore, a more profound inhibition was observed with high KCl Krebs compared to PNU37883A in the mesenteric artery, suggesting that additional potassium channels besides K_{ATP} are also involved. This is consistent with my findings demonstrating the role of additional potassium channels, which include IK_{Ca}, BK_{Ca} and K_v7 channels, in n-3 PUFA mediated relaxation. As mentioned before, these findings also demonstrate heterogeneity in the vasodilation mechanisms depending upon both the type of artery and n-3 PUFA.

Taking into consideration that PNU37883A selectively blocks vascular K_{ATP} channels (Kir6.1/SUR2B) (Kovalev et al. 2004), findings from the myograph experiments demonstrated a significant role for K_{ATP} channels in n-3 PUFA-induced relaxation of both rat aorta and mesenteric arteries. Given that the n-3 PUFAs can directly activate BK_{Ca}

channels (Toshinori Hoshi, Wissuwa, et al. 2013), it is reasonable to assume their direct actions on other potassium channels such as K_{ATP}. However, currently there are no studies that have investigated this possibility. To address this question, I generated a stable cell line that expressed the major vascular isoform of K_{ATP}, by transfecting SUR2B and transducing Kir6.1 subunit into HEK cells (chapter 5, section 5.2.3-5.2.4). The expression of vascular K_{ATP} subunits were then confirmed using immunocytochemistry and western blotting (Fig 5.11 and 5.14). Using whole cell patch clamp with the stable cells, functional K_{ATP} channels were detected as demonstrated by the significant increase in current density following K_{ATP} agonist application, and subsequent abrogation of this effect with the perfusion of the K_{ATP} inhibitor (Fig 5.15). Application of DHA failed to enhance K_{ATP} currents, indicating that that a direct modulation of channel activity does not occur during relaxation mediated by DHA.

EETs have been reported to mediate vasodilation by indirectly activating K_{ATP} channels through a PKA-dependent pathway in rat mesenteric arteries (Ye et al. 2005). Further investigation into the mechanisms revealed that EETs activated $G\alpha_s$ protein resulting in subsequent activation of PKA which phosphorylated and enhanced K_{ATP} channel opening (Ye et al. 2006). Due to the nature of the pathway the authors suggested the presence of an EET surface receptor, which remains to identified. There is evidence indicating that EETs can activate free fatty acid receptor 1 (GPR40), which is a GPCR found in vascular ECs and SMCs (Park et al. 2018). EETs were found to elevate $[Ca^{2+}]_i$ levels via GPR40 in HEK cells, however, this receptor was not involved in the EET-induced relaxation of bovine coronary arteries (Park et al. 2018). A recent study indicated that resolvins, which are n-3 PUFA metabolites involved in the resolution of inflammation, can inhibit TP receptor-mediated constriction in rat aorta and human pulmonary artery following activation of chemerin receptors (a GPCR) (Jannaway et al. 2018). As a result, it can be

speculated that the stable cells used for my patch clamp experiments lacked the necessary receptors or the cellular environment involved in the indirect modulation of K_{ATP} by n-3 PUFAs. Furthermore, we have preliminary patch clamp data (personal communication, professor Andrew Tinker) demonstrating enhancement of PNU37883A-sensitive currents in murine aortic SMCs following acute application of DHA.

Consistent with an indirect effect of n-3 PUFAS on K_{ATP}, activation of cardiac K_{ATP} channels by AA was dependent upon CYP (Lu et al. 2006). EETs were reported to directly modulate cardiac K_{ATP} channels and this modulatory effect was indicated to be stereospecific, since 11(*S*), 12(*R*)-EET enhanced K_{ATP} currents, whereas 11(*R*), 12(*S*)-EET did not elicit any effects (Lu et al. 2002; Lu et al. 2006). Furthermore, using EET analogs, K_{ATP} activation was increased when a double bond was introduced at the n-3 position of EETs, indicating the possibility of channel modulation by n-3 PUFA metabolites (Lu et al. 2002). These findings highlight how the correct metabolites of AA are required for K_{ATP} activation; hence, it is possible that metabolites of DHA and EPA are primarily involved in stimulating K_{ATP} and therefore, the stable HEK cells may lack the necessary enzymes required to produce these metabolites. As my findings indicated that CYP is not involved in DHA-induced relaxation, perhaps metabolites such as 17S-HDHA and resolvins, derived from other vascular enzymes may have a role (Jannaway et al. 2018). In contrast to DHA, EPA-mediated relaxation was sensitive to CYP inhibition in both rat aorta and mesenteric artery, as a result, EPETEs may be involved in K_{ATP} modulation. Thus, future electrophysiological experiments should involve: (1) the use of native vascular cells and (2) the use of different vasoactive metabolites of DHA and EPA, to further examine if an indirect pathway is involved in K_{ATP} activation during n-3 PUFA-induced vasodilation.

Our findings indicate that n-3 PUFAs are possibly involved in the indirect activation of K_{ATP} channels in rat arteries. There is evidence indicating that the vascular K_{ATP} is mostly composed of Kir6.1/SUR2B subunits (Foster and Coetzee 2016). Animal studies have demonstrated the expression of these channels in various vascular beds such as aorta (Blanco-Rivero et al. 2008), coronary (Miyoshi et al. 1992; Morrissey et al. 2005) and mesenteric arteries (Tang et al. 2005). The role of each K_{ATP} subunit in the cardiovascular system has been investigated using KO models. A study demonstrated that the genetic loss of Kir6.1 was associated with complete inhibition of K_{ATP}-induced hyperpolarization and vasodilation of aorta (Miki et al. 2002). Furthermore, these mice had a higher rate of developing sudden cardiac death compared to the wild-type controls (Miki et al. 2002). Genetic loss of SUR2 was also associated with focal constriction of coronary arteries resulting in vasospasms (Chutkow et al. 2002). An increase in resting blood pressure and sudden death was also reported in the SUR2 KO mice (Chutkow et al. 2002). In humans, expression of K_{ATP} channels has been confirmed in coronary (Yoshida et al. 2004), meningeal (Ploug et al. 2008) and pulmonary arteries (Cui et al. 2002) (Table 1.2). Although these findings indicate the potential role of K_{ATP} channels as a therapeutic target, there is also evidence indicating that loss of function mutations of the Kir6.1 and SUR2B were not associated with hypertension (Ellis et al. 2010; Duan et al. 2011). This is perhaps explained by the compensatory role of other vasodilation mechanisms such as BK_{Ca} channels and EDH response that have been indicated to prevent the development of hypertension in various studies (Scotland et al. 2005; Chang et al. 2006). However, a selective K_{ATP} opener, iptakalim, was reported to elicit potent blood pressure lowering effects in hypertensive animals and humans (Pan et al. 2010). Furthermore, these effects were completely absent in the normotensive controls. The enhanced effectiveness of iptakalim was associated with its increased selectivity towards the vascular

Kir6.1/SUR2B subtype and therefore iptakalim was reported to have a better safety and tolerability profile compared to the previous K_{ATP} openers (Pan et al. 2010). Although direct activation of K_{ATP} channels by n-3 PUFAs was not observed according to my patch-clamp data (Fig 5.15), profound reduction in relaxation was observed in both arteries with K_{ATP} inhibition, indicating a possible indirect interaction between the channel and n-3 PUFAs (Fig 5.7-5.8). Therefore, it is plausible to suggest that the therapeutic effects observed with n-3 PUFA supplementation may involve activation of K_{ATP} channels, however additional studies involving Kir6.1 and/or SUR2B KO animal models are required to further confirm whether a similar inhibition in n-3 PUFA-induced relaxation is observed as demonstrated following treatment with PNU-37883A.

6.5 The role of K_v7 in n-3 PUFA mediated vasodilation

After examining the findings from the myograph experiments (Fig 5.1-5.8), it can be argued that high KCl Krebs was marginally more effective compared to PNU37883A (K_{ATP} channel inhibitor) in inhibiting the n-3 PUFA-mediated relaxation, especially involving EPA. Furthermore, my patch clamp data demonstrated that DHA is not involved in direct activation of vascular K_{ATP} channels expressed in HEK cells and as a result, it is possible that PNU37883A is not selective and may inhibit other vascular potassium channels. In fact some studies have reported that although PNU37883A (also known as U-37883A) is more selective to Kir6.1 containing K_{ATP} channels, it can also inhibit other potassium channels present in the vasculature (Teramoto 2006). However, a considerably higher concentration (100 μM) of PNU37883A was reported to inhibit both K_V and Kir channels (channel subtypes were not specified) present in SMCs derived from rat mesenteric artery (Wellman et al. 1999). Recent studies have reported that acute application of both DHA and EPA can activate the cardiac I_{KS} channel, composed of $K_v7.1$/KCNE1 subunits, and neuronal M-channel, composed of $K_v7.2/K_v7.3$ subunits

(Liin et al. 2014; Moreno et al. 2015; Liin et al. 2016). Currently there are no studies that have investigated whether n-3 PUFAs also modulate the vascular K_v7 channels (mainly $K_v7.4$ and 7.5) involved in vasodilation and therefore, the final part of my project focussed in examining the role of K_v7 channels in n-3 PUFA-induced relaxation of rat arteries.

In rat mesenteric artery, both DHA- and EPA-mediated relaxations were partially inhibited following the blockade of K_v7 channels with XE991 (non-selective inhibitor of Kv7) (Fig 5.18). This inhibition of relaxation was considerably smaller compared to PNU37883A-mediated attenuation in rat mesenteric artery (Fig 5.7). Surprisingly in rat aorta, inhibition of n-3 PUFA-mediated relaxation with XE991 appeared to be almost identical to the effects observed with the K_{ATP} blockade. It is interesting that the magnitude of inhibition mediated by XE991 and PNU37883A was different in rat mesenteric artery. This is perhaps explained by the non-selectivity of PNU37883A to vascular potassium channels, although a lower concentration (3 µM) of this blocker was used in my experiments. There is evidence indicating that PNU37883A is involved in inhibition of K_V channels at higher concentration (100 µM), however the channel isoforms were not identified (Wellman et al. 1999). Studies have demonstrated that the role of EDH in vasodilation and the expression of SK_{Ca} increases with decreasing arterial size (Hilgers et al. 2006), therefore, it is possible that other potassium channels, such as K_v7, could also have differential expression depending upon the vascular bed. In fact, a study confirmed that although $K_v7.1$ and $K_v7.4$ subunit expressions were observed in mouse vascular beds, a higher expression of $K_v7.4$ was demonstrated in cerebral compared to coronary arteries (Lee et al. 2015). Similarly, using wire myograph, pharmacological modulation of K_v7 channel activity had a greater effect in the regulation of cerebral vascular tone in comparison to coronary arteries (Lee et al. 2015). This

heterogeneity in the contribution of K_v7 was also observed in other arteries, since K_v7 inhibitors such as linopirdine and XE991 were reported to elicit constrictions in rat and mouse pulmonary arteries whereas the contractile tone of mesenteric arteries were unaffected by these inhibitors (Joshi et al. 2006). Furthermore, regional differences of K_v7 contribution in the same artery was also reported; for example, cAMP-mediated relaxation was more profound in the left compared to right coronary artery due to the higher activity and expression of $K_v7.1$ and $K_v7.5$ (Morales-Cano et al. 2015). Although extensive evidence indicates that $K_v7.1$ channels are not associated with regulation of resting arterial tone, activation of these channels were associated with relaxation of preconstricted arteries (Bett et al. 2006; Lerche et al. 2007; Preet S Chadha et al. 2012). Furthermore, $K_v7.1$ was reported to be expressed in both rat aorta and mesenteric artery; however, relaxation induced by the activation of $K_v7.1$ channels was more potent in the mesenteric artery, indicating variability in the contribution of K_v7 channels in the regulation of vascular tone (Preet S Chadha et al. 2012). Therefore, the variable expression and contribution of potassium channels in the relaxation of blood vessels, may provide an explanation for the observed heterogeneity in our findings. For example, in rat mesenteric artery, perhaps the expression of K_{ATP} channels is higher compared to K_v7 and hence PNU37883A (Fig 5.7) elicited a more potent inhibition in relaxation compared to XE991 (Fig 5.18). In rat aorta on the other hand, it is possible that the basal expression of K_v7 is greater than K_{ATP}, therefore, both inhibitors had a similar effect as the relaxation was mostly dependent upon K_v7 activity. It would be completely ignorant to not consider the possibility that perhaps the K_{ATP} and K_v7 channels interact with each other to elicit vasodilation and therefore, this could explain why my findings indicated that the individual blockade of each channel can elicit an inhibition of a similar magnitude, especially in n-3 PUFA-induced relaxation of rat aorta. However, currently there is no

evidence demonstrating the presence of such interactions between K_v7 and K_{ATP} channels in vasodilation.

The residual relaxation that was observed with EPA in rat aorta, following the pre-treatment with PNU37883A, demonstrates the involvement of other potassium channels, since high KCl Krebs completely abolished this relaxation. Findings from my previous myograph experiments indicate that K_{Ca} channels are not involved in EPA-induced relaxation of aorta (Fig 19). Although I have mentioned the non-selectivity of PNU37883A, perhaps combined blockade of both K_{ATP} and K_v7 would mimic the effects observed with high KCl Krebs. In rat mesenteric artery, residual relaxation was observed with high KCl Krebs for both n-3 PUFAs indicating the presence of vasodilation mechanism(s) that are independent of potassium channels, these pathways may involve voltage-gated sodium and calcium channels as there is evidence of their modulation by PUFAs (Elinder and Liin 2017).

As mentioned previously, studies have demonstrated expression and activity of K_v7 channels in various murine vascular beds such as aorta (Preet S Chadha et al. 2012), cerebral (Lee et al. 2015), coronary (Morales-Cano et al. 2015), pulmonary (Joshi et al. 2006) and mesenteric arteries (Preet S Chadha et al. 2012). The expression and the functional role of K_v7 channels were also investigated in human adipose and mesenteric arteries (Ng et al. 2011). The findings from this study demonstrated that $K_v7.4$ was consistently expressed in all the arterial samples whereas variable expression of $K_v7.1$, $K_v7.3$ and $K_v7.5$ was reported (Ng et al. 2011). Furthermore, $K_v7.4$ was predominantly involved in vasodilation whereas $K_v7.1$ did not have a functional role in the regulation of vascular tone (Ng et al. 2011). Several animal studies have indicated that K_v7 channels are associated with CVDs. For example; in SHR compared to normotensive controls, a reduction in $K_v7.4$ expression and agonist-induced relaxation was demonstrated in

various vascular beds such as aorta, coronary, mesenteric and renal arteries (Jepps et al. 2011; P. S. Chadha et al. 2012). In humans, currently there is limited evidence indicating the therapeutic effects of K_v7 activation in hypertension. Although flupirtine, a K_v7 opener, was reported to attenuate right ventricular pressure and hypertrophy in pulmonary hypertensive mice (Morecroft et al. 2009), two human studies reported contrasting effects on blood pressure depending upon the duration of the treatments with this opener (Herrmann et al. 1987; Hummel et al. 1991). Besides the vasculature, K_v7 subunits are also expressed in cardiac muscle cells (I_{KS} channel composed of $K_v7.1$) and neurons (M-channel composed of $K_v7.2$, $K_v7.3$ and $K_v7.5$), therefore, it is important to consider that K_v7 openers could possibly elicit effects in more than one type of tissue. Selective K_v7 openers that are targeted more towards the $K_v7.4$ subunits should be investigated to assess if these openers provide a better therapeutic efficacy and safety profile when targeting CVDs, compared to the less-selective openers. My novel findings indicate that the K_v7 has a major role in n-3 PUFA-induced relaxation. Although direct activation of I_{KS} and M-channels has been previously indicated in cardiac and neuronal cells (Liin et al. 2014; Moreno et al. 2015; Liin et al. 2016), additional studies need to be conducted to fully confirm that n-3 PUFAs can also regulate the activity of K_v7 subtypes present in the vasculature. Findings from these experiments would be indispensable for studies investigating the prospect of using novel analogues that can selectively target specific pathways, such as $K_v7.4$ channels, for the treatment of CVDs.

6.6 Conclusion and future experiments

This is the first comprehensive characterisation of the mechanisms underlying DHA- and EPA-mediated relaxation of rat conduit and resistance arteries. According to my control curve data, DHA was significantly more potent than EPA in both arteries, however, there was no difference in the maximal response of n-3 PUFAs in either artery (Log EC_{50} and E_{max} values can be found in table 6.1). Consistent with my findings, previous studies have indicated that DHA is generally more effective than EPA in activating potassium channels. DHA was reported to be more potent in enhancing BK_{Ca} currents due to its longer acyl chain length compared to EPA (Toshinori Hoshi, Xu, et al. 2013). There is also evidence indicating that the negative charge of various PUFAs is crucial in the activation of *Shaker* and $K_v7.1$ channels (Börjesson et al. 2008; Liin et al. 2015). Furthermore, acute treatment with DHA was reported to elicit the largest enhancement of *Shaker* channel currents compared to EPA and in contrast to BK_{Ca} channels, the charge and the presence of two or more methylene-interrupted *cis* double bonds were the most important structural features of PUFAs in channel modulation, as opposed to acyl chain length (Börjesson et al. 2008). The findings from my myograph experiments indicated that endothelium has a minor role in these relaxations, since NO and COX were not involved whereas CYP metabolism only had a small effect in EPA-induced relaxation. IK_{Ca} and BK_{Ca} channels were both involved in DHA-induced relaxation of both arteries whereas only BK_{Ca} channels were involved in EPA mediated relaxation of rat mesenteric artery. This is the first study demonstrating the novel role of IK_{Ca} in n-3 PUFA-mediated relaxation. These findings are summarised in Fig 6.2 and they clearly demonstrate heterogeneity in the vasodilation mechanisms of n-3 PUFAs, depending upon both the type of n-3 PUFA and the vascular bed. Another novel finding of this study is the role of TRPV4 in the acute relaxation effect of DHA in rat mesenteric artery, which is possibly

involved in the regulation of the IK_{Ca} component. n-3 PUFA-mediated relaxation in rat aorta was completely dependent upon potassium channels and further characterisation revealed that K_{ATP} channels were involved. This is also the first study that demonstrated the role of K_v7 channels in n-3 PUFA-induced relaxation. The general consensus is that both K_{ATP} and K_v7 channels are predominately expressed in the vascular SMCs (Fosmo and Skraastad 2017). This is consistent with my findings as n-3 PUFA-induced relaxation was primarily regulated by endothelium-independent mechanisms. This project was focussed on completely characterizing the pathways involved with n-3 PUFA-induced relaxation using a conduit and a resistance artery, as most of the previous vascular studies are limited to a certain type of vascular bed and n-3 PUFA. We have partly met this goal as my findings indicate that n-3 PUFA-induced relaxation in rat aorta is completely dependent upon potassium channels. However, in rat mesenteric artery, there was still some remaining residual relaxation with high KCl Krebs, indicating the presence of vasodilation mechanism(s) that are independent of potassium channels. Additional myograph experiments should be conducted to fully characterize these pathways which may involve voltage-gated sodium and calcium channels as there is some evidence indicating modulation of their activity by PUFAs (Elinder and Liin 2017).

Although my mesenteric data demonstrated a TRPV4 component in DHA-induced relaxation, direct activation of these channels by n-3 PUFAs was not observed in our stable cells. This was also validated by a recent study using whole cell patch clamp (Caires et al. 2017). Acute pre-treatment (1 h) of these stable cells with EPA did not evoke any changes in TRPV4 activity. However, an enhancement in TRPV4 currents was reported in human microvascular ECs following overnight supplementation with EPA (Caires et al. 2017). It is possible that perhaps acute treatment does not result in optimum membrane incorporation of n-3 PUFAs, therefore as a possible future experiment it would

be interesting to assess if overnight n-3 PUFA supplementation of the stable HEK cells could modify TRPV4 currents. It is quite evident from my findings that a heterologous expression system might not be ideal, especially if the pathways involve microdomains that are unique to the native tissue. n-3 PUFAs were unable to directly activate both K_{ATP} and TRPV4 channels and therefore, future electrophysiological experiments should involve the use of native vascular cells to further investigate the presence of any indirect interaction between these channels and n-3 PUFAs. In fact, due to our collaboration with professor Andrew Tinker, we have preliminary data (not shown) demonstrating an upregulation in K_{ATP} currents following acute application of DHA in murine vascular cells. This suggests that there is possibly an indirect pathway that leads to K_{ATP} activation following acute application of n-3 PUFAs.

One of the highlights of my findings is the crucial role of the hyperpolarization response mediated by the potassium channels. Multiple channels including BK_{Ca}, IK_{Ca}, K_{ATP} and K_v7 channels were found to be involved indicating that perhaps a unifying upstream pathway could be involved in the subsequent activation of these potassium channels, although there is also evidence indicating direct activation of BK_{Ca} and $K_v7.1$ by n-3 PUFAs (Toshinori Hoshi, Wissuwa, et al. 2013; Liin et al. 2015). This upstream pathway perhaps involves the activation of PKA as it can activate multiple potassium channels including BK_{Ca} (Imig et al. 1999; Fukao et al. 2001; Dimitropoulou et al. 2007), K_{ATP} (Ye et al. 2005; Ye et al. 2006; Yang et al. 2008) and K_v7 (Stott et al. 2015; Mani et al. 2016; Stott et al. 2016). Furthermore, several studies have indicated that n-3 PUFAs can activate PKA in cardiac myocytes, epithelial and hepatoma cell lines (Mies et al. 2004; Szentandrássy et al. 2007; Tai et al. 2009). Similar to EETs (Ye et al. 2006), it is plausible to suggest that n-3 PUFAs are possibly involved in the initial activation of PKA resulting in subsequent stimulation of the potassium channels involved in vasodilation. Therefore,

additional myograph experiments should be conducted to investigate the role of PKA in n-3 PUFA-induced relaxation.

Studies report that the vasculature is mostly composed of $K_v7.1$, $K_v7.4$ and $K_v7.5$ subunits (Ng et al. 2011). However, there is evidence indicating that $K_v7.4$ is the predominant subunit involved in vasodilation of both murine and human vascular beds (Ng et al. 2011; Lee et al. 2015). My experiments involved the use of XE991 which is a non-selective K_v7 inhibitor, therefore, the specific channel subtype(s) involved with n-3 PUFAs was not identified. Studies that demonstrated direct activation of K_v7 channels by n-3 PUFAs were conducted using cardiac I_{KS} and neuronal M-channels, which were composed of $K_v7.1$, $K_v7.2$ and $K_v7.3$ subunits (Liin et al. 2014; Moreno et al. 2015; Liin et al. 2016). Therefore, additional experiments are required to investigate whether n-3 PUFAs also elicit an identical effect with the $K_v7.4$ channels. Similar to my project, these experiments could be carried out by generating stable cell lines expressing $K_v7.4$ tetramers, followed by patch clamp electrophysiology to detect any changes in channel activity with acute application of n-3 PUFAs. As our myograph experiments indicated that pathways involved in n-3 PUFA-induced vasodilation were primarily endothelium-independent, native vascular SMCs could then be used to further confirm if the acute treatments with DHA and EPA can enhance K_v7 currents.

The gene-targeting techniques are significantly more advanced in mice compared to rats, as a result mice have been used as the preferred mammalian model for genetic modifications over the years (Homberg et al. 2017). However, rats have several experimental advantages over mice for cardiovascular research due to their larger size. Different types of tissue including blood vessels are significantly smaller in mice compared to rats, therefore, performing functional myograph experiments with the smaller vascular beds such as cerebral and mesenteric arteries would be impossible.

Furthermore, the measurement of physiological parameters is also more challenging in mice compared to rats; for example, studies have indicated that the telemetric measurement of blood pressure via the insertion of implants into mice arteries can result in the obstruction blood flow, whereas in rats this is does not occur due to the larger size of the vessels (Homberg et al. 2017). There is also an increased difficulty in performing precise surgical manipulations in mice without the risk of damaging the target tissue. Therefore, functional cardiovascular studies should ideally involve the use rats due to its superiority as an experimental model in comparison to mice.

To further validate my findings, additional supplementation studies using KO and disease animal models are required. My myograph experiments indicated that NO pathway is not involved in n-3 PUFA-induced vascular relaxation, however supplementation studies have reported an increase in NO production following n-3 PUFA treatment. It is possible that this enhancement in the NO pathway is only observed via chronic exposure with n-3 PUFAs, as the treatments for most of these studies lasted for more than a week (Hirafuji et al. 2002). Furthermore, these studies involved the use of vascular cells rather than arterial tissues and therefore lacked functional evidence that demonstrated effects of n-3 PUFA supplementation on vascular relaxation (Omura et al. 2001; Hirafuji et al. 2002; López et al. 2004; Raimondi et al. 2005). To address this discrepancy, future experiments with animal models should investigate whether variations in the duration of n-3 PUFA supplementation alters NO production and arterial tissues derived from these animals should be used to asses if any functional changes in n-3 PUFA-induced vasodilation involves the NO pathway.

My myograph experiments demonstrated that K_{ATP} channel inhibition with PNU37883A elicited significant reduction in n-3 PUFA-induced relaxation of rat arteries. Therefore, to further confirm these findings, an immediate future experiment would be to investigate

if similar effects are observed with K_{ATP} KO mice which will be kindly provided by professor Andrew Tinker (William Harvey Heart Centre, Queen Mary University of London). Native vascular cells and arterial tissue derived from these mice could then be used to assess the acute effects of n-3 PUFAs, using techniques such as wire myograph and patch clamp electrophysiology. Inhibition of K_v7 channels also led to significant attenuation in vasodilation mediated by n-3 PUFAs. Due to evidence demonstrating the predominance of $K_v7.4$ subunit in the vasodilation of both murine and human vascular beds (Ng et al. 2011; Lee et al. 2015), $K_v7.4$ KO mice can be used to further corroborate my findings.

The incorporation of EPA into the plasma membrane following overnight supplementation has been reported to enhance TRPV4 activity in human microvascular ECs (Caires et al. 2017). Therefore, an interesting avenue for supplementation studies would be to investigate whether the activity of vascular potassium channels is also enhanced due to membrane incorporation of n-3 PUFAs. Although multiple animal and human studies have confirmed the protective role of n-3 PUFAs in hypertension (Vaskonen et al. 1996; Geleijnse et al. 2002; Campbell et al. 2013; Miller et al. 2014), these studies usually only employ physiological parameters to demonstrate the therapeutic effects and therefore lack the mechanistic investigation of pathways involved. The expression profile of potassium channels has been reported to alter in hypertension depending upon the type of vascular bed and ion channel; for example, in SHR compared to normotensive controls, an enhancement of the BK_{Ca} β1 subunit expression was reported in the mesenteric artery (Chang et al. 2006) whereas reduction in $K_v7.4$ expression was demonstrated in various vascular beds such as aorta, coronary, mesenteric and renal arteries (Jepps et al. 2011; P. S. Chadha et al. 2012). Most disease model studies, involving n-3 PUFA supplementation, usually only investigate a particular type of

potassium channel and artery. Therefore, more comprehensive supplementation studies are required to investigate the effects of CVDs and n-3 PUFA treatment in the expression and functional activity of more than one type of vascular potassium channels. The findings from these studies would be invaluable for differentiating impaired versus compensatory vasodilation pathways in various CVDs which can subsequently facilitate the use of more targeted approach for cardiovascular treatments depending upon the disorder.

In conclusion, my study provides evidence of the role of IK_{Ca}, K_{ATP} and K_v7 in n-3 PUFA-mediated relaxation of rat aorta and mesenteric artery. The heterogeneity in these mechanisms were dependent upon both the type of blood vessels and the n-3 PUFA. Compared to healthy individuals, the therapeutic benefits of n-3 PUFAs have been reported to be more prominent in individuals with disorders such as hypertension (Morris et al. 1993). Therefore, the findings from this project will be invaluable for future vascular studies that investigate the prospect of using n-3 PUFA and novel analogues as treatments that target specific pathways involved in providing therapeutic effects against cardiovascular disorders.

Chapter 7

References

Abramovitz, M., Adam, M., Boie, Y., Carrière, M., Denis, D., Godbout, C., Lamontagne, S., Rochette, C., Sawyer, N., Tremblay, N.M., Belley, M., Gallant, M., Dufresne, C., Gareau, Y., Ruel, R., Juteau, H., Labelle, M., Ouimet, N., and Metters, K.M., 2000. The utilization of recombinant prostanoid receptors to determine the affinities and selectivities of prostaglandins and related analogs. *Biochimica et biophysica acta*, 1483(2), pp.285–93.

Adeagbo, A.S., 1997. Endothelium-derived hyperpolarizing factor: characterization as a cytochrome P450 1A-linked metabolite of arachidonic acid in perfused rat mesenteric prearteriolar bed. *American journal of hypertension*, 10(7 Pt 1), pp.763–71.

Adela, R., Nethi, S.K., Bagul, P.K., Barui, A.K., Mattapally, S., Kuncha, M., Patra, C.R., Reddy, P.N.C., and Banerjee, S.K., 2015. Hyperglycaemia Enhances Nitric Oxide Production in Diabetes: A Study from South Indian Patients. A. V. Gomes, ed. *PLOS ONE*, 10(4), p.e0125270.

Agostoni, A. and Cugno, M., 2001. The kinin system: biological mechanisms and clinical implications. *Recenti progressi in medicina*, 92(12), pp.764–73.

Al-Allaf, F.A., Tolmachov, O.E., Zambetti, L.P., Tchetchelnitski, V., and Mehmet, H., 2013. Remarkable stability of an instability-prone lentiviral vector plasmid in Escherichia coli Stbl3. *3 Biotech*, 3(1), pp.61–70.

Allen, B.G. and Walsh, M.P., 1994. The biochemical basis of the regulation of smooth-muscle contraction. *Trends in Biochemical Sciences*, 19(9), pp.362–368.

Amberg, G.C., Bonev, A.D., Rossow, C.F., Nelson, M.T., and Santana, L.F., 2003. Modulation of the molecular composition of large conductance, Ca(2+) activated K(+) channels in vascular smooth muscle during hypertension. *The Journal of clinical investigation*, 112(5), pp.717–24.

Amberg, G.C. and Santana, L.F., 2003. Downregulation of the BK Channel 1 Subunit in Genetic Hypertension. *Circulation Research*, 93(10), pp.965–971.

Andoh, T. and Kuraishi, Y., 2003. Nitric oxide enhances substance P-induced itch-associated responses in mice. *British journal of pharmacology*, 138(1), pp.202–8.

Anon, 2018. *UniProt* [Online]. Available from: http://www.uniprot.org/ [Accessed 1 February 2018].

Archer, S.L., Gragasin, F.S., Wu, X., Wang, S., McMurtry, S., Kim, D.H., Platonov, M., Koshal, A., Hashimoto, K., Campbell, W.B., Falck, J.R., and Michelakis, E.D., 2003. Endothelium-derived hyperpolarizing factor in human internal mammary artery is 11,12-epoxyeicosatrienoic acid and causes relaxation by activating smooth muscle BK(Ca) channels. *Circulation*, 107(5), pp.769–76.

Archer, S.L., Huang, J.M., Hampl, V., Nelson, D.P., Shultz, P.J., and Weir, E.K., 1994. Nitric oxide and cGMP cause vasorelaxation by activation of a charybdotoxin-sensitive K channel by cGMP-dependent protein kinase. *Proceedings of the National Academy of Sciences of the United States of America*, 91(16), pp.7583–7.

Arehart, E., Stitham, J., Asselbergs, F.W., Douville, K., MacKenzie, T., Fetalvero, K.M., Gleim, S., Kasza, Z., Rao, Y., Martel, L., Segel, S., Robb, J., Kaplan, A., Simons, M., Powell, R.J., Moore, J.H., Rimm, E.B., Martin, K.A., and Hwa, J., 2008. Acceleration of cardiovascular disease by a dysfunctional prostacyclin receptor mutation: potential implications for cyclooxygenase-2 inhibition. *Circulation research*, 102(8), pp.986–93.

Arnold, C., Konkel, A., Fischer, R., and Schunck, W.-H., 2010. Cytochrome P450-dependent metabolism of omega-6 and omega-3 long-chain polyunsaturated fatty acids. *Pharmacological reports : PR*, 62(3), pp.536–47.

Arnold, C., Markovic, M., Blossey, K., Wallukat, G., Fischer, R., Dechend, R., Konkel,

A., von Schacky, C., Luft, F.C., Muller, D.N., Rothe, M., and Schunck, W.-H., 2010. Arachidonic Acid-metabolizing Cytochrome P450 Enzymes Are Targets of ω-3 Fatty Acids. *Journal of Biological Chemistry*, 285(43), pp.32720–32733.

Arun Kumar, A.S., Chakradhara Rao, U.S., Umamaheswaran, G., Ramu, P., Kesavan, R., Shewade, D.G., Balachandar, J., and Adithan, C., 2011. Haplotype Structures of Common Variants of CYP2C8 , CYP2C9 , and ADRB1 Genes in a South Indian Population. *Genetic Testing and Molecular Biomarkers*, 15(6), pp.407–413.

Ashcroft, F.M., Harrison, D.E., and Ashcroft, S.J.H., 1984. Glucose induces closure of single potassium channels in isolated rat pancreatic β-cells. *Nature*, 312(5993), pp.446–448.

Ashcroft, F.M. and Rorsman, P., 1990. ATP-sensitive K+ channels: a link between B-cell metabolism and insulin secretion. *Biochemical Society transactions*, 18(1), pp.109–11.

Aung, T., Halsey, J., Kromhout, D., Gerstein, H.C., Marchioli, R., Tavazzi, L., Geleijnse, J.M., Rauch, B., Ness, A., Galan, P., Chew, E.Y., Bosch, J., Collins, R., Lewington, S., Armitage, J., Clarke, R., and Omega-3 Treatment Trialists' Collaboration, 2018. Associations of Omega-3 Fatty Acid Supplement Use With Cardiovascular Disease Risks. *JAMA Cardiology*, 3(3), p.225.

Bagher, P., Beleznai, T., Kansui, Y., Mitchell, R., Garland, C.J., and Dora, K.A., 2012. Low intravascular pressure activates endothelial cell TRPV4 channels, local Ca2+ events, and IKCa channels, reducing arteriolar tone. *Proceedings of the National Academy of Sciences*, 109(44), pp.18174–18179.

Bang, H.O., Dyerberg, J., and Hjøorne, N., 1976. The composition of food consumed by Greenland Eskimos. *Acta medica Scandinavica*, 200(1–2), pp.69–73.

Bayliss, W.M., 1902. On the local reactions of the arterial wall to changes of internal

pressure. *The Journal of physiology*, 28(3), pp.220–31.

Bentzen, B.H., Olesen, S.-P., Rønn, L.C.B., and Grunnet, M., 2014. BK channel activators and their therapeutic perspectives. *Frontiers in physiology*, 5, p.389.

Bergstroem, S., Danielsson, H., and Samuelsson, B., 1964. The enzymatic formation of prostaglandin E2 from arachidonic acid. Prostaglandins and related factors 32. *Biochimica et biophysica acta*, 90, pp.207–10.

Berridge, M.J., 1987. Inositol Trisphosphate and Diacylglycerol: Two Interacting Second Messengers. *Annual Review of Biochemistry*, 56(1), pp.159–193.

Beswick, R.A., Dorrance, A.M., Leite, R., and Webb, R.C., 2001. NADH/NADPH oxidase and enhanced superoxide production in the mineralocorticoid hypertensive rat. *Hypertension (Dallas, Tex. : 1979)*, 38(5), pp.1107–11.

Bett, G.C.L., Morales, M.J., Beahm, D.L., Duffey, M.E., and Rasmusson, R.L., 2006. Ancillary subunits and stimulation frequency determine the potency of chromanol 293B block of the KCNQ1 potassium channel. *The Journal of Physiology*, 576(3), pp.755–767.

Betts, J.G., Desaix, P., Johnson, E. (Edward W.., Johnson, J.E., Korol, O., Kruse, D., Poe, B., Wise, J., Womble, M.D., Young, K.A., and OpenStax College, 2013. *Anatomy and Physiology*. 1st ed. OpenStax. Available from: http://cnx.org/contents/14fb4ad7-39a1-4eee-ab6e-3ef2482e3e22@8.24 [Accessed 7 August 2018].

Billaud, M., Lohman, A.W., Johnstone, S.R., Biwer, L.A., Mutchler, S., and Isakson, B.E., 2014. Regulation of Cellular Communication by Signaling Microdomains in the Blood Vessel Wall. *Pharmacological Reviews*, 66(2), pp.513–569.

Blackshaw, L.A., Brierley, S.M., and Hughes, P.A., 2010. TRP channels: new targets for visceral pain. *Gut*, 59(01), pp.126–135.

Blackwell, K.A., Sorenson, J.P., Richardson, D.M., Smith, L.A., Suda, O., Nath, K., and Katusic, Z.S., 2004. Mechanisms of aging-induced impairment of endothelium-dependent relaxation: role of tetrahydrobiopterin. *American Journal of Physiology-Heart and Circulatory Physiology*, 287(6), pp.H2448–H2453.

Blanco-Rivero, J., Gamallo, C., Aras-López, R., Cobeño, L., Cogolludo, A., Pérez-Vizcaino, F., Ferrer, M., and Balfagon, G., 2008. Decreased expression of aortic KIR6.1 and SUR2B in hypertension does not correlate with changes in the functional role of KATP channels. *European Journal of Pharmacology*, 587(1–3), pp.204–208.

Blank, T., Nijholt, I., Kye, M.-J., and Spiess, J., 2004. Small Conductance Ca2+-Activated K+ Channels as Targets of CNS Drug Development. *Current Drug Target -CNS & Neurological Disorders*, 3(3), pp.161–167.

Bogatcheva, N. V., Sergeeva, M.G., Dudek, S.M., and Verin, A.D., 2005. Arachidonic acid cascade in endothelial pathobiology. *Microvascular Research*, 69(3), pp.107–127.

Böger, R.H., Bode-Böger, S.M., Szuba, A., Tsao, P.S., Chan, J.R., Tangphao, O., Blaschke, T.F., and Cooke, J.P., 1998. Asymmetric dimethylarginine (ADMA): a novel risk factor for endothelial dysfunction: its role in hypercholesterolemia. *Circulation*, 98(18), pp.1842–7.

Bolton, T.B. and Imaizumi, Y., 1996. Spontaneous transient outward currents in smooth muscle cells. *Cell calcium*, 20(2), pp.141–52.

Bolton, T.B., Lang, R.J., and Takewaki, T., 1984. Mechanisms of action of noradrenaline and carbachol on smooth muscle of guinea-pig anterior mesenteric artery. *The Journal of physiology*, 351, pp.549–72.

Bonnet, S., Dumas-de-La-Roque, E., Begueret, H., Marthan, R., Fayon, M., Dos Santos,

P., Savineau, J.-P., and Baulieu, E.-E., 2003. Dehydroepiandrosterone (DHEA) prevents and reverses chronic hypoxic pulmonary hypertension. *Proceedings of the National Academy of Sciences*, 100(16), pp.9488–9493.

Börjesson, S.I., Hammarström, S., and Elinder, F., 2008. Lipoelectric Modification of Ion Channel Voltage Gating by Polyunsaturated Fatty Acids. *Biophysical Journal*, 95(5), pp.2242–2253.

Boussif, O., Lezoualc'h, F., Zanta, M.A., Mergny, M.D., Scherman, D., Demeneix, B., and Behr, J.P., 1995. A versatile vector for gene and oligonucleotide transfer into cells in culture and in vivo: polyethylenimine. *Proceedings of the National Academy of Sciences of the United States of America*, 92(16), pp.7297–301.

Bradley, K.K., Jaggar, J.H., Bonev, A.D., Heppner, T.J., Flynn, E.R., Nelson, M.T., and Horowitz, B., 1999. Kir2.1 encodes the inward rectifier potassium channel in rat arterial smooth muscle cells. *The Journal of physiology*, 515 (Pt 3, pp.639–51.

Brandes, R.P., Behra, A., Lebherz, C., Böger, R.H., Bode-Böger, S.M., Phivthong-Ngam, L., and Mügge, A., 1997. N(G)-nitro-L-arginine- and indomethacin-resistant endothelium-dependent relaxation in the rabbit renal artery: effect of hypercholesterolemia. *Atherosclerosis*, 135(1), pp.49–55.

Bratz, I.N., Dick, G.M., Partridge, L.D., and Kanagy, N.L., 2005. Reduced molecular expression of K + channel proteins in vascular smooth muscle from rats made hypertensive with N ω -nitro- l -arginine. *American Journal of Physiology-Heart and Circulatory Physiology*, 289(3), pp.H1277–H1283.

Brown, D.A. and Passmore, G.M., 2009. Neural KCNQ (Kv7) channels. *British Journal of Pharmacology*, 156(8), pp.1185–1195.

Brown, N.K., Zhou, Z., Zhang, J., Zeng, R., Wu, J., Eitzman, D.T., Chen, Y.E., and Chang, L., 2014. Perivascular adipose tissue in vascular function and disease: a

review of current research and animal models. *Arteriosclerosis, thrombosis, and vascular biology*, 34(8), pp.1621–30.

Bubolz, A.H., Mendoza, S.A., Zheng, X., Zinkevich, N.S., Li, R., Gutterman, D.D., and Zhang, D.X., 2012. Activation of endothelial TRPV4 channels mediates flow-induced dilation in human coronary arterioles: role of Ca 2+ entry and mitochondrial ROS signaling. *American Journal of Physiology-Heart and Circulatory Physiology*, 302(3), pp.H634–H642.

Buchholz, F., Ringrose, L., Angrand, P.O., Rossi, F., and Stewart, A.F., 1996. Different thermostabilities of FLP and Cre recombinases: implications for applied site-specific recombination. *Nucleic acids research*, 24(21), pp.4256–62.

Bunting, S., Gryglewski, R., Moncada, S., and Vane, J.R., 1976. Arterial walls generate from prostaglandin endoperoxides a substance (prostaglandin X) which relaxes strips of mesenteric and coeliac ateries and inhibits platelet aggregation. *Prostaglandins*, 12(6), pp.897–913.

Burdge, G.C., Jones, A.E., and Wootton, S.A., 2002. Eicosapentaenoic and docosapentaenoic acids are the principal products of α-linolenic acid metabolism in young men. *British Journal of Nutrition*, 88(04), p.355.

Burr, G. 0 and Burr, M.M., 1929. A new deficiency disease produced by the rigid exclusion of fat from the diet. *Journal of Biological Chemistry*, 82, pp.345–367.

Burr, G. 0 and Burr, M.M., 1930. On the nature and role of the fatty acids essential in nutrition. *Journal of Biological Chemistry*, 86, pp.587–621.

Busse, R. and Fleming, I., 2003. Regulation of endothelium-derived vasoactive autacoid production by hemodynamic forces. *Trends in pharmacological sciences*, 24(1), pp.24–9.

Cabral, P.D. and Garvin, J.L., 2014. TRPV4 activation mediates flow-induced nitric

oxide production in the rat thick ascending limb. *American Journal of Physiology-Renal Physiology*, 307(6), pp.F666–F672.

Caires, R., Sierra-Valdez, F.J., Millet, J.R.M., Herwig, J.D., Roan, E., Vásquez, V., and Cordero-Morales, J.F., 2017. Omega-3 Fatty Acids Modulate TRPV4 Function through Plasma Membrane Remodeling. *Cell Reports*, 21(1), pp.246–258.

Campbell, F., Dickinson, H.O., Critchley, J.A., Ford, G.A., and Bradburn, M., 2013. A systematic review of fish-oil supplements for the prevention and treatment of hypertension. *European Journal of Preventive Cardiology*, 20(1), pp.107–120.

Campbell, W.B., Gebremedhin, D., Pratt, P.F., and Harder, D.R., 1996. Identification of epoxyeicosatrienoic acids as endothelium-derived hyperpolarizing factors. *Circulation research*, 78(3), pp.415–23.

Campbell, W.B., Holmes, B.B., Falck, J.R., Capdevila, J.H., and Gauthier, K.M., 2006. Regulation of potassium channels in coronary smooth muscle by adenoviral expression of cytochrome P -450 epoxygenase. *American Journal of Physiology-Heart and Circulatory Physiology*, 290(1), pp.H64–H71.

Capdevila, J.H., Pidkovka, N., Mei, S., Gong, Y., Falck, J.R., Imig, J.D., Harris, R.C., and Wang, W., 2014. The Cyp2c44 epoxygenase regulates epithelial sodium channel activity and the blood pressure responses to increased dietary salt. *The Journal of biological chemistry*, 289(7), pp.4377–86.

Casós, K., Zaragozá, M.C., Zarkovic, N., Zarkovic, K., Andrisic, L., Portero-Otín, M., Cacabelos, D., and Mitjavila, M.T., 2010. A fish oil-rich diet reduces vascular oxidative stress in apoE –/– mice. *Free Radical Research*, 44(7), pp.821–829.

CELL BIOLABS, I., 2017. *ViraBind™ Lentivirus Purification Kit* [Online]. Available from: https://www.cellbiolabs.com/sites/default/files/VPK-104-lentiviral-purification-kit.pdf [Accessed 1 February 2018].

Chadha, P.S., Liu, L., Rikard-Bell, M., Senadheera, S., Howitt, L., Bertrand, R.L., Grayson, T.H., Murphy, T. V, and Sandow, S.L., 2011. Endothelium-dependent vasodilation in human mesenteric artery is primarily mediated by myoendothelial gap junctions intermediate conductance calcium-activated K+ channel and nitric oxide. *The Journal of pharmacology and experimental therapeutics*, 336(3), pp.701–8.

Chadha, Preet S, Zunke, F., Davis, A.J., Jepps, T.A., Linders, J.T.M., Schwake, M., Towart, R., and Greenwood, I.A., 2012. Pharmacological dissection of K(v)7.1 channels in systemic and pulmonary arteries. *British journal of pharmacology*, 166(4), pp.1377–87.

Chadha, P. S., Zunke, F., Zhu, H.-L., Davis, A.J., Jepps, T.A., Olesen, S.P., Cole, W.C., Moffatt, J.D., and Greenwood, I.A., 2012. Reduced KCNQ4-Encoded Voltage-Dependent Potassium Channel Activity Underlies Impaired -Adrenoceptor-Mediated Relaxation of Renal Arteries in Hypertension. *Hypertension*, 59(4), pp.877–884.

Chang, T., Wu, L., and Wang, R., 2006. Altered Expression of BK Channel β1 Subunit in Vascular Tissues from Spontaneously Hypertensive Rats. *American Journal of Hypertension*, 19(7), pp.678–685.

Chen, G., Suzuki, H., and Weston, A.H., 1988. Acetylcholine releases endothelium-derived hyperpolarizing factor and EDRF from rat blood vessels. *British journal of pharmacology*, 95(4), pp.1165–74.

Chen, I.S., Hotta, S.S., Ikeda, I., Cassidy, M.M., Sheppard, A.J., and Vahouny, G. V., 1987. Digestion, Absorption and Effects on Cholesterol Absorption of Menhaden Oil, Fish Oil Concentrate and Corn Oil by Rats. *The Journal of Nutrition*, 117(10), pp.1676–1680.

Chen, X., Li, Y., Hollenberg, M., Triggle, C.R., and Ding, H., 2012. The Contribution of d-Tubocurarine–sensitive and Apamin-sensitive K-channels to EDHF-mediated Relaxation of Mesenteric Arteries From eNOS−/− Mice. *Journal of Cardiovascular Pharmacology*, 59(5), pp.413–425.

Chen, Y., Shen, F., Liu, J., and Yang, G.-Y., 2017. Arterial stiffness and stroke: de-stiffening strategy, a therapeutic target for stroke. *Stroke and Vascular Neurology*, 2(2), pp.65–72.

Cheng, K., Khurana, S., Chen, Y., Kennedy, R.H., Zimniak, P., and Raufman, J.-P., 2002. Lithocholylcholine, a Bile Acid/Acetylcholine Hybrid, Is a Muscarinic Receptor Antagonist. *Journal of Pharmacology and Experimental Therapeutics*, 303(1), pp.29–35.

Chin, J.P., Gust, A.P., and Dart, A.M., 1993. Indomethacin inhibits the effects of dietary supplementation with marine oils on vasoconstriction of human forearm resistance vessels in vivo. *Journal of hypertension*, 11(11), pp.1229–34.

Chou, T.C., Yen, M.H., Li, C.Y., and Ding, Y.A., 1998. Alterations of nitric oxide synthase expression with aging and hypertension in rats. *Hypertension (Dallas, Tex. : 1979)*, 31(2), pp.643–8.

Christman, B.W., McPherson, C.D., Newman, J.H., King, G.A., Bernard, G.R., Groves, B.M., and Loyd, J.E., 1992. An Imbalance between the Excretion of Thromboxane and Prostacyclin Metabolites in Pulmonary Hypertension. *New England Journal of Medicine*, 327(2), pp.70–75.

Chutkow, W.A., Pu, J., Wheeler, M.T., Wada, T., Makielski, J.C., Burant, C.F., and McNally, E.M., 2002. Episodic coronary artery vasospasm and hypertension develop in the absence of Sur2 KATP channels. *Journal of Clinical Investigation*, 110(2), pp.203–208.

Chutkow, W.A., Simon, M.C., Le Beau, M.M., and Burant, C.F., 1996. Cloning, tissue expression, and chromosomal localization of SUR2, the putative drug-binding subunit of cardiac, skeletal muscle, and vascular KATP channels. *Diabetes*, 45(10), pp.1439–45.

Clapp, L.H., Turcato, S., Hall, S., and Baloch, M., 1998. Evidence that Ca2+-activated K+ channels play a major role in mediating the vascular effects of iloprost and cicaprost. *European journal of pharmacology*, 356(2–3), pp.215–24.

Clark, J.D., Lin, L.L., Kriz, R.W., Ramesha, C.S., Sultzman, L.A., Lin, A.Y., Milona, N., and Knopf, J.L., 1991. A novel arachidonic acid-selective cytosolic PLA2 contains a Ca(2+)-dependent translocation domain with homology to PKC and GAP. *Cell*, 65(6), pp.1043–51.

Clarke, A.L., Petrou, S., Walsh, J. V, and Singer, J.J., 2002. Modulation of BK Ca channel activity by fatty acids: structural requirements and mechanism of action. *American Journal of Physiology-Cell Physiology*, 283, p.66.

Clements, R.T., Terentyev, D., and Sellke, F.W., 2015. Ca^{2+}-Activated K^{+} Channels as Therapeutic Targets for Myocardial and Vascular Protection. *Circulation Journal*, 79(3), pp.455–462.

Cocks, T.M., King, S.J., and Angus, J.A., 1990. Glibenclamide is a competitive antagonist of the thromboxane A2 receptor in dog coronary artery in vitro. *British journal of pharmacology*, 100(2), pp.375–8.

Conquer, J.A. and Holub, B.J., 1998. Effect of supplementation with different doses of DHA on the levels of circulating DHA as non-esterified fatty acid in subjects of Asian Indian background. *Journal of lipid research*, 39(2), pp.286–92.

Corbin, J.D. and Francis, S.H., 1999. Cyclic GMP phosphodiesterase-5: target of sildenafil. *The Journal of biological chemistry*, 274(20), pp.13729–32.

Cornwell, T.L., Pryzwansky, K.B., Wyatt, T.A., and Lincoln, T.M., 1991. Regulation of sarcoplasmic reticulum protein phosphorylation by localized cyclic GMP-dependent protein kinase in vascular smooth muscle cells. *Molecular pharmacology*, 40(6), pp.923–31.

Covic, A., Goldsmith, D.J.A., Panaghiu, L., Covic, M., and Sedor, J., 2000. Analysis of the effect of hemodialysis on peripheral and central arterial pressure waveforms. *Kidney International*, 57(6), pp.2634–2643.

Crane, G.J. and Garland, C.J., 2004. Thromboxane receptor stimulation associated with loss of SK_{Ca} activity and reduced EDHF responses in the rat isolated mesenteric artery. *British Journal of Pharmacology*, 142(1), pp.43–50.

Csiszar, A., Labinskyy, N., Orosz, Z., Xiangmin, Z., Buffenstein, R., and Ungvari, Z., 2007. Vascular aging in the longest-living rodent, the naked mole rat. *American Journal of Physiology-Heart and Circulatory Physiology*, 293(2), pp.H919–H927.

Cui, Y., Tran, S., Tinker, A., and Clapp, L.H., 2002. The Molecular Composition of K ATP Channels in Human Pulmonary Artery Smooth Muscle Cells and Their Modulation by Growth. *American Journal of Respiratory Cell and Molecular Biology*, 26(1), pp.135–143.

Dabrowska, R., Hinkins, S., Walsh, M.P., and Hartshorne, D.J., 1982. The binding of smooth muscle myosin light chain kinase to actin. *Biochemical and Biophysical Research Communications*, 107(4), pp.1524–1531.

Dalby, B., Cates, S., Harris, A., Ohki, E.C., Tilkins, M.L., Price, P.J., and Ciccarone, V.C., 2004. Advanced transfection with Lipofectamine 2000 reagent: primary neurons, siRNA, and high-throughput applications. *Methods*, 33(2), pp.95–103.

Danish Myo Technology, 2017. *DMT Normalization Guide vol.2.1* [Online]. Available from: https://www.dmt.dk/blog/normalization-guide [Accessed 18 February 2019].

Dart, C. and Standen, N.B., 1993. Adenosine-activated potassium current in smooth muscle cells isolated from the pig coronary artery. *The Journal of physiology*, 471, pp.767–86.

Davis, M.J., 2012. Perspective: Physiological Role(s) of the Vascular Myogenic Response. *Microcirculation*, 19(2), pp.99–114.

Davis, M.J., Ferrer, P.N., and Gore, R.W., 1986. Vascular anatomy and hydrostatic pressure profile in the hamster cheek pouch. *American Journal of Physiology-Heart and Circulatory Physiology*, 250(2), pp.H291–H303.

Daykin, K., Widdop, S., and Hall, I.P., 1993. Control of histamine induced inositol phospholipid hydrolysis in cultured human tracheal smooth muscle cells. *European Journal of Pharmacology: Molecular Pharmacology*, 246(2), pp.135–140.

Dennis, E.A., 1994. Diversity of group types, regulation, and function of phospholipase A2. *The Journal of biological chemistry*, 269(18), pp.13057–60.

Dhakam, Z., McEniery, C.M., Yasmin, Cockroft, J.R., Brown, M.J., and Wilkinson, I.B., 2006. Atenolol and Eprosartan: Differential Effects on Central Blood Pressure and Aortic Pulse Wave Velocity. *American Journal of Hypertension*, 19(2), pp.214–219.

Dimitropoulou, C., West, L., Field, M.B., White, R.E., Reddy, L.M., Falck, J.R., and Imig, J.D., 2007. Protein phosphatase 2A and Ca2+-activated K+ channels contribute to 11,12-epoxyeicosatrienoic acid analog mediated mesenteric arterial relaxation. *Prostaglandins & Other Lipid Mediators*, 83(1–2), pp.50–61.

Ding, H., Hashem, M., Wiehler, W.B., Lau, W., Martin, J., Reid, J., and Triggle, C., 2009. Endothelial dysfunction in the streptozotocin-induced diabetic apoE-deficient mouse. *British Journal of Pharmacology*, 146(8), pp.1110–1118.

Ding, H., Kubes, P., and Triggle, C., 2000. Potassium- and acetylcholine-induced vasorelaxation in mice lacking endothelial nitric oxide synthase. *British Journal of Pharmacology*, 129(6), pp.1194–1200.

Dong, H., Waldron, G.J., Cole, W.C., and Triggle, C.R., 1998. Roles of calcium-activated and voltage-gated delayed rectifier potassium channels in endothelium-dependent vasorelaxation of the rabbit middle cerebral artery. *British Journal of Pharmacology*, 123(5), pp.821–832.

Dong, H., Waldron, G.J., Galipeau, D., Cole, W.C., and Triggle, C.R., 1997. NO/PGI 2 -independent vasorelaxation and the cytochrome P450 pathway in rabbit carotid artery. *British Journal of Pharmacology*, 120(4), pp.695–701.

Doolan, G.K., Panchal, R.G., Fonnes, E.L., Clarke, A.L., Williams, D.A., and Petrou, S., 2002. Fatty acid augmentation of the cardiac slowly activating delayed rectifier current (I Ks) is conferred by hminK. *The FASEB Journal*, 16(12), pp.1662–1664.

Van Dorp, D.A., Beerthuis, R.K., Nugteren, D.H., and Vonkeman, H., 1964. The biosynthesis of prostaglandins. *Biochimica et biophysica acta*, 90, pp.204–7.

Dreisbach, A.W., Japa, S., Sigel, A., Parenti, M.B., Hess, A.E., Srinouanprachanh, S.L., Rettie, A.E., Kim, H., Farin, F.M., Hamm, L.L., and Lertora, J.J.L., 2005. The Prevalence of CYP2C8, 2C9, 2J2, and Soluble Epoxide Hydrolase Polymorphisms in African Americans With Hypertension. *American Journal of Hypertension*, 18(10), pp.1276–1281.

Duan, R., Cui, W., and Wang, H., 2011. Mutational analysis of the Kir6.1 gene in Chinese hypertensive patients treated with the novel ATP-sensitive potassium channel opener iptakalim. *Experimental and therapeutic medicine*, 2(4), pp.757–760.

Dudley, D.T., Pang, L., Decker, S.J., Bridges, A.J., Saltiel, A.R., Bourcier, T., Weksler,

B.B., and Caterina, R. De, 1995. A synthetic inhibitor of the mitogen-activated protein kinase cascade. *Proceedings of the National Academy of Sciences of the United States of America*, 92(17), pp.7686–9.

Dumas, M., Dumas, J.-P., Rochette, L., Advenier, C., and Giudicelli, J.-F., 1997. Role of potassium channels and nitric oxide in the effects of iloprost and prostaglandin E 1 on hypoxic vasoconstriction in the isolated perfused lung of the rat. *British Journal of Pharmacology*, 120(3), pp.405–410.

Dumoulin, M., Salvail, D., Gaudreault, S.B., Cadieux, A., and Rousseau, E., 1998. Epoxyeicosatrienoic acids relax airway smooth muscles and directly activate reconstituted K Ca channels. *American Journal of Physiology-Lung Cellular and Molecular Physiology*, 275(3), pp.L423–L431.

Dusting, G.J., Moncada, S., and Vane, J.R., 1977. Prostacyclin (PGX) is the endogenous metabolite responsible for relaxation of coronary arteries induced by arachindonic acid. *Prostaglandins*, 13(1), pp.3–15.

Earley, S., 2012. TRPA1 channels in the vasculature. *British journal of pharmacology*, 167(1), pp.13–22.

Earley, S., Gonzales, A.L., and Crnich, R., 2009. Endothelium-Dependent Cerebral Artery Dilation Mediated by TRPA1 and Ca 2+ -Activated K + Channels. *Circulation Research*, 104(8), pp.987–994.

Earley, S., Heppner, T.J., Nelson, M.T., and Brayden, J.E., 2005. TRPV4 Forms a Novel Ca2+ Signaling Complex With Ryanodine Receptors and BKCa Channels. *Circulation Research*, 97(12), pp.1270–1279.

Earley, S., Pauyo, T., Drapp, R., Tavares, M.J., Liedtke, W., and Brayden, J.E., 2009. TRPV4-dependent dilation of peripheral resistance arteries influences arterial pressure. *American journal of physiology. Heart and circulatory physiology*,

297(3), pp.H1096-102.

Eckman, D.M., Hopkins, N., Mcbride, C., and Keef, K.D., 1998. Endothelium-dependent relaxation and hyperpolarization in guinea-pig coronary artery: role of epoxyeicosatrienoic acid. *British Journal of Pharmacology*, 124(1), pp.181–189.

Edwards, G., Dora, K.A., Gardener, M.J., Garland, C.J., and Weston, A.H., 1998. K+ is an endothelium-derived hyperpolarizing factor in rat arteries. *Nature*, 396(6708), pp.269–272.

Edwards, G., Félétou, M., and Weston, A.H., 2010. Endothelium-derived hyperpolarising factors and associated pathways: a synopsis. *Pflügers Archiv - European Journal of Physiology*, 459(6), pp.863–879.

Edwards, R.M., 1983. Segmental effects of norepinephrine and angiotensin II on isolated renal microvessels. *American Journal of Physiology-Renal Physiology*, 244(5), pp.F526–F534.

Egan, K.M., Lawson, J.A., Fries, S., Koller, B., Rader, D.J., Smyth, E.M., and Fitzgerald, G.A., 2004. COX-2-Derived Prostacyclin Confers Atheroprotection on Female Mice. *Science*, 306(5703), pp.1954–1957.

Eglen, R.M. and Whiting, R.L., 1990. Heterogeneity of vascular muscarinic receptors. *Journal of autonomic pharmacology*, 10(4), pp.233–45.

Elinder, F. and Liin, S.I., 2017. Actions and Mechanisms of Polyunsaturated Fatty Acids on Voltage-Gated Ion Channels. *Frontiers in physiology*, 8, p.43.

Ellis, J.A., Lamantia, A., Chavez, R., Scurrah, K.J., Nichols, C.G., and Harrap, S.B., 2010. Genes controlling postural changes in blood pressure: comprehensive association analysis of ATP-sensitive potassium channel genes *KCNJ8* and *ABCC9*. *Physiological Genomics*, 40(3), pp.184–188.

Engler, M.B. and Engler, M.M., 2000. Docosahexaenoic Acid-Induced Vasorelaxation

in Hypertensive Rats: Mechanisms of Action. *Biological Research For Nursing*, 2(2), pp.85–95.

Engler, M.B., Engler, M.M., Browne, A., Sun, Y.-P., and Sievers, R., 2000. Mechanisms of vasorelaxation induced by eicosapentaenoic acid (20:5n-3) in WKY rat aorta. *British Journal of Pharmacology*, 131(8), pp.1793–1799.

Eto, M., Ohmori, T., Suzuki, M., Furuya, K., and Morita, F., 1995. A novel protein phosphatase-1 inhibitory protein potentiated by protein kinase C. Isolation from porcine aorta media and characterization. *Journal of biochemistry*, 118(6), pp.1104–7.

Everaerts, W. and Owsianik, G., 2010. The vanilloid transient receptor potential channel TRPV4: From structure to disease. *Progress in Biophysics and Molecular Biology*, 103(1), pp.2–17.

Everaerts, W., Zhen, X., Ghosh, D., Vriens, J., Gevaert, T., Gilbert, J.P., Hayward, N.J., McNamara, C.R., Xue, F., Moran, M.M., Strassmaier, T., Uykal, E., Owsianik, G., Vennekens, R., De Ridder, D., Nilius, B., Fanger, C.M., and Voets, T., 2010. Inhibition of the cation channel TRPV4 improves bladder function in mice and rats with cyclophosphamide-induced cystitis. *Proceedings of the National Academy of Sciences*, 107(44), pp.19084–19089.

ExPASy, 2018. *Translate tool* [Online]. Available from: https://web.expasy.org/translate/ [Accessed 1 February 2018].

Exton, J.H., 1985. Mechanisms involved in alpha-adrenergic phenomena. *American Journal of Physiology-Endocrinology and Metabolism*, 248(6), pp.E633–E647.

Fahs, C.A., Yan, H., Ranadive, S., Rossow, L.M., Agiovlasitis, S., Wilund, K.R., and Fernhall, B., 2010. The effect of acute fish-oil supplementation on endothelial function and arterial stiffness following a high-fat meal. *Applied Physiology,*

Nutrition, and Metabolism, 35(3), pp.294–302.

Falcone, J.C., Davis, M.J., and Meininger, G.A., 1991. Endothelial independence of myogenic response in isolated skeletal muscle arterioles. *American Journal of Physiology-Heart and Circulatory Physiology*, 260(1), pp.H130–H135.

Fanger, C.M., Ghanshani, S., Logsdon, N.J., Rauer, H., Kalman, K., Zhou, J., Beckingham, K., Chandy, K.G., Cahalan, M.D., and Aiyar, J., 1999. Calmodulin mediates calcium-dependent activation of the intermediate conductance KCa channel, IKCa1. *The Journal of biological chemistry*, 274(9), pp.5746–54.

Félétou, M., 2009. Calcium-activated potassium channels and endothelial dysfunction: therapeutic options? *British journal of pharmacology*, 156(4), pp.545–62.

Feletou, M. and Vanhoutte, P.M., 2004. EDHF: new therapeutic targets? *Pharmacological Research*, 49(6), pp.565–580.

Feletou, M. and Vanhoutte, P.M., 2006. Endothelium-Derived Hyperpolarizing Factor: Where Are We Now? *Arteriosclerosis, Thrombosis, and Vascular Biology*, 26(6), pp.1215–1225.

Félétou, M. and Vanhoutte, P.M., 2009. EDHF: an update. *Clinical Science*, 117(4), pp.139–155.

Feng, J, Ito, M., Ichikawa, K., Isaka, N., Nishikawa, M., Hartshorne, D.J., and Nakano, T., 1999. Inhibitory phosphorylation site for Rho-associated kinase on smooth muscle myosin phosphatase. *The Journal of biological chemistry*, 274(52), pp.37385–90.

Feng, Jianhua, Ito, M., Nishikawa, M., Okinaka, T., Isaka, N., Hartshorne, D.J., and Nakano, T., 1999. Dephosphorylation of distinct sites on the 20 kDa myosin light chain by smooth muscle myosin phosphatase. *FEBS Letters*, 448(1), pp.101–104.

Feng, J., Liu, Y., Clements, R.T., Sodha, N.R., Khabbaz, K.R., Senthilnathan, V.,

Nishimura, K.K., Alper, S.L., and Sellke, F.W., 2008. Calcium-activated potassium channels contribute to human coronary microvascular dysfunction after cardioplegic arrest. *Circulation*, 118(14 Suppl), pp.S46-51.

Filosa, J.A., Yao, X., and Rath, G., 2013. TRPV4 and the regulation of vascular tone. *Journal of cardiovascular pharmacology*, 61(2), pp.113–9.

Fleming, I., 2016. The factor in EDHF: Cytochrome P450 derived lipid mediators and vascular signaling. *Vascular Pharmacology*, 86, pp.31–40.

Forstermann, U. and Münzel, T., 2006. Endothelial Nitric Oxide Synthase in Vascular Disease: From Marvel to Menace. *Circulation*, 113(13), pp.1708–1714.

Fosmo, A.L. and Skraastad, Ø.B., 2017. The Kv7 Channel and Cardiovascular Risk Factors. *Frontiers in cardiovascular medicine*, 4, p.75.

Foster, M.N. and Coetzee, W.A., 2016. K ATP Channels in the Cardiovascular System. *Physiological Reviews*, 96(1), pp.177–252.

Frangos, S.G., Gahtan, V., and Sumpio, B., 1999. Localization of Atherosclerosis. *Archives of Surgery*, 134(10), p.1142.

Fukao, M., Mason, H.S., Kenyon, J.L., Horowitz, B., and Keef, K.D., 2001. Regulation of BK(Ca) channels expressed in human embryonic kidney 293 cells by epoxyeicosatrienoic acid. *Molecular pharmacology*, 59(1), pp.16–23.

Fukui, T., Ishizaka, N., Rajagopalan, S., Laursen, J.B., Capers, Q., Taylor, W.R., Harrison, D.G., de Leon, H., Wilcox, J.N., and Griendling, K.K., 1997. p22phox mRNA expression and NADPH oxidase activity are increased in aortas from hypertensive rats. *Circulation research*, 80(1), pp.45–51.

Furchgott, R.F., Cherry, P.D., Zawadzki, J. V, and Jothianandan, D., 1984. Endothelial cells as mediators of vasodilation of arteries. *Journal of cardiovascular pharmacology*, 6 Suppl 2, pp.S336-43.

Furchgott, R.F. and Zawadzki, J. V, 1980. The obligatory role of endothelial cells in the relaxation of arterial smooth muscle by acetylcholine. *Nature*, 288(5789), pp.373–6.

Garavito, R.M. and DeWitt, D.L., 1999. The cyclooxygenase isoforms: structural insights into the conversion of arachidonic acid to prostaglandins. *Biochimica et Biophysica Acta (BBA) - Molecular and Cell Biology of Lipids*, 1441(2–3), pp.278–287.

Garcia, M.C., Sprecher, H., and Rosenthal, M.D., 1990. Chain elongation of polyunsaturated fatty acids by vascular endothelial cells: studies with arachidonate analogues. *Lipids*, 25(4), pp.211–5.

Garcia, M.L., Knaus, H.G., Munujos, P., Slaughter, R.S., and Kaczorowski, G.J., 1995. Charybdotoxin and its effects on potassium channels. *The American journal of physiology*, 269(1 Pt 1), pp.C1-10.

Gauthier, K.M., Campbell, W.B., and McNeish, A.J., 2014. Regulation of K_{Ca} 2.3 and endothelium-dependent hyperpolarization (EDH) in the rat middle cerebral artery: the role of lipoxygenase metabolites and isoprostanes. *PeerJ*, 2, p.e414.

Gebremedhin, D., Lange, A.R., Narayanan, J., Aebly, M.R., Jacobs, E.R., and Harder, D.R., 1998. Cat cerebral arterial smooth muscle cells express cytochrome P450 4A2 enzyme and produce the vasoconstrictor 20-HETE which enhances L-type Ca2+ current. *The Journal of physiology*, 507 (Pt 3, pp.771–81.

Gee, K.R., Brown, K.A., Chen, W.-N.U., Bishop-Stewart, J., Gray, D., and Johnson, I., 2000. Chemical and physiological characterization of fluo-4 Ca2+-indicator dyes. *Cell Calcium*, 27(2), pp.97–106.

Geleijnse, J.M., Giltay, E.J., Grobbee, D.E., Donders, A.R.T., and Kok, F.J., 2002. Blood pressure response to fish oil supplementation: metaregression analysis of

randomized trials. *Journal of hypertension*, 20(8), pp.1493–9.

Gibbs, R.A., 1990. DNA amplification by the polymerase chain reaction. *Analytical chemistry*, 62(13), pp.1202–14.

Gillham, J.C., Myers, J.E., Baker, P.N., and Taggart, M.J., 2007. Regulation of Endothelial-Dependent Relaxation in Human Systemic Arteries by SK Ca and IK Ca Channels. *Reproductive Sciences*, 14(1), pp.43–50.

Glagov, S., Zarins, C., Giddens, D.P., and Ku, D.N., 1988. Hemodynamics and atherosclerosis. Insights and perspectives gained from studies of human arteries. *Archives of pathology & laboratory medicine*, 112(10), pp.1018–31.

Grace, M.S., Bonvini, S.J., Belvisi, M.G., and McIntyre, P., 2017. Modulation of the TRPV4 ion channel as a therapeutic target for disease. *Pharmacology & Therapeutics*, 177, pp.9–22.

Green, M.R. and Sambrook, J., 2016. Precipitation of DNA with Ethanol. *Cold Spring Harbor Protocols*, 2016(12), p.pdb.prot093377.

Green, M.R. and Sambrook, J., 2017. Precipitation of DNA with Isopropanol. *Cold Spring Harbor Protocols*, 2017(8), p.pdb.prot093385.

Greene, D.L. and Hoshi, N., 2017. Modulation of Kv7 channels and excitability in the brain. *Cellular and molecular life sciences : CMLS*, 74(3), pp.495–508.

Grgic, I., Eichler, I., Heinau, P., Si, H., Brakemeier, S., Hoyer, J., and Köhler, R., 2005. Selective Blockade of the Intermediate-Conductance Ca2+-Activated K+ Channel Suppresses Proliferation of Microvascular and Macrovascular Endothelial Cells and Angiogenesis In Vivo. *Arteriosclerosis, Thrombosis, and Vascular Biology*, 25(4), pp.704–709.

Grgic, I., Kaistha, B.P., Hoyer, J., and Köhler, R., 2009. Endothelial Ca+-activated K+ channels in normal and impaired EDHF-dilator responses--relevance to

cardiovascular pathologies and drug discovery. *British journal of pharmacology*, 157(4), pp.509–26.

Gruhn, N., Boesgaard, S., Eiberg, J., Bang, L., Thiis, J., Schroeder, T. V, and Aldershvile, J., 2002. Effects of large conductance Ca(2+)-activated K(+) channels on nitroglycerin-mediated vasorelaxation in humans. *European journal of pharmacology*, 446(1–3), pp.145–50.

Guéguinou, M., Chantôme, A., Fromont, G., Bougnoux, P., Vandier, C., and Potier-Cartereau, M., 2014. KCa and Ca2 + channels: The complex thought. *Biochimica et Biophysica Acta (BBA) - Molecular Cell Research*, 1843(10), pp.2322–2333.

Guzik, T.J., Hoch, N.E., Brown, K.A., McCann, L.A., Rahman, A., Dikalov, S., Goronzy, J., Weyand, C., and Harrison, D.G., 2007. Role of the T cell in the genesis of angiotensin II induced hypertension and vascular dysfunction. *The Journal of experimental medicine*, 204(10), pp.2449–60.

Haddock, R.E., Grayson, T.H., Brackenbury, T.D., Meaney, K.R., Neylon, C.B., Sandow, S.L., and Hill, C.E., 2006. Endothelial coordination of cerebral vasomotion via myoendothelial gap junctions containing connexins 37 and 40. *American Journal of Physiology-Heart and Circulatory Physiology*, 291(5), pp.H2047–H2056.

Haddy, F.J., Vanhoutte, P.M., and Feletou, M., 2006. Role of potassium in regulating blood flow and blood pressure. *American Journal of Physiology-Regulatory, Integrative and Comparative Physiology*, 290(3), pp.R546–R552.

Hadi, H.A.R., Carr, C.S., and Al Suwaidi, J., 2005. Endothelial dysfunction: cardiovascular risk factors, therapy, and outcome. *Vascular health and risk management*, 1(3), pp.183–98.

Hamilton, C.A., Brosnan, M.J., Al-Benna, S., Berg, G., and Dominiczak, A.F., 2002.

NAD(P)H oxidase inhibition improves endothelial function in rat and human blood vessels. *Hypertension (Dallas, Tex. : 1979)*, 40(5), pp.755–62.

Hansen, T.R. and Bohr, D.F., 1975. Hypertension, transmural pressure, and vascular smooth muscle response in rats. *Circulation Research*, 36(5), pp.590–598.

Harder, D.R., Gebremedhin, D., Narayanan, J., Jefcoat, C., Falck, J.R., Campbell, W.B., and Roman, R., 1994. Formation and action of a P-450 4A metabolite of arachidonic acid in cat cerebral microvessels. *American Journal of Physiology-Heart and Circulatory Physiology*, 266(5), pp.H2098–H2107.

Harder, D R, Gebremedhin, D., Pratt, P.F., and Harder, David R., 1984. Pressure-dependent membrane depolarization in cat middle cerebral artery. *Circulation research*, 55(2), pp.197–202.

Harmon, S.D., Kaduce, T.L., Manuel, T.D., and Spector, A.A., 2003. Effect of the delta6-desaturase inhibitor SC-26196 on PUFA metabolism in human cells. *Lipids*, 38(4), pp.469–76.

Harris, W.S., 1997. n-3 fatty acids and serum lipoproteins: human studies. *The American Journal of Clinical Nutrition*, 65(5), pp.1645S-1654S.

Harris, W.S., Connor, W.E., Alam, N., and Illingworth, D.R., 1988. Reduction of postprandial triglyceridemia in humans by dietary n-3 fatty acids. *Journal of lipid research*, 29(11), pp.1451–60.

Hartmannsgruber, V., Heyken, W.-T., Kacik, M., Kaistha, A., Grgic, I., Harteneck, C., Liedtke, W., Hoyer, J., and Köhler, R., 2007. Arterial Response to Shear Stress Critically Depends on Endothelial TRPV4 Expression. H. Mansvelder, ed. *PLoS ONE*, 2(9), p.e827.

Hata, A.N. and Breyer, R.M., 2004. Pharmacology and signaling of prostaglandin receptors: Multiple roles in inflammation and immune modulation. *Pharmacology*

& Therapeutics, 103(2), pp.147–166.

Hercule, H.C., Salanova, B., Essin, K., Honeck, H., Falck, J.R., Sausbier, M., Ruth, P., Schunck, W.-H., Luft, F.C., and Gollasch, M., 2007. The vasodilator 17,18-epoxyeicosatetraenoic acid targets the pore-forming BK alpha channel subunit in rodents. *Experimental physiology*, 92(6), pp.1067–76.

Hermann, M., Flammer, A., and Lscher, T.F., 2006. Nitric Oxide in Hypertension. *The Journal of Clinical Hypertension*, 8(2 Suppl 4), pp.17–29.

Herrmann, W.M., Kern, U., and Aigner, M., 1987. On the adverse reactions and efficacy of long-term treatment with flupirtine: preliminary results of an ongoing twelve-month study with 200 patients suffering from chronic pain states in arthrosis or arthritis. *Postgraduate medical journal*, 63 Suppl 3, pp.87–103.

Hilgers, R.H.P., Todd, J., and Webb, R.C., 2006. Regional heterogeneity in acetylcholine-induced relaxation in rat vascular bed: role of calcium-activated K + channels. *American Journal of Physiology-Heart and Circulatory Physiology*, 291(1), pp.H216–H222.

Hirafuji, M., Machida, T., Tsunoda, M., Miyamoto, A., and Minami, M., 2002. Docosahexaenoic acid potentiates interleukin-1β induction of nitric oxide synthase through mechanism involving p44/42 MAPK activation in rat vascular smooth muscle cells. *British Journal of Pharmacology*, 136(4), pp.613–619.

Hirai, A., Hamazaki, T., Terano, T., Nishikawa, T., Tamura, Y., Kamugai, A., and Jajiki, J., 1980. Eicosapentaenoic acid and platelet function in Japanese. *Lancet (London, England)*, 2(8204), pp.1132–3.

Hirata, M., Kohse, K.P., Chang, C.H., Ikebe, T., and Murad, F., 1990. Mechanism of cyclic GMP inhibition of inositol phosphate formation in rat aorta segments and cultured bovine aortic smooth muscle cells. *The Journal of biological chemistry*,

265(3), pp.1268–73.

Ho, W.S. V, Zheng, X., and Zhang, D.X., 2015. Role of endothelial TRPV4 channels in vascular actions of the endocannabinoid, 2-arachidonoylglycerol. *British Journal of Pharmacology*, 172(22), pp.5251–5264.

Holman, R.T. and Burr, G.O., 1948. Alkali conjugation of the unsaturated fatty acids. *Archives of biochemistry*, 19(3), pp.474–82.

Homberg, J.R., Wöhr, M., and Alenina, N., 2017. Comeback of the Rat in Biomedical Research. *ACS Chemical Neuroscience*, 8(5), pp.900–903.

Hong, K., Zhao, G., Hong, Z., Sun, Z., Yang, Y., Clifford, P.S., Davis, M.J., Meininger, G.A., and Hill, M.A., 2016. Mechanical activation of angiotensin II type 1 receptors causes actin remodelling and myogenic responsiveness in skeletal muscle arterioles. *The Journal of Physiology*, 594(23), pp.7027–7047.

Horman, S., Morel, N., Vertommen, D., Hussain, N., Neumann, D., Beauloye, C., El Najjar, N., Forcet, C., Viollet, B., Walsh, M.P., Hue, L., and Rider, M.H., 2008. AMP-activated protein kinase phosphorylates and desensitizes smooth muscle myosin light chain kinase. *The Journal of biological chemistry*, 283(27), pp.18505–12.

Hoshi, T., Tian, Y., Xu, R., Heinemann, S.H., and Hou, S., 2013. Mechanism of the modulation of BK potassium channel complexes with different auxiliary subunit compositions by the omega-3 fatty acid DHA. *Proceedings of the National Academy of Sciences*, 110(12), pp.4822–4827.

Hoshi, Toshinori, Wissuwa, B., Tian, Y., Tajima, N., Xu, R., Bauer, M., Heinemann, S.H., and Hou, S., 2013. Omega-3 fatty acids lower blood pressure by directly activating large-conductance Ca^{2+}-dependent K^{+} channels. *Proceedings of the National Academy of Sciences of the United States of America*, 110(12), pp.4816–

21.

Hoshi, Toshinori, Xu, R., Hou, S., Heinemann, S.H., and Tian, Y., 2013. A point mutation in the human Slo1 channel that impairs its sensitivity to omega-3 docosahexaenoic acid. *The Journal of General Physiology*, 142(5), pp.507–522.

Hrabie, J.A., Klose, J.R., Wink, D.A., and Keefer, L.K., 1993. New nitric oxide-releasing zwitterions derived from polyamines. *The Journal of Organic Chemistry*, 58(6), pp.1472–1476.

Huang, A., Sun, D., Carroll, M.A., Jiang, H., Smith, C.J., Connetta, J.A., Falck, J.R., Shesely, E.G., Koller, A., and Kaley, G., 2001. EDHF mediates flow-induced dilation in skeletal muscle arterioles of female eNOS-KO mice. *American Journal of Physiology-Heart and Circulatory Physiology*, 280(6), pp.H2462–H2469.

Huang, A., Sun, D., Smith, C.J., Connetta, J.A., Shesely, E.G., Koller, A., and Kaley, G., 2000. In eNOS knockout mice skeletal muscle arteriolar dilation to acetylcholine is mediated by EDHF. *American Journal of Physiology-Heart and Circulatory Physiology*, 278(3), pp.H762–H768.

Huang, P.L., Huang, Z., Mashimo, H., Bloch, K., D., Moskowitz, M.A., Bevan, J., A., and Fishman, M.C., 1995. Hypertension in mice lacking the gene for endothelial nitric oxide synthase. *Nature*, 377(6546), pp.239–242.

Hummel, T., Friedmann, T., Pauli, E., Niebch, G., Borbe, H.O., and Kobal, G., 1991. Dose-related analgesic effects of flupirtine. *British journal of clinical pharmacology*, 32(1), pp.69–76.

Ignarro, L.J., Buga, G.M., Wood, K.S., Byrns, R.E., and Chaudhuri, G., 1987. Endothelium-derived relaxing factor produced and released from artery and vein is nitric oxide. *Proceedings of the National Academy of Sciences of the United States of America*, 84(24), pp.9265–9.

Ignarro, L.J. and Napoli, C., 2005. Novel features of nitric oxide, endothelial nitric oxide synthase, and atherosclerosis. *Current diabetes reports*, 5(1), pp.17–23.

Im, E.J., Bais, A.J., Yang, W., Ma, Q., Guo, X., Sepe, S.M., and Junghans, R.P., 2014. Recombination–deletion between homologous cassettes in retrovirus is suppressed via a strategy of degenerate codon substitution. *Molecular Therapy - Methods & Clinical Development*, 1, p.14022.

Imhoff, B.R. and Hansen, J.M., 2009. Extracellular redox status regulates Nrf2 activation through mitochondrial reactive oxygen species. *Biochemical Journal*, 424(3), pp.491–500.

Imig, J.D., 2012. Epoxides and Soluble Epoxide Hydrolase in Cardiovascular Physiology. *Physiological Reviews*, 92(1), pp.101–130.

Imig, J.D., 2016. Epoxyeicosatrienoic Acids and 20-Hydroxyeicosatetraenoic Acid on Endothelial and Vascular Function. *Advances in pharmacology*, 77, pp.105–41.

Imig, J.D. and Hammock, B.D., 2009. Soluble epoxide hydrolase as a therapeutic target for cardiovascular diseases. *Nature Reviews Drug Discovery*, 8(10), pp.794–805.

Imig, J.D., Inscho, E.W., Deichmann, P.C., Reddy, K.M., and Falck, J.R., 1999. Afferent arteriolar vasodilation to the sulfonimide analog of 11, 12-epoxyeicosatrienoic acid involves protein kinase A. *Hypertension*, 33(1 Pt 2), pp.408–13.

Imig, J.D., Zhao, X., Capdevila, J.H., Morisseau, C., and Hammock, B.D., 2002. Soluble epoxide hydrolase inhibition lowers arterial blood pressure in angiotensin II hypertension. *Hypertension*, 39(2 Pt 2), pp.690–4.

Inagaki, N., Gonoi, T., Iv, J.P.C., Wang, C.-Z., Aguilar-Bryan, L., Bryan, J., and Seino, S., 1996. A Family of Sulfonylurea Receptors Determines the Pharmacological Properties of ATP-Sensitive K+ Channels. *Neuron*, 16(5), pp.1011–1017.

Inagaki, N., Tsuura, Y., Namba, N., Masuda, K., Gonoi, T., Horie, M., Seino, Y., Mizuta, M., and Seino, S., 1995. Cloning and functional characterization of a novel ATP-sensitive potassium channel ubiquitously expressed in rat tissues, including pancreatic islets, pituitary, skeletal muscle, and heart. *The Journal of biological chemistry*, 270(11), pp.5691–4.

Inoue, H., Nojima, H., and Okayama, H., 1990. High efficiency transformation of Escherichia coli with plasmids. *Gene*, 96(1), pp.23–28.

Isomoto, S., Kondo, C., Yamada, M., Matsumoto, S., Higashiguchi, O., Horio, Y., Matsuzawa, Y., and Kurachi, Y., 1996. A novel sulfonylurea receptor forms with BIR (Kir6.2) a smooth muscle type ATP-sensitive K+ channel. *The Journal of biological chemistry*, 271(40), pp.24321–4.

Jackson, K.G., Armah, C.K., Doman, I., James, L., Cheghani, F., and Minihane, A.M., 2009. The impact of age on the postprandial vascular response to a fish oil-enriched meal. *British Journal of Nutrition*, 102(10), p.1414.

Jager, H., Dreker, T., Buck, A., Giehl, K., Gress, T., and Grissmer, S., 2004. Blockage of Intermediate-Conductance Ca2+-Activated K+ Channels Inhibit Human Pancreatic Cancer Cell Growth in Vitro. *Molecular Pharmacology*, 65(3), pp.630–638.

Janigro, D., West, G.A., Gordon, E.L., and Winn, H.R., 1993. ATP-sensitive K+ channels in rat aorta and brain microvascular endothelial cells. *The American journal of physiology*, 265(3 Pt 1), pp.C812-21.

Jannaway, M., Torrens, C., Warner, J.A., and Sampson, A.P., 2018. Resolvin E1, resolvin D1 and resolvin D2 inhibit constriction of rat thoracic aorta and human pulmonary artery induced by the thromboxane mimetic U46619. *British Journal of Pharmacology*, 175(7), pp.1100–1108.

Jepps, T.A., Chadha, P.S., Davis, A.J., Harhun, M.I., Cockerill, G.W., Olesen, S.P., Hansen, R.S., and Greenwood, I.A., 2011. Downregulation of Kv7.4 Channel Activity in Primary and Secondary Hypertension. *Circulation*, 124(5), pp.602–611.

Joshi, S., Balan, P., and Gurney, A.M., 2006. Pulmonary vasoconstrictor action of KCNQ potassium channel blockers. *Respiratory Research*, 7(1), p.31.

Kacik, M., Oliván-Viguera, A., and Köhler, R., 2014. Modulation of KCa3.1 Channels by Eicosanoids, Omega-3 Fatty Acids, and Molecular Determinants. A. G. Obukhov, ed. *PLoS ONE*, 9(11), p.e112081.

Kagota, S., Tamashiro, A., Yamaguchi, Y., Nakamura, K., and Kunitomo, M., 1999. Excessive salt or cholesterol intake alters the balance among endothelium-derived factors released from renal arteries in spontaneously hypertensive rats. *Journal of cardiovascular pharmacology*, 34(4), pp.533–9.

Kampus, P., Serg, M., Kals, J., Zagura, M., Muda, P., Karu, K., Zilmer, M., and Eha, J., 2011. Differential Effects of Nebivolol and Metoprolol on Central Aortic Pressure and Left Ventricular Wall Thickness. *Hypertension*, 57(6), pp.1122–1128.

Kassab, S.E., Khedr, M.A., Ali, H.I., and Abdalla, M.M., 2017. Discovery of new indomethacin-based analogs with potentially selective cyclooxygenase-2 inhibition and observed diminishing to PGE2 activities. *European Journal of Medicinal Chemistry*, 141, pp.306–321.

Kauffenstein, G., Tamareille, S., Prunier, F., Roy, C., Ayer, A., Toutain, B., Billaud, M., Isakson, B.E., Grimaud, L., Loufrani, L., Rousseau, P., Abraham, P., Procaccio, V., Monyer, H., de Wit, C., Boeynaems, J.-M., Robaye, B., Kwak, B.R., and Henrion, D., 2016. Central Role of P2Y6 UDP Receptor in Arteriolar Myogenic Tone. *Arteriosclerosis, thrombosis, and vascular biology*, 36(8),

pp.1598–606.

De Keulenaer, G.W., Alexander, R.W., Ushio-Fukai, M., Ishizaka, N., and Griendling, K.K., 1998. Tumour necrosis factor alpha activates a p22phox-based NADH oxidase in vascular smooth muscle. *The Biochemical journal*, 329 (Pt 3, pp.653–7.

Kirber, M.T., Ordway, R.W., Clapp, L.H., Walsh, J. V., and Singer, J.J., 1992. Both membrane stretch and fatty acids directly activate large conductance Ca2+-activated K+ channels in vascular smooth muscle cells. *FEBS Letters*, 297(1–2), pp.24–28.

Kitamura, K. and Kuriyama, H., 1979. Effects of acetylcholine on the smooth muscle cell of isolated main coronary artery of the guinea-pig. *The Journal of physiology*, 293, pp.119–33.

Kitazawa, T., Takizawa, N., Ikebe, M., and Eto, M., 1999. Reconstitution of protein kinase C-induced contractile Ca2+ sensitization in triton X-100-demembranated rabbit arterial smooth muscle. *The Journal of physiology*, 520 Pt 1(Pt 1), pp.139–52.

Kobayashi, T., Tahara, Y., Matsumoto, M., Iguchi, M., Sano, H., Murayama, T., Arai, H., Oida, H., Yurugi-Kobayashi, T., Yamashita, J.K., Katagiri, H., Majima, M., Yokode, M., Kita, T., and Narumiya, S., 2004. Roles of thromboxane A2 and prostacyclin in the development of atherosclerosis in apoE-deficient mice. *Journal of Clinical Investigation*, 114(6), pp.784–794.

Kohler, R., Wulff, H., Eichler, I., Kneifel, M., Neumann, D., Knorr, A., Grgic, I., Kämpfe, D., Si, H., Wibawa, J., Real, R., Borner, K., Brakemeier, S., Orzechowski, H.-D., Reusch, H.-P., Paul, M., Chandy, K.G., and Hoyer, J., 2003. Blockade of the Intermediate-Conductance Calcium-Activated Potassium Channel as a New Therapeutic Strategy for Restenosis. *Circulation*, 108(9), pp.1119–1125.

Komalavilas, P. and Lincoln, T.M., 1994. Phosphorylation of the inositol 1,4,5-trisphosphate receptor by cyclic GMP-dependent protein kinase. *The Journal of biological chemistry*, 269(12), pp.8701–7.

Komalavilas, P. and Lincoln, T.M., 1996. Phosphorylation of the inositol 1,4,5-trisphosphate receptor. Cyclic GMP-dependent protein kinase mediates cAMP and cGMP dependent phosphorylation in the intact rat aorta. *The Journal of biological chemistry*, 271(36), pp.21933–8.

Kovalev, H., Quayle, J.M., Kamishima, T., and Lodwick, D., 2004. Molecular analysis of the subtype-selective inhibition of cloned KATP channels by PNU-37883A. *British journal of pharmacology*, 141(5), pp.867–73.

Krummen, S., Falck, J.R., and Thorin, E., 2005. Two distinct pathways account for EDHF-dependent dilatation in the gracilis artery of dyslipidaemic hApoB+/+ mice. *British journal of pharmacology*, 145(2), pp.264–70.

Kuhlencordt, P.J., Gyurko, R., Han, F., Scherrer-Crosbie, M., Aretz, T.H., Hajjar, R., Picard, M.H., and Huang, P.L., 2001. Accelerated atherosclerosis, aortic aneurysm formation, and ischemic heart disease in apolipoprotein E/endothelial nitric oxide synthase double-knockout mice. *Circulation*, 104(4), pp.448–54.

Kuriyama, H. and Suzuki, H., 1978. The effects of acetylcholine on the membrane and contractile properties of smooth muscle cells of the rabbit superior mesenteric artery. *British journal of pharmacology*, 64(4), pp.493–501.

Kuzkaya, N., Weissmann, N., Harrison, D.G., and Dikalov, S., 2003. Interactions of Peroxynitrite, Tetrahydrobiopterin, Ascorbic Acid, and Thiols. *Journal of Biological Chemistry*, 278(25), pp.22546–22554.

Lai, L., Wang, R., Jiang, W., Yang, X., Song, J., Li, X., and Tao, G., 2009. Effects of docosahexaenoic acid on large-conductance Ca2+-activated K+ channels and

voltage-dependent K+ channels in rat coronary artery smooth muscle cells. *Acta Pharmacologica Sinica*, 30(3), pp.314–320.

Lakshmikanthan, S., Zieba, B.J., Ge, Z.-D., Momotani, K., Zheng, X., Lund, H., Artamonov, M. V., Maas, J.E., Szabo, A., Zhang, D.X., Auchampach, J.A., Mattson, D.L., Somlyo, A. V., and Chrzanowska-Wodnicka, M., 2014. Rap1b in Smooth Muscle and Endothelium Is Required for Maintenance of Vascular Tone and Normal Blood Pressure. *Arteriosclerosis, Thrombosis, and Vascular Biology*, 34(7), pp.1486–1494.

Lang, N.N., Luksha, L., Newby, D.E., and Kublickiene, K., 2007. Connexin 43 mediates endothelium-derived hyperpolarizing factor-induced vasodilatation in subcutaneous resistance arteries from healthy pregnant women. *American Journal of Physiology-Heart and Circulatory Physiology*, 292(2), pp.H1026–H1032.

Lange, A., Gebremedhin, D., Narayanan, J., and Harder, D., 1997. 20-Hydroxyeicosatetraenoic acid-induced vasoconstriction and inhibition of potassium current in cerebral vascular smooth muscle is dependent on activation of protein kinase C. *The Journal of biological chemistry*, 272(43), pp.27345–52.

Laurent, S., Cockcroft, J., Van Bortel, L., Boutouyrie, P., Giannattasio, C., Hayoz, D., Pannier, B., Vlachopoulos, C., Wilkinson, I., and Struijker-Boudier, H., 2007. Abridged version of the expert consensus document on arterial stiffness. *Artery Research*, 1(1), pp.2–12.

Laursen, J.B., Somers, M., Kurz, S., McCann, L., Warnholtz, A., Freeman, B.A., Tarpey, M., Fukai, T., and Harrison, D.G., 2001. Endothelial regulation of vasomotion in apoE-deficient mice: implications for interactions between peroxynitrite and tetrahydrobiopterin. *Circulation*, 103(9), pp.1282–8.

Lazaar, A.L., Yang, L., Boardley, R.L., Goyal, N.S., Robertson, J., Baldwin, S.J.,

Newby, D.E., Wilkinson, I.B., Tal-Singer, R., Mayer, R.J., and Cheriyan, J., 2016. Pharmacokinetics, pharmacodynamics and adverse event profile of GSK2256294, a novel soluble epoxide hydrolase inhibitor. *British journal of clinical pharmacology*, 81(5), pp.971–9.

Lee, C.R., North, K.E., Bray, M.S., Couper, D.J., Heiss, G., and Zeldin, D.C., 2007. CYP2J2 and CYP2C8 polymorphisms and coronary heart disease risk: the Atherosclerosis Risk in Communities (ARIC) study. *Pharmacogenetics and Genomics*, 17(5), pp.349–358.

Lee, M.R., Li, L., and Kitazawa, T., 1997. Cyclic GMP causes Ca2+ desensitization in vascular smooth muscle by activating the myosin light chain phosphatase. *The Journal of biological chemistry*, 272(8), pp.5063–8.

Lee, S., Yang, Y., Tanner, M.A., Li, M., and Hill, M.A., 2015. Heterogeneity in Kv7 channel function in the cerebral and coronary circulation. *Microcirculation (New York, N.Y. : 1994)*, 22(2), pp.109–121.

Lee, S.A., Kim, H.J., Chang, K.C., Baek, J.C., Park, J.K., Shin, J.K., Choi, W.J., Lee, J.H., and Paik, W.Y., 2009. DHA and EPA Down-regulate COX-2 Expression through Suppression of NF-kappaB Activity in LPS-treated Human Umbilical Vein Endothelial Cells. *The Korean journal of physiology & pharmacology : official journal of the Korean Physiological Society and the Korean Society of Pharmacology*, 13(4), pp.301–7.

Lee, U.S. and Cui, J., 2010. BK channel activation: structural and functional insights. *Trends in neurosciences*, 33(9), pp.415–23.

Lerche, C., Bruhova, I., Lerche, H., Steinmeyer, K., Wei, A.D., Strutz-Seebohm, N., Lang, F., Busch, A.E., Zhorov, B.S., and Seebohm, G., 2007. Chromanol 293B Binding in KCNQ1 (Kv7.1) Channels Involves Electrostatic Interactions with a

Potassium Ion in the Selectivity Filter. *Molecular Pharmacology*, 71(6), pp.1503–1511.

Lesniewski, L.A., Connell, M.L., Durrant, J.R., Folian, B.J., Anderson, M.C., Donato, A.J., and Seals, D.R., 2009. B6D2F1 Mice Are a Suitable Model of Oxidative Stress-Mediated Impaired Endothelium-Dependent Dilation With Aging. *The Journals of Gerontology Series A: Biological Sciences and Medical Sciences*, 64A(1), pp.9–20.

Li, L., Eto, M., Lee, M.R., Morita, F., Yazawa, M., and Kitazawa, T., 1998. Possible involvement of the novel CPI-17 protein in protein kinase C signal transduction of rabbit arterial smooth muscle. *The Journal of physiology*, 508 (Pt 3, pp.871–81.

Li, P.-L., Zhang, D.X., Ge, Z.-D., and Campbell, W.B., 2002. Role of ADP-ribose in 11,12-EET-induced activation of K Ca channels in coronary arterial smooth muscle cells. *American Journal of Physiology-Heart and Circulatory Physiology*, 282(4), pp.H1229–H1236.

Li, X., Hong, S., Li, P.-L., and Zhang, Y., 2011. Docosahexanoic acid-induced coronary arterial dilation: actions of 17S-hydroxy docosahexanoic acid on K+ channel activity. *The Journal of pharmacology and experimental therapeutics*, 336(3), pp.891–9.

Liang, G.H., Adebiyi, A., Leo, M.D., McNally, E.M., Leffler, C.W., and Jaggar, J.H., 2011. Hydrogen sulfide dilates cerebral arterioles by activating smooth muscle cell plasma membrane K ATP channels. *American Journal of Physiology-Heart and Circulatory Physiology*, 300(6), pp.H2088–H2095.

Liao, J.C. and Kuo, L., 1997. Interaction between adenosine and flow-induced dilation in coronary microvascular network. *American Journal of Physiology-Heart and Circulatory Physiology*, 272(4), pp.H1571–H1581.

Libby, P., Ridker, P.M., and Maseri, A., 2002. Inflammation and atherosclerosis. *Circulation*, 105(9), pp.1135–43.

Liin, S.I., Karlsson, U., Bentzen, B.H., Schmitt, N., and Elinder, F., 2016. Polyunsaturated fatty acids are potent openers of human M-channels expressed in Xenopus laevis oocytes. *Acta Physiologica*, 218(1), pp.7–9.

Liin, S.I., Schmitt, N., Larsson, J., Starck Härlin, F., Bentzen, B.H., Larsson, H.P., and Elinder, F., 2014. KCNE1 Modulates the Sensitivity of Kv7.1 to Polyunsaturated Fatty Acids. *Biophysical Journal*, 106(2), p.143a.

Liin, S.I., Silverå Ejneby, M., Barro-Soria, R., Skarsfeldt, M.A., Larsson, J.E., Starck Härlin, F., Parkkari, T., Bentzen, B.H., Schmitt, N., Larsson, H.P., and Elinder, F., 2015. Polyunsaturated fatty acid analogs act antiarrhythmically on the cardiac IKs channel. *Proceedings of the National Academy of Sciences of the United States of America*, 112(18), pp.5714–9.

Limbu, R., Cottrell, G.S., and McNeish, A.J., 2018. Characterisation of the vasodilation effects of DHA and EPA, n-3 PUFAs (fish oils), in rat aorta and mesenteric resistance arteries. *Plos One*, 13(2), p.e0192484.

Lin, M.T., Jian, M.-Y., Taylor, M.S., Cioffi, D.L., Yap, F.C., Liedtke, W., and Townsley, M.I., 2015. Functional coupling of TRPV4, IK, and SK channels contributes to Ca(2+)-dependent endothelial injury in rodent lung. *Pulmonary circulation*, 5(2), pp.279–90.

Lischke, V., Busse, R., and Hecker, M., 1995. Selective inhibition by barbiturates of the synthesis of endothelium-derived hyperpolarizing factor in the rabbit carotid artery. *British journal of pharmacology*, 115(6), pp.969–74.

Liu, Y. and Gutterman, D.D., 2002. The coronary circulation in diabetes:: Influence of reactive oxygen species on K+ channel-mediated vasodilation. *Vascular*

Pharmacology, 38(1), pp.43–49.

Liu, Y., Hudetz, A.G., Knaus, H.G., and Rusch, N.J., 1998. Increased expression of Ca2+-sensitive K+ channels in the cerebral microcirculation of genetically hypertensive rats: evidence for their protection against cerebral vasospasm. *Circulation research*, 82(6), pp.729–37.

Liu, Y., Sellke, E.W., Feng, J., Clements, R.T., Sodha, N.R., Khabbaz, K.R., Senthilnathan, V., Alper, S.L., and Sellke, F.W., 2008. Calcium-activated potassium channels contribute to human skeletal muscle microvascular endothelial dysfunction related to cardiopulmonary bypass. *Surgery*, 144(2), pp.239–244.

London, G.M., 1997. Large arteries haemodynamics: conduit versus cushioning function. *Blood pressure. Supplement*, 2, pp.48–51.

López, D., Orta, X., Casós, K., Sáiz, M.P., Puig-Parellada, P., Farriol, M., and Mitjavila, M.T., 2004. Upregulation of endothelial nitric oxide synthase in rat aorta after ingestion of fish oil-rich diet. *American Journal of Physiology-Heart and Circulatory Physiology*, 287(2), pp.H567–H572.

Lu, T., Hong, M.-P., and Lee, H.-C., 2005. Molecular determinants of cardiac K(ATP) channel activation by epoxyeicosatrienoic acids. *The Journal of biological chemistry*, 280(19), pp.19097–104.

Lu, T., Hoshi, T., Weintraub, N.L., Spector, A.A., and Lee, H.C., 2001. Activation of ATP-sensitive K(+) channels by epoxyeicosatrienoic acids in rat cardiac ventricular myocytes. *The Journal of physiology*, 537(Pt 3), pp.811–27.

Lu, T., Katakam, P. V, VanRollins, M., Weintraub, N.L., Spector, A.A., and Lee, H.C., 2001. Dihydroxyeicosatrienoic acids are potent activators of Ca(2+)-activated K(+) channels in isolated rat coronary arterial myocytes. *The Journal of physiology*, 534(Pt 3), pp.651–67.

Lu, T., VanRollins, M., and Lee, H.-C., 2002. Stereospecific activation of cardiac ATP-sensitive K(+) channels by epoxyeicosatrienoic acids: a structural determinant study. *Molecular pharmacology*, 62(5), pp.1076–83.

Lu, T., Ye, D., Wang, X., Seubert, J.M., Graves, J.P., Bradbury, J.A., Zeldin, D.C., and Lee, H.-C., 2006. Cardiac and vascular K ATP channels in rats are activated by endogenous epoxyeicosatrienoic acids through different mechanisms. *The Journal of Physiology*, 575(2), pp.627–644.

Lynch, F.M., Withers, S.B., Yao, Z., Werner, M.E., Edwards, G., Weston, A.H., and Heagerty, A.M., 2013. Perivascular adipose tissue-derived adiponectin activates BK_{Ca} channels to induce anticontractile responses. *American Journal of Physiology-Heart and Circulatory Physiology*, 304(6), pp.H786–H795.

Ma, X., Du, J., Zhang, P., Deng, J., Liu, J., Lam, F.F.-Y., Li, R.A., Huang, Y., Jin, J., and Yao, X., 2013. Functional Role of TRPV4-KCa2.3 Signaling in Vascular Endothelial Cells in Normal and Streptozotocin-Induced Diabetic Rats. *Hypertension*, 62(1), pp.134–139.

Ma, Y., Zhang, P., Li, J., Lu, J., Ge, J., Zhao, Z., Ma, X., Wan, S., Yao, X., and Shen, B., 2015. Epoxyeicosatrienoic acids act through TRPV4–TRPC1–KCa1.1 complex to induce smooth muscle membrane hyperpolarization and relaxation in human internal mammary arteries. *Biochimica et Biophysica Acta (BBA) - Molecular Basis of Disease*, 1852(3), pp.552–559.

Madhur, M.S., Lob, H.E., McCann, L.A., Iwakura, Y., Blinder, Y., Guzik, T.J., and Harrison, D.G., 2010. Interleukin 17 Promotes Angiotensin II–Induced Hypertension and Vascular Dysfunction. *Hypertension*, 55(2), pp.500–507.

Majed, B.H. and Khalil, R.A., 2012. Molecular mechanisms regulating the vascular prostacyclin pathways and their adaptation during pregnancy and in the newborn.

Pharmacological reviews, 64(3), pp.540–82.

Malerba, M., D Amato, M., Radaeli, A., Giacovelli, G., Rovati, L., Arshad, S.H., and Holgate, S.T., 2015. Efficacy of Andolast in Mild to Moderate Asthma: A Randomized, Controlled, Double-Blind Multicenter Study (The Andast Trial). *Current pharmaceutical design*, 21(26), pp.3835–43.

Mani, B.K., Robakowski, C., Brueggemann, L.I., Cribbs, L.L., Tripathi, A., Majetschak, M., and Byron, K.L., 2016. Kv7.5 Potassium Channel Subunits Are the Primary Targets for PKA-Dependent Enhancement of Vascular Smooth Muscle Kv7 Currents. *Molecular Pharmacology*, 89(3), pp.323–334.

Manikandan, P. and Nagini, S., 2018. Cytochrome P450 Structure, Function and Clinical Significance: A Review. *Current Drug Targets*, 19(1), pp.38–54.

Marchais, S.J., Guerin, A.P., Pannier, B., Delavaud, G., and London, G.M., 1993. Arterial Compliance and Blood Pressure. *Drugs*, 46(Supplement 2), pp.82–87.

Marchenko, S.M. and Sage, S.O., 1996. Calcium-activated potassium channels in the endothelium of intact rat aorta. *The Journal of Physiology*, 492(1), pp.53–60.

Marieb, E.N., 2014. *ESSENTIALS of Human Anatomy & Physiology*. 11th ed. Pearson.

Marijic, J., Li, Q., Song, M., Nishimaru, K., Stefani, E., and Toro, L., 2001. Decreased Expression of Voltage- and Ca 2+ -Activated K + Channels in Coronary Smooth Muscle During Aging. *Circulation Research*, 88(2), pp.210–216.

Marji, J.S., Wang, M.-H., and Laniado-Schwartzman, M., 2002. Cytochrome P -450 4A isoform expression and 20-HETE synthesis in renal preglomerular arteries. *American Journal of Physiology-Renal Physiology*, 283(1), pp.F60–F67.

Marlettaz, M.A., 1993. Nitric Oxide Synthase Structure and Mechanism. *The Journal of biological chemistry*, 268(17), pp.12231–12234.

Martín, P., Moncada, M., Enrique, N., Asuaje, A., Valdez Capuccino, J.M., Gonzalez,

C., and Milesi, V., 2014. Arachidonic acid activation of BKCa (Slo1) channels associated to the β1-subunit in human vascular smooth muscle cells. *Pflügers Archiv - European Journal of Physiology*, 466(9), pp.1779–1792.

Matchkov, V. V., Rahman, A., Bakker, L.M., Griffith, T.M., Nilsson, H., and Aalkjær, C., 2006. Analysis of effects of connexin-mimetic peptides in rat mesenteric small arteries. *American Journal of Physiology-Heart and Circulatory Physiology*, 291(1), pp.H357–H367.

Matsumoto, T., Kobayashi, T., Wakabayashi, K., and Kamata, K., 2005. Cilostazol improves endothelium-derived hyperpolarizing factor-type relaxation in mesenteric arteries from diabetic rats. *American Journal of Physiology-Heart and Circulatory Physiology*, 289(5), pp.H1933–H1940.

Matta, J.A., Miyares, R.L., and Ahern, G.P., 2007. TRPV1 is a novel target for omega-3 polyunsaturated fatty acids. *The Journal of physiology*, 578(Pt 2), pp.397–411.

McCobb, D.P., Fowler, N.L., Featherstone, T., Lingle, C.J., Saito, M., Krause, J.E., and Salkoff, L., 1995. A human calcium-activated potassium channel gene expressed in vascular smooth muscle. *American Journal of Physiology-Heart and Circulatory Physiology*, 269(3), pp.H767–H777.

McEniery, C.M., Cockcroft, J.R., Roman, M.J., Franklin, S.S., and Wilkinson, I.B., 2014. Central blood pressure: current evidence and clinical importance. *European Heart Journal*, 35(26), pp.1719–1725.

McEniery, C.M., McDonnell, B.J., So, A., Aitken, S., Bolton, C.E., Munnery, M., Hickson, S.S., Yasmin, Maki-Petaja, K.M., Cockcroft, J.R., Dixon, A.K., Wilkinson, I.B., and Anglo-Cardiff Collaboration Trial Investigators, 2009. Aortic Calcification Is Associated With Aortic Stiffness and Isolated Systolic Hypertension in Healthy Individuals. *Hypertension*, 53(3), pp.524–531.

McEniery, C.M., Schmitt, M., Qasem, A., Webb, D.J., Avolio, A.P., Wilkinson, I.B., and Cockcroft, J.R., 2004. Nebivolol Increases Arterial Distensibility In Vivo. *Hypertension*, 44(3), pp.305–310.

McManus, O.B., 1991. Calcium-activated potassium channels: regulation by calcium. *Journal of bioenergetics and biomembranes*, 23(4), pp.537–60.

McNeish, A.J. and Garland, C.J., 2007. Thromboxane A2 inhibition of SKCa after NO synthase block in rat middle cerebral artery. *British Journal of Pharmacology*, 151(4), pp.441–449.

McNeish, A.J., Jimenez-Altayo, F., Cottrell, G.S., and Garland, C.J., 2012. Statins and Selective Inhibition of Rho Kinase Protect Small Conductance Calcium-Activated Potassium Channel Function (KCa2.3) in Cerebral Arteries. Y. Huang, ed. *PLoS ONE*, 7(10), p.e46735.

McPherson, G.A., 1992. Assessing vascular reactivity of arteries in the small vessel myograph. *Clinical and experimental pharmacology & physiology*, 19(12), pp.815–25.

Mederos y Schnitzler, M., Derst, C., Daut, J., and Preisig-Müller, R., 2000. ATP-sensitive potassium channels in capillaries isolated from guinea-pig heart. *The Journal of physiology*, 525 Pt 2(Pt 2), pp.307–17.

Mendoza, S.A., Fang, J., Gutterman, D.D., Wilcox, D.A., Bubolz, A.H., Li, R., Suzuki, M., and Zhang, D.X., 2010. TRPV4-mediated endothelial Ca 2+ influx and vasodilation in response to shear stress. *American Journal of Physiology-Heart and Circulatory Physiology*, 298(2), pp.H466–H476.

Merten, O.-W., Hebben, M., and Bovolenta, C., 2016. Production of lentiviral vectors. *Molecular therapy. Methods & clinical development*, 3, p.16017.

Mies, F., Shlyonsky, V., Goolaerts, A., and Sariban-Sohraby, S., 2004. Modulation of

epithelial Na $^{+}$ channel activity by long-chain n–3 fatty acids. *American Journal of Physiology-Renal Physiology*, 287(4), pp.F850–F855.

Miki, T., Suzuki, M., Shibasaki, T., Uemura, H., Sato, T., Yamaguchi, K., Koseki, H., Iwanaga, T., Nakaya, H., and Seino, S., 2002. Mouse model of Prinzmetal angina by disruption of the inward rectifier Kir6.1. *Nature Medicine*, 8(5), pp.466–472.

Miller, P.E., Van Elswyk, M., and Alexander, D.D., 2014. Long-chain omega-3 fatty acids eicosapentaenoic acid and docosahexaenoic acid and blood pressure: a meta-analysis of randomized controlled trials. *American journal of hypertension*, 27(7), pp.885–96.

Mistry, D.K. and Garland, C.J., 1998. Nitric oxide (NO)-induced activation of large conductance Ca2+-dependent K+ channels (BK(Ca)) in smooth muscle cells isolated from the rat mesenteric artery. *British journal of pharmacology*, 124(6), pp.1131–40.

Mitchell, J.A., Ahmetaj-Shala, B., Kirkby, N.S., Wright, W.R., Mackenzie, L.S., Reed, D.M., and Mohamed, N., 2014. Role of prostacyclin in pulmonary hypertension. *Global cardiology science & practice*, 2014(4), pp.382–93.

Miyoshi, Y., Nakaya, Y., Wakatsuki, T., Nakaya, S., Fujino, K., Saito, K., and Inoue, I., 1992. Endothelin blocks ATP-sensitive K+ channels and depolarizes smooth muscle cells of porcine coronary artery. *Circulation research*, 70(3), pp.612–6.

Moers, A., Wettschureck, N., Grüner, S., Nieswandt, B., and Offermanns, S., 2004. Unresponsiveness of platelets lacking both Galpha(q) and Galpha(13). Implications for collagen-induced platelet activation. *The Journal of biological chemistry*, 279(44), pp.45354–9.

Mollnau, H., Wendt, M., Szöcs, K., Lassègue, B., Schulz, E., Oelze, M., Li, H., Bodenschatz, M., August, M., Kleschyov, A.L., Tsilimingas, N., Walter, U.,

Förstermann, U., Meinertz, T., Griendling, K., and Münzel, T., 2002. Effects of angiotensin II infusion on the expression and function of NAD(P)H oxidase and components of nitric oxide/cGMP signaling. *Circulation research*, 90(4), pp.E58-65.

Moncada, S., Palmer, R.M., and Higgs, E.A., 1991. Nitric oxide: physiology, pathophysiology, and pharmacology. *Pharmacological reviews*, 43(2), pp.109–42.

Morales-Cano, D., Moreno, L., Barreira, B., Pandolfi, R., Chamorro, V., Jimenez, R., Villamor, E., Duarte, J., Perez-Vizcaino, F., and Cogolludo, A., 2015. Kv7 channels critically determine coronary artery reactivity: left-right differences and down-regulation by hyperglycaemia. *Cardiovascular Research*, 106(1), pp.98–108.

Morecroft, I., Murray, A., Nilsen, M., Gurney, A.M., and MacLean, M.R., 2009. Treatment with the Kv7 potassium channel activator flupirtine is beneficial in two independent mouse models of pulmonary hypertension. *British journal of pharmacology*, 157(7), pp.1241–9.

Moreno, C., de la Cruz, A., Oliveras, A., Kharche, S.R., Guizy, M., Comes, N., Starý, T., Ronchi, C., Rocchetti, M., Baró, I., Loussouarn, G., Zaza, A., Severi, S., Felipe, A., and Valenzuela, C., 2015. Marine n-3 PUFAs modulate IKs gating, channel expression, and location in membrane microdomains. *Cardiovascular Research*, 105(2), pp.223–232.

Mori, T.A., 2014. Omega-3 fatty acids and cardiovascular disease: epidemiology and effects on cardiometabolic risk factors. *Food & function*, 5(9), pp.2004–19.

Morris, M.C., Sacks, F., and Rosner, B., 1993. Does fish oil lower blood pressure? A meta-analysis of controlled trials. *Circulation*, 88(2), pp.523–33.

Morrissey, A., Rosner, E., Lanning, J., Parachuru, L., Dhar Chowdhury, P., Han, S.,

Lopez, G., Tong, X., Yoshida, H., Nakamura, T.Y., Artman, M., Giblin, J.P., Tinker, A., and Coetzee, W.A., 2005. Immunolocalization of K ATP channel subunits in mouse and rat cardiac myocytes and the coronary vasculature. *BMC Physiology*, 5(1), p.1.

Motter, A.L. and Ahern, G.P., 2012. TRPA1 is a polyunsaturated fatty acid sensor in mammals. *PloS one*, 7(6), p.e38439.

Mozaffarian, D. and Wu, J.H.Y., 2011. Omega-3 Fatty Acids and Cardiovascular Disease. *Journal of the American College of Cardiology*, 58(20), pp.2047–2067.

Mulvany, M.J. and Halpern, W., 1976. Mechanical properties of vascular smooth muscle cells in situ. *Nature*, 260(5552), pp.617–619.

Mulvany, M.J. and Halpern, W., 1977. Contractile properties of small arterial resistance vessels in spontaneously hypertensive and normotensive rats. *Circulation research*, 41(1), pp.19–26.

Murphy, M.E. and Brayden, J.E., 1995. Nitric oxide hyperpolarizes rabbit mesenteric arteries via ATP-sensitive potassium channels. *The Journal of physiology*, 486 (Pt 1(Pt 1), pp.47–58.

Musicki, B., Liu, T., Strong, T., Jin, L., Laughlin, M.H., Turk, J.R., and Burnett, A.L., 2008. Low-fat diet and exercise preserve eNOS regulation and endothelial function in the penis of early atherosclerotic pigs: a molecular analysis. *The journal of sexual medicine*, 5(3), pp.552–61.

Muthalif, M.M., Benter, I.F., Karzoun, N., Fatima, S., Harper, J., Uddin, M.R., and Malik, K.U., 1998. 20-Hydroxyeicosatetraenoic acid mediates calcium/calmodulin-dependent protein kinase II-induced mitogen-activated protein kinase activation in vascular smooth muscle cells. *Proceedings of the National Academy of Sciences of the United States of America*, 95(21), pp.12701–6.

Nagaraj, C., Tang, B., Nagy, B.M., Papp, R., Jain, P.P., Marsh, L.M., Meredith, A.L., Ghanim, B., Klepetko, W., Kwapiszewska, G., Weir, E.K., Olschewski, H., and Olschewski, A., 2016. Docosahexaenoic acid causes rapid pulmonary arterial relaxation via KCa channel-mediated hyperpolarisation in pulmonary hypertension. *The European respiratory journal*, 48(4), pp.1127–1136.

Naraba, H., Murakami, M., Matsumoto, H., Shimbara, S., Ueno, A., Kudo, I., and Oh-ishi, S., 1998. Segregated coupling of phospholipases A2, cyclooxygenases, and terminal prostanoid synthases in different phases of prostanoid biosynthesis in rat peritoneal macrophages. *Journal of immunology (Baltimore, Md. : 1950)*, 160(6), pp.2974–82.

Nardi, A. and Olesen, S.-P., 2008. BK channel modulators: a comprehensive overview. *Current medicinal chemistry*, 15(11), pp.1126–46.

Nebert, D.W., Wikvall, K., and Miller, W.L., 2013. Human cytochromes P450 in health and disease. *Philosophical transactions of the Royal Society of London. Series B, Biological sciences*, 368(1612), p.20120431.

New England Biolabs, 2019. *PCR Using Q5® Hot Start High-Fidelity DNA Polymerase (M0493)* [Online]. Available from: https://international.neb.com/protocols/2012/08/30/pcr-using-q5-hot-start-high-fidelity-dna-polymerase-m0493 [Accessed 18 February 2019].

New England BioLabs, 2018. *NEBcutter V2.0* [Online]. Available from: http://nc2.neb.com/NEBcutter2/ [Accessed 1 February 2018].

Newens, K.J., Thompson, A.K., Jackson, K.G., Wright, J., and Williams, C.M., 2011. DHA-rich fish oil reverses the detrimental effects of saturated fatty acids on postprandial vascular reactivity. *American Journal of Clinical Nutrition*, 94(3), pp.742–748.

Neylon, C.B., Lang, R.J., Fu, Y., Bobik, A., and Reinhart, P.H., 1999. Molecular cloning and characterization of the intermediate-conductance Ca(2+)-activated K(+) channel in vascular smooth muscle: relationship between K(Ca) channel diversity and smooth muscle cell function. *Circulation research*, 85(9), pp.e33-43.

Ng, F.L., Davis, A.J., Jepps, T.A., Harhun, M.I., Yeung, S.Y., Wan, A., Reddy, M., Melville, D., Nardi, A., Khong, T.K., and Greenwood, I.A., 2011. Expression and function of the K+ channel KCNQ genes in human arteries. *British journal of pharmacology*, 162(1), pp.42–53.

NICE, 2019a. *Antihypertensive drugs* [Online]. Available from: https://bnf.nice.org.uk/treatment-summary/antihypertensive-drugs.html [Accessed 26 August 2018].

NICE, 2019b. *EPOPROSTENOL* [Online]. NICE. Available from: https://bnf.nice.org.uk/drug/epoprostenol.html [Accessed 26 June 2018].

NICE, 2019c. *ILOPROST* [Online]. NICE. Available from: https://bnf.nice.org.uk/drug/iloprost.html [Accessed 26 June 2018].

NICE, 2019d. *MINOXIDIL* [Online]. NICE. Available from: https://bnf.nice.org.uk/drug/minoxidil.html#indicationsAndDoses [Accessed 26 June 2018].

NICE, 2019e. *NICORANDIL* [Online]. NICE. Available from: https://bnf.nice.org.uk/drug/nicorandil.html [Accessed 26 August 2018].

NICE, 2019f. *SODIUM NITROPRUSSIDE* [Online]. Available from: https://bnf.nice.org.uk/drug/sodium-nitroprusside.html [Accessed 26 June 2018].

Nichols, C.G., Singh, G.K., and Grange, D.K., 2013. KATP channels and cardiovascular disease: suddenly a syndrome. *Circulation research*, 112(7), pp.1059–72.

Nicholson, W.T., Vaa, B., Hesse, C., Eisenach, J.H., and Joyner, M.J., 2009. Aging Is Associated With Reduced Prostacyclin-Mediated Dilation in the Human Forearm. *Hypertension*, 53(6), pp.973–978.

Nieves-Cintrón, M., Syed, A.U., Buonarati, O.R., Rigor, R.R., Nystoriak, M.A., Ghosh, D., Sasse, K.C., Ward, S.M., Santana, L.F., Hell, J.W., and Navedo, M.F., 2017. Impaired BKCa channel function in native vascular smooth muscle from humans with type 2 diabetes. *Scientific reports*, 7(1), p.14058.

Nishimaru, K., Eghbali, M., Lu, R., Marijic, J., Stefani, E., and Toro, L., 2004. Functional and molecular evidence of MaxiK channel β1 subunit decrease with coronary artery ageing in the rat. *The Journal of Physiology*, 559(3), pp.849–862.

Nishimaru, K., Eghbali, M., Stefani, E., and Toro, L., 2004. Function and clustered expression of MaxiK channels in cerebral myocytes remain intact with aging. *Experimental Gerontology*, 39(5), pp.831–839.

Niwano, K., Arai, M., Tomaru, K., Uchiyama, T., Ohyama, Y., and Kurabayashi, M., 2003. Transcriptional Stimulation of the eNOS Gene by the Stable Prostacyclin Analogue Beraprost Is Mediated Through cAMP-Responsive Element in Vascular Endothelial Cells: Close Link Between PGI2 Signal and NO Pathways. *Circulation Research*, 93(6), pp.523–530.

Node, K., Huo, Y., Ruan, X., Yang, B., Spiecker, M., Ley, K., Zeldin, D.C., and Liao, J.K., 1999. Anti-inflammatory properties of cytochrome P450 epoxygenase-derived eicosanoids. *Science (New York, N.Y.)*, 285(5431), pp.1276–9.

Noma, A., 1983. ATP-regulated K+ channels in cardiac muscle. *Nature*, 305(5930), pp.147–8.

Nunn, L.C. and Smedley-Maclean, I., 1938. The nature of the fatty acids stored by the liver in the fat-deficiency disease of rats. *The Biochemical journal*, 32(12),

pp.2178–84.

Nyby, M., Matsumoto, K., Yamamoto, K., Abedi, K., Eslami, P., Hernandez, G., Smutko, V., Berger, M., and Tuck, M., 2005. Dietary fish oil prevents vascular dysfunction and oxidative stress in hyperinsulinemic rats. *American Journal of Hypertension*, 18(2), pp.213–219.

O'Gorman, S., Fox, D., and Wahl, G., 1991. Recombinase-mediated gene activation and site-specific integration in mammalian cells. *Science*, 251(4999), pp.1351–1355.

Oltman, C.L., Weintraub, N.L., VanRollins, M., and Dellsperger, K.C., 1998. Epoxyeicosatrienoic acids and dihydroxyeicosatrienoic acids are potent vasodilators in the canine coronary microcirculation. *Circulation research*, 83(9), pp.932–9.

Omura, M., Kobayashi, S., Mizukami, Y., Mogami, K., Todoroki-Ikeda, N., Miyake, T., and Matsuzaki, M., 2001. Eicosapentaenoic acid (EPA) induces Ca(2+)-independent activation and translocation of endothelial nitric oxide synthase and endothelium-dependent vasorelaxation. *FEBS letters*, 487(3), pp.361–6.

Orstavik, S., Natarajan, V., Taskén, K., Jahnsen, T., and Sandberg, M., 1997. Characterization of the Human Gene Encoding the Type Iα and Type Iβ cGMP-Dependent Protein Kinase (PRKG1). *Genomics*, 42(2), pp.311–318.

Ortiz, P., Stoos, B.A., Hong, N.J., Boesch, D.M., Plato, C.F., and Garvin, J.L., 2003. High-Salt Diet Increases Sensitivity to NO and eNOS Expression But Not NO Production in THALs. *Hypertension*, 41(3), pp.682–687.

Osteen, J.D., Sampson, K.J., and Kass, R.S., 2010. The cardiac IKs channel, complex indeed. *Proceedings of the National Academy of Sciences of the United States of America*, 107(44), pp.18751–2.

Oyekan, A.O., McGiff, J.C., and Quilley, J., 1991. Cytochrome P-450-dependent vasodilator responses to arachidonic acid in the isolated, perfused kidney of the rat. *Circulation Research*, 68(4), pp.958–965.

Ozkor, M.A. and Quyyumi, A.A., 2011. Endothelium-derived hyperpolarizing factor and vascular function. *Cardiology research and practice*, 2011, p.156146.

Pan, Z., Huang, J., Cui, W., Long, C., Zhang, Y., and Wang, H., 2010. Targeting Hypertension With a New Adenosine Triphosphate–sensitive Potassium Channel Opener Iptakalim. *Journal of Cardiovascular Pharmacology*, 56(3), pp.215–228.

Panigrahy, D., Kaipainen, A., Greene, E.R., and Huang, S., 2010. Cytochrome P450-derived eicosanoids: the neglected pathway in cancer. *Cancer metastasis reviews*, 29(4), pp.723–35.

Panza, J.A., Quyyumi, A.A., Brush, J.E., and Epstein, S.E., 1990. Abnormal Endothelium-Dependent Vascular Relaxation in Patients with Essential Hypertension. *New England Journal of Medicine*, 323(1), pp.22–27.

Park, S.-H., Cho, G., and Park, S.-G., 2014. NF-κB Activation in T Helper 17 Cell Differentiation. *Immune network*, 14(1), pp.14–20.

Park, S.-K., Herrnreiter, A., Pfister, S.L., Gauthier, K.M., Falck, B.A., Falck, J.R., and Campbell, W.B., 2018. GPR40 is a low-affinity epoxyeicosatrienoic acid receptor in vascular cells. *Journal of Biological Chemistry*, 293(27), pp.10675–10691.

Patel, S., Joseph, S.K., and Thomas, A.P., 1999. Molecular properties of inositol 1,4,5-trisphosphate receptors. *Cell Calcium*, 25(3), pp.247–264.

Patterson, A.J., Henrie-Olson, J., and Brenner, R., 2002. Vasoregulation at the molecular level: a role for the beta1 subunit of the calcium-activated potassium (BK) channel. *Trends in cardiovascular medicine*, 12(2), pp.78–82.

Pear, W.S., Nolan, G.P., Scott, M.L., and Baltimore, D., 1993. Production of high-titer

helper-free retroviruses by transient transfection. *Proceedings of the National Academy of Sciences of the United States of America*, 90(18), pp.8392–6.

Peters, T., 1991. Gel Electrophoresis of Proteins: A Practical Approach (Second Edition). *Biochemical Education*, 19(1), p.39.

Pfeifer, A., Nürnberg, B., Kamm, S., Uhde, M., Schultz, G., Ruth, P., and Hofmann, F., 1995. Cyclic GMP-dependent protein kinase blocks pertussis toxin-sensitive hormone receptor signaling pathways in Chinese hamster ovary cells. *The Journal of biological chemistry*, 270(16), pp.9052–9.

Pfitzner, J., 1976. Poiseuille and his law. *Anaesthesia*, 3(1), pp.273–275.

Pikuleva, I.A. and Waterman, M.R., 2013. Cytochromes p450: roles in diseases. *The Journal of biological chemistry*, 288(24), pp.17091–8.

Ploug, K.B., Sørensen, M.A., Strøbech, L., Klaerke, D.A., Hay-Schmidt, A., Sheykhzade, M., Olesen, J., and Jansen-Olesen, I., 2008. KATP channels in pig and human intracranial arteries. *European Journal of Pharmacology*, 601(1–3), pp.43–49.

Pocock, G., Richards, C.D., and Richards, D.A., 2013. The circulation. In: *Human Physiology*. Oxford University Press, pp.410–517.

Prior, H.M., Webster, N., Quinn, K., Beech, D.J., and Yates, M.S., 1998. K(+)-induced dilation of a small renal artery: no role for inward rectifier K+ channels. *Cardiovascular research*, 37(3), pp.780–90.

Purves, G.I., Kamishima, T., Davies, L.M., Quayle, J.M., and Dart, C., 2009. Exchange protein activated by cAMP (Epac) mediates cAMP-dependent but protein kinase A-insensitive modulation of vascular ATP-sensitive potassium channels. *The Journal of Physiology*, 587(14), pp.3639–3650.

QIAGEN, 2012a. *(EN) - EndoFree Plasmid Purification Handbook - QIAGEN*

[Online]. Available from: https://www.qiagen.com/gb/resources/resourcedetail?id=f8ed5bab-15c3-4211-bfa8-4fbe207aad74&lang=en [Accessed 27 May 2018].

QIAGEN, 2012b. *QIAprep Spin Miniprep Kit High-Yield Protocol - (EN)* [Online]. Available from: https://www.qiagen.com/dk/resources/resourcedetail?id=89bfa021-7310-4c0f-90e0-6a9c84f66cee&lang=en [Accessed 17 May 2018].

QIAGEN, 2015. *(EN)-QIAquick Spin Handbook* [Online]. Available from: https://www.qiagen.com/gb/resources/resourcedetail?id=3987caa6-ef28-4abd-927e-d5759d986658&lang=en [Accessed 5 February 2018].

Qian, L.-L., Sun, M.-Q., Wang, R.-X., Lu, T., Wu, Y., Dang, S.-P., Tang, X., Ji, Y., Liu, X.-Y., Zhao, X.-X., Wang, W., Chai, Q., Pan, M., Yi, F., Zhang, D.-M., and Lee, H.-C., 2018. Mechanisms of BK Channel Activation by Docosahexaenoic Acid in Rat Coronary Arterial Smooth Muscle Cells. *Frontiers in pharmacology*, 9, p.223.

Qu, Y.-J., Zhang, X., Fan, Z.-Z., Huai, J., Teng, Y.-B., Zhang, Y., and Yue, S.-W., 2016. Effect of TRPV4-p38 MAPK Pathway on Neuropathic Pain in Rats with Chronic Compression of the Dorsal Root Ganglion. *BioMed Research International*, 2016, pp.1–12.

Quayle, J.M., Bonev, A.D., Brayden, J.E., and Nelson, M.T., 1994. Calcitonin gene-related peptide activated ATP-sensitive K+ currents in rabbit arterial smooth muscle via protein kinase A. *The Journal of physiology*, 475(1), pp.9–13.

Rahaman, S.O., Grove, L.M., Paruchuri, S., Southern, B.D., Abraham, S., Niese, K.A., Scheraga, R.G., Ghosh, S., Thodeti, C.K., Zhang, D.X., Moran, M.M., Schilling, W.P., Tschumperlin, D.J., and Olman, M.A., 2014. TRPV4 mediates

myofibroblast differentiation and pulmonary fibrosis in mice. *Journal of Clinical Investigation*, 124(12), pp.5225–5238.

Raimondi, L., Lodovici, M., Visioli, F., Sartiani, L., Cioni, L., Alfarano, C., Banchelli, G., Pirisino, R., Cecchi, E., Cerbai, E., and Mugelli, A., 2005. n–3 polyunsaturated fatty acids supplementation decreases asymmetric dimethyl arginine and arachidonate accumulation in aging spontaneously hypertensive rats. *European Journal of Nutrition*, 44(6), pp.327–333.

Randriamboavonjy, V., Busse, R., and Fleming, I., 2003. 20-HETE–Induced Contraction of Small Coronary Arteries Depends on the Activation of Rho-Kinase. *Hypertension*, 41(3), pp.801–806.

Rees, D.D., Palmer, R.M., Schulz, R., Hodson, H.F., and Moncada, S., 1990. Characterization of three inhibitors of endothelial nitric oxide synthase in vitro and in vivo. *British journal of pharmacology*, 101(3), pp.746–52.

Reiter, B., Kraft, R., Günzel, D., Zeissig, S., Schulzke, J.-D., Fromm, M., and Harteneck, C., 2006. TRPV4-mediated regulation of epithelial permeability. *The FASEB Journal*, 20(11), pp.1802–1812.

Ricciotti, E. and FitzGerald, G.A., 2011. Prostaglandins and Inflammation. *Arteriosclerosis, Thrombosis, and Vascular Biology*, 31(5), pp.986–1000.

Ricciotti, E., Yu, Y., Grosser, T., and Fitzgerald, G.A., 2013. COX-2, the dominant source of prostacyclin. *Proceedings of the National Academy of Sciences of the United States of America*, 110(3), p.E183.

Rieckenhoff, I.G., Holman, R.T., and Burr, G.O., 1949. Polyethenoid fatty acid metabolism; effect of dietary fat on polyethenoid fatty acids of rat tissues. *Archives of biochemistry*, 20(2), pp.331–40.

Riobo, N.A. and Manning, D.R., 2005. Receptors coupled to heterotrimeric G proteins

of the G12 family. *Trends in Pharmacological Sciences*, 26(3), pp.146–154.

Rodrigo, R., González, J., and Paoletto, F., 2011. The role of oxidative stress in the pathophysiology of hypertension. *Hypertension Research*, 34(4), pp.431–440.

Roman, M.J., Okin, P.M., Kizer, J.R., Lee, E.T., Howard, B. V, and Devereux, R.B., 2010. Relations of central and brachial blood pressure to left ventricular hypertrophy and geometry: the Strong Heart Study. *Journal of Hypertension*, 28(2), pp.384–388.

Roman, R.J., 2002. P -450 Metabolites of Arachidonic Acid in the Control of Cardiovascular Function. *Physiological Reviews*, 82(1), pp.131–185.

Rosenthal, M.D. and Whitehurst, M.C., 1983. Fatty acyl delta 6 desaturation activity of cultured human endothelial cells. Modulation by fetal bovine serum. *Biochimica et biophysica acta*, 750(3), pp.490–6.

Rosolowsky, M. and Campbell, W.B., 1993. Role of PGI2 and epoxyeicosatrienoic acids in relaxation of bovine coronary arteries to arachidonic acid. *American Journal of Physiology-Heart and Circulatory Physiology*, 264(2), pp.H327–H335.

Rosolowsky, M. and Campbell, W.B., 1996. Synthesis of hydroxyeicosatetraenoic (HETEs) and epoxyeicosatrienoic acids (EETs) by cultured bovine coronary artery endothelial cells. *Biochimica et biophysica acta*, 1299(2), pp.267–77.

Rosolowsky, M., Falck, J.R., Willerson, J.T., and Campbell, W.B., 1990. Synthesis of lipoxygenase and epoxygenase products of arachidonic acid by normal and stenosed canine coronary arteries. *Circulation Research*, 66(3), pp.608–621.

Roux, B.T., Bauer, C.C., McNeish, A.J., Ward, S.G., and Cottrell, G.S., 2017. The Role of Ubiquitination and Hepatocyte Growth Factor-Regulated Tyrosine Kinase Substrate in the Degradation of the Adrenomedullin Type I Receptor. *Scientific Reports*, 7(1), p.12389.

Russ, U., Metzger, F., Kickenweiz, E., Hambrock, A., Krippeit-Drews, P., and Quast, U., 1997. Binding and effects of KATP channel openers in the vascular smooth muscle cell line, A10. *British journal of pharmacology*, 122(6), pp.1119–26.

Rzehak, P., Thijs, C., Standl, M., Mommers, M., Glaser, C., Jansen, E., Klopp, N., Koppelman, G.H., Singmann, P., Postma, D.S., Sausenthaler, S., Dagnelie, P.C., van den Brandt, P.A., Koletzko, B., Heinrich, J., and Group, for the K. and the L. study, 2010. Variants of the FADS1 FADS2 Gene Cluster, Blood Levels of Polyunsaturated Fatty Acids and Eczema in Children within the First 2 Years of Life. D. Hartl, ed. *PLoS ONE*, 5(10), p.e13261.

Sacerdoti, D., Bolognesi, M., Di Pascoli, M., Gatta, A., McGiff, J.C., Schwartzman, M.L., and Abraham, N.G., 2006. Rat mesenteric arterial dilator response to 11,12-epoxyeicosatrienoic acid is mediated by activating heme oxygenase. *American Journal of Physiology-Heart and Circulatory Physiology*, 291(4), pp.H1999–H2002.

Sanchez, M. and McManus, O.B., 1996. Paxilline inhibition of the alpha-subunit of the high-conductance calcium-activated potassium channel. *Neuropharmacology*, 35(7), pp.963–8.

Sandow, S.L. and Hill, C.E., 2000. Incidence of myoendothelial gap junctions in the proximal and distal mesenteric arteries of the rat is suggestive of a role in endothelium-derived hyperpolarizing factor-mediated responses. *Circulation research*, 86(3), pp.341–6.

Sanger, F., Nicklen, S., and Coulson, A.R., 1977. DNA sequencing with chain-terminating inhibitors. *Proceedings of the National Academy of Sciences of the United States of America*, 74(12), pp.5463–7.

Sato, K., Chino, D., Nishioka, N., Kanai, K., Aoki, M., Obara, K., Miyauchi, S., and

Tanaka, Y., 2014. Pharmacological Evidence Showing Significant Roles for Potassium Channels and CYP Epoxygenase Metabolites in the Relaxant Effects of Docosahexaenoic Acid on the Rat Aorta Contracted with U46619. *Biological and Pharmaceutical Bulletin*, 37(3), pp.394–403.

Schiffrin, E.L., 1992. Reactivity of small blood vessels in hypertension: relation with structural changes. State of the art lecture. *Hypertension*, 19(2 Suppl), pp.II1-9.

Schroeder, B.C., Hechenberger, M., Weinreich, F., Kubisch, C., and Jentsch, T.J., 2000. KCNQ5, a Novel Potassium Channel Broadly Expressed in Brain, Mediates M-type Currents. *Journal of Biological Chemistry*, 275(31), pp.24089–24095.

Scotland, R.S., Madhani, M., Chauhan, S., Moncada, S., Andresen, J., Nilsson, H., Hobbs, A.J., and Ahluwalia, A., 2005. Investigation of Vascular Responses in Endothelial Nitric Oxide Synthase/Cyclooxygenase-1 Double-Knockout Mice: Key Role for Endothelium-Derived Hyperpolarizing Factor in the Regulation of Blood Pressure in Vivo. *Circulation*, 111(6), pp.796–803.

Seals, D.R., Jablonski, K.L., and Donato, A.J., 2011. Aging and vascular endothelial function in humans. *Clinical Science*, 120(9), pp.357–375.

Sedivy, V., Joshi, S., Ghaly, Y., Mizera, R., Zaloudikova, M., Brennan, S., Novotna, J., Herget, J., and Gurney, A.M., 2015. Role of Kv7 channels in responses of the pulmonary circulation to hypoxia. *American journal of physiology. Lung cellular and molecular physiology*, 308(1), pp.L48-57.

Seino, S., 1999. ATP-SENSITIVE POTASSIUM CHANNELS: A Model of Heteromultimeric Potassium Channel/Receptor Assemblies. *Annual Review of Physiology*, 61(1), pp.337–362.

Sen, C.K. and Packer, L., 1996. Antioxidant and redox regulation of gene transcription. *FASEB journal : official publication of the Federation of American Societies for*

Experimental Biology, 10(7), pp.709–20.

Sharan, S.K., Thomason, L.C., Kuznetsov, S.G., and Court, D.L., 2009. Recombineering: a homologous recombination-based method of genetic engineering. *Nature protocols*, 4(2), pp.206–23.

Shi, B., Shin, Y.K., Hassanali, A.A., and Singer, S.J., 2015. DNA Binding to the Silica Surface. *The Journal of Physical Chemistry B*, 119(34), pp.11030–11040.

Shi, Q. and Jackowski, G., 1998. One-dimensional polyacrylamide gel electrophoresis. In: B. D. Hames, ed. *Gel Electrophoresis of Proteins: A Practical Approach*. Oxford: Oxford University Press, pp.1–52.

Shi, W.-W., Yang, Y., Shi, Y., and Jiang, C., 2012. K(ATP) channel action in vascular tone regulation: from genetics to diseases. *Sheng li xue bao : [Acta physiologica Sinica]*, 64(1), pp.1–13.

Shi, Y., Wu, Z., Cui, N., Shi, W., Yang, Y., Zhang, X., Rojas, A., Ha, B.T., and Jiang, C., 2007. PKA phosphorylation of SUR2B subunit underscores vascular K ATP channel activation by beta-adrenergic receptors. *American Journal of Physiology-Regulatory, Integrative and Comparative Physiology*, 293(3), pp.R1205–R1214.

Shimokawa, H., Yasutake, H., Fujii, K., Owada, M.K., Nakaike, R., Fukumoto, Y., Takayanagi, T., Nagao, T., Egashira, K., Fujishima, M., and Takeshita, A., 1996. The importance of the hyperpolarizing mechanism increases as the vessel size decreases in endothelium-dependent relaxations in rat mesenteric circulation. *Journal of cardiovascular pharmacology*, 28(5), pp.703–11.

Si, H., 2006. Impaired Endothelium-Derived Hyperpolarizing Factor-Mediated Dilations and Increased Blood Pressure in Mice Deficient of the Intermediate-Conductance Ca2+-Activated K+ Channel. *Circulation Research*, 99(5), pp.537–544.

Silva, B.R., Paula, T.D., Paulo, M., and Bendhack, L.M., 2016. Nitric oxide signaling and the cross talk with prostanoids pathways in vascular system. *Medicinal chemistry (Shariqah (United Arab Emirates))*, 13(4), pp.319–333.

Singh, U. and Jialal, I., 2006. Oxidative stress and atherosclerosis. *Pathophysiology*, 13(3), pp.129–42.

Sinha, S., Sinharoy, P., Bratz, I.N., and Damron, D.S., 2015. Propofol causes vasodilation in vivo via TRPA1 ion channels: role of nitric oxide and BKCa channels. *PloS one*, 10(4), p.e0122189.

Sitia, S., Tomasoni, L., Atzeni, F., Ambrosio, G., Cordiano, C., Catapano, A., Tramontana, S., Perticone, F., Naccarato, P., Camici, P., Picano, E., Cortigiani, L., Bevilacqua, M., Milazzo, L., Cusi, D., Barlassina, C., Sarzi-Puttini, P., and Turiel, M., 2010. From endothelial dysfunction to atherosclerosis. *Autoimmunity Reviews*, 9(12), pp.830–834.

Van Sloten, T.T., Protogerou, A.D., Henry, R.M.A., Schram, M.T., Launer, L.J., and Stehouwer, C.D.A., 2015. Association between arterial stiffness, cerebral small vessel disease and cognitive impairment: A systematic review and meta-analysis. *Neuroscience & Biobehavioral Reviews*, 53, pp.121–130.

Smith, L.M., Fung, S., Hunkapiller, M.W., Hunkapiller, T.J., and Hood, L.E., 1985. The synthesis of oligonucleotides containing an aliphatic amino group at the 5' terminus: synthesis of fluorescent DNA primers for use in DNA sequence analysis. *Nucleic acids research*, 13(7), pp.2399–412.

Smith, L.M., Sanders, J.Z., Kaiser, R.J., Hughes, P., Dodd, C., Connell, C.R., Heiner, C., Kent, S.B.H., and Hood, L.E., 1986. Fluorescence detection in automated DNA sequence analysis. *Nature*, 321(6071), pp.674–679.

Smith, P.K., Krohn, R.I., Hermanson, G.T., Mallia, A.K., Gartner, F.H., Provenzano,

M.D., Fujimoto, E.K., Goeke, N.M., Olson, B.J., and Klenk, D.C., 1985. Measurement of protein using bicinchoninic acid. *Analytical biochemistry*, 150(1), pp.76–85.

Smith, W.L., DeWitt, D.L., and Garavito, R.M., 2000. Cyclooxygenases: Structural, Cellular, and Molecular Biology. *Annual Review of Biochemistry*, 69(1), pp.145–182.

Smyth, E.M., Grosser, T., Wang, M., Yu, Y., and FitzGerald, G.A., 2009. Prostanoids in health and disease. *Journal of lipid research*, 50 Suppl(Suppl), pp.S423-8.

Søgaard, R., Ljungstrøm, T., Pedersen, K.A., Olesen, S.-P., and Jensen, B.S., 2001. KCNQ4 channels expressed in mammalian cells: functional characteristics and pharmacology. *American Journal of Physiology-Cell Physiology*, 280(4), pp.C859–C866.

Somlyo, A.P. and Somlyo, A. V, 2000. Signal transduction by G-proteins, rho-kinase and protein phosphatase to smooth muscle and non-muscle myosin II. *The Journal of physiology*, 522 Pt 2, pp.177–85.

Sonkusare, S.K., Bonev, A.D., Ledoux, J., Liedtke, W., Kotlikoff, M.I., Heppner, T.J., Hill-Eubanks, D.C., and Nelson, M.T., 2012. Elementary Ca2+ signals through endothelial TRPV4 channels regulate vascular function. *Science (New York, N.Y.)*, 336(6081), pp.597–601.

Sonkusare, S.K., Dalsgaard, T., Bonev, A.D., Hill-Eubanks, D.C., Kotlikoff, M.I., Scott, J.D., Santana, L.F., and Nelson, M.T., 2014. AKAP150-dependent cooperative TRPV4 channel gating is central to endothelium-dependent vasodilation and is disrupted in hypertension. *Science signaling*, 7(333), p.ra66.

Spector, A.A. and Kim, H.-Y., 2015. Discovery of essential fatty acids. *Journal of lipid research*, 56(1), pp.11–21.

Spruce, A.E., Standen, N.B., and Stanfield, P.R., 1985. Voltage-dependent ATP-sensitive potassium channels of skeletal muscle membrane. *Nature*, 316(6030), pp.736–738.

Standen, N.B., Quayle, J.M., Davies, N.W., Brayden, J.E., Huang, Y., and Nelson, M.T., 1989. Hyperpolarizing vasodilators activate ATP-sensitive K+ channels in arterial smooth muscle. *Science (New York, N.Y.)*, 245(4914), pp.177–80.

Stewart, J., Manmathan, G., and Wilkinson, P., 2017. Primary prevention of cardiovascular disease: A review of contemporary guidance and literature. *JRSM Cardiovascular Disease*, 6, p.204800401668721.

Stoller, D.A., Fahrenbach, J.P., Chalupsky, K., Tan, B.-H., Aggarwal, N., Metcalfe, J., Hadhazy, M., Shi, N.-Q., Makielski, J.C., and McNally, E.M., 2010. Cardiomyocyte sulfonylurea receptor 2-KATP channel mediates cardioprotection and ST segment elevation. *American journal of physiology. Heart and circulatory physiology*, 299(4), pp.H1100-8.

Stott, J.B., Barrese, V., and Greenwood, I.A., 2016. Kv7 Channel Activation Underpins EPAC-Dependent Relaxations of Rat Arteries. *Arteriosclerosis, Thrombosis, and Vascular Biology*, 36(12), pp.2404–2411.

Stott, J.B., Barrese, V., Jepps, T.A., Leighton, E. V., and Greenwood, I.A., 2015. Contribution of Kv7 Channels to Natriuretic Peptide Mediated Vasodilation in Normal and Hypertensive RatsNovelty and Significance. *Hypertension*, 65(3), pp.676–682.

Sukumaran, S. V., Singh, T.U., Parida, S., Narasimha Reddy, C.E., Thangamalai, R., Kandasamy, K., Singh, V., and Mishra, S.K., 2013. TRPV4 channel activation leads to endothelium-dependent relaxation mediated by nitric oxide and endothelium-derived hyperpolarizing factor in rat pulmonary artery.

Pharmacological Research, 78, pp.18–27.

Sullivan, J.M., Zimanyi, C.M., Aisenberg, W., Bears, B., Chen, D.-H., Day, J.W., Bird, T.D., Siskind, C.E., Gaudet, R., and Sumner, C.J., 2015. Novel mutations highlight the key role of the ankyrin repeat domain in TRPV4-mediated neuropathy. *Neurology. Genetics*, 1(4), p.e29.

Sun, C.W., Falck, J.R., Harder, D.R., and Roman, R.J., 1999. Role of tyrosine kinase and PKC in the vasoconstrictor response to 20-HETE in renal arterioles. *Hypertension (Dallas, Tex. : 1979)*, 33(1 Pt 2), pp.414–8.

Sun, D., Messina, E.J., Kaley, G., and Koller, A., 1992. Characteristics and origin of myogenic response in isolated mesenteric arterioles. *American Journal of Physiology-Heart and Circulatory Physiology*, 263(5), pp.H1486–H1491.

Swärd, K., Mita, M., Wilson, D.P., Deng, J.T., Susnjar, M., and Walsh, M.P., 2003. The role of RhoA and Rho-associated kinase in vascular smooth muscle contraction. *Current hypertension reports*, 5(1), pp.66–72.

Szentandrássy, N., Pérez-Bido, M.R., Alonzo, E., Negretti, N., and O'Neill, S.C., 2007. Protein kinase A is activated by the n-3 polyunsaturated fatty acid eicosapentaenoic acid in rat ventricular muscle. *The Journal of physiology*, 582(Pt 1), pp.349–58.

Tagawa, H., Shimokawa, H., Tagawa, T., Kuroiwa-Matsumoto, M., Hirooka, Y., and Takeshita, A., 1999. Long-term treatment with eicosapentaenoic acid augments both nitric oxide-mediated and non-nitric oxide-mediated endothelium-dependent forearm vasodilatation in patients with coronary artery disease. *Journal of cardiovascular pharmacology*, 33(4), pp.633–40.

Tai, C.C., Chen, C.Y., Lee, H.S., Wang, Y.C., Li, T.K., Mersamm, H.J., Ding, S.T., and Wang, P.H., 2009. Docosahexaenoic Acid Enhances Hepatic Serum Amyloid A

Expression via Protein Kinase A-dependent Mechanism. *Journal of Biological Chemistry*, 284(47), pp.32239–32247.

Takahashi, N., Hamada-Nakahara, S., Itoh, Y., Takemura, K., Shimada, A., Ueda, Y., Kitamata, M., Matsuoka, R., Hanawa-Suetsugu, K., Senju, Y., Mori, M.X., Kiyonaka, S., Kohda, D., Kitao, A., Mori, Y., and Suetsugu, S., 2014. TRPV4 channel activity is modulated by direct interaction of the ankyrin domain to PI(4,5)P2. *Nature Communications*, 5(1), p.4994.

Takai, J., Santu, A., Zheng, H., Koh, S.D., Ohta, M., Filimban, L.M., Lemaître, V., Teraoka, R., Jo, H., and Miura, H., 2013. Laminar shear stress upregulates endothelial Ca 2+ -activated K + channels KCa2.3 and KCa3.1 via a Ca 2+ /calmodulin-dependent protein kinase kinase/Akt/p300 cascade. *American Journal of Physiology-Heart and Circulatory Physiology*, 305(4), pp.H484–H493.

Tamura, N., Itoh, H., Ogawa, Y., Nakagawa, O., Harada, M., Chun, T.H., Suga, S., Yoshimasa, T., and Nakao, K., 1996. cDNA cloning and gene expression of human type Ialpha cGMP-dependent protein kinase. *Hypertension (Dallas, Tex. : 1979)*, 27(3 Pt 2), pp.552–7.

Tanaka, Y., Meera, P., Song, M., Knaus, H.G., and Toro, L., 1997. Molecular constituents of maxi KCa channels in human coronary smooth muscle: predominant alpha + beta subunit complexes. *The Journal of physiology*, 502 (Pt 3, pp.545–57.

Tang, G., Wu, L., Liang, W., and Wang, R., 2005. Direct stimulation of KATP channels by exogenous and endogenous hydrogen sulfide in vascular smooth muscle. *Molecular Pharmacology*, 68(6), pp.1757–64.

Taniguchi, J., Honda, H., Shibusawa, Y., Iwata, T., and Notoya, Y., 2005. Alteration in endothelial function and modulation by treatment with pioglitazone in rabbit renal

artery from short-term hypercholesterolemia. *Vascular Pharmacology*, 43(1), pp.47–55.

Taylor, M.S., Bonev, A.D., Gross, T.P., Eckman, D.M., Brayden, J.E., Bond, C.T., Adelman, J.P., and Nelson, M.T., 2003. Altered Expression of Small-Conductance Ca2+-Activated K+ (SK3) Channels Modulates Arterial Tone and Blood Pressure. *Circulation Research*, 93(2), pp.124–131.

Taylor, S.G. and Weston, A.H., 1988. Endothelium-derived hyperpolarizing factor: a new endogenous inhibitor from the vascular endothelium. *Trends in pharmacological sciences*, 9(8), pp.272–4.

Teramoto, N., 2006. Pharmacological Profile of U-37883A, a Channel Blocker of Smooth Muscle-Type ATP-Sensitive K+ Channels. *Cardiovascular Drug Reviews*, 24(1), pp.25–32.

Tharp, D.L., Wamhoff, B.R., Turk, J.R., and Bowles, D.K., 2006. Upregulation of intermediate-conductance Ca 2+ -activated K + channel (IKCa1) mediates phenotypic modulation of coronary smooth muscle. *American Journal of Physiology-Heart and Circulatory Physiology*, 291(5), pp.H2493–H2503.

Thermofisher, 2010. *pLenti6.3_7.3_V5_TOPO TA Cloning Kits* [Online]. Available from: https://www.thermofisher.com/document-connect/document-connect.html?url=https%3A%2F%2Fassets.thermofisher.com%2FTFS-Assets%2FLSG%2Fmanuals%2Fplenti6_3_7_3_v5_topo_ta_man.pdf&title=cExlbnRpNi4zXzcuM19WNV9UT1BPIFRBIENsb25pbmcgS2l0cw== [Accessed 4 March 2019].

ThermoFisher, 2010. *Flp-In™ T-REx™ 293 Cell Line* [Online]. Available from: https://www.thermofisher.com/order/catalog/product/R78007 [Accessed 5 February 2018].

ThermoFisher, 2012. *Flp-recombinase expression vector designed for use with the Flp-In™ System* [Online]. Available from: https://assets.thermofisher.com/TFS-Assets/LSG/manuals/flpin_pog44_man.pdf [Accessed 28 February 2018].

ThermoFisher, 2018. *Flp-In System: For Generating Constitutive Expression Cell Lines* [Online]. Available from: https://www.thermofisher.com/uk/en/home/references/protocols/proteins-expression-isolation-and-analysis/protein-expression-protocol/flp-in-system-for-generating-constitutive-expression-cell-lines.html [Accessed 2 February 2018].

Thomson, S.J., Askari, A., and Bishop-Bailey, D., 2012. Anti-Inflammatory Effects of Epoxyeicosatrienoic Acids. *International Journal of Vascular Medicine*, 2012, pp.1–7.

Tinker, A., Aziz, Q., and Thomas, A., 2014. The role of ATP-sensitive potassium channels in cellular function and protection in the cardiovascular system. *British journal of pharmacology*, 171(1), pp.12–23.

Tran, L.T., MacLeod, K.M., and McNeill, J.H., 2009. Chronic etanercept treatment prevents the development of hypertension in fructose-fed rats. *Molecular and Cellular Biochemistry*, 330(1–2), pp.219–228.

Triggle, C.R. and Ding, H., 2011. The endothelium in compliance and resistance vessels. *Frontiers in bioscience (Scholar edition)*, 3, pp.730–44.

Ueda, A., Ohyanagi, M., Koida, S., and Iwasaki, T., 2005. Enhanced release of endothelium-derived hyperpolarizing factor in small coronary arteries from rats with congestive heart failure. *Clinical and Experimental Pharmacology and Physiology*, 32(8), pp.615–621.

Urakami-Harasawa, L., Shimokawa, H., Nakashima, M., Egashira, K., and Takeshita, A., 1997. Importance of endothelium-derived hyperpolarizing factor in human

arteries. *Journal of Clinical Investigation*, 100(11), pp.2793–2799.

Vaskonen, T., Laakso, J., Mervaala, E., Sievi, E., and Karppanen, H., 1996. Interrelationships between salt and fish oil in stroke-prone spontaneously hypertensive rat. *Blood pressure*, 5(3), pp.178–89.

Vázquez, J., Feigenbaum, P., King, V.F., Kaczorowski, G.J., and Garcia, M.L., 1990. Characterization of high affinity binding sites for charybdotoxin in synaptic plasma membranes from rat brain. Evidence for a direct association with an inactivating, voltage-dependent, potassium channel. *The Journal of biological chemistry*, 265(26), pp.15564–71.

Vellani, V., Mapplebeck, S., Moriondo, A., Davis, J.B., and McNaughton, P.A., 2001. Protein kinase C activation potentiates gating of the vanilloid receptor VR1 by capsaicin, protons, heat and anandamide. *The Journal of physiology*, 534(Pt 3), pp.813–25.

Venegas-Pont, M., Manigrasso, M.B., Grifoni, S.C., LaMarca, B.B., Maric, C., Racusen, L.C., Glover, P.H., Jones, A. V, Drummond, H.A., and Ryan, M.J., 2010. Tumor necrosis factor-alpha antagonist etanercept decreases blood pressure and protects the kidney in a mouse model of systemic lupus erythematosus. *Hypertension (Dallas, Tex. : 1979)*, 56(4), pp.643–9.

Verkerk, A., Vanginneken, A., Berecki, G., Denruijter, H., Schumacher, C., Veldkamp, M., Baartscheer, A., Casini, S., Opthof, T., Hovenier, R., Fiolet, J.W.T., Zock, P.L., and Coronel, R., 2006. Incorporated sarcolemmal fish oil fatty acids shorten pig ventricular action potentials. *Cardiovascular Research*, 70(3), pp.509–520.

Villalpando, D.M., Navarro, R., Del Campo, L., Largo, C., Muñoz, D., Tabernero, M., Baeza, R., Otero, C., García, H.S., and Ferrer, M., 2015. Effect of Dietary Docosahexaenoic Acid Supplementation on the Participation of Vasodilator

Factors in Aorta from Orchidectomized Rats. *PloS one*, 10(11), p.e0142039.

Villarroel, A., 1994. On the role of arachidonic acid in M-current modulation by muscarine in bullfrog sympathetic neurons. *The Journal of neuroscience : the official journal of the Society for Neuroscience*, 14(11 Pt 2), pp.7053–66.

Vincent, F., Acevedo, A., Nguyen, M.T., Dourado, M., DeFalco, J., Gustafson, A., Spiro, P., Emerling, D.E., Kelly, M.G., and Duncton, M.A.J., 2009. Identification and characterization of novel TRPV4 modulators. *Biochemical and Biophysical Research Communications*, 389(3), pp.490–494.

Vriens, J., Owsianik, G., Fisslthaler, B., Suzuki, M., Janssens, A., Voets, T., Morisseau, C., Hammock, B.D., Fleming, I., Busse, R., and Nilius, B., 2005. Modulation of the Ca2 Permeable Cation Channel TRPV4 by Cytochrome P450 Epoxygenases in Vascular Endothelium. *Circulation Research*, 97(9), pp.908–915.

Waldron, G.J., Ding, H., Lovren, F., Kubes, P., and Triggle, C.R., 1999. Acetylcholine-induced relaxation of peripheral arteries isolated from mice lacking endothelial nitric oxide synthase. *British Journal of Pharmacology*, 128(3), pp.653–658.

Wallace, S.M.L., Yasmin, McEniery, C.M., Mäki-Petäjä, K.M., Booth, A.D., Cockcroft, J.R., and Wilkinson, I.B., 2007. Isolated Systolic Hypertension Is Characterized by Increased Aortic Stiffness and Endothelial Dysfunction. *Hypertension*, 50(1), pp.228–233.

Walz, W., Boulton, A.A., and Baker, G.B., 2002. *Patch-Clamp Analysis*. Humana Press.

Wang, K.-L., Cheng, H.-M., Chuang, S.-Y., Spurgeon, H.A., Ting, C.-T., Lakatta, E.G., Yin, F.C.P., Chou, P., and Chen, C.-H., 2009. Central or peripheral systolic or pulse pressure: which best relates to target organs and future mortality? *Journal of hypertension*, 27(3), pp.461–7.

Wang, R. -x., Chai, Q., Lu, T., and Lee, H.-C., 2011. Activation of vascular BK channels by docosahexaenoic acid is dependent on cytochrome P450 epoxygenase activity. *Cardiovascular Research*, 90(2), pp.344–352.

Wang, Z., Shi, H., and Wang, H., 2004. Functional M3 muscarinic acetylcholine receptors in mammalian hearts. *British journal of pharmacology*, 142(3), pp.395–408.

Wang, Z.H., Shen, B., Yao, H.L., Jia, Y.C., Ren, J., Feng, Y.J., and Wang, Y.Z., 2007. Blockage of intermediate-conductance-Ca2+-activated K+ channels inhibits progression of human endometrial cancer. *Oncogene*, 26(35), pp.5107–5114.

Wassmann, S., Laufs, U., Bäumer, A.T., Müller, K., Ahlbory, K., Linz, W., Itter, G., Rösen, R., Böhm, M., and Nickenig, G., 2001. HMG-CoA reductase inhibitors improve endothelial dysfunction in normocholesterolemic hypertension via reduced production of reactive oxygen species. *Hypertension (Dallas, Tex. : 1979)*, 37(6), pp.1450–7.

Wassmann, S., Laufs, U., Müller, K., Konkol, C., Ahlbory, K., Bäumer, A.T., Linz, W., Böhm, M., and Nickenig, G., 2002. Cellular antioxidant effects of atorvastatin in vitro and in vivo. *Arteriosclerosis, thrombosis, and vascular biology*, 22(2), pp.300–5.

Watanabe, H., Vriens, J., Prenen, J., Droogmans, G., Voets, T., and Nilius, B., 2003. Anandamide and arachidonic acid use epoxyeicosatrienoic acids to activate TRPV4 channels. *Nature*, 424(6947), pp.434–438.

Wellman, G.C., Barrett-Jolley, R., Köppel, H., Everitt, D., and Quayle, J.M., 1999. Inhibition of vascular K_{ATP} channels by U-37883A: a comparison with cardiac and skeletal muscle. *British Journal of Pharmacology*, 128(4), pp.909–916.

Wellman, G.C., Quayle, J.M., and Standen, N.B., 1998. ATP-sensitive K+ channel

activation by calcitonin gene-related peptide and protein kinase A in pig coronary arterial smooth muscle. *The Journal of physiology*, 507 (Pt 1(Pt 1), pp.117–29.

Werner, M.E., Meredith, A.L., Aldrich, R.W., and Nelson, M.T., 2008. Hypercontractility and impaired sildenafil relaxations in the BK Ca channel deletion model of erectile dysfunction. *American Journal of Physiology-Regulatory, Integrative and Comparative Physiology*, 295(1), pp.R181–R188.

WHO, 2017. *Cardiovascular diseases (CVDs)* [Online]. Available from: http://www.who.int/en/news-room/fact-sheets/detail/cardiovascular-diseases-(cvds) [Accessed 30 August 2018].

Widmer, C. and Holman, R.T., 1950. Polyethenoid fatty acid metabolism; deposition of polyunsaturated fatty acids in fat-deficient rats upon single fatty acid supplementation. *Archives of biochemistry*, 25(1), pp.1–12.

Wikström, K., Kavanagh, D.J., Reid, H.M., and Kinsella, B.T., 2008. Differential regulation of RhoA-mediated signaling by the TPalpha and TPbeta isoforms of the human thromboxane A2 receptor: independent modulation of TPalpha signaling by prostacyclin and nitric oxide. *Cellular signalling*, 20(8), pp.1497–512.

Wilkinson, I.B., Franklin, S.S., and Cockcroft, J.R., 2004. Nitric Oxide and the Regulation of Large Artery Stiffness. *Hypertension*, 44(2), pp.112–116.

Wilkinson, I.B., MacCallum, H., Cockcroft, J.R., and Webb, D.J., 2002. Inhibition of basal nitric oxide synthesis increases aortic augmentation index and pulse wave velocity in vivo. *British Journal of Clinical Pharmacology*, 53(2), pp.189–192.

Willette, R.N., Bao, W., Nerurkar, S., Yue, T. -l., Doe, C.P., Stankus, G., Turner, G.H., Ju, H., Thomas, H., Fishman, C.E., Sulpizio, A., Behm, D.J., Hoffman, S., Lin, Z., Lozinskaya, I., Casillas, L.N., Lin, M., Trout, R.E.L., Votta, B.J., Thorneloe, K., Lashinger, E.S.R., Figueroa, D.J., Marquis, R., and Xu, X., 2008. Systemic

Activation of the Transient Receptor Potential Vanilloid Subtype 4 Channel Causes Endothelial Failure and Circulatory Collapse: Part 2. *Journal of Pharmacology and Experimental Therapeutics*, 326(2), pp.443–452.

de Wit, C., Boettcher, M., and Schmidt, V.J., 2008. Signaling across Myoendothelial Gap Junctions—Fact or fiction? *Cell Communication & Adhesion*, 15(3), pp.231–245.

Withers, S.B., Simpson, L., Fattah, S., Werner, M.E., and Heagerty, A.M., 2014. cGMP-dependent protein kinase (PKG) mediates the anticontractile capacity of perivascular adipose tissue. *Cardiovascular Research*, 101(1), pp.130–137.

Woodman, C.R., Thompson, M.A., Turk, J.R., and Laughlin, M.H., 2005. Endurance exercise training improves endothelium-dependent relaxation in brachial arteries from hypercholesterolemic male pigs. *Journal of Applied Physiology*, 99(4), pp.1412–1421.

Wu, K.-T., Huang, C.-T., Wei, J., Tsait, L.-M., Hsu, C.-H., Chen, Y.-C., Yangs, J.-M., and Lin, C.-I., 2007. Vasodilator action of docosahexaenoic acid (DHA) in human coronary arteries in vitro. *The Chinese journal of physiology*, 50(4), pp.164–70.

Wu, P.-R., Kuo, C.-C., Yet, S.-F., Liou, J.-Y., Wu, K.K., and Chen, P.-F., 2012. Lobe-Specific Calcium Binding in Calmodulin Regulates Endothelial Nitric Oxide Synthase Activation. A. Hofmann, ed. *PLoS ONE*, 7(6), p.e39851.

Wu, X., Somlyo, A. V, and Somlyo, A.P., 1996. Cyclic GMP-dependent stimulation reverses G-protein-coupled inhibition of smooth muscle myosin light chain phosphate. *Biochemical and biophysical research communications*, 220(3), pp.658–63.

Wulff, H., Miller, M.J., Hansel, W., Grissmer, S., Cahalan, M.D., and Chandy, K.G., 2000. Design of a potent and selective inhibitor of the intermediate-conductance

Ca2+-activated K+ channel, IKCa1: a potential immunosuppressant. *Proceedings of the National Academy of Sciences of the United States of America*, 97(14), pp.8151–6.

Xia, X.-M., Fakler, B., Rivard, A., Wayman, G., Johnson-Pais, T., Keen, J.E., Ishii, T., Hirschberg, B., Bond, C.T., Lutsenko, S., Maylie, J., and Adelman, J.P., 1998. Mechanism of calcium gating in small-conductance calcium-activated potassium channels. *Nature*, 395(6701), pp.503–507.

Yamakage, M., Hirshman, C.A., and Croxton, T.L., 1996. Sodium nitroprusside stimulates Ca2+ -activated K+ channels in porcine tracheal smooth muscle cells. *American Journal of Physiology-Lung Cellular and Molecular Physiology*, 270(3), pp.L338–L345.

Yang, L., Cheriyan, J., Gutterman, D.D., Mayer, R.J., Ament, Z., Griffin, J.L., Lazaar, A.L., Newby, D.E., Tal-Singer, R., and Wilkinson, I.B., 2017. Mechanisms of Vascular Dysfunction in COPD and Effects of a Novel Soluble Epoxide Hydrolase Inhibitor in Smokers. *Chest*, 151(3), pp.555–563.

Yang, Y., Li, P.-Y., Cheng, J., Mao, L., Wen, J., Tan, X.-Q., Liu, Z.-F., and Zeng, X.-R., 2013. Function of BK Ca Channels Is Reduced in Human Vascular Smooth Muscle Cells From Han Chinese Patients With Hypertension. *Hypertension*, 61(2), pp.519–525.

Yang, Y., Shi, Y., Guo, S., Zhang, S., Cui, N., Shi, W., Zhu, D., and Jiang, C., 2008. PKA-dependent activation of the vascular smooth muscle isoform of KATP channels by vasoactive intestinal polypeptide and its effect on relaxation of the mesenteric resistance artery. *Biochimica et biophysica acta*, 1778(1), pp.88–96.

Yap, F.C., Taylor, M.S., and Lin, M.T., 2014. Ovariectomy-Induced Reductions in Endothelial SK3 Channel Activity and Endothelium-Dependent Vasorelaxation in

Murine Mesenteric Arteries. X.-F. Yang, ed. *PLoS ONE*, 9(8), p.e104686.

Ye, D., Zhang, D., Oltman, C., Dellsperger, K., Lee, H.-C., and VanRollins, M., 2002. Cytochrome p-450 epoxygenase metabolites of docosahexaenoate potently dilate coronary arterioles by activating large-conductance calcium-activated potassium channels. *The Journal of pharmacology and experimental therapeutics*, 303(2), pp.768–76.

Ye, D., Zhou, W., and Lee, H.-C., 2005. Activation of rat mesenteric arterial K ATP channels by 11,12-epoxyeicosatrienoic acid. *American Journal of Physiology-Heart and Circulatory Physiology*, 288(1), pp.H358–H364.

Ye, D., Zhou, W., Lu, T., Jagadeesh, S.G., Falck, J.R., and Lee, H.-C., 2006. Mechanism of rat mesenteric arterial K ATP channel activation by 14,15-epoxyeicosatrienoic acid. *American Journal of Physiology-Heart and Circulatory Physiology*, 290(4), pp.H1326–H1336.

Yoshida, H., Feig, J.E., Morrissey, A., Ghiu, I.A., Artman, M., and Coetzee, W.A., 2004. KATP channels of primary human coronary artery endothelial cells consist of a heteromultimeric complex of Kir6.1, Kir6.2, and SUR2B subunits. *Journal of Molecular and Cellular Cardiology*, 37(4), pp.857–869.

Yu, S.P., 1995. Roles of arachidonic acid, lipoxygenases and phosphatases in calcium-dependent modulation of M-current in bullfrog sympathetic neurons. *The Journal of physiology*, 487 (Pt 3(Pt 3), pp.797–811.

Yu, Z., Xu, F., Huse, L.M., Morisseau, C., Draper, A.J., Newman, J.W., Parker, C., Graham, L., Engler, M.M., Hammock, B.D., Zeldin, D.C., and Kroetz, D.L., 2000. Soluble epoxide hydrolase regulates hydrolysis of vasoactive epoxyeicosatrienoic acids. *Circulation research*, 87(11), pp.992–8.

Yucel, C., Demir, S., Demir, M., Tufenk, M., Nas, K., Molnar, F., Illyes, M., and

Acarturk, E., 2015. Left ventricular hypertrophy and arterial stiffness in essential hypertension. *Bratislavske lekarske listy*, 116(12), pp.714–8.

Zalba, G., Beaumont, F.J., San José, G., Fortuño, A., Fortuño, M.A., Etayo, J.C., and Díez, J., 2000. Vascular NADH/NADPH oxidase is involved in enhanced superoxide production in spontaneously hypertensive rats. *Hypertension (Dallas, Tex. : 1979)*, 35(5), pp.1055–61.

Zanetti, M., Gortan Cappellari, G., Barbetta, D., Semolic, A., and Barazzoni, R., 2017. Omega 3 Polyunsaturated Fatty Acids Improve Endothelial Dysfunction in Chronic Renal Failure: Role of eNOS Activation and of Oxidative Stress. *Nutrients*, 9(8), p.895.

Zeldin, D.C., 2001. Epoxygenase Pathways of Arachidonic Acid Metabolism. *Journal of Biological Chemistry*, 276(39), pp.36059–36062.

Zhang, D.X., Mendoza, S.A., Bubolz, A.H., Mizuno, A., Ge, Z.-D., Li, R., Warltier, D.C., Suzuki, M., and Gutterman, D.D., 2009. Transient Receptor Potential Vanilloid Type 4-Deficient Mice Exhibit Impaired Endothelium-Dependent Relaxation Induced by Acetylcholine In Vitro and In Vivo. *Hypertension*, 53(3), pp.532–538.

Zhang, F., Wang, M.H., Krishna, U.M., Falck, J.R., Laniado-Schwartzman, M., and Nasjletti, A., 2001. Modulation by 20-HETE of phenylephrine-induced mesenteric artery contraction in spontaneously hypertensive and Wistar-Kyoto rats. *Hypertension (Dallas, Tex. : 1979)*, 38(6), pp.1311–5.

Zhao, W. and Wang, R., 2002. H 2 S-induced vasorelaxation and underlying cellular and molecular mechanisms. *American Journal of Physiology-Heart and Circulatory Physiology*, 283(2), pp.H474–H480.

Zhao, X., Pollock, D.M., Inscho, E.W., Zeldin, D.C., and Imig, J.D., 2003. Decreased

Renal Cytochrome P450 2C Enzymes and Impaired Vasodilation Are Associated With Angiotensin Salt-Sensitive Hypertension. *Hypertension*, 41(3), pp.709–714.

Zhao, X., Yamamoto, T., Newman, J.W., Kim, I.-H., Watanabe, T., Hammock, B.D., Stewart, J., Pollock, J.S., Pollock, D.M., and Imig, J.D., 2004. Soluble epoxide hydrolase inhibition protects the kidney from hypertension-induced damage. *Journal of the American Society of Nephrology : JASN*, 15(5), pp.1244–53.

Zhao, Y., Vanhoutte, P.M., and Leung, S.W.S., 2015. Vascular nitric oxide: Beyond eNOS. *Journal of Pharmacological Sciences*, 129(2), pp.83–94.

Zheng, X., Zinkevich, N.S., Gebremedhin, D., Gauthier, K.M., Nishijima, Y., Fang, J., Wilcox, D.A., Campbell, W.B., Gutterman, D.D., and Zhang, D.X., 2013. Arachidonic acid-induced dilation in human coronary arterioles: convergence of signaling mechanisms on endothelial TRPV4-mediated Ca2+ entry. *Journal of the American Heart Association*, 2(3), p.e000080.

Zhou, A., Jiang, X., and Xu, X., 1997. Improved Alkaline Lysis Method for Rapid Isolation of Plasmid DNA. *BioTechniques*, 23(4), pp.592–594.

Zhou, W., Hong, M., Zhang, K., Chen, D., Han, W., Shen, W., Zhu, D., and Gao, P., 2014. Mechanisms of Improved Aortic Stiffness by Arotinolol in Spontaneously Hypertensive Rats. S. E. Bearden, ed. *PLoS ONE*, 9(2), p.e88722.

Zhou, X.-B., Schlossmann, J., Hofmann, F., Ruth, P., and Korth, M., 1998. Regulation of stably expressed and native BK channels from human myometrium by cGMP- and cAMP-dependent protein kinase. *Pflügers Archiv European Journal of Physiology*, 436(5), pp.725–734.

Zhu, D., Zhang, C., Medhora, M., and Jacobs, E.R., 2002. CYP4A mRNA, protein, and product in rat lungs: novel localization in vascular endothelium. *Journal of Applied Physiology*, 93(1), pp.330–337.

Zhuge, R., Fogarty, K.E., Tuft, R.A., Walsh, J. V, and Jr, 2002. Spontaneous transient outward currents arise from microdomains where BK channels are exposed to a mean Ca(2+) concentration on the order of 10 microM during a Ca(2+) spark. *The Journal of general physiology*, 120(1), pp.15–27.

Zordoky, B.N.M. and El-Kadi, A.O.S., 2010. Effect of cytochrome P450 polymorphism on arachidonic acid metabolism and their impact on cardiovascular diseases. *Pharmacology & Therapeutics*, 125(3), pp.446–463.

Zou, A.P., Fleming, J.T., Falck, J.R., Jacobs, E.R., Gebremedhin, D., Harder, D.R., and Roman, R.J., 1996. Stereospecific effects of epoxyeicosatrienoic acids on renal vascular tone and K(+)-channel activity. *American Journal of Physiology-Renal Physiology*, 270(5), pp.F822–F832.

Zygmunt, P.M. and Högestätt, E.D., 1996. Role of potassium channels in endothelium-dependent relaxation resistant to nitroarginine in the rat hepatic artery. *British journal of pharmacology*, 117(7), pp.1600–6.